

The Effect of Hydrogen Concentration on the Flame Stability and Laminar Burning Velocity of Hydrogen-Hydrocarbon-Carbon Dioxide Mixtures



A thesis submitted to the Department of Chemical and Biological
Engineering of the University of Sheffield, UK
for the degree of Doctor of Philosophy

presented by

Fei Teng

Supervisor: Dr. Yajue Wu

Sheffield, November 2014

Summary

Syngas as a renewable energy source can be produced from Biomass gasification. Generally, syngas consists of H_2 , CO_2 , CO and C_1 - C_4 hydrocarbons. The gaseous mixtures are also produced from many other chemical processes, such as coal gasification and methane reforming, as products or by-products. Also there is increasing interest in the utilisation of Hydrogen-Hydrocarbon gaseous fuels as alternative energy sources instead of conventional fossil fuels. The gaseous mixtures can be used in burners and gas turbines involved in combustion processes. The utilisation of such gaseous mixture is able to reduce CO_2 emission and fossil fuels consumption in combustion processes. However, the fluctuation in H_2 concentration causes difficulties to predict the laminar burning velocity and flame stability characteristics of the mixtures. These issues lead to the challenges on combustion performance and safe handling. The objectives of this study are to experimentally determine the effect of H_2 and CO_2 addition on the flame lift-off and blow-out characteristics, and also numerically modelling the laminar burning velocity of the Hydrogen-Hydrocarbon gaseous mixtures to determine the effect of H_2 concentration on the laminar burning velocity of the mixtures.

The flame stability experiments are carried out to determine the lift-off heights, lift-off velocities and blow-out velocities of H_2 - CO_2 , H_2 - CH_4 , H_2 - C_2H_6 , H_2 - C_3H_8 and H_2 - CH_4 - CO_2 flames. The H_2 concentration varies from 59% to 100%. The results show that the flame lift-off and blow-out characteristics are mainly governed by the H_2 concentration in the mixtures. With varying hydrocarbons or CO_2 concentrations, the flame lift-off and blow-out parameters can be predicted by the inlet H_2 velocity. The flame can be stabilised by adjusting the H_2 inlet velocity.

The reaction kinetics of H_2 - CH_4 , H_2 - C_2H_6 and H_2 - C_3H_8 gaseous mixtures is

simulated to determine the species concentration and reaction rate of the key components in the mixtures, such as H, OH, CH, H₂ and C₁-C₃. The results show that the consumption rate of CH₄ increases with H₂ concentration while C₂H₆ and C₃H₈ are not so sensitive to the H₂ concentration. However when H₂ concentration is greater than 60%, all mixtures show the overall reaction rate is increased rapidly with H₂ concentration.

The species pathway analysis is employed to determine the consumption and production paths of H, OH, CH, H₂ and C₁-C₃. For H₂-CH₄ mixture, the CH₄ consumption is mainly through the elementary reactions with H and OH. The increasing H₂ concentration in the mixture enhances the decomposition rate of both CH₄ and H₂. For H₂-C₂H₆ and H₂-C₃H₈ mixtures, the primary decompositions of C₂H₆ and C₃H₈ are to form C₂H₅ and C₂H₄. However, the influence of H and OH on the consumption rates of C₂H₆ and C₃H₈ is very weak. They are not directly related to the primary consumption paths of C₂H₆ and C₃H₈.

The laminar burning velocities of the mixtures are determined numerically. When H₂ concentration is less than 60%, the laminar burning velocities increase steadily with H₂ concentration. When H₂ concentration is greater than 60%, the laminar burning velocities increase steeply. It is shown that H₂ concentration has stronger influence on the laminar burning velocity of CH₄-H₂ and the laminar burning velocity of H₂-CH₄ is greater than that of H₂-C₂H₆ and H₂-C₃H₈.

A correlation between the laminar burning velocity and H₂ concentration is established and applied to analyse flame lift-off height data. Based on Kalghatgi's premixed stabilisation theory, the lifted flame base is stabilised at a position which is balanced by the local burning velocity and inlet jet velocity.

Acknowledgements

First of all, I hereby would like to present my sincere gratitude to my supervisor, Dr. Yajue Wu, who has patiently guided me on my PhD studies. Her valuably academic suggestions bring a lot of supports to my works. Her patience, responsibility and encouragement have been with me through my PhD studies. These help me a lot on my development.

I also like to appreciate Prof. Zhang and Dr. Huang from the Department of Mechanical Engineering. They have given me a load of supports on my experiments. I would also like to thank the staffs working at Buxton laboratory, Mike and Dave, and the members of Dr. Wu's group. They bring a lot of helps and happiness to my PhD life.

Moreover, I would like to say thanks to my parents. I could not get this far without their loves. They have been supporting and encouraging me everyday upon my studies and livings, though they are not in the UK.

Fei Teng

Sheffield, 2014

Contents

Chapter 1: Introduction	1
1.1 Background	1
1.2 The Approach and Objectives of the Research	7
1.2.1 Research Approach	7
1.2.2 Objectives	7
1.3 Layout of the Thesis	8
Chapter 2: Literature Review of the Laminar Burning Velocity of	
Hydrogen-Hydrocarbon Gaseous Mixtures	10
2.1 The Definition of Laminar Burning Velocity	10
2.2 The Experimental Methods	12
2.2.1 Stationary Flames	13
2.2.2 Propagation Flames	15
2.3 Numerical Modelling Methods	17
2.4 The Laminar Burning Velocity of H ₂ -Air	19
2.5 The Laminar Burning velocity of CH ₄ -Air and H ₂ -CH ₄	20
2.6 The Laminar Burning Velocity of C ₂ H ₆ -Air and C ₂ H ₆ -H ₂ -Air	25
2.7 The Laminar Burning Velocity of C ₃ H ₈ -Air and C ₃ H ₈ -H ₂ -Air	29
2.8 Summary	32
Chapter 3: Numerical Modelling of Reaction Kinetics and Review of	
Reaction mechanisms	34
3.1 Chemical Reaction Kinetics	34
3.1.1 Molecularity and Reaction Order	34
3.1.2 Rate Laws and Rate Constant	36
3.1.3 Reaction Mechanism	44
3.2 Reaction Mechanism of H ₂ -Air Oxidation	47
3.3 Reaction Mechanism of Hydrocarbon Combustion	50
3.4 CHEMKIN Kinetics Analysis Application	55
3.5 Summary	61

Chapter 4: Literature Review of Flame Stability Mechanism	62
4.1 Definitions of Flame Lift-Off and Blow-Out Parameters	62
4.2 Flame Stabilisation Models	65
4.3 Relationship of Burning Velocity with Flame Lift-Off and Blow-Out Characteristics	67
4.4 Flame Stability of Hydrogen and Hydrocarbons	69
4.5 Summary	71
Chapter 5: Experimental Study of the Lift-off and Blow-out Stability of Hydrogen/hydrocarbon Flames	72
5.1 Experiment Programme	72
5.1.1 Experimental Method	72
5.1.2 Experimental Rig	73
5.1.3 The Gaseous Mixtures Preparing and Mixing	76
5.2 Experimental Results	79
5.2.1 Experimental Results for Pure H ₂ Flames	79
5.2.2 Experimental Results for H ₂ -CH ₄ Flames	80
5.2.3 Experimental Results for H ₂ –C ₂ H ₆ Flames	81
5.2.4 Experimental Results for H ₂ -C ₃ H ₈ Flames	83
5.2.5 Experimental Results for H ₂ -CH ₄ -CO ₂ Flames	84
5.2.6 Experimental Results for H ₂ -CO ₂ Flames	90
5.3 Discussion	94
5.3.1 The Lift-off Heights	94
5.3.2 The Lift-Off jet Velocities	99
5.3.3 The Blow-Out /Off Velocities	100
5.4 Error Analysis	103
5.5 Summary	104
Chapter 6: Numerical Modelling of Reaction Kinetics	105
6.1 Computational Simulation Method	105
6.1.1 Compositions of the Initial Reactants	106
6.1.2 Apply Thermodynamic Data into Numerical Model	106

6.1.3 Determine the Detailed Reaction Mechanism	107
6.2 Reaction Kinetics Simulation of H ₂ -CH ₄ -Air Mixture	111
6.3 Reaction Kinetics Simulation of H ₂ -C ₂ H ₆ -Air Mixture	117
6.4 Reaction Kinetics Simulation of H ₂ -C ₃ H ₈ -Air Mixture	123
6.5 Summary	127
Chapter 7: Species Pathway Analysis	129
7.1 Introduction	129
7.2 Pathway Analysis of the Reactions of CH ₄ -H ₂ Mixtures	131
7.2.1 Pathway Analysis of H ₂	131
7.2.2 Pathway Analysis of CH ₄	132
7.2.3 Pathway Analysis of H	134
7.2.4 Pathway Analysis of OH	138
7.2.5 Pathway Analysis of CH	141
7.2.6 The Main Reaction Pathways	144
7.3 Pathway Analysis of the Reactions of C ₂ H ₆ -H ₂ Mixtures	147
7.3.1 Pathway Analysis of H ₂	147
7.3.2 Pathway Analysis of C ₂ H ₆	147
7.3.3 Pathway Analysis of H	148
7.3.4 Pathway Analysis of OH	149
7.3.5 Pathway Analysis of CH	151
7.3.6 The Main Reaction Pathways	152
7.4 Pathway Analysis of the Reactions of C ₃ H ₈ -H ₂ Mixtures	155
7.4.1 Pathway Analysis of H ₂	155
7.4.2 Pathway Analysis of C ₃ H ₈	155
7.4.3 Pathway Analysis of H	156
7.4.4 Pathway Analysis of OH	158
7.4.5 Pathway Analysis of CH	159
7.4.6 The Main Reaction Pathways	160
7.5 Summary	162
Chapter 8: Numerical Modelling of the Laminar Burning Velocity	163

8.1 The Laminar Burning Velocity Modeling Method	163
8.2 Transport Coefficients	166
8.3 1-D laminar Burning Velocity Simulations	167
8.3.1 Laminar Burning Velocity of Pure CH ₄	167
8.3.2 Laminar Burning Velocity of Pure C ₂ H ₆	169
8.3.3 Laminar Burning Velocity of C ₃ H ₈	172
8.3.4 The Comparison for the Laminar Burning Velocity of H ₂ with CH ₄ , C ₂ H ₆ and C ₃ H ₈ Flames	175
8.4 The Laminar Burning Velocity Simulation of the CH ₄ -H ₂ , C ₂ H ₆ -H ₂ and C ₃ H ₈ -H ₂ mixtures	181
8.5 Summary	183
Chapter 9: Discuss the Correlation of the Laminar Burring Velocity with the Flame Stability and Reaction Kinetics	185
9.1 Laminar Burning and Reaction Kinetics	185
9.1.1 Laminar Burning Velocity	185
9.1.2 The Effect of H ₂ on Reaction Rates	186
9.1.3 The Reaction Pathways	188
9.2 The Laminar Burning Velocity and the Flame Stability Parameters	191
Chapter 10: Conclusions and Further Considerations	203
References	212
Appendix A: Warnatz and Heghes (2006) C ₁ -C ₃ Hydrocarbon Oxidation Mechanism	224
Appendix B: A 19 Elementary Reactions Mechanism used in CHMKIN	231
Appendix C: Complete H ₂ Combustion Mechanism	232
Appendix D: Kinetics Analysis of Propane Combustion in CHEMKIN	233
Appendix E: Gri-Mech 3.0 Methane Combustion Mechanism	234
Appendix F: The Test Condition for H ₂ -CH ₄ Jet Diffusion Flames	242
Appendix G: The Test Condition for H ₂ -C ₂ H ₆ Jet Diffusion Flames	244
Appendix H: The Test Conditions for H ₂ -C ₃ H ₈ Jet Diffusion Flames	246
Appendix I: The Test Conditions for H ₂ -CH ₄ -CO ₂ Jet Diffusion Flames, at H ₂ Flowrate of 20 l/min	247
Appendix J: The Test Condition for H ₂ -CH ₄ -CO ₂ Jet Diffusion Flames, at H ₂ Flowrate of 40 l/min	253
Appendix K: The Test Conditions for H ₂ -CO ₂ Jet Diffusion Flames	257

Appendix L: The Test Conditions for Pure H ₂ Jet Diffusion Flames	263
Appendix M: The Initial Composition of H ₂ -CH ₄ , H ₂ -C ₂ H ₆ and H ₂ -C ₃ H ₈ Mixtures applied in Equilibrium Kinetics Simulation	264
Appendix N: CHEMKIN Output File of the Final Solution of Laminar Burning Velocity Simulation for CH ₄ /Air	265
Appendix O: CHEMKIN Output File of the Final Solution of Laminar Burning Velocity Simulation for C ₂ H ₆ /Air	266
Appendix P: CHEMKIN Output File of the Final Solution of Laminar Burning Velocity Simulation for C ₃ H ₈ /Air	267
Appendix Q: CHEMKIN Output File of the Final Solution of Laminar Burning Velocity Simulation for H ₂ /Air	268

List of Tables

Table 1.1: The composition of syngas from biomass pyrolysis/gasification system	3
Table 1.2: The composition of syngas produced from coal gasification	4
Table 1.3: The comparison of the physical properties for H ₂ , CH ₄ and C ₃ H ₈	5
Table 5.1: The lift-off heights and lift-off velocities for pure H ₂ flames	79
Table 5.2: The lift-off heights, lift-off velocities and blow-out velocities for H ₂ -CH ₄ flames	80
Table 5.3: The lift-off heights, lift-off velocities and blow-out velocities for H ₂ -C ₂ H ₆ flames	82
Table 5.4: The lift-off height, lift-off velocities and blow-out velocities for H ₂ -C ₃ H ₈ flames	83
Table 5.5: the lift-off heights, lift-off velocities and blow-out velocities for H ₂ -CH ₄ -CO ₂ flames with initial hydrogen flowrate at 20 l/min	85
Table 5.6: The lift-off heights, lift-off velocities and blow-out velocities for H ₂ -CH ₄ -CO ₂ flames with hydrogen flowrate of 40 l/min	86
Table 5.7: The lift-off heights, lift-off velocities and blow-out velocities for H ₂ -CO ₂ flames	90
Table 6.1: The comparison between Gri-Mech 3.0 and Warnatz reaction mechanism for C ₂ H ₆ oxidation	110
Table 6.2: The comparison between Gri-Mech 3.0 and Warnatz reaction mechanism for C ₃ H ₈ oxidation	110
Table 7.1: H ₂ consumption pathway of the oxidation of H ₂ -CH ₄ mixtures	132
Table 7.2: CH ₄ consumption pathway of the oxidation of H ₂ -CH ₄ mixtures	134
Table 7.3: H consumption and generation pathways of the oxidation of H ₂ -CH ₄ mixtures	138
Table 7.4: OH consumption and generation pathways of the oxidation of H ₂ -CH ₄ mixtures	140

Table 7.5: CH consumption and generation pathways of the oxidation of H ₂ -CH ₄ mixtures	142
Table 7.6: C ₂ H ₆ consumption pathways of the oxidation of H ₂ -C ₂ H ₆ mixtures	148
Table 7.7: H formation and consumption pathways of the oxidation of H ₂ -C ₂ H ₆ mixtures	149
Table 7.8: OH formation and consumption pathways of the oxidation of H ₂ -C ₂ H ₆ mixtures	150
Table 7.9: CH formation and consumption pathways of the oxidation of H ₂ -C ₂ H ₆ mixtures	151
Table 7.10: H ₂ consumption pathway of the oxidation of H ₂ -C ₃ H ₈ mixtures	155
Table 7.11: C ₃ H ₈ consumption pathways of the oxidation of H ₂ -C ₃ H ₈ mixtures	156
Table 7.12: H formation and consumption pathways of the oxidation of H ₂ -C ₃ H ₈ mixtures	157
Table 7.13: OH formation and consumption pathways of the oxidation of H ₂ -C ₃ H ₈ mixtures	158
Table 7.14: CH formation and consumption pathways of the oxidation of H ₂ -C ₃ H ₈ mixtures	159
Table 8.1: The reactants and products mol fractions for the Laminar burning velocity calculation of the combustion of CH ₄ -air mixture	167
Table 8.2: The reactants and products mol fractions for the laminar burning velocity calculation of the combustion of C ₂ H ₆ -air mixture	170
Table 8.3 The reactants and products mol fractions for the laminar burning velocity calculation of the combustion of C ₃ H ₈ -air mixture	173
Table 9.1: The physical and thermodynamic properties of H ₂ , CH ₄ , C ₂ H ₆ and C ₃ H ₈ at 1atm and 300 K	196
Table 9.2: The calculations of $C_2 \left(\frac{\bar{\rho}}{\rho}\right)^{1.5} v_e$ based on Kalghatgi's correlation	197

List of Figures

Figure 1.1: The world energy consumption share 2012	2
Figure 2.1: The Schematic illustration of a plane front propagating in an unconfined fuel mixture	11
Figure 2.2: The comparison of the laminar burning velocity data of H ₂ -air mixtures	20
Figure 2.3: The comparison of the laminar burning velocity data of CH ₄ -air mixture	22
Figure 2.4: The effect of hydrogen concentration on the laminar burning velocity of H ₂ -CH ₄ mixture at stoichiometric condition	24
Figure 2.5: The comparison of the laminar burning velocity data of C ₂ H ₆ -air	26
Figure 2.6: The correlation of the laminar burning velocity of H ₂ -C ₂ H ₆ with the hydrogen concentration at equivalence ratio of 1	28
Figure 2.7: The correlation of laminar burning velocity of the flame of hydrogen-ethane-air with the hydrogen concentration in the mixture	27
Figure 2.8: The comparison of the laminar burning velocity data of C ₃ H ₈ -air mixture	31
Figure 2.9: The laminar burning velocity of H ₂ -C ₃ H ₈ over a range of equivalence ratio at 80%, 60%, 40% and 20% hydrogen concentration	31
Figure 2.10: The correlation of laminar burning velocity of H ₂ -C ₃ H ₈ with the hydrogen concentration at equivalence ratio of 1	32
Figure 3.1: Plot of concentration of A with time for zero order reaction	37
Figure 3.2: The concentration of the reactant against time for first order reaction	38
Figure 3.3: The correlation of reactant and product with time for first order reaction	39
Figure 3.4: Plot of 1/[A] with time for second order reaction	39

Figure 3.5: Arrhenius plot, the relation between reactant concentration and temperature	41
Figure 3.6: Arrhenius plot, the relation between reactant concentration and temperature	43
Figure 3.6: The activation energy in collision theory	41
Figure 4.1: Schematic of a lifted jet diffusion flame	63
Figure 4.3: The illustration of premixed flame model	65
Figure 5.1: The rig employed in the flame stability experiment	74
Figure 5.2: The schematic and geometry of the burner used in the experiment	75
Figure 5.3: Schematic of the stability experimental set-up	78
Figure 5.4: the images of lifted pure H ₂ flames	79
Figure 5.5: The flame images for H ₂ -CH ₄ flames at lift-off and blow-out conditions	81
Figure 5.6: The flame images for H ₂ -C ₂ H ₆ flames at lift-off and blow-out conditions	82
Figure 5.7: The flame images for H ₂ -C ₃ H ₈ flames at lift-off and blow-out conditions	84
Figure 5.8: The flame images for H ₂ -CH ₄ -CO ₂ mixtures at lift-off condition, for 20 l/min H ₂ flowrate	88
Figure 5.9: The flame images for H ₂ -CH ₄ -CO ₂ flames at lift-off condition with hydrogen flowrate at 40 l/min	89
Figure 5.10 (a): The flame images for H ₂ - CO ₂ flames at lift-off condition	92
Figure 5.10 (b): The flame images for H ₂ - CO ₂ flames at lift-off condition	93
Figure 5.11: The lift-off height against exit jet velocity for pure H ₂ and H ₂ -hydrocarbon flames	94
Figure 5.12: The flame lift-off height against hydrogen concentration for H ₂ -hydrocarbon flames	95
Figure 5.13: The lift-off velocity against jet velocity for pure H ₂ and H ₂ -CO ₂ flames	96

Figure 5.14: The lift-off height against jet velocity for H ₂ -CH ₄ , H ₂ -C ₂ H ₆ , H ₂ -C ₃ H ₈ and H ₂ -CH ₄ -CO ₂ flames, with initial H ₂ flowrate of 20 l/min	96
Figure 5.15: The lift-off height against jet velocity for H ₂ -CH ₄ , H ₂ -C ₂ H ₆ , H ₂ -C ₃ H ₈ and H ₂ -CH ₄ -CO ₂ flames, with initial H ₂ flowrate of 40 l/min	97
Figure 5.16: The lift-off heights against CH ₄ concentration of H ₂ -CH ₄ -CO ₂ flames for 20 l/min initial H ₂ flowrate	98
Figure 5.17: The lift-off heights against CH ₄ concentration of H ₂ -CH ₄ -CO ₂ flames at 40 l/min initial H ₂ flowrate	99
Figure 5.18: The lift-off jet velocity against the H ₂ concentration for H ₂ -CH ₄ -CO ₂ and H ₂ -hydrocarbon flames	100
Figure 5.19: The blow-out velocity against hydrogen concentration for H ₂ -hydrocarbon and H ₂ -CO ₂ flames	101
Figure 5.20: The blow-out/off velocity against CH ₄ concentration of H ₂ -CH ₄ -CO ₂ flames	103
Figure 6.1: The comparison between Gri-Mech 3.0 and Warnatz reaction mechanisms for the oxidation of H ₂ -CH ₄ mixture of 80%H ₂	108
Figure 6.2: The comparison between Gri-Mech 3.0 and Warnatz reaction mechanisms for the oxidation of H ₂ -CH ₄ mixture of 80%H ₂	108
Figure 6.3: The comparison of the temperature profile between Gri-Mech 3.0 and Warnatz of the combustion of H ₂ -CH ₄ mixture of 80%H ₂ ...	106
Figure 6.4: The change of H ₂ molar fraction over time for H ₂ -CH ₄ reactions, at 2500 K and 1 atm	113
Figure 6.5: The change H ₂ concentration over time for H ₂ -CH ₄ , at 2500 K and 1 atm	113
Figure 6.6: The change of CH ₄ molar fraction over time for H ₂ -CH ₄ reaction, at 2500K and 1 atm	114
Figure 6.7: The CH ₄ concentration over time for H ₂ -CH ₄ reaction, at 2500K and 1 atm	114

Figure 6.8: The OH concentration over time for H ₂ -CH ₄ reaction, at 2500K and 1 atm	116
Figure 6.9: The H concentration over time for H ₂ -CH ₄ reaction, at 2500K and 1 atm	116
Figure 6.10: The Temperature profile of H ₂ -CH ₄ reactions	117
Figure 6.11: The H ₂ concentration over time for H ₂ -C ₂ H ₆ reaction, at 2500K and 1 atm	114
Figure 6.12: The number of mole of H ₂ over time for H ₂ -C ₂ H ₆ reaction, at 2500K and 1 atm	119
Figure 6.13: The C ₂ H ₆ concentration over time for H ₂ -C ₂ H ₆ reaction, at 2500 K and 1 atm	120
Figure 6.14: The number of mole of C ₂ H ₆ over time for H ₂ -C ₂ H ₆ reaction, at 2500 K and 1 atm	121
Figure 6.15: The H concentration over time for H ₂ -C ₂ H ₆ reaction, at 2500 K and 1 atm	122
Figure 6.16: The OH concentration over time for H ₂ -C ₂ H ₆ reaction, at 2500 K and 1 atm	122
Figure 6.17: The Temperature profile of H ₂ -C ₂ H ₆ reactions	123
Figure 6.18: The H ₂ concentration over time for H ₂ -C ₃ H ₈ reaction, at 2500 K and 1 atm	124
Figure 6.19: The C ₃ H ₈ concentration over the time of the reaction of H ₂ -C ₃ H ₈ /air combustion, at 2500 K and 1 atm	125
Figure 6.20: The OH concentration over time for H ₂ -C ₃ H ₈ / reaction, at 2500 K and 1 atm	126
Figure 6.21: The H concentration over time for H ₂ -C ₃ H ₈ reaction, at 2500 K and 1 atm	126
Figure 6.22: The temperature profile for H ₂ -C ₃ H ₈ reactions	127
Figure 7.1: The production paths of C ₂ H and C ₂ H ₂	137
Figure 7.2: The production paths of CHO, CH ₂ O and CH ₃	137
Figure 7.3: The production paths of HCCO	143

Figure 7.4: The main paths for CH ₄ and H ₂ in the oxidation of CH ₄ -H ₂	145
Figure 7.5: The formation and consumption of H and OH in the oxidation of CH ₄ -H ₂	146
Figure 7.6: The main paths for C ₂ H ₆ and H ₂ in the oxidation of C ₂ H ₆ -H ₂	154
Figure 7.7: The main contributors of the formation and consumption of H and OH in the oxidation of C ₂ H ₆ -H ₂	154
Figure 7.8: The main paths for C ₃ H ₈ and H ₂ in the oxidation of C ₃ H ₈ -H ₂	161
Figure 8.1: The temperature and species gradients through a flame front	165
Figure 8.2: The gas temperature above burner for the CH ₄ -air flame	168
Figure 8.3: The axial velocity profile above burner for the CH ₄ -air flame	169
Figure 8.4: The comparison of the laminar burning velocity of CH ₄ -air of current study with previous studies	169
Figure 8.5: The gas temperature above burner for the C ₂ H ₆ -air flame	171
Figure 8.6: The axial velocity profile above burner for the C ₂ H ₆ -Air flame	171
Figure 8.7: The comparison of the laminar burning velocity of C ₂ H ₆ -air of current study with previous studies	172
Figure 8.8: The gas temperature above burner for the C ₃ H ₈ -air flame	173
Figure 8.9: The axial velocity profile above burner for the C ₃ H ₈ -air flame	174
Figure 8.10: The comparison of the laminar burning velocity of C ₃ H ₈ -air of current study with previous studies	175
Figure 8.11: The comparison of the laminar burning velocity of H ₂ -air of current study with previous studies	176
Figure 8.12: The distribution of the molar fraction of H above burner for the flames of H ₂ , CH ₄ , C ₂ H ₆ and C ₃ H ₈ oxidation	177
Figure 8.13: The distribution of the molar fraction of OH above burner for the flames of H ₂ , CH ₄ , C ₂ H ₆ and C ₃ H ₈ oxidation	178
Figure 8.14: The distribution of the molar fraction of CH above burner for the flames of H ₂ , CH ₄ , C ₂ H ₆ and C ₃ H ₈ oxidation	178
Figure 8.15: The distribution of the molar fraction of CH ₃ , C ₂ H ₄ and C ₂ H ₅ radicals above burner for the C ₂ H ₆ -air flame	179

Figure 8.16: The distribution of the molar fraction of CH ₃ , C ₂ H ₄ and C ₂ H ₅ radicals above the burner for the C ₃ H ₈ -air flame	180
Figure 8.17: The distribution of the molar fraction of CH ₃ , C ₂ H ₄ and C ₂ H ₅ radicals above burner for the CH ₄ -air flame	180
Figure 8.18: The laminar burning velocity of CH ₄ -H ₂ , C ₂ H ₆ -H ₂ and C ₃ H ₈ -H ₂ mixtures, at 1 atm and stoichiometric condition	182
Figure 8.19: The comparison of the laminar burning velocity of methane-hydrogen mixture of current study with previous study ..	183
Figure 9.1: The laminar burning velocity ratio of CH ₄ -H ₂ , C ₂ H ₆ -H ₂ and C ₃ H ₈ -H ₂ to pure H ₂ over a range of H ₂ concentration, at 1 atm and stoichiometric condition	186
Figure 9.2: The average reaction rate of CH ₄ , C ₂ H ₆ , C ₃ H ₈ and H ₂ over the time of the combustion reaction of H ₂ -CH ₄ /C ₂ H ₆ C ₃ H ₈ with air, at 2500 K and 1 atm	188
Figure 9.3: The H concentration and H ₂ reaction rate against the H ₂ addition concentration for H ₂ -CH ₄ , H ₂ -C ₂ H ₆ and H ₂ -C ₃ H ₈ mixtures	190
Figure 9.4: The OH concentration and H ₂ reaction rate against the H ₂ addition concentration for H ₂ -CH ₄ , H ₂ -C ₂ H ₆ and H ₂ -C ₃ H ₈ mixtures	190
Figure 9.5: The flame lift-off height and corresponding jet velocity against the laminar burning velocity for H ₂ -CH ₄ , H ₂ -C ₂ H ₆ and H ₂ -C ₃ H ₈ lifted flames	192
Figure 9.6: The correlation between h and U_0/S_L^2 for lifted H ₂ -CH ₄ flames	194
Figure 9.7: The correlation between h and U_0/S_L^2 for lifted H ₂ -C ₂ H ₆ flames	194
Figure 9.8: The correlation between h and U_0/S_L^2 for lifted H ₂ -C ₃ H ₈ flames	195
Figure 9.9: The correlation between h and U_0/S_L^2 for pure H ₂ lifted flames	195
Figure 9.10: The comparison of the laminar burning velocity correlation between Ilbas and current study on Kalghatgi's correlation	199
Figure 9.11: The laminar burning velocity correlation of H ₂ -CH ₄ at stoichiometric condition and H ₂ <60%	200

Figure 9.12: The laminar burning velocity correlation of H ₂ -CH ₄ at stoichiometric condition and H ₂ ≥ 60%	201
Figure 9.13: The laminar burning velocity correlation of H ₂ -C ₂ H ₆ at stoichiometric condition and H ₂ < 60%	201
Figure 9.14: The laminar burning velocity correlation of H ₂ -C ₂ H ₆ at stoichiometric condition and H ₂ ≥ 60%	202
Figure 10.1: Schematic of the setup of the spectral analysis system	208
Figure 10.2: The internal structure of the spectrometer	209
Figure 10.3: The dimensionless plot of lift-off height with laminar burning velocity based on Kalghatgi's correlation	211

Nomenclature

Symbol	Description	SI Units
a_n	coefficients of fits to thermodynamic data	
A	The pre-exponential factor of Arrhenius equation	
A_c	Cross-section area	m^2
[A]	The concentration of species A	mol/m^3
[A_0]	The initial concentration of species A	mol/m^3
b_n	coefficients of fits to thermodynamic data	
[B]	The concentration of species B	mol/m^3
C	Species concentration	mol/m^3
C_p	Specific heat capacity	J/mol K
d_0	Burner inner diameter	m
d_n	coefficients of fits to thermodynamic data	
D_{kn}	Mixture-averaged diffusion coefficient of the k^{th} species	m^2/s
D_{kj}	Binary diffusion coefficient	m^2/s
Ea	Activation energy	J/mol
F	Flowrate of gas mixture	m^3/s
h	Flame lift-off height	m
H	Specific enthalpy	J/kg
H_h	Dimensionless height	
ΔH	Heat of formation	J/mol

H^0	Standard state molar enthalpy	J/mol
Subscript i	The i^{th} reaction	
k	Rate constant	Depending on reaction order
Subscript k	The k^{th} species	-
k_f	Forward rate constant	Depending on reaction order
k_r	Reverse rate constant	Depending on reaction order
K_c	The Equilibrium constant in concentration units	Depending on reaction
K_p	The Equilibrium constant in pressure units	Depending on reaction
k_s	Flame stretch factor	s^{-1}
L	Markstein length	m
m	Mass	kg
M	Molecular weight	kg/mol
\dot{M}	Mass flow rate	kg/s
Subscript n	The number of coefficients in polynomial fits	
n	The temperature independent constant in modified Arrhenius equation	
P_{atm}	Pressure of one standard atmosphere	Pa
q	Rate of production	$\text{mol/m}^3 \text{ s}$
r	Rate of reaction	$\text{mol/m}^3 \text{ s}$
R	The gas constant	J/mol K
Re_t	Turbulent Reynolds number	

Re_H	Reynolds number based on dimensionless height	
S^0	Standard state molar entropy	J/mol K
S_L	Laminar burning velocity	m/s
S_{Lf}	Flame propagation rate relative to the unburned gas	m/s
S_{L0}	Laminar burning velocity at unstretched condition	m/s
S_t	The velocity corrected from laminar burning velocity depending on the turbulence level	m/s
S_T	Total turbulent burning velocity	m/s
t	time	s
T	Temperature	K
u	Velocity of the fluid mixture	m/s
u'_{rms}	The root mean square fluctuations of turbulent velocity	m/s
U_g	Inlet gas velocity	m/s
U_0	Inlet jet velocity	m/s
U_b	Blow-out velocity	m/s
ν	The stoichiometric coefficient	
ν_D	Ordinary diffusion velocity	m/s
V	Diffusion velocity	m/s
V_f	Volumetric flowrate	m ³ /s
w	Thermal diffusion velocity	m/s
W	Molecular weight	kg/mol
\bar{W}	Mean molecular weight	kg/mol

X	Mole concentration	mol/m^3
Y	Mass fraction	
Y_0	Mass fraction at burner exit	
Y_{ST}	The stoichiometric mass fraction	
ε_{in}	Inlet reactant fraction of a species	
η	Dynamic viscosity	Pa s
θ	Thermal diffusion ratio	
λ	Thermal conductivity	J/m s K
μ	Dynamic viscosity	kg/m s
ν_e	Kinematic viscosity	m^2/s
ρ	Density	kg/m^3
$\frac{\rho}{\rho_0}$	Density ratio of the density of the gas at the jet exit to the density of the ambient air	
ρ_e	Density of the gas at the jet exit	kg/m^3
ρ_∞	Density of the ambient air	kg/m^3
Ψ	The stoichiometric air to fuel ratio	
\mathcal{D}	Diffusivity	m^2/s
$\dot{\omega}_k$	Molar rate of production	$\text{mol/m}^3 \text{ s}$

Chapter 1

Introduction

1.1 Background

As the consumption of fossil fuels such as coal, oil and natural gas, keeps increase over the last few decades, the global resource of the fossil fuels face immense pressure to meet the demand of the energy sources for power generation, heating/cooling and transport. As reported in the study conducted by Yeh et. al (2012), there was a increase in the consumption of coal, oil and gas in 1990 to 2007 and the consumption of the fossil fuels was expected to continue increase worldwide. Bilgen (2014) indicated that there was a 5% increase in the consumption of natural gas for energy generation in 2011 to 2012. However, the consumption of petroleum and other liquid fuels reduced from 36.56 quadrillion Btu in 2011 to 35.87 quadrillion Btu in 2012 and the consumption of coal decreased from 19.62 to 17.34 quadrillion Btu. However, the use of fossil fuels for energy production is still far higher than the utilisation of renewable energy sources. As shown in Figure 1.1, the world energy consumption through renewable fuels only accounted for 19%. This value was far lower than the 78.4% of the fossil fuels. The utilisation of renewable energy sources to replace fossil fuels is still facing some technical and economic issues.

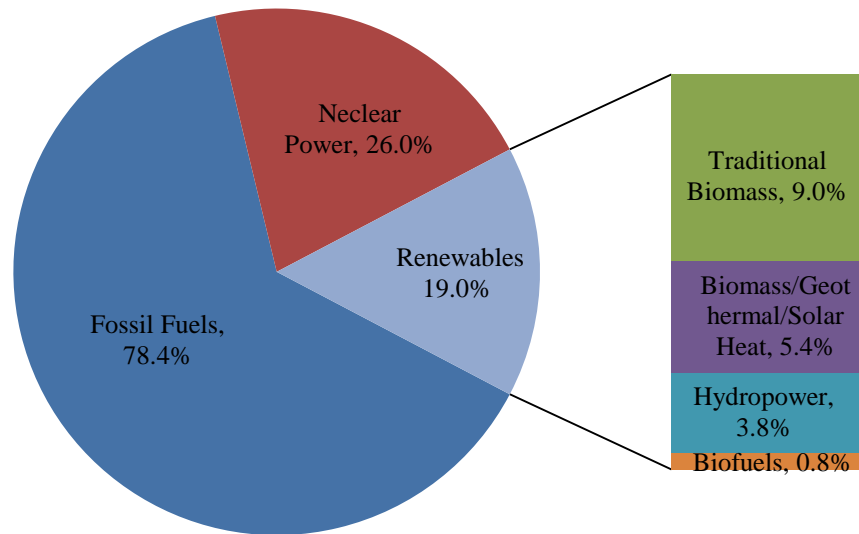


Figure 1.1: The world energy consumption share 2012 (REN21, 2014)

Apart from the exhaustion of the fossil fuels reserve, one of the main issues of utilising fossil fuel for energy generation and transport is the CO₂ emission. CO₂ is the main contributor of the green house effect which results in global warming. CO₂ are counted for more than half of the composition of the green house gases (Nicoletti et al., 2014; Nicoletti et al., 2009; Report Kyoto Protocol, 2009). The combustion of fossil fuels is the major source to produce CO₂ emission. Approximately 73% of the CO₂ originates from the combustion of fossil fuels (Nicoletti et al., 2014; Bruzzi, L., 2007; Weimer, T., 1997). It was also estimated by Meng and Niu (2011) that the CO₂ produced from the combustion of fossil fuels accounts for approximate 60% of the total global CO₂ emitted. Therefore, it is very important to reduce the CO₂ emission in combustion technology, and to use alternative fuels to reduce the strain from the consumption of fossil fuels.

In order to reduce carbon emission, recently, biomass is used as an alternative fuel

to replace some of the conventional fossil fuels. The biomass pyrolysis and gasification process can be employed to convert biomass into hydrogen based syngas. The components of syngas mainly include H₂, CO, CO₂, CH₄ and other hydrocarbons. The composition of syngas depends on the biomass properties and gasifier operating conditions (Chhiti and Kemiha 2013). A syngas composition from a fixed bed biomass gasification system is given in Table 1.1.

Table 1.1: The composition of syngas from biomass pyrolysis/gasification system

Component	Concentration vol.%
CO	25
H ₂	40
CO ₂	24
CH ₄	8-9
C ₂ -C ₄	2

(Olaleye et al., 2014)

Biomass also can be applied in fermentation process, in which macromolecule, such as carbohydrates, fats and proteins are initially converted into organic acids and alcohols, and then ultimately to methane and CO₂ based biogas (Methling et al., 2014). Usually, the main component of biogas is methane, over 50%, and CO₂, approximately 40% (Herout, 2011).

It has been shown that coal gasification technology can be used to produce H₂ with CO₂ capturing (Herdem et al., 2014; Chiesa et al., 2005; Williams et al., 2005). Approximately 19% of hydrogen production is contributed by coal gasification process (Stiegel and Ramezan, 2006). The coal gasification process basically includes pyrolysis and gasification processes. These processes take place simultaneously to form syngas mainly consisting of H₂, CO₂, CO and CH₄. The composition of syngas can vary significantly due to the process parameters and the feedstock properties. Table 1.2 shows a typical syngas composition from coal

gasification process.

Table 1.2: The composition of syngas produced from coal gasification

Component	Concentration %
CO	30-60
H ₂	25-30
CO ₂	5-15
CH ₄	0-5

The steam reforming of natural gas is widely used as a method to produce hydrogen. It was indicated that 95% of hydrogen production rises from the steam reforming of natural gas (Silva and Muller, 2011; Anderson et al., 2014). The conventional steam methane reforming process consists of syngas production through steam reforming and water gas shift reaction. The overall reaction is to form hydrogen enriched syngas with CO, CO₂ and methane. Advanced steam reforming of combustion engines process allows high content of methane and hydrogen in the gas production.

It has been demonstrated that syngas, containing H₂, CO₂ and hydrocarbons, can be produced from many processes as products or by-products. The hydrogen-hydrocarbon based syngas can be utilised in the gas turbine in Combined Heat and Power system (CHP) or in a Combined Cycles gas turbine (CCGT) (Chacartegui et al., 2013; Cormos et al., 2009). Furthermore, there is substantial interest in the use of hydrogen/hydrocarbon synthesised gas as an alternative fuel in combustion processes for advanced performance and extended flammability limits, and to use hydrogen addition to aid the combustion of hydrocarbon fuels. Hydrogen has very different physical properties from conventional hydrocarbons. As shown in the Table 1.3, hydrogen has advantages

upon the higher value in burning velocity, heat of combustion, gaseous detonation sensitivity, energy density by weight. H₂ also have wider flammability limits and lower ignition energy.

Table 1.3: The comparison of the physical properties for H₂, CH₄ and C₃H₈

Physical Properties	H ₂	CH ₄	C ₃ H ₈
Specific gravity relative to air at NTP	0.07	0.55	1.52
Density of gas at NTP (kg/m ³)	0.089	0.668	1.882
Diffusion coefficients in air at NTP (cm ² /s)	0.61	0.16	0.1
Limits of flammability (vol. %)	4.0-75.0	5.3-15.0	2.1-10.4
Minimum energy for ignition in air (mJ)	0.02	0.29	0.305
Maximum burning velocity (cm/s)	270-350	32-44	40-52
Heat of combustion (MJ/kg)	143	51.9	50.4
Heat of combustoin (MJ/m ³)	10.8	37.8	49600

The change of the composition of the gaseous mixture results in the challenges to predict the physical properties of the mixture. To utilise syngas and biogas, which are mixtures of H₂, hydrocarbons (C₁-C₄), CO and CO₂, the main issues in combustion of the mixtures are the H₂ content fluctuation in the mixtures and its effect on the flame burning velocity and flame stability. The difference in the burning velocity, transport properties and heat capacity between hydrogen and hydrocarbons causes the combustion in the gas turbine strongly depends on the composition of the syngas fuel. In terms of safely handling, when there is a fluctuation in the hydrogen concentration, the flame can become unstable due to suddenly increased or decreased laminar burning velocity. The effect of short self-ignition delay and high burning velocity of hydrogen causes unacceptable risk of flame propagation. This upstream flam propagation can cause flash back in combustion chamber and burner. The reduction in the laminar burning velocity of the mixture also can cause flame blow-out.

At the moment, there is very limited data on the burning velocity and flame stability of syngas and biogas mixtures. There is no reliable correlation to predict the burning velocity and flame stability of the mixtures. The safe usage of such gaseous mixture needs more precisely interpretations on the reaction kinetics and flame stability mechanism for such gaseous mixtures, which however is not well understood. Therefore, the objective of this PhD thesis is to establish the effect of hydrogen concentration on the laminar burning velocity and flame stability of H₂-hydrocarbon-CO₂ mixtures. Laminar burning velocity and flame stability are important for design and safely handling of the combustion systems that use syngas and biogas. It is desirable to develop a numerical correlation between hydrogen concentration and the laminar burning velocity and flame stability parameters for such gas mixtures.

1.2 The Approach and Objectives of the Research

1.2.1 Research Approach

The research is conducted by combining experimental study and computational modelling. The syngas and biogas are represented by using a mixture of H₂, CH₄, C₂H₆, C₃H₈ and CO₂. A flame stability experiment rig with 2mm diameter burner is employed to produce jet diffusion flames to measure the flame stability parameters of the mixtures. A digital camera was used to capture the flame images, and to determine flame lift-off height and guide the calculations of flame lift-off and blow-out velocities.

The combustion kinetics modelling and analysis are used to determine the reaction rates and reaction pathways for some key components such as H₂, H, OH, CH₄, C₂H₆ and C₃H₈, and also to calculate the laminar burning velocity of the H₂-hydrocarbon mixtures. The numerically determined burning velocities and reaction pathways are used to analyse and carry out data treatment of the

experimentally measured flame lift-off and blow-out parameters.

1.2.2 Objectives

This study is aimed at determining the effect of hydrogen concentration in hydrogen enriched hydrocarbon and CO₂ mixtures on the flame laminar burning velocity and the flame lift-off and blow-out stability.

The objectives of the study are to:

1. Carry out experimental tests systematically to measure the flame lift-off and blow-out stability parameters for or H₂-CH₄, H₂-C₂H₆, H₂-C₃H₈, H₂-CO₂ and H₂-CH₄-CO₂ flames.
2. Determine the effects of H₂ and CO₂ addition on the flame lift-off and blow-out characteristics.
3. Determine suitable chemical kinetics reaction mechanisms for the numerical modelling of chemical reactions hydrogen-hydrocarbon gaseous mixtures.
4. Carry out kinetic modelling to determine the effect of hydrogen concentration on the reaction kinetics and reaction pathways of the main components, such as H, OH and C₁-C₃, of the H₂-CH₄, H₂-C₂H₆ and H₂-C₃H₈ mixtures.
5. Calculate the laminar burning velocity of H₂-CH₄, H₂-C₂H₆ and H₂-C₃H₈ mixtures over a large range of H₂ concentration through numerical modelling.
6. Establish a correlation between the effect of H₂ concentration on the laminar burning velocity and flame stability parameters for the hydrogen-hydrocarbon gaseous mixtures.
7. Apply the kinetics analysis and the burning velocity correlation in the analysis and data treatment of flame lift-off and blow-out stability parameters.

1.3 Layout of the Thesis

Chapter 2 presents a literature review on experimental and numerical methods of measuring laminar burning velocity. The experimental programme and numerical

governing equations are introduced. The challenges upon measuring laminar burning velocity are also included in this chapter. The data concerning the laminar burning velocity of H₂, CH₄, C₂H₆ and C₃H₈ collected from previous studies is also presented in this chapter.

Chapter 3 includes the basic theories of reaction kinetics and reaction mechanisms. It also presents the literature review on the reaction mechanism of H₂ and hydrocarbon oxidation.

Chapter 4 firstly gives the definitions of the flame stability parameters, lift-off height, lift-off velocity, blow-out/off velocity and flash back. It then introduces three flame stability models describing the flame lift-off and blow-out theories. A literature review of the flame stability parameters of H₂ and hydrocarbons is given in last section of the chapter.

Chapter 5 presents the experimental programme rig of a gas preparing system and a burner to produce jet diffusion flames. The experimental results concerning flame lift-off height, lift-off velocity and blow-out velocity are given along with corresponding flame images. The discussion section presents the correlation between H₂ concentration and flame lift-off and blow-out characteristics. The results demonstrate the effect of H₂ and CO₂ addition on the flame stability of H₂-hydrocarbon-CO₂ mixtures.

The numerical modelling of species concentrations and reaction rates is presented in Chapter 6. The reaction rates and concentrations of H, OH, CH, CH₄, C₂H₆ and C₃H₈ of H₂-hydrocarbon mixtures are shown in this chapter. The discussions correlate the H₂ concentration with the species concentrations and reaction rates.

Chapter 7 concerns the species pathway analysis. It illustrates the consumption and production paths of H, OH, CH, CH₄, C₂H₆ and C₃H₈ of H₂-hydrocarbon

mixtures. It also discusses the differences of CH₄-H₂ oxidation pathways from C₂H₆-H₂ and C₃H₈-H₂.

Chapter 8 shows the results from computational modelling of the laminar burning velocity of CH₄-H₂, C₂H₆-H₂ and C₃H₈-H₂ mixtures. It discusses the effect of H₂ concentration on the laminar burning velocity of the mixtures.

Chapter 9 presents the correlation of the experimentally measured flame stability parameters with the numerically simulated laminar burning velocity data. The results from the species pathway analysis and reaction kinetics modelling are used to explain the effect of H₂ concentration on flame burning velocity. Finally, the conclusions are given in Chapter 10.

Chapter 2

Literature Review of the Laminar Burning Velocity of Hydrogen-Hydrocarbon Gaseous Mixtures

Laminar burning velocity is an important parameter of a gaseous fuel and directly determined by the reactivity of the gaseous mixture. This chapter firstly gives the definition of the laminar burning velocity and the factors influencing its value. A literature review of the experimental and numerical modelling methods to determine the value of the burning velocity is presented. The values of the laminar burning velocity of H₂, CH₄, C₂H₆, C₃H₈, H₂-CH₄, H₂-C₂H₆ and H₂-C₃H₈ gaseous mixtures are collected through the literature review and presented in this chapter.

2.1 The Definition of the Laminar Burning Velocity

Burning velocity is the physicochemical constant for a specified combustible gaseous mixture (Andrews and Bradley, 1972). Lewis and von Elbe (1951) defined the laminar burning velocity as the velocity with which a plane of flame front moves normal to its surface through the adjacent unburnt gas. Figure 2.1 shows a typical model of describing the laminar burning velocity. As shown in Figure 2.1, a plane of flame front moves to the unburned gas and S_L indicates the laminar burning velocity of the flame. The laminar burning velocity of the flame can be expressed as:

$$S_L = \left(\frac{1}{A_c \rho} \right) \left(\frac{dm}{dt} \right) \tag{Eq.2-1}$$

Where A_c is the cross section area of the tube (flame front), ρ is the density of the unburned gas adjacent to the flame front and $\frac{dm}{dt}$ represents the mass flow rate of the unburned gas into the flame front (Rallis and Garforth, 1980).

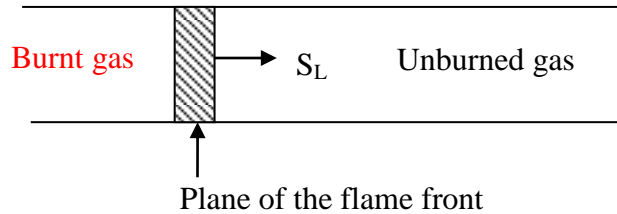


Figure 2.1: The Schematic illustration of a plane front propagating in an unconfined fuel mixture

As the laminar burning velocity is defined as the relative velocity with respect to the unburned gas, when the flame front remains as stationary the laminar burning velocity equals to the unburned gas velocity immediately adjacent to the flame front. The laminar burning velocity is an intrinsic property for a specific combustible mixture. However, flame stretch, turbulent flow and the expansion due to pressure built up on burned gaseous products have impact on accurate prediction of the laminar burning velocity. Markstein (1964) proposed a relationship representing the effect of flame stretch rate on laminar burning velocity, as shown below:

$$S_{L_f} = S_{L_0} - Lk_s \quad \text{Eq.2-2}$$

Where S_{L_f} is the flame propagation rate relative to the unburned gas, S_{L_0} is the laminar flame speed at the unstretched condition, k_s is the flame stretch factor and L is the Markstein length (Kuo, 2005). Kwon et al. (1992) showed that the Markstein length is proportional to the characteristic flame thickness. Tseng et al. (1993) conducted an experimental study on the effect of flame stretch on the laminar burning velocities of hydrocarbon-air flames. A windowed test chamber

developed by Groff (1982) was used to produce an outward-propagating spherical flame with the reactants at 298 K and 1 atm. Their study showed significant effect of flame stretch on typical laboratory measurement of the laminar burning velocity and practical turbulent premixed flames. In addition, Markstein numbers varied linearly with fuel-equivalence ratio.

Differentiating from the laminar burning velocity, turbulent burning velocity is used when the effect of turbulent on combustion can not be ignored. The flame can be considered as a wrinkled laminar flame with turbulence taken into account. Karlovitz et al. (1951) conducted experimental studies to determine the turbulent burning velocity. They corrected turbulent burning velocity from the laminar burning velocity as shown below:

$$S_T = S_L + S_t \quad \text{Eq.2-3}$$

$$\begin{aligned} S_t &= (2S_L u'_{rms})^{1/2}, & \text{strong turbulence} \\ S_t &= (2S_L u'_{rms})^{1/2} (1 - S_L / u'_{rms}) (1 - \exp(-u'_{rms} / S_L))^{1/2}, & \text{int ermediate turbulence} \\ S_t &= u'_{rms}, & \text{very weak turbulence} \end{aligned}$$

Eq.2-4

Where S_T is the total turbulent burning velocity, S_L is the laminar burning velocity and S_t is the velocity corrected from laminar burning velocity depending on the turbulence level, and u'_{rms} is root mean square fluctuations of turbulent velocity (Kuo and Acharya, 2012).

2.2 The Experimental Methods

The experimental methods of determining the laminar burning velocity has been developed for many decades. However, there still are some challenges in these

methods. The experimental methods can be classified by stationary flames and propagating flames.

2.2.1 Stationary Flames

Generally, the measurement of the laminar burning velocity using stationary flames is achieved by introducing a premixed combustible gaseous mixture to enter a stationary flame front as laminar flow. The velocity of gaseous flow equals to the laminar burning velocity (Rallis and Garforth, 1980). However, the stationary flame front is unstable, so that it is difficult to ensure the flame front is an ideal plane. Usually, the flame front in such method is distorted to some extent.

The early studies (Gaydon and Wolfarrd, 1953; Linnett, 1953; Lewis and Elbe, 1961; Andrew and Bradley, 1972) used burner method to obtain the data of the laminar burning velocity. In these studies, a range of burners had been used including circular tube, shaped nozzle and rectangular slot. Basically, these studies established the laminar flow in the vertical tube, at the top end of which the flame was held as stationary by the up forward moving combustible gas flow. Thus, at the point on the flame front surface, the laminar burning velocity equals to the normal component of the gas velocity at the point. The average burning velocity over the flame front cone can be calculated from the mass continuity equation. Lewis and von Elbe (1961) and Levy and Weinberg (1959) added particle tracking technology into burner method to measure both of the velocity and the direction of the containing stream tube. This approach allowed them to demonstrate that the flame velocity was constant over most of the flame front. In addition, some studies (Klaukens and Wolfhard, 1948; Andrew and Bradley, 1972) used the Schlieren photography system to observe the flow above the burner nozzle. Guntrher and Janisch (1972) used a Mache-Hebra nozzle burner, managing to produce uniform velocity profile at the centre of the flow, with particle tracking photography technology to measure the laminar burning velocity of H₂-air and CH₄-air flames. The results showed that the laminar burning velocity of H₂-air

was about 280 cm/s at equivalence ratio of 1, and of CH₄-air was about 42 cm/s at the equivalence ratio of 1. The maximum laminar burning velocity of H₂-air was just above 350 cm/s at the equivalence ratio of approximately 1.6. They suggested that the surrounding air flowing into the flame cone near the burner rim affects the accuracy of the measurement. Their study was compared by Liu and MacFarlane (1983), in which a constant velocity Mache-Hebra nozzle burner was applied to produce a conical flame and both laser-Doppler velocimetry and Schlieren photography are used to determine the local velocity and the flame angle. Their results agreed well with Guntrher and Janisch (1972). Pareja et al. (2010) also used particle tracking velocimetry and Schlieren photography technology to measure the laminar burning velocity of H₂-air premixed flame. They employed a small burner with a contoured slot type nozzle to reduce the effects of flame stretch and flame curvature. The design of the nozzle was expected to supply nearly uniform exit velocity profile. The results were compared with the previous studies (Guntrher and Janisch, 1972; Liu and MacFarlane, 1983; Wu and Law, 1985) that also used burner method. The laminar burning velocity of H₂-air flame obtained by Pareja (2010) was 237 cm/s at the equivalence ratio of 1 and the maximum value was about 310 cm/s at the equivalence ratio of 1.6. These values are lower than the conventional angle method. The result was also compared with computational modelling using Gri-Mech 3.0 and the mechanism developed by Mueller et al. (1999). The experimental results are well agreed with the computational simulation when the equivalence ratio is lower than 1. However, there are some disadvantages for employing the burner method. The burning velocity profile over the flame surface is not uniform enough in the region between the flame tip and the burner rim. The unstable flame front thickness and the curvature of the flame cone also have impact on the accuracy of the result.

Cylindrical burner tube with flat flame was also conducted by some studies (Powling, 1961; Levy and Weinberg, 1959; Botha and Spalding, 1954; Dixon-Lewis and Wilson, 1967; Edmondson and Heap, 1970). In which Powling

(1961) provided a close approximation to one-dimensional flat flame, however, it was limited to low burning velocity (< 20 cm/s). In his method, the inlet premixed combustible gaseous mixture was introduced into a cylindrical burner tube and went through tube matrix, glass bead packing, glass bead packing, fine diffusion screens and channels matrix. This design was managed to eliminate the turbulent effect. The flame was resulted as a flat disk above the burner associated with a wire gauze. The laminar burning velocity was calculated from dividing the volumetric flow rate of the mixture into the area of the disk. Kumar and Meyer (2013) used a stainless steel tube burner and CCD camera to produce and capture the flame image. The flame surface area was calculated from the image analysis. The results were compared with computational simulation using Gri-Mech 3.0. They concluded that the configuration underestimated the adiabatic flame burning velocity by 25-30% at high equivalence ratio due to the effect of heat losses. However, both of the unburned gas escaped from the flame edge and the heat loss of the flame caused less accurate value of the laminar burning velocity.

2.2.2 Propagation Flames

The propagation flame methods usually used cylindrical tubes, soap bubble and constant volume spherical vessel. The vessel is filled with homogeneous combustible gaseous mixture and the ignition starts from the inside of the vessel to produce flame propagation. The laminar burning velocity is determined through the movement of the flame front surface between the mixture and its surroundings (Rallis and Garforth, 1980).

The adaption of the conventional cylindrical tube methods was implemented by Fuller et al. (1969). They used double igniting method to produce a double flame kernel associated with flat flame front. This increased the accuracy upon determining the area of the flame front. However, the effect of the wall interaction caused the accuracy of this method was not reliable enough.

A relatively popular method is the spherical constant-volume vessel method. This technology has been used by many studies (O'Donovan and Rallis, 1959; Raezer and Olsen, 1962; Rallies and Tremeer, 1963; Rallis et al., 1965; Garforth, 1974; Garforth and Rallis, 1975). The initial development of the method for determining laminar burning velocity was by Lewis and Elbe. In this method, the combustible mixture was contained in the closed spherical vessel and ignited at the centre. The change of the flame front position was associated with the changes in pressure and temperature. Dowdy et al. (1990) used expanding spherical flame technique, associated with high-speed schlieren cine-photography system, to measure the burning velocity of H₂-air mixtures, in which flames were produced in a spherical bomb with central ignition and the front propagation was captured by high-speed cine-photography image system. The experiment was conducted at 296 K and 1 atm. The result showed that the laminar burning velocity of H₂-air mixture was about 210 cm/s at equivalence ratio of 1 and 285 cm/s at equivalence ratio of 1.4. Aung et al. (1998) employed spherical windowed chamber to test the effect of N₂ dilution and flame stretch on the laminar burning velocity of H₂-O₂-N₂ mixture. The gaseous mixture was ignited at the centre of the vessel. The initial pressure was in the range of 0.35-4 atm while the initial temperature was at 298 K. Their results showed that the laminar burning velocity of H₂-air was about 200 cm/s at 1 atm and equivalence ratio of 1. This value was corrected from flame stretch and a bit lower than the computational prediction by using Gri-Mech 3.0. They pointed out that the flame stretch had significant effect on the laboratory measurements of the laminar burning velocity and the other properties of turbulent premixed flames. The same apparatus were employed by Kwon and Faeth (2001) who showed the effect of flame stretch interactions could be correlated based on the Markstein numbers for given reactant conditions and the effect of flame stretch on the laminar burning velocity was substantial. The bomb used by Tse et al. (2000) consisted of an inner cylindrical vessel and an outer chamber. Two Quartz windows were set at both sides. The flame propagation was started from the centre of the inner vessel through spark discharge. The movement of the flame

was observed by applying Schlieren cinematography system. The laminar burning velocities of H₂-air mixtures evaluated by them were lower than the data developed by Aung et al. (1998) and Kwon and Faeth (2001) when the equivalence ratio was smaller than 1.5. As illustrated in Pareja et al. (2010), the results from Burner method were greater than the data obtained from the Bomb method. However, same as Burner method there are some restrictions related to spherical constant volume vessel method. The complexity of the flame front, the non-uniformity of the pressure, the curvature of the flame front and heat loss all have impact on the accuracy of the determination of the laminar burning velocity.

2.3 Numerical Modelling Methods

Essentially, the laminar burning velocity is only meaningful when it is related to a planar flame front occurred in one-dimensional flow system (Dixon-Lewis and Islam, 1982). The measured data is frequently curved and not in one-dimensional flow system. Some studies (Sarli and Benedetto, 2007; Smooke, 2013) have demonstrated through the application of CHEMKIN package to numerically simulate the one-dimensional laminar flame burning velocity. Kee et al. (1998) introduced the programme of employing the PREMIX programme in conjunction with CHEMKIN for numerically modelling the laminar burning velocity for one-dimensional flames. A detailed description of the governing equations, mixture-averaged transport properties equations is given in Chapter 3.

Smooke (2013) proposed a study that introduced the method of computationally modelling of the laminar flames. The study introduced a spatial (3-D) numerical model and one-dimensional premixed flame model for flame propagation. However, if the flame was adiabatic with neglecting viscous effects, body forces, radiation heat transfer and the diffusion of heat resulting from concentration gradients, the 3-dimensional governing equations were simplified to ordinary differential equations for one-dimensional isobaric flame. The application of the

governing equations was to predict the species fractions and temperature profile as the function of the independent distance above the burner (Smooke, 2013). The governing equations are introduced in Chapter 3. The specific heat, enthalpies dynamic viscosity, the thermal conductivity, and the mixture-averaged diffusion coefficients required in the governing equations are provided by the thermodynamic and transport coefficients. Spalding (1956) solved the governing equations of the adiabatic problem by considering the model as a relaxation of a time dependent system, in which the initial concentration and temperature profile of the gaseous mixture was assumed and the standard finite difference technique was applied. The assumption of the temperature distribution over the distance, x , above the burner gives the temperature, T , in the energy equations is expressed as $T(x)$. Smooke (2013) introduced the Newton's steady state solution algorithm employed in various software packages including CHEMKIN. The governing equations were solved by adaptive finite difference method.

The computational simulations of the hybrid flames have been implemented by many studies (Sarli and Di Benedetto, 2007; Sher and Refael, 1988; Refael and Sher, 1989; Kuniishi and Fukutani, 1992; Gauducheau et al., 1998; Kee et al., 1985). Most of the studies used CHEMKIN in which the detailed kinetic reaction mechanism is given. Sarli and Di Benedetto (2007) applied the one-dimensional freely propagating premixed flame model to numerically predict the laminar burning velocity of hydrogen-methane-air flames. In his study, the flames were assumed to be one-dimensional unstretched laminar flame with planar flame front, adiabatic and steady conditions. The Gri-Mech 3.0, which is discussed in Chapter 3 and shown in Appendix E, was employed as the reaction mechanism in the modelling. Their study used the same governing equations and the mixture-averaged formulas as described by Smooke (2013). The inlet temperature was set at 300 K and the pressure was constant at 1 atm. The location of the flame was fixed at the point at which the temperature reaching 400 K. The continuity equation was then solved to give the laminar burning velocity. For the equivalence

ratio of 1, at 30% hydrogen the S_L of the mixture was near 50 cm/s; at 60% hydrogen, the S_L was near 90 cm/s; at 90% hydrogen the value of S_L was about 150 cm/s. The laminar burning velocity of stoichiometric CH_4 -air was 37-38 cm/s, which was given by Dixon-Lewis and Islam (1982). The laminar burning velocity of H_2 -air modelled by CHEMKIN with using Gri-Mech 3.0 given in Pareja (2010) showed that the maximum value was about 280 cm/s and the stoichiometric value was about 200 cm/s.

2.4 The Laminar Burning Velocity of H_2 -Air

The laminar burning velocity of H_2 -air was measured from many previous studies. (eg. Lamoureux et al., 2003; Liu et al., 1983; Ilbas et al., 2006; Milton 1984), and numerically simulated by some studies (eg. Williams and Grcar, 2009). The value of the maximum laminar burning velocity of hydrogen-air mixture in varied from approximately 250cm/s to 350 cm/s. The variation of the values is mainly caused by if the flame expansion was taken into account.

A comparison of the values of the laminar burning velocity of H_2 -air of previous studies is shown in Figure 2.2. These studies have performed the measurements of laminar burning velocity of hydrogen/air combustion at atmospheric pressure and 293 K. It can be seen from the Figure 2.2 that the laminar burning velocities from these measurements are over a wide range of equivalence ratio. The previous studies have shown that the laminar burning velocity of hydrogen-air flames varies from 210-280 cm/s at the equivalence ratio of 1. The maximum values vary from 290 cm/s to just above 350 cm/s, at the equivalence ratio of 1.6.

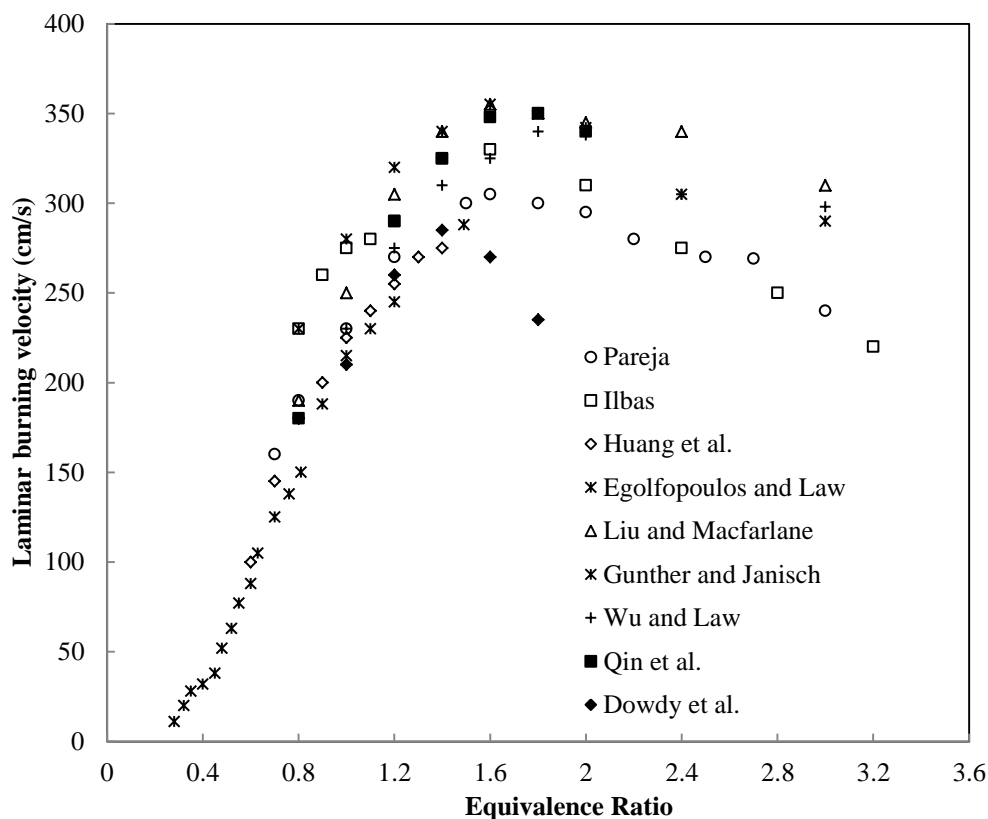


Figure 2.2: The comparison of the laminar burning velocity data of H₂-air mixtures

2.5 The Laminar Burning velocity of CH₄-Air and H₂-CH₄

CH₄-Air

Experimental study of laminar burning velocity of methane-air mixtures was conducted by Ulinski et al. (1998). The results showed the laminar burning velocity for methane-air gaseous mixtures in a certain pressure and temperature range, 1.0-3.0 atm, 298-500 K, by using constant volume combustion vessel. Their study represented the laminar burning velocities of methane-air-diluents mixtures for the equivalence ratio of 0.65-1.1 and 0-10 % diluents. The results from the experiments were compared with previous studies (Agrawal, 1981; Egolfopoulos et al., 1989; Van Oostendorp and Levinsky, 1990). This study indicated that the maximum laminar burning velocity of methane-air mixture is

0.35 m/s at fuel/air equivalence ratio of about 1.03. From the previous studies mentioned in Ulinski's study, it can be realised that the maximum laminar burning velocity of methane-air mixture are in the range of 37 to 43 cm/s, and at the equivalence of 1.0.

A more detailed measurement of laminar burning velocity of methane-air mixture using a Slot and Bunsen burner was conducted by Buffam et al. (2008). Their study used two different experimental methods, and the flame angle and flame area were estimated by using a digital camera. The influence of flame stretch was considered in their study. It was indicated that the maximum burning velocity of methane-air mixture is 0.35 m/s which agrees with the experimental study conducted by Ulinski et al. (1998). The result was from the experiment using slot burner. The maximum burning velocity of 0.35m/s appears at the equivalence ratio of 1.1. The paper also introduced Lewis' study to indicate the relationship between equivalence ratio and burning velocity.

A comparison of the laminar burning velocity data of CH₄-air from different studies is listed in Figure 2.3. In Lewis's bell-shaped correlation between burning velocity and equivalence ratio, the maximum laminar burning velocity for methane-air mixture is 44 cm/s at the equivalence ratio of 1. There are also many other studies which have published the data of laminar burning velocity of methane-air combustion over a range of equivalence ratio at 1 atm. (Yu et al., 1986; Egolfopoulos et al., 1991; Serrano et al., 2008; Uykur et al., 2001) By considering with other studies on the laminar burning velocity of methane-air mixtures, it has been realised that the laminar burning velocity for methane-air mixtures is in the range of 32-44 cm/s at the equivalence ratio of approximately 1.

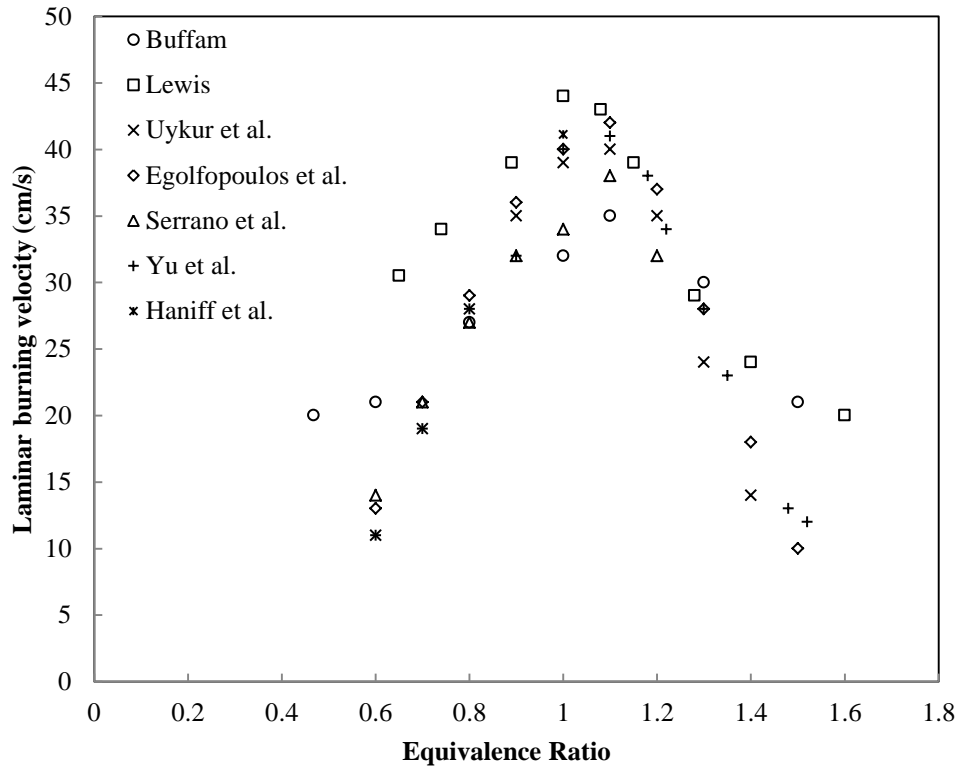


Figure 2.3: The comparison of the laminar burning velocity data of CH₄-air mixture

H₂-CH₄ Mixture

The studies (eg. Di Sarli and Benedetto, 2007; Wu et al., 2009) focused on the combustion characteristics of hydrogen-hydrocarbon mixtures have highlighted the effects of hydrogen addition on combustion characteristics of hydrocarbons. As hydrogen has been appearing its advantages in combustion, the combustion characteristics of hydrogen-methane mixtures have been studied by many researchers. Some of the studies show the combustion characteristics of hydrogen-methane fuels and illustrate the effect of hydrogen concentration on the burning velocity of methane.

The paper, concerning the measurements of laminar burning velocities for natural gas-hydrogen-air mixtures, published by Huang et al. (2006) introduced their study on natural gas-hydrogen-air mixture. The experimental apparatus was

similar to most previous studies, which used a constant volume bomb. The ranges of volume fraction (0-100%) and equivalence ratio (0.6-1.4) used in this study was wider compared with previous studies. The influence of stretch rate on flame was also analysed in this study. It indicated that the maximum unstretched laminar burning velocity for natural gas-hydrogen-air mixture is about 270 cm/s. From this study, it can be realised that the addition of hydrogen into methane can result in a dramatic increase in the laminar burning velocity. The study also considered the relationship between the laminar burning velocity of the mixture and the hydrogen concentration at different equivalence ratios. It showed that laminar burning velocities increase exponentially with the increase of hydrogen concentration at high hydrogen composition.

A more comprehensive study by Ilbas et al. (2006) conducted the laminar burning velocity measurements for H₂-CH₄ mixtures. The laminar burning velocities of H₂-air and different composition of H₂-CH₄-air mixtures have been measured at ambient temperatures for different equivalence ratios in the range of 0.8 to 3.2. It was shown that the laminar burning velocity of H₂-CH₄ increases with the addition of hydrogen. The amount of the increase strongly depends on the hydrogen concentration. The result is shown in Figure 2.4. The correlation of the burning velocity of hydrogen-methane mixtures with hydrogen concentration showed that within about 20% of hydrogen concentration, the effect of increasing in burning velocity is moderated. On the other hand, when hydrogen concentration is increased to above 70%, the burning velocity starts to increase sharply with the hydrogen concentration. This means that correlation between the hydrogen concentration and the laminar burning velocity is not a linear relation. Only if the hydrogen concentration in the mixture is high enough, the addition of hydrogen will effectively increase the laminar burning velocity.

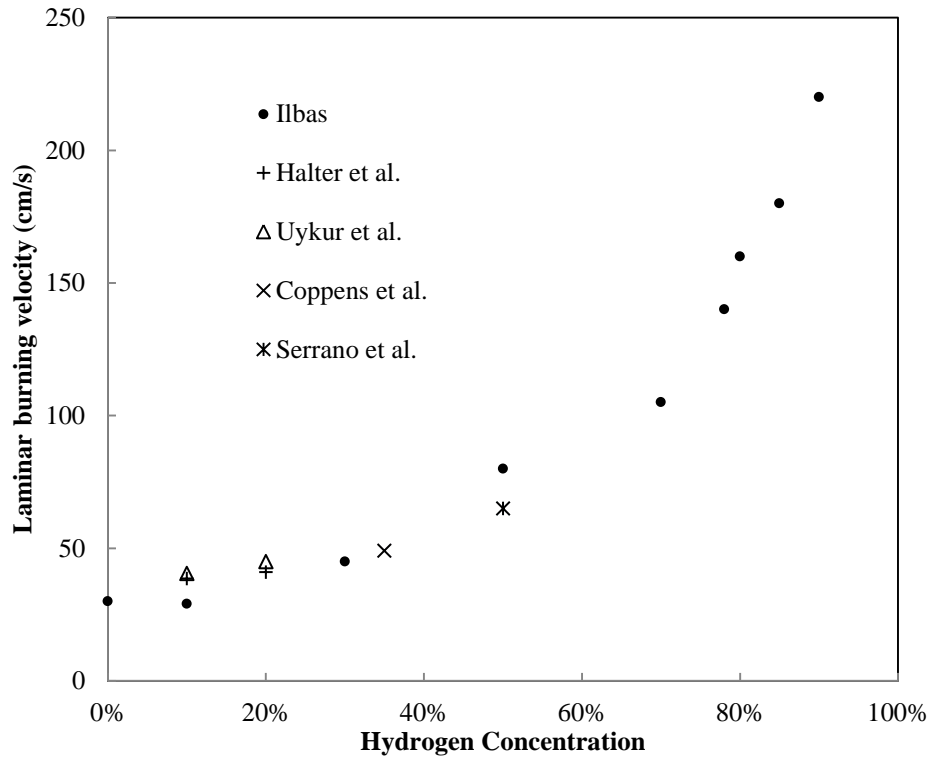


Figure 2.4: The effect of hydrogen concentration on the laminar burning velocity of H₂-CH₄ mixture at stoichiometric condition

Halter et al. (2004) showed that at 10% and 20% hydrogen addition in methane, the increase on the laminar burning velocity of methane is very slight. The laminar burning velocity of methane-hydrogen does not exceed 50 cm/s for the hydrogen concentration of 0-20%. Their findings also showed that the laminar burning velocity of hydrogen-methane mixture is far lower than those of pure hydrogen. For 50% hydrogen, the maximum burning velocity is 70 cm/s and appears at equivalence ratio of 1. It is agreed with Lewis' study motioned above. It was concluded in their study that the ignition could not be performed at equivalence ratio of 1.4 or above for pure methane-air mixtures, while that was easily performed at very high equivalence ratios up to 3.2 due to low ignition energy needed for hydrogen combustion compared with methane combustion. In addition, the influence of methane addition on flammability of hydrogen was also investigated. The flammable regions were widened with hydrogen content

increased in the mixtures.

More recently, Di Sarli and Benedetto (2007) simulated laminar burning velocity of hydrogen-methane-air premixed flames. The calculations in their study used CHEMKIN PREMIX code with the Gri-Mech mechanism. The equivalence ratio and the fuel composition were varied from lean to rich and from pure methane to pure hydrogen. They found that the laminar burning velocities are always smaller than the ones obtained by averaging the values of the pure fuels. They defined three regimes for the effect of hydrogen concentration on laminar burning velocity of methane. At low hydrogen concentration (0-50%), the combustion is dominated by methane and the addition of hydrogen results in a linear and slight increase of the methane laminar burning velocity. At high hydrogen contents (90-100%), the combustion of methane inhibited by hydrogen takes place corresponding to linear and sharp increase of the methane laminar burning velocity. A transition regime is found at the concentration of hydrogen between 50% and 90%. The results showed that at 85% H₂ addition, the laminar burning velocity of the mixture was about 190 cm/s at equivalence ratio of 1. On the other hand at 10% H₂ addition, the lamina burning velocity was about 49 cm/s at equivalence ratio of 1. An exponential increase in the laminar burning velocity was found when H₂ addition exceeded 80%.

2.6 The Laminar Burning Velocity of C₂H₆-Air and C₂H₆-H₂-Air

C₂H₆-Air

The study concerning the measurement of burning velocity for ethane-oxygen-nitrogen and ethane-oxygen-argon mixtures was conducted by Konnov et al. (2003). A counterflow flame technique was employed by Egolfopoulos et al (1991) and, Vagelopoulos and Egolfopoulos (1998) to evaluate the laminar burning velocity of ethane-air combustion. A more recently study conducted by Jomaas et al. (2005) has shown the laminar burning velocity of

ethane-air flames by using constant pressure bomb technique. They showed the results of different methods evaluating the ethane-air laminar burning velocity. It is shown in Figure 2.5. As shown in the figure, the laminar burning velocity of ethane-air flame is approximately 40 cm/s at equivalence ratio of 1. The maximum laminar burning velocity of ethane-air flames concentrate at the equivalence ratio of near 1.2.

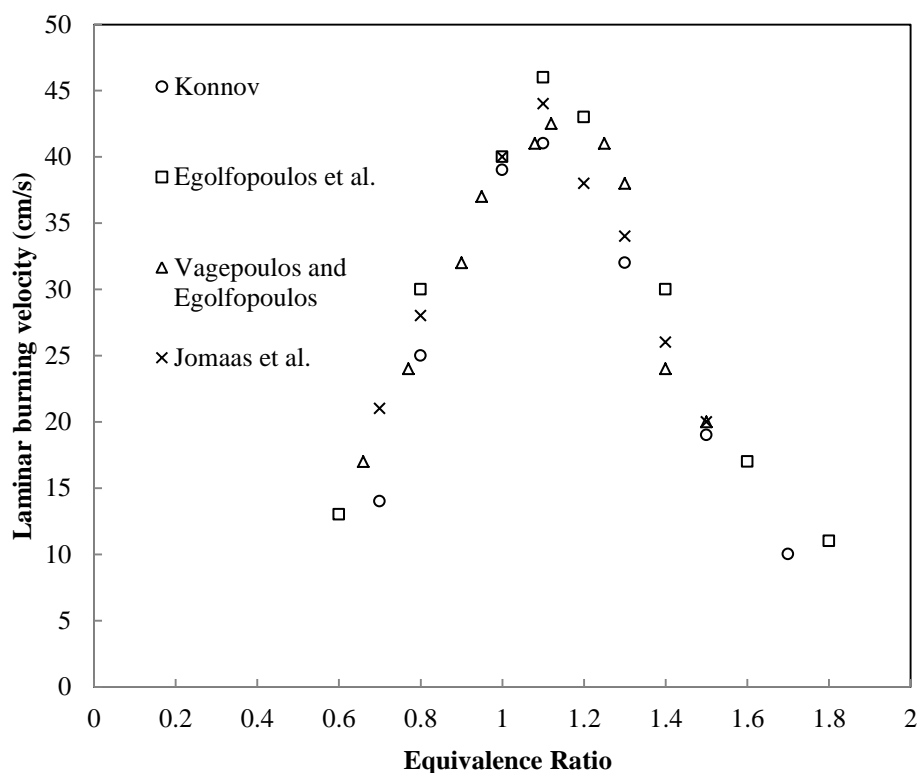


Figure 2.5: The comparison of the laminar burning velocity data of C_2H_6 -air

Furthermore, the previous studies implemented by Gibbs et al. (1959), Scholte and Vaags (1959) and Law showed that that the maximum laminar burning velocity of ethane-air is about 50 cm/s at equivalence ratio at about 1.1.

H_2 - C_2H_6 Mixtures

In terms of ethane-hydrogen mixture combustion, the previous studies concerning

the measurement of laminar burning velocity are really rare. The investigation implemented by Kido et al. (1994) illustrated the correlation of hydrogen addition into ethane-air flames with the laminar burning velocity of the mixture at 1 bar and 298 K. The constant volume spherical explosion bomb approach was employed. The adiabatic combustion condition was assumed in their study. The data gained from their study is illustrated in Figure 2.6. As shown in the figure, their study showed that the laminar burning velocity of the combustion of ethane-hydrogen mixture increases with the hydrogen addition concentration in the mixture, as well as the equivalence ratio. The increase was more efficient with high hydrogen concentration in the reactant. Since the study of mine does not focus on the effect of equivalence ratio on laminar burning velocity, but the hydrogen concentration in the mixture. Thus Figure 2.6 can be plotted as laminar burning velocity against hydrogen concentration at equivalence ratio of 1. This is shown in Figure 2.7. The previous studies, shown in Figure 2.5, showed that the laminar burning velocity of ethane-air combustion was about 40 cm/s at equivalence of 1.

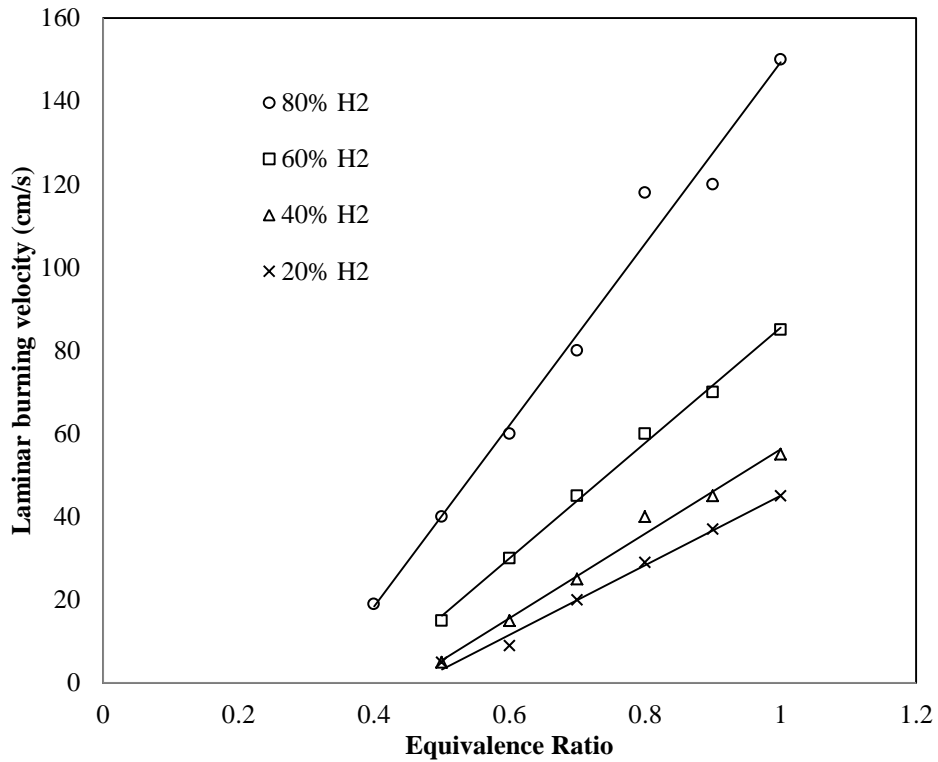


Figure 2.6: The laminar burning velocity of $H_2-C_2H_6$ over a range of equivalence ratio at 80%, 60%, 40% and 20% hydrogen concentration, adapted from Kido et al. (1994)

Thus, considering with the results gained by Kido et al. (1994), at low hydrogen concentration (20%) in the mixture the laminar burning velocity of the mixture was basically same as that of pure ethane-air flame. On the other hand, at 80% hydrogen in the mixture the laminar burning velocity of the mixture had experienced a dramatic increase.

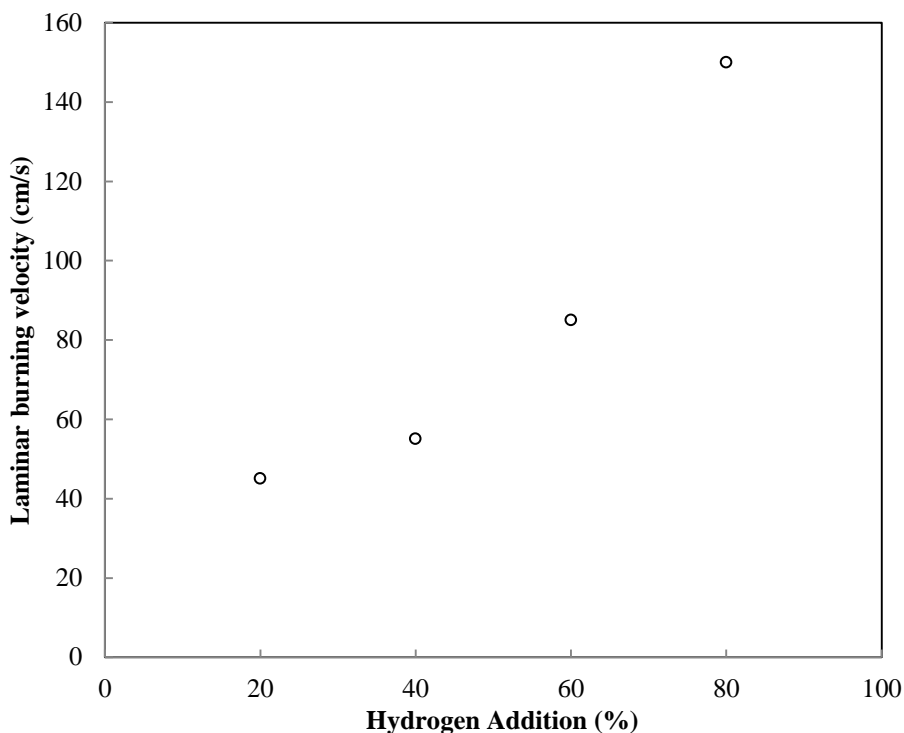


Figure 2.7: The correlation of the laminar burning velocity of $H_2-C_2H_6$ with the hydrogen concentration at equivalence ratio of 1, adapted from Kido et al. (1994)

2.7 The Laminar Burning Velocity of C_3H_8 -Air and $C_3H_8-H_2$ -Air

C_3H_8 -Air

For propane-air mixtures, there also are large numbers of literatures (Methalchi and Keck, 1980; Razus et al., 2010). From the studies on the laminar burning velocity of hydrocarbons fuels it was found that the laminar burning velocities of hydrocarbons increase as the content of carbon increases.

Hung (1986) conducted a study to assess the effects of adding propane or ethane on laminar burning velocity of methane-air mixtures. The results from their study represented that the addition of propane or ethane increases the burning velocity of methane-air, and the amount of the increase depending on the concentration of the additives. It also showed that ethane appears to be more effective than propane

at the same volume percent. In Tripathi et al. (2010) study, the maximum laminar burning velocity of LPG was shown as 57.5 cm/s at equivalence ratio of 1.2. The laminar burning velocity of propane-air combustion over different equivalence ratio has also been performed in other studies.

Egolfopoulos et al. (1991) used counterflow flame technique, on the other hand, the constant volume spherical bomb method was employed by Huzayyin et al. (2008) and Liao et al. (2007). These studies are illustrated in Figure 2.8. As shown in the figure, the data gained by Liao et al. (2007) were agreed with that by Egolfopoulos et al. (1991). The laminar burning velocity of propane-air flame was about 44 cm/s at the equivalence ratio of 1. Lee et al. (2010) employed spherical constant volume chamber and measured the laminar burning velocity of H₂-air, CH₄-air and C₃H₈-air mixtures at normal temperature and pressure condition. They showed that the laminar burning velocity of propane flame was lower than 50cm/s at equivalence ratio of 1 and was higher than that of methane flame.

C₃H₈-H₂ Mixture

Tang et al. (2008) evaluated the laminar burning velocity of propane-hydrogen-air flame over a range of equivalence ratio corresponding to different hydrogen addition. This is illustrated in Figure 2.9. The study showed that at same equivalence ratio the laminar burning velocity increased as the hydrogen concentration in the mixture. In addition, the increase from 60%-80% hydrogen addition was far higher than that from 20%-40%.

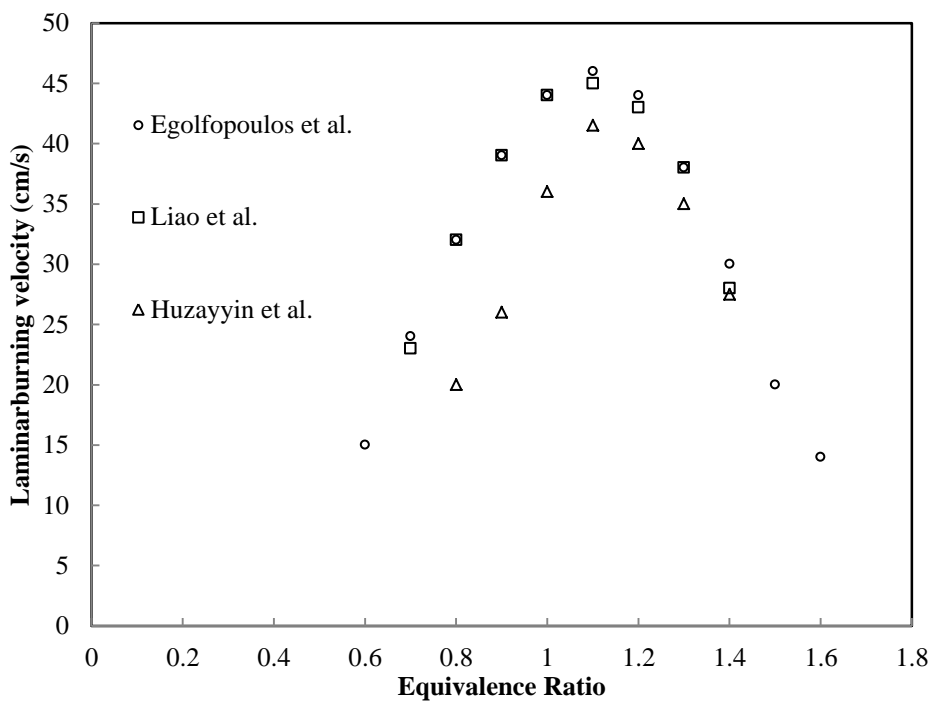


Figure 2.8: The comparison of the laminar burning velocity data of C_3H_8 -air mixture

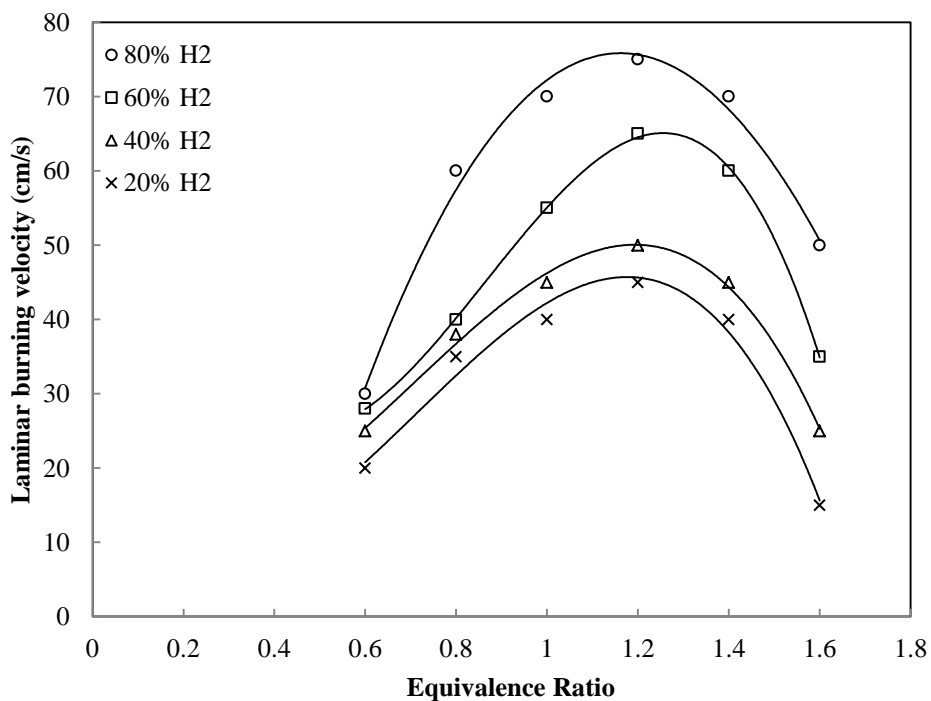


Figure 2.9: The laminar burning velocity of H_2 - C_3H_8 over a range of equivalence ratio at 80%, 60%, 40% and 20% hydrogen concentration, adapted from Tang et al. (2008)

Figure 2.9 also can be plotted as the laminar burning velocity against hydrogen addition concentration at equivalence ratio of 1. This is illustrated in Figure 2.10. As shown in the figure, their study found an exponential increase in the lamina flame speed at high hydrogen addition concentration (>60%).

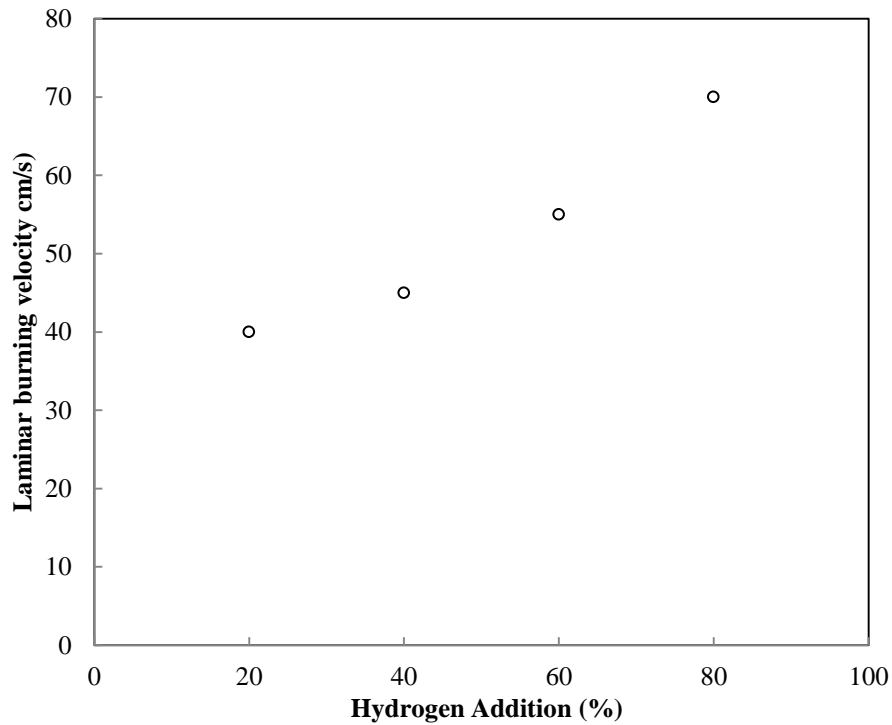


Figure 2.10: The correlation of laminar burning velocity of $H_2-C_3H_8$ with the hydrogen concentration at equivalence ratio of 1, adapted from Tang et al. (2008)

2.8 Summary

- The literature review of the experimental measurement on laminar burning velocity showed that the experiment has to consider the effect of non-one-dimensional flame front. The heat loss from the edge of the flame front also influences the accuracy of the experimental measurements.
- The laminar burning velocity of hydrogen-air flames varies from 210-280 cm/s at the equivalence ratio of 1. The peaked value varies from 250-370

cm/s at equivalence ratio of 1.6.

- The laminar burning velocity for methane-air mixtures is in the range of 32-44 cm/s at the equivalence ratio of approximately 1. In terms of methane-hydrogen mixture, the laminar burning velocity of the mixture increases exponentially with hydrogen concentration. With hydrogen addition is over 80%, the lamina burning velocity of the mixture exceeds 200 cm/s.
- The laminar burning velocity of ethane-air flame is approximately 35-40 cm/s at equivalence ratio of 1. The laminar burning velocity of ethane-hydrogen mixture is about 150 cm/s at 80% H₂ addition.
- The laminar burning velocity of propane-air flame was about 44 cm/s at the equivalence ratio of 1. For propane-hydrogen mixture, the laminar burning velocity is about 70 cm/s at 80% H₂ addition.
- The laminar burning velocities of H₂-CH₄, H₂-C₂H₆ and H₂-C₃H₈ are dependent of the equivalence ratio of the gaseous mixture, and strongly depending on the H₂ concentration in the gaseous mixture.

Chapter 3

Numerical Modelling of Reaction Kinetics and Review of Reaction mechanisms

Chapter 2 has already mentioned laminar burning velocity is determined by the reactivity of the gaseous mixture. The numerical simulation of the laminar burning velocity requires the understanding of the reaction kinetics modelling and the reaction mechanism.

This chapter presents the detailed theories applied in the reaction kinetics modelling. The reaction mechanisms of H_2 and hydrocarbons (C_1 - C_3) are also discussed in this chapter.

3.1 Chemical Reaction Kinetics

Chemical kinetics is the one used to describe the rate of chemical processes. In combustion, thermochemistry considers the heat, work and temperature of the combustion. On the other hand, the rate at which the combustion processes take place is concerned by chemical kinetics.

3.1.1 Molecularity and Reaction Order

The term “molecularity” is the number of molecules involved in the reaction (Levenspiel, 1999). The molecularity of a reaction must be integer, since it is used to describe the mechanism of the reaction and only applies to elementary reactions. Considering a chemical reaction involving reactants A, B, C and D has a rate expression as following (Levenspiel, 1999):

$$-r_A = k_A C_A^a C_B^b C_C^c C_D^d \quad \text{Eq. 3-1}$$

In which, a, b, c and d are not essentially represented the stoichiometric coefficients with corresponding reactants. They are called the order of the corresponding reactants, the summation of them respects to the overall reaction order for the chemical reaction. Being differ from the molecularity, the order refers to the empirically found rate expression (Levenspiel, 1999).

Chemical reactions can be classified into two distinguished types of reactions which are elementary reactions and overall reactions. Provided the collision and interaction of two single molecules are involved in the rate-controlling mechanism, the number of collisions of the molecules will be proportional to the rate of the reaction. However, at a given temperature, the collisions depend upon the concentration of the reactants in the mixtures. The elementary reactions occur at molecular level as a result of a collision process. The elementary reactions depend on the intermolecular potential forces existing during the collision encounter, the quantum states of the molecules, and the transfer of energy (Heghes, 2006). The equations representing the elementary reactions basically show both the molecularity and the rate constant. For example a second order chemical reaction:



As shown in the reaction, the reaction order coincides with the molecularity of the reaction. The elementary reactions include unimolecular, bimolecular and trimolecular reactions. The unimolecular reactions are the dissociations of reactive molecules to form products. This kind of reactions belongs to first-order reactions, in which the reaction rate is proportional to the concentration of a single reactant raised to the first power. The collision of two same or different molecules

produces bimolecular reactions, in which reaction rate is proportional to either the concentration of a reactant squared, or the product of concentrations of two reactants. The reactions involving three reactive molecules are trimolecular reactions. The trimolecular reactions are of important and of course more complicated than unimolecular and bimolecular reactions. The trimolecular reactions can be considered as the process of recombination. This kind of reactions obeys third-order reactions. A detailed description will be given in later section.

On the other hand, the overall reactions are the consequence of series elementary reactions. For the nonelementary reactions, there is no direct correspondence between stoichiometry and rate. Thus, the nonelementary reactions have a more complex rate laws compared with the elementary reactions. Generally, the order of nonelementary reactions is not integer.

3.1.2 Rate Laws and Rate Constant

The reaction rates depend on the concentration of each species involved in the reaction. The relationship between the concentration and rates can be expressed mathematically. The mathematical expression for the dependence of reaction rates on concentration is called rate law. Therefore, rate law represents reaction rates in terms of concentration of the component involved in the reaction. Rate laws can be expressed in differential forms or integrated forms.

For a chemical reaction:



For zero order reaction, the rate of the reaction is constant and independent of the concentration of the materials involved in the reaction. The rate law is written as:

$$r = -\frac{d[A]}{dt} = k \quad \text{Eq. 3-2}$$

It is shown in the equation that the rate is only dependent on the rate constant.

By integrating the rate expression:

$$[A] = -kt \quad \text{Eq. 3-3}$$

This gives a linear correlation between the concentration of the reactant and the time as shown in Figure. 3.1

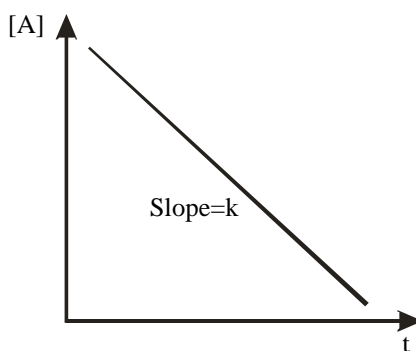


Figure 3.1: Plot of concentration of A with time for zero order reaction

For first order reaction, the reaction rate is proportional to the concentration of a single reactant raised to the first power. The rate equation is written as following:

$$r = -\frac{d[A]}{dt} = k[A] \quad \text{Eq. 3-4}$$

By integrating the rate expression:

$$\ln \frac{[A]}{[A_0]} = -kt \quad \text{Eq. 3-5}$$

Or

$$[A] = [A_0] \times e^{-kt} \quad \text{Eq.3-6}$$

Plotting $\ln [A] / [A_0]$ against time creates a straight line with slope of $-k$. On the other hand, plotting the concentration of the reactant against time shows the concentration falls exponentially from the initial concentration to zero. It is shown in the Figure. 3.2.

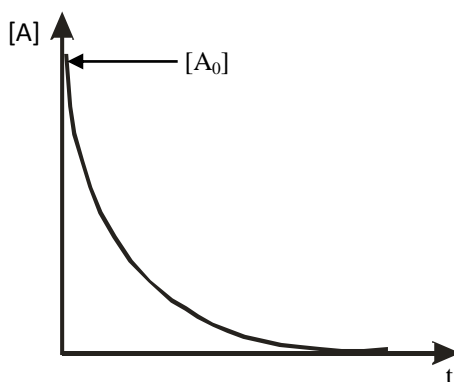


Figure 3.2: The concentration of the reactant against time for first order reaction

Considering the correlation of concentration with time for both reactant and product, the rate equation can be written as:

$$[Product] = [A_0](1 - e^{-kt}) \quad \text{Eq. 3-7}$$

Figure 3.3 reflects the rate equation as shown as following:

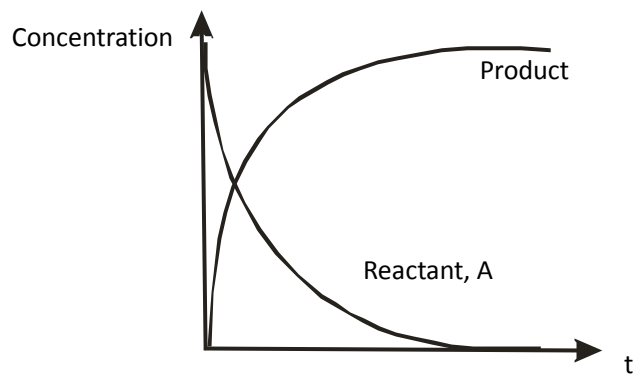


Figure 3.3: The correlation of reactant and product with time for first order reaction

For a second order reaction, the rate law is written as:

$$\frac{d[A]}{dt} = -k[A]^2 \quad \text{Eq. 3-8}$$

By integrating the rate law:

$$\frac{1}{[A]} - \frac{1}{[A_0]} = kt \quad \text{Eq. 3-9}$$

The plot of $1/[A]$ versus time produces a straight line with slope k and intercept $1/[A_0]$. The relationship is shown as following:

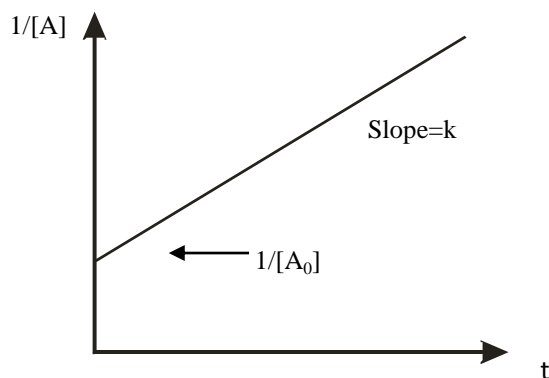


Figure 3.4: Plot of $1/[A]$ with time for second order reaction

It is different from the situation of the first order reactions, the detailed concentration is needed to find out the rate constant. When considering the second order reaction:



If the concentrations of A and B are equal at initial situation, time zero. The rate law is expressed as the one given above. On the other hand, if the starting concentrations of the two reactants are different, the situation will be more complex. The rate law is expressed as:

$$\frac{d[A]}{dt} = -k[A][B] \qquad \text{Eq. 3-10}$$

There are many chemical reactions having such rate law expression. For this kind of rate law, it is very complicated to carry out differential and to predict the correlation of concentration with time.

The rate law, and hence associated with the rate constant, can be measured experimentally. This can give a comparison of the measured rate constant with the one predicted by theory. In addition, one of the importance roles of rate law is that the form of the rate law can give the information about the mechanism of a chemical reaction. The rate of a reaction associated with several elementary reactions mechanism is often affected by the slowest step. The transition state with the highest energy is the rate determining step of a reaction.

The rate of chemical reactions also depends on the temperature. Thus, for many chemical reactions, particularly elementary reactions, the rate expression can be written in terms of temperature-dependent function and composition dependent function. The high temperature increases the probability of the collision of two

molecules. The higher collision rate is the result of high average kinetic energy. It has been found that the reactions, temperature dependent, can be described by Arrhenius equation, which determines the relationship between rate constant and temperature. The Arrhenius equation is given below:

$$k = A \times e^{-\frac{E_a}{RT}} \quad \text{Eq. 3-11}$$

Where E_a is the activation energy, R is the gas constant ($8.314 \times 10^{-3} \text{ kJ mole}^{-1} \text{ K}^{-1}$), A is the pre-exponential factor or frequency factor, k is the rate constant for the reaction and T indicates the absolute temperature (K).

The Arrhenius equation can also be written as:

$$\ln k = -\frac{E_a}{RT} + \ln A \quad \text{Eq. 3-12}$$

It can be seen from the equation, that plotting $\ln k$ against $1/T$ gives a straight line with the slope of E_a/R . This is called Arrhenius plot, shown in Figure 3.5.

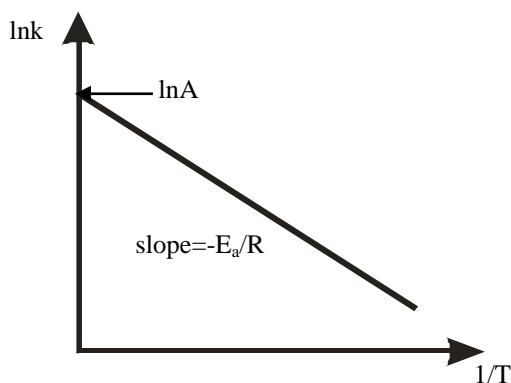


Figure 3.5: Arrhenius plot, the relation between reactant concentration and temperature

As shown in Figure 3.5, the activation energy can be calculated from the slope of the straight line and the intercept corresponds to $\ln A$. It means that A can be identified as the possibly maximum rate constant. A indicates the effect of the collision orientation, colliding molecules and temperature dependence of the preexponential factor. Thus, the value of $\ln A$ will move up when the slope, and hence the activation energy, increases. Compared with the reaction having relative low activation energy, the reactions with high activation energy are very temperature sensitive. However, Arrhenius relation does not hold the reactions with low activation energy and radical recombination. In the process of a simple radical recombination to form a single product, energy must be removed from the product formation to stabilise it. Thus, a third body is required to carry the energy. The third body can be any radicals in the reservoir of the reaction system. Thus, for a third body recombination reaction, pressure dependence becomes quite important rather than the temperature (Kuo, 2005). Typically, the third body effect is for recombination and dissociation reactions.

The Arrhenius equation is based on the collision theory. It is not the fact that all of the collisions between reactant molecules are effective and convert reactants into products. There are two factors deciding if the collision is effective, which are kinetic energy and orientation. To convert reactants into products, the molecules must collide with both the correct orientation and sufficient kinetic energy. This is described in Figure 3.6.

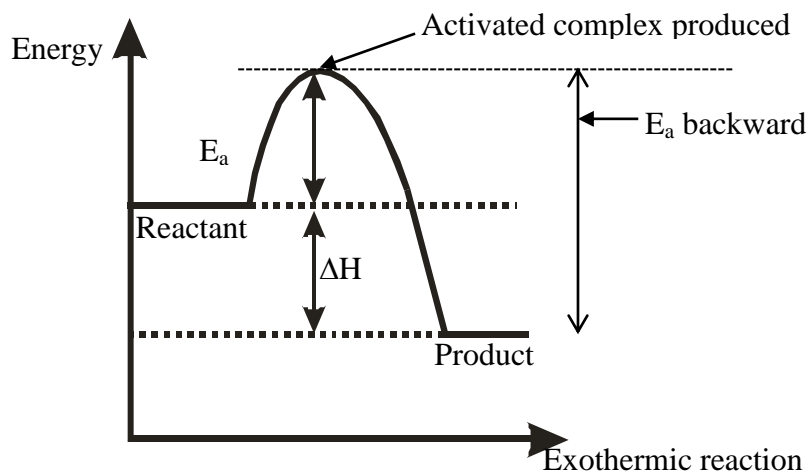


Figure 3.6: The activation energy in collision theory

In Figure 3.6, ΔH refers to the energy difference between reactant and product. It is the energy used in bond breaking reaction minus the energy released in bond forming. In molecules collision, the kinetic energy carried by molecules must be higher than the activation energy in order to achieve the conversion of reactant to product. Basically, the activation energy is recovered by the heat generated during the reaction. As shown in the figure, the activated complex is first formed through molecular collisions, and then it results in products formation. The forward and backward reactions require different activation energy so different specific reaction rate constant. At the highest point where the activated complex formed, it must have lower energy above the reactants than other reaction paths. Thus, the highest point in the figure also indicates the reaction path (Kuo, 2005).

However, some reactions do not appear the linear relation in Arrhenius plot. The nonlinear behaviour can be predicted theoretically and the reaction rate for those reactions has the expression as give:

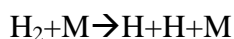
$$k = AT^n e^{\left(\frac{E_a}{RT}\right)} \quad \text{Eq. 3-13}$$

Same as A and E_a , n is temperature-independent constant. The values for A and E_a can be obtained from experiment or statistical mechanics calculations. They are based on the nature of the elementary reaction. In the modified Arrhenius equation, AT^n represents the collision frequency while the exponential factor indicates the fraction of the collision that has energy levels greater than the activation energy. Both of the Arrhenius and this modified Arrhenius are the expressions based on experimental data.

3.1.3 Reaction Mechanism

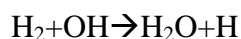
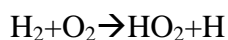
With empirical rate expressions, the mechanism of chemical reactions can be taken into account. The nonelementary reactions result from a sequence of elementary reactions. Thus the nonelementary reactions represent the overall effect of the elementary reactions. In the process from initial reactant to final product, there are many intermediates formed, they are only appeared in a short time and hard to be observed. There are many different types of intermediates. Free radicals refer to the atoms or large fragments of stable molecules that have unpaired electrons. Basically, the free radicals are unstable and thus highly reactive. The electrically charged atoms and molecules can act as active intermediates in reactions. Some molecules with very small lifetime in reactions can be considered as reactive intermediates. The energy released from the collisions between reactant molecules can result in strained bonds, unstable forms of molecules, or unstable association of molecules. These can either decompose to form products, or return to normal state (Levenspiel, 1999). These unstable forms are referred to as transition complexes. In nonchain reactions, the intermediates are formed in the first reaction and then it gives to product in further reaction. On the other hand, in chain reactions, the intermediates are formed in the first reaction, the chain initiation step. In the chain propagation steps, the formed intermediates take part in the production of either product or more intermediates. All of the intermediates are destroyed in the chain termination step.

The mechanism of elementary reactions can be described in terms of unimolecular, bimolecular and termolecular steps. Unimolecular reactions are achieved by the collision between one reactive molecule and an unspecified molecule, or when an already excited molecule hits another and decomposes. The momentum and energy of the unimolecular chemical change is balanced by the unspecified molecule. Generally, unimolecular reactions take place at relative high temperature. An example of unimolecular reaction is give below:



In which M refers to as the unspecified molecule.

Bimolecular reactions are the reactions in which two reactive molecules recombine by collision. The molecules are with high relative speed or they are already excited. The examples can be found from the combustion of hydrogen:



If three molecules collide together at the same time, the reaction will be called termolecular reaction. Compared with unimolecular and bimolecular reactions, the termolecular reactions have relative high possibility of redistributing the momentum and energy. A very important elementary reaction in combustion of hydrogen represents the characteristics of termolecular reaction, which is:



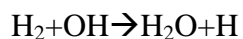
In solution and gas elementary reactions, termolecular, three molecules colliding simultaneously, is relatively rare. In addition, a bimolecular reaction with third body effect is also considered as termolecular reaction. Most of the time, the

reaction mechanism is dependent on the range of temperatures and pressures involved in the combustion (Isidoro Martinez,2011).

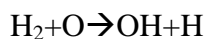
The elementary reactions can include first order, second order and third order reactions according to the reaction order. The mechanism of first order reactions serve to decomposition reactions when the concentration of the unspecified molecule is larger than that of reactant (Isidoro Martinez,2011). The mechanism of most of the elementary reactions fits second order reactions. The elementary reactions also can be classified by considering their effect. The types include chain initiation, propagation and termination, and chain branching. The radicals are formed from relative stable molecules in initiation step. The formation of final product and destroying of radicals take place in the termination step. There are two examples for initiation and termination reactions.



The chain propagation reactions are responsible for producing new radicals from consuming other radicals. An example is shown below:



The chain branching takes place when the collision between a stable molecule and one radical produces more than one radical (Isidoro Martinez, 2011). The production of increased number of active radicals results in the reactions become more and more productive. An example of chain branching elementary reaction is shown as below:



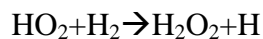
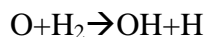
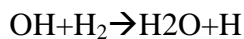
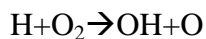
The free radicals generated from chain branching reactions are terminated at wall

through recombination reaction processes. However, above certain temperature, the chain branching reactions become strongly activated and frequent, so that the multiplication of the free radicals are caused. This may lead to chain branching explosions and thermal explosions (Kuo, 2005). The chain branching explosions result in reaction rate increases without limit, on the other hand, the thermal explosions cause an exponential increase in reaction rate due to heat released from exothermic chemical reaction and in the magnitude of the specific reaction rate constant.

3.2 Reaction Mechanism of H₂-Air Oxidation

Compared with the combustion of hydrocarbons, the mechanism and kinetics of hydrogen combustion are relatively simple. However, the combustion kinetics of hydrogen combustion is of important for studying the combustion of hydrogen-hydrocarbon mixtures.

The combustion of hydrogen may occur as either a slow reaction or an explosion, depending on the experimental conditions. (Kassel, 1937) The basic principles and general features of combustion have been studied by many previous studies. The ignition region is defined by chain reaction which generally starts from the wall but few examples originate in the gas phase. The branching elementary reactions occur in the gas phase. Ignition takes place when the rate of branching is higher than that of breaking. This mechanism gives the upper and lower limits of the ignition. (Kassel, 1937) Considering with specific case, hydrogen combustion, the branching took place at collisions between H and O₂, and breaking by $H+O_2+M \rightarrow HO_2+M$ (Kassel and Storch 1935). The effective slow chain step has been pointed out by von Elbe and Lewis (1937), which is $H+O_2 \rightarrow OH+O$. This gives the complete mechanism to be considered for the ignition region for hydrogen combustion. The mechanism includes following elementary reactions:



The mostly used mechanism for kinetics modelling of hydrogen combustion includes about 20 elementary reactions. The one given by CHEMKIN database has 19 elementary reactions (see Appendix C). The complete mechanism of hydrogen combustion includes the following species: H_2 , O_2 , OH , H , O , HO_2 , H_2O and H_2O_2 . The maximum complete mechanism has been given in the early study by Dimitrov and Azatyan (1975). It included 30 elementary reactions and 4 quenching reactions. It is shown in appendix D.

The kinetic analysis of hydrogen combustion can be carried out either experimentally or computationally. From the studies in previous literatures, it has shown that the majority of the studies used computational kinetic modelling to analysis hydrogen combustion. This method is essentially the computational calculation that determines the species concentration with time of the considered elementary reactions, associated with the Arrhenius parameters. The Arrhenius equation has been described in previous chapter. Most of the studies on computational kinetics modelling of hydrogen combustion have some common elementary reactions such as $\text{H} + \text{O}_2 + \text{M} \rightarrow \text{HO}_2 + \text{M}$.

A more recent study focusing on kinetic simulation of hydrogen combustion was implemented by Goncalves et al. (2010) who conducted the kinetic simulation for hydrogen combustion in a homogeneous reactor. In their study, the combustion kinetics simulation was carried out in the software CHEMKIN, and the results from which were compared with the one published by Connaire et al., (2004). The elementary reactions used and the corresponding kinetic parameters is shown as

Appendix C. The results were then compared and standardised with the calculated results by MP2 molecular quantum chemistry method. The agreement meant that the MP2 calculation method can be used for the calculation for the reactions which cannot be determined experimentally. There were 18 elementary reactions used in their study. Their study gave a typical example of simulating hydrogen combustion kinetics by CHEMKIN.

Different with Goncalves et al. (2010), the hydrogen combustion kinetics study by Dougherty and Rabitz (1980) used different elementary reactions and method. This study emphasized the importance of the step that $\text{H} + \text{O}_2 + \text{M} \rightarrow \text{HO}_2 + \text{M}$. They gave 15 elementary reactions for the slow reaction between the second and third explosion limits and 13 elementary reactions for the second explosion limit. The study listed 12 insignificant reactions for the H_2/O_2 system, which are radical-radical or endothermic reactions. It was found that the reactions involving HO_2 are important in the regime between the second and third explosion limits. The finding by Westbrook et al., (1977) was mentioned that the branching ratio of $\text{H} + \text{O}_2 \rightarrow \text{OH} + \text{O}$ and $\text{H} + \text{O}_2 + \text{M} \rightarrow \text{HO}_2 + \text{M}$ is critical in determining the length of the induction period for methane combustion. Compared with Goncalves' study, Dougherty and Rabitz (1980) attempted to link the hydrogen kinetics model with other hydrocarbons.

The study conducted by Gontkovskaya et al., (1981) aimed to select the most important elementary processes for H_2/O_2 system. There were 18 reactions used for the simulation, including the one suggested by Dougherty and Rabitz (1980), which is $\text{H} + \text{O}_2 + \text{M} \rightarrow \text{HO}_2 + \text{M}$. However, the reactions are different with Goncalves' study. For Goncalves' study, the data for the reaction kinetic parameters were obtained from the database of CHEMKIN.

A recently comprehensive study by Li et al., (2004) updated the H_2/O_2 reaction mechanism of Mueller et al., (1999). The result included 19 elementary reactions,

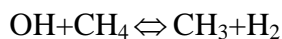
including $\text{H}+\text{O}_2+\text{M}\rightarrow\text{HO}_2+\text{M}$ and $\text{H}_2+\text{OH}\rightarrow\text{H}_2\text{O}+\text{H}$. Their study showed the importance of the elementary reactions depending on temperature range. The analysis also showed that the reaction, $\text{H}_2+\text{OH}\rightarrow\text{H}_2\text{O}+\text{H}$, is important for observing the flames propagation at high pressure. Similar to the simulation conducted by Goncalves et al. (2010), CHEMKIN transport package was used for achieving flame propagation model performance. In terms of the flame propagation, the competition between the chain branching and recombination reactions can result in the increase and reduction in the laminar burning velocity (Hu et al., 2012). Their study indicated that $\text{H}+\text{O}_2\rightleftharpoons\text{O}+\text{OH}$, $\text{O}+\text{H}_2\rightleftharpoons\text{H}+\text{OH}$, $\text{OH}+\text{H}_2\rightleftharpoons\text{H}+\text{H}_2\text{O}$ and $\text{HO}+\text{H}\rightleftharpoons\text{OH}+\text{OH}$ are the main chain branching reactions in hydrogen oxidation mechanism. These reactions are responsible for the increase in concentration of the H, O and OH radicals and thus enhance the reactions.

3.3 Reaction mechanism of Hydrocarbon Combustion

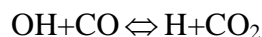
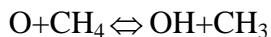
Santoro et al. (2010) conducted an experimental and chemical kinetics study for the combustion of syngas. They emphasized the H_2/O_2 system was the core subset mechanism for all hydrocarbon fuels. Their study considered the effects of pressure and CH/CO addition on the kinetics and developed an improved kinetic model. It showed HO_2 paths were terminating at low pressure and temperature and the competition between OH and HO_2 still controlled pressure dependence. They traced the H flux to observe the effect pressure on kinetics. It showed the increased flux through $\text{H}+\text{O}_2+\text{M}$ and H_2 channels. An updated H_2/O_2 kinetic model, which used 19-reaction mechanism and based on Li et al. (2004), was used the model to predict the H_2 with CH_4 , C_2H_4 and C_2H_6 additions.

The chain character of reactions for $\text{H}_2\text{-O}_2$ system has been well studied by Semenov (1935) and Hinshelwood (1940). The basic principles of chain branching and propagation to give ignition can be applied to hydrocarbon

combustion. In hydrocarbons oxidation, the chain carriers are radical species H, O, OH, CH₃ and HO₂ (Westbrook, 2000). The system of hydrocarbon combustion has been well studied as well as the optimisation of the combustion mechanism. In the study by Di Sarli and Benedetto (2007), they gave 6 elementary reactions that contribute to the kinetic control of the methane-hydrogen-air combustion, which are given below:



At low hydrogen concentration, the methane conversion is governed by $\text{H} + \text{O}_2 \Leftrightarrow \text{O} + \text{OH}$. Many literatures (for example, Sher et al., 1988; Refael and Sher, 1989; EI-Sherif, 2000; Daugaut and Nicolle, 2005) have demonstrated the relevance between this elementary reaction and hydrocarbons combustion. It was found by Ren et al. (2001) that methane is mainly consumed through $\text{OH} + \text{CH}_4 \Leftrightarrow \text{CH}_3 + \text{H}_2$. This was confirmed by Daugaut and Nicolle (2005). They stated that the combustion of methane basically proceeds through the elementary reactions involving OH radicals. They also found that $\text{OH} + \text{CH}_4 \Leftrightarrow \text{CH}_3 + \text{H}_2$ is the main agent of methane oxidation. It was shown in Di Sarli and Benedetto (2007), at high hydrogen concentration, $\text{H} + \text{CH}_4 \Leftrightarrow \text{CH}_3 + \text{H}_2$ controls both the stoichiometric and rich flames. They employed the sensitivity factor equation to calculate the methane mole fraction sensitivity factors. Compared with the study by Di Sarli and Benedetto, the research conducted by Hu et al. (2009) gave different opinion. They suggested 7 elementary reactions that mainly contribute to the kinetic control of the methane-hydrogen combustion. These reactions are listed below:



It was found that the consumption reactions of methane in the flame are attacked by H, O and OH. CH₃ radical is produced from the attack. Same as the view of Di Sarli and Benedetto, they indicated that the branching reaction $\text{H} + \text{O}_2 \Leftrightarrow \text{O} + \text{OH}$ has the highest sensitivity for CH₄ conversion. This was also confirmed by Law (2006). Hu et al. also thought that methane combustion mostly proceeds through the reactions not only with OH radicals but also H radicals. The generation of H radicals accelerates the reaction, $\text{H} + \text{O}_2 \Leftrightarrow \text{O} + \text{OH}$, and thus enhances the burning intensity. They also found that hydrogen radicals participate in the termination reactions, $\text{H} + \text{O}_2 + \text{H}_2\text{O} \Leftrightarrow \text{HO}_2 + \text{H}_2\text{O}$ and $\text{H} + \text{CH}_3 + \text{M} \Leftrightarrow \text{CH}_4 + \text{M}$, competing for H radical. It was shown that the sensitivity factors of $\text{H} + \text{CH}_3 + \text{M} \Leftrightarrow \text{CH}_4 + \text{M}$ and $\text{H} + \text{O}_2 + \text{H}_2\text{O} \Leftrightarrow \text{HO}_2 + \text{H}_2\text{O}$ are positive for which they gave the explanation that the reactions retard the reactions of methane conversion. It has been shown from these studies, for the combustion of methane-hydrogen-air syngas, CH and OH are two important radicals for assessing the combustion characteristics.

In the study by Berman and Lin (1983), it was pointed out that it is useful to focus on the CH+CH₄ reaction in discussing the mechanisms of the reactions of CH with saturated hydrocarbons. They illustrated the energies of some important pathways for the reactions of CH+R→Products. So far, the most comprehensive mechanism of methane combustion consists of more than 300 elementary reactions and over 50 species. There have been many versions of the reduced mechanism for numerical modelling methane combustion and kinetics analysis.

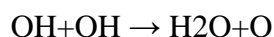
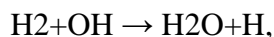
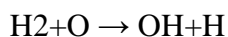
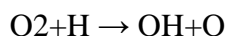
The mechanism of propane combustion is more complex than that of methane. Jachimowski (1984) developed a propane combustion mechanism consisting of 83 elementary reactions. And the kinetics study, temperature range 1600-1000K for pressure from 0.5-50atm, in his work showed that propane is consumed and to form primary products, CH₄, C₂H₄ and C₃H₆ during the ignition delay period. A detailed kinetic model of ignition and combustion of propane-air mixtures was developed in Titova, et al. (2010). The mechanism included 599 reactions with 92 species for both high temperature and low temperature.

Qin et al. (2000) conducted a study upon optimisation of the reaction mechanism of propane combustion. It was interested that the optimised mechanism was tested by integrating with the flame speed of propane and CHEMKIN program was employed for conducting the kinetic modelling. The result is shown in Appendix E. They used 9 targeted elementary reactions for ignition delays and 12 targeted elementary reactions for flame speed. The elementary reactions with high sensitivity to slower and faster combustion were important for the ignition and flame speed of propane combustion. The results were expected to add the optimising rate parameters of C₃ combustion chemistry mechanism into C_{<3} mechanism. However, they concluded that it is not possible to add the C₃ combustion mechanism while keep the C_{<3} rate parameters only by optimising the rate parameters of C₃ combustion mechanism.

Many studies have been done for experimental or computational evaluating the combustion mechanism of hydrocarbons, (for example Borisov et al., 1982; Warnatz, 1984) so that there are many published version of completed or reduced mechanism for hydrocarbons combustion. For example, the mostly used mechanism for kinetic modeling methane combustion is GRI-MECH. The last version of it is Gri-Mech 3.0 by Smith et. al, 1999. The mechanism consists of 325 reactions that involve 53 species. The data supplied by Gri-Mech laboratory shows that the laminar burning velocity of H₂-air is about 200 cm/s at equivalence

ratio of 1. This is agreed well with Dowdy et al. (1990) and Law and Egolfopoulos (1990). The laminar burning velocity of CH₄-H₂ is about 42 cm/s at 1 atm and equivalence ratio of 1. It agrees with Vagelopoulos and Egolfopoulos (1998). The laminar burning velocities of C₂H₆-H₂ and C₃H₈ are 40 cm/s and 51 cm/s respectively. The Gri-Mech 3.0 reaction mechanism is shown in APPENDIX E.

Warnatz and Heghes (2006) developed a C₁-C₄ hydrocarbon oxidation mechanism, which is shown in APPENDIX A. This relatively comprehensive mechanism also included H₂ oxidation. There were 20 elementary reactions and 9 species for the hydrogen oxidation mechanism. They indicated the most important steps providing the chain branching in H₂-O₂ system as shown as follow:



In terms of methane, their study showed that one of the the primary products CH₃ results from the attack of the O, OH, H and H₂O radicals on CH₄. The oxidation of CH₃ is competed with CH₃+CH₃+M <=>C₂H₆ +M. The oxidation of C₂H₆ results in the production of C₂H₅, C₂H₄ and C₂H₂. Compared with CH₄, the initial step of large hydrocarbon decomposition is the break of C-C bond rather than C-H bond. In terms of C₃H₈, the chain initiating step is C₃H₈+M → CH₃+C₂H₅ +M as indicated in their study.

The selection of the reduced mechanism for kinetics modelling depends on the purpose of the study and the experimental condition. For example, a four-step reduced mechanism of Peters (1985) was used in the study by Pantano (2004). This mechanism was used for direct simulation of non-premixed flame in a

methane-air jet.

3.4 CHEMKIN Kinetics Analysis Application

CHEMKIN was developed by Kee et al. and has become a widely used tool in combustion engineering especially in chemical reaction dynamics. It is a software package with a collection of programmes to be able to solve gas phase reaction kinetics problems. The software consists of five key components, which are gas phase kinetics subroutine, the surface kinetics subroutine, the transport property subroutine, the thermodynamic property database and a two-point boundary solver (Kuo, 2005). The users are required to supply the gas phase thermodynamic and transport properties for the gaseous mixtures and define the model input file. The results and analysis are obtained in postprocessors. In CHEMKIN, the gaseous mixture is assumed to be ideal gas.

In this study, the applied CHEMIN programmes include gas phase chemical reaction rate modelling associated with a closed homogenous model, the one-dimensional laminar premixed flame model and the species pathway analysis of using rate of production calculation.

In gas phase reaction kinetics modelling, each species in a reaction must be associated with thermodynamic data that are used to calculate equilibrium constants and reverse-rate coefficients for the elementary reactions. In CHEMKIN, the thermodynamic properties are presented in the form of polynomial fits to the specific heats and constant pressure. It is presumed that the standard state thermodynamic properties of all gas species are functions of temperature only. Furthermore, the specific heat is expressed as polynomial fit of arbitrary order of temperature (Kuo, 2005). There are many elementary reactions not governed by Arrhenius expression. In summary, the reaction rate subroutines include:

- Arrhenius temperature-dependent
- Pressure dependent
- Vibration energy transfer reactions
- Enhanced third body effect reactions
- Reverse reactions

The chemical rate expressions build on the thermodynamic expression. The reaction rate can depend on species composition, temperature and pressure. In CHEMKIN the production rate of the k^{th} species is written as a summation of the rate of progress variables for all reactions including the k^{th} species. The equation is given below:

$$\dot{r}_k = \sum_{i=1}^I v_{ki} q_i \quad (k=1, \dots, K) \quad \text{Eq. 3-14}$$

Where \dot{r}_k is the production rate of the k^{th} species and v_{ki} presents the stoichiometric coefficient. The rate of progress variable q_i for the reaction is obtained by the difference between the forward and reverse rate, as shown below:

$$q_i = k_{fi} \prod_{k=1}^K [X_k]^{v_{ki}'} - k_{ri} \prod_{k=1}^K [X_k]^{v_{ki}''} \quad \text{Eq. 3-15}$$

Where X_k is the mole concentration of the k^{th} species, and k_{fi} and k_{ri} are the forward and reverse rate constants of the i^{th} reaction. As shown in the equation, it uses the concentration of each reactant or product raised to the power of its stoichiometric coefficient. v_{ki}' is the stoichiometric coefficient in forward reaction and v_{ki}'' represents the coefficient in the reverse reaction.

In CHEMKIN, the forward rate constant of the reaction is assumed to be temperature dependence based on the modified Arrhenius equation as shown as Eq. 3-16. The reverse rate constant, k_{ri} , related to the forward rate constant through the equilibrium constant. The relationship is shown below:

$$K_c = \frac{k_f}{k_r} \tag{Eq. 3-16}$$

The equilibrium constant, K_c is calculated from thermodynamic properties, as shown below:

$$K_{ci} = K_{pi} \left(\frac{P_{atm}}{RT} \right)^{\sum_{k=1}^K v_{ki}} \tag{Eq. 3-17}$$

and

$$K_{pi} = \exp\left(\frac{\Delta S_i^\circ}{R} - \frac{\Delta H_i^\circ}{RT}\right) \tag{Eq. 3-18}$$

Where i means the i^{th} reaction, S° is entropy and H° is enthalpy. The Δ refers to the change that occurs in passing completely from reactants to products in the i^{th} reaction.

The change in the standard-state molar enthalpy is shown as following:

$$\frac{\Delta H_i^0}{R} = \sum_{k=1}^K v_{ki} \frac{H_i^0}{RT} \tag{Eq. 3-19}$$

And the change in the standard-state molar entropy is given by:

$$\frac{\Delta S_i^0}{R} = \sum_{k=1}^K v_{ki} \frac{S_i^0}{RT} \quad \text{Eq. 3-20}$$

where v_{ki} is obtained from the reverse stoichiometric coefficients minus the forward stoichiometric coefficients for the k^{th} species in the i^{th} reaction.

In the one-dimensional premixed flame model, both of thermodynamic and transport properties are required. The model is capable of solving the governing differential equations which determine the flame dynamics. The finite difference method is applied in this model. Furthermore, the mesh is optimised by applying coarse to fine grid refinement approach. The governing equations, mixed-average transport equations and boundary conditions are shown as following;

The energy conservation equation:

$$\dot{M} \frac{dT}{dx} - \frac{1}{c_p} \frac{d\left(\lambda A_c \frac{dT}{dx}\right)}{dx} + \frac{A_c}{c_p} \sum_{k=1}^K \dot{\omega}_k h_k W_k = 0 \quad \text{Eq.3-21}$$

Where, x is the coordinate system of the flame, \dot{M} is the mass flow rate, T indicates the temperature, λ is the thermal conductivity of the mixture, C_p represents the specific heat capacity of the mixture at constant pressure, A_c is the cross-sectional area of the stream, encompassing the flame, $\dot{\omega}_k$ is the molar rate of production by chemical reaction of the k^{th} species per unit volume, h_k is the specific enthalpy of the k^{th} species and W_k is the molecular weight of the k^{th} species.

The species equation:

$$\dot{M} \frac{dY_k}{dx} + \frac{d(\rho A_c Y_k V_k)}{dx} - A_c \dot{\omega}_k W_k = 0 \quad \text{Eq.3-22}$$

Where, Y_k is the mass fraction of the species, V_k is the diffusion velocity of the species and ρ is the mass density.

The state equations:

$$\rho = \frac{P \bar{W}}{RT} \quad \text{Eq. 3-23}$$

The continuity equation:

$$\dot{M} = \rho u A_c \quad \text{Eq. 3-24}$$

Where u is the velocity of the fluid mixture is, \bar{W} is the mean molecular weight of the mixture, P indicates the pressure and R is the gas constant.

In the governing conservation equations, the molar production rate of a species, $\dot{\omega}_k$, is actually related to the reaction kinetics of the elementary reactions involving the species. Therefore, the rate constant of the species is in the modified Arrhenius equation which is employed in the reaction kinetics simulation. The modified Arrhenius form is also shown as below:

$$k = AT^n \exp(-E_a / RT) \quad \text{Eq. 3-25}$$

Apart from the reaction rates and the basic governing conservation equations, the transport properties of the species are also be considered. The equations for transport properties are listed below:

$$v_{Dk} = D_{km} \frac{1}{X_k} \frac{dX_k}{dx} \quad \text{Eq. 3-26}$$

Where v_{Dk} is the ordinary diffusion velocity, X_k is the mole fraction of the species and D_{km} is evaluated from the binary diffusion coefficients, D_{kj} .

$$D_{km} = \frac{1 - Y_k}{\sum_{j \neq k}^K \frac{X_j}{D_{kj}}} \quad \text{Eq. 3-27}$$

The calculation of the thermal diffusion velocity is given as the equation shown below:

$$w_k = \frac{D_{km} \theta_k}{X_k} \frac{1}{T} \frac{dT}{dx} \quad \text{Eq. 3-28}$$

The boundary conditions were derived from the early works implemented by Hirschfelder and Curtiss (1949). The mass flux fraction and temperature are specified at the clod boundary, and solving the equations:

$$\epsilon_{in} - Y_c - \left(\frac{\rho A Y V}{\dot{M}} \right) = 0 \quad \text{Eq. 3-29}$$

and

$$T_{in} - T_f = 0 \quad \text{Eq. 3-30}$$

Where ε_m is the inlet reactant fraction of the species, Y_c is the mass fraction of the species at clod boundary, T_{in} is the temperature of inlet flow and T_f is the fixed temperature at clod boundary.

On the other hand, the species and temperature gradients vanish at the hot boundary:

$$\frac{Y_j - Y_{j-1}}{X_j - X_{j-1}} \quad \text{Eq. 3-31}$$

and

$$\frac{T_j - T_{j-1}}{X_j - X_{j-1}} \quad \text{Eq. 3-32}$$

Where j indicates the grind point at the hot boundary.

3.5 Summary

- A brief introduction on the numerical reaction kinetics modelling shows that to carry out chemical kinetics simulation it is necessary to employ Arrhenius equation. The governing equations applied in CHEMKIN code for reaction kinetics equilibrium simulation are given.
- The thermodynamic data, such as enthalpy of formation and specific heat, is required associated with Arrhenius equation to calculate the rate constant and reaction rate. The species enthalpy and entropy are required to calculate equilibrium constant K_c and forward rate constant k_f to obtain the production rate and species concentration.
- The chain branching reactions are responsible for producing free radicals and sensitive to combustion reaction rates. They play important role in H_2 and hydrocarbon oxidation reactions and also have the impact on the laminar burning velocity.
- A relatively comprehensive combustion mechanism covering C_1 - C_4 was

developed by Warnatz and Heghes (2006). The important chain branching reactions in H₂ oxidation mechanism and the decomposition of methane, ethane and propane are included in the mechanism.

Chapter 4

Literature Review of Flame Stability Mechanism

The flame stability mechanism is determined by local flame speed and local inlet flow velocity. The flame lift-off and blow-out characteristics influence the performance of gas turbines and gas burners. It also can cause safe handling issues in combustions.

This chapter gives the definitions of the flame lift-off and blow-out parameters. It also presents the relationships of the flame burning velocity with stability parameters. A literature review of flame lift-off and blow-out characteristics of H₂ and hydrocarbon is also given in this chapter.

4.1 Definitions of Flame Lift-Off and Blow-Out Parameters

The light emitted from the flame is due to the heat of the flame and the chemical reactions within the flame zone. The basis of the flame is formed by the combustion of gas. The temperature gradient and the flame zone in which chemical reactions take place decide the location of the flame. The flame stability is often associated with the phenomena which are presented as a result of the balance between the flow velocity and the flame speed. The phenomena includes three flame stability mechanisms, consisting of the attached flame on the burner rim, the lifted base of the flame from the burner rim and the flame being extinguished as a lifted flame or an attached flame (Wu, 2010). For a fixed flame above a stabilised burner, when the flame speed is far greater than the inlet velocity of the fuel supply, the flame will propagate into the cross-section area of

the barrel of the burner to cause flashback. However, on the other hand, when the flame speed is too small compared with the inlet velocity the flame will approach blow-out/off situation (Kuo, 2005). The flame stability is usually referred to as liftoff height, liftoff velocity and blow-out velocity. The blowout velocity indicates the velocity at which the reaction cannot be sustained and the flame is extinguished. The lift-off velocity is defined as the inlet gas velocity at which the flame is lifted above the burner rim (Wu, 2010). A sketch of a lifted jet diffusion flame is shown in Figure 4.1. As shown in the figure, flame liftoff height is the height that the flame lifted from the exit of the burner due to high jet velocity. At relative low jet exit velocity, the flame is attached at the exit of the jet. With increased jet velocity, the flame starts to be lifted and the liftoff height increases with increased jet velocity. As the definition of laminar burning velocity, the flame plane moves to the unreacted gas. This can be described by reaction kinetics. So, the laminar burning velocity makes the flame moves against the jet velocity. As keeping increased jet velocity, a turbulent mixing region occurs under the flame base and the flame attempts to move down to reach the stabilised state.

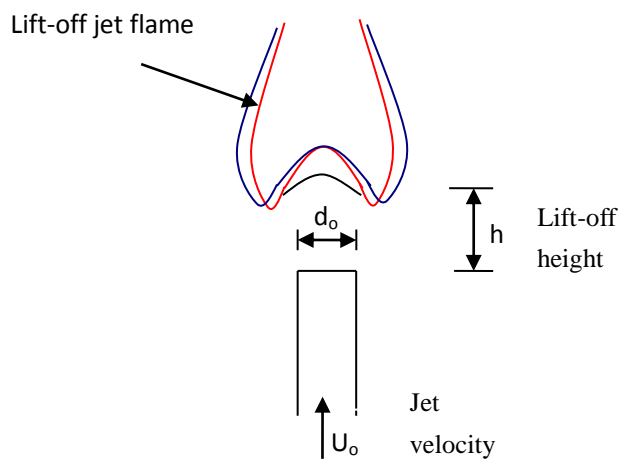


Figure 4.1: Schematic of a lifted jet diffusion flame

The flame is extinguished not only for a lifted flame but also an attached flame. The flame reaches the blow-out condition without experiencing lift-off stage. This phenomenon is referred to as flame blow-off, which is distinguished with blow-out (Wu, 2010). On the other hand, if the flame velocity is higher than the jet flow velocity, the flame can propagate into the upstream through the burner barrel or port without quenching to result in flashback situation (Kuo, 2005). Lewis and von Elbe (1961) proposed a velocity profile that assumed a flame just entering the burner tube and described the velocity gradients slightly inside the tube. The distance from the tube wall while the flame just entered the tube is half of the quenching distance, d_q . When the distance is smaller than the quenching distance the flame can not propagate into the tube (Kuo, 2005). If the inlet gas velocity is greater than the burning velocity, the flame inside the tube will then be blown out from the tube. The critical flashback condition is reached when the local gas velocity equals to the burning velocity.

4.2 Flame Stabilisation Models

Generally, the flame stabilisation models can be classified into three categories, which include the premixed flame propagation models, the laminar flamelet models and the large-scale turbulent structural mixing models (Wu, 2010).

In the premixed flame propagation models, the premixing condition ahead of the flame front of lifted flame is considered. Vanquickenborne and van Tiggelen (1966) conducted experimental measurements for turbulent jet methane flames over a range of jet exit diameter and inlet jet velocity. They showed that the lifted diffusion flame stabilised at the position at which the flame base was anchored in a turbulent mixing region, in which the turbulent burning velocity was balanced by the inlet gas velocity. In addition, at that position, the time-averaged reactant mass fraction equalled to stoichiometric condition at the flame base. The model is described in Figure 4.2.

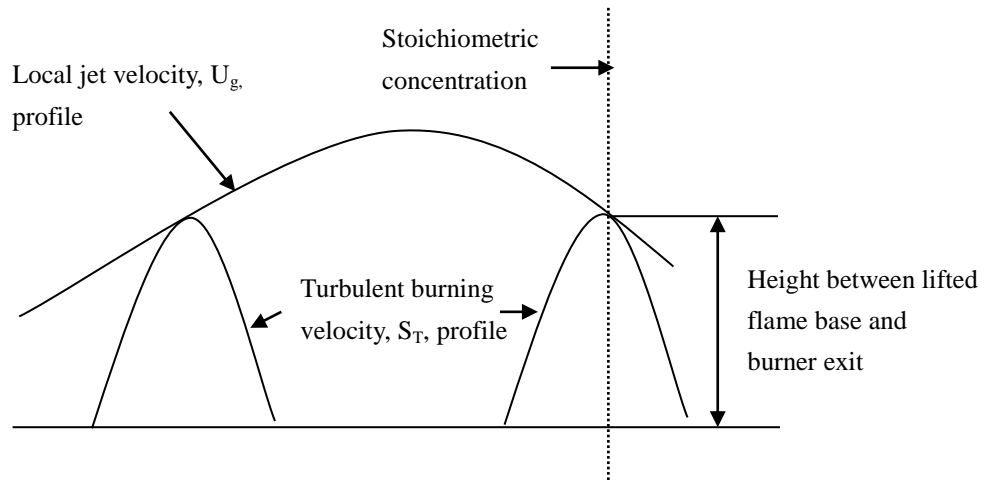


Figure 4.2: The illustration of premixed flame model

As shown in Figure 4.2, the model proposes that in the region between the lifted flame base and the inlet gas exist the flame lift-off height provides enough space for the gaseous fuel and the diffusing air to reach the premixed condition. When the lifted flame base is at the position in which fuel rich or fuel lean condition is reached, the balance between the flame burning velocity and the local jet velocity no longer exists and then the flame reaches blow-out condition. Many studies (Eickhoff et al., 1984 and Waston et al., 1999) have been conducted to testify the premixed flame propagation model. In these studies, the premixing region was found to take place ahead of the lifted flame base.

In the laminar flamelet models, the flame lift-off is considered as the result of laminar flamelets quenching (Wu, 2010). It was suggested in the studies (Peters and Williams 1983 and Peters, 1986) the flame lift-off was the result of flame extinction taking place in the turbulent structures near the unburned gaseous mixture. The typical lift-off heights, 30-300 mm, were too short for the gaseous mixture to reach premixing condition in the turbulent jets. They described the diffusion flames as an ensemble of laminar diffusion flamelets, which were anchored by the influence of local turbulence. The flame was stabilised at the

position in which the combustion extinction and flame propagation were in balance. However, this hypothesis was not supported by Eickhoff et al. (1984), Waston et al. (1999) and Everest et al. (1996). In these studies, the premixing was found between the inlet unburned gaseous mixture and the lifted flame base.

The large scale structural mixing model assumed the flame lift-off is caused by the flame extinction resulting from the large scale turbulent structures. The principle of this model was proposed by Broadwell et al. (1983). In this model, the blow-out phenomena are contributed by the entrainment of the burned gases with the mixture of non-flammable jet gases under large scale turbulent structures (Wu, 2010). Before the unburned gaseous mixture is ignited by the hot gases, the hot gaseous products are entrained by the incoming non-flammable gases, which are able to quench the hot gases.

4.3 Relationship of Burning Velocity with Flame Lift-Off and Blow-Out Characteristics

The experimental investigations of the flame lift-off have been conducted by many studies (Eickhoff et al, 1985; Savas and Gollahali, 1986; Wohl et al., 1949; Scholefield and Garside, 1949). The premixed flame propagation model proposed by Vanquickenborne and van Tiggelen (1966) was agreed with the results from the experiments implemented by Hall et al. (1980). They also indicated in that at the flame base the fuel-air mixture had the maximum laminar burning velocity. Compared with their studies, Kalghatgi (1984) conducted an extensive experimental investigation upon the flame lift-off. This investigation reported that the lift-off height increased linearly with the inlet gas velocity and it was inversely proportional to the square of the maximum lamina burning velocity of the gaseous mixture. He also showed that the lift-off height was independent of the diameter of the jet exit for a given inlet gas velocity. Hall et al (1980) and Gunther et al

(1981) proposed an identical model to correlate laminar burning velocity and turbulent burning velocity by the local turbulence properties. It is shown below:

$$S_t / S_L = k \times \text{Re}_t \quad \text{Eq. 4-1}$$

Where k is a constant, Re_t is the turbulent Reynolds number resulted from the velocity fluctuations and local kinetic viscosity, S_t is the turbulent burning velocity and S_L represents the laminar burning velocity.

Kalghatgi (1984) correlated the experimental results by assuming the flame stability model proposed by Vanquickenborne and van Tiggelen (1966). Thus, the liftoff height of a flame is governed by the laminar burning velocity and the jet velocity. The correlation between flame liftoff height and laminar burning velocity was given by Kalghatgi (1984). It is shown as below and this experimental correlation can be applied to help to predict the relationship between laminar burning velocity and flame stability.

$$h = C_2 \left(\frac{U_o}{S_L} \right) \left(\frac{\rho}{\rho_e} \right)^{1.5} \nu_e \quad \text{Eq. 4-2}$$

Where, h is the lift-off height, S_L is the laminar burning velocity, ν_e is the kinematic viscosity at the jet exit, C_2 is Constant equaling to 50, U_o is the gas velocity at the jet exit, $\frac{\rho}{\rho_e}$ = density ratio of the density of the gas at the jet exit, ρ_e , to the density of the ambient air, ρ_∞

However, Pitts (1988) implied that the empirical correlation of Kalghatgi (1984) can be correlated to be more accurate. The correlation is written as:

$$h \propto \frac{U_0}{S_L^2} \quad \text{Eq. 4-3}$$

This expression implies that the lift-off height is independent of jet exit diameter, kinetic viscosity and mass fraction.

Based on the premixed flame propagation model, Kalghatgi (1981) also developed an experimental correlation between the blow-out velocity and burner diameters for CH₄-air, CH₄-CO₂, C₃H₈-air and C₃H₈-CO₂ mixtures. It is expressed as below:

$$U_b = S_L \left(\frac{\rho_\infty}{\rho_e} \right)^{1.5} \times 0.017 \text{Re}_H \left(1 - 3.5 \times 10^{-6} \text{Re}_H \right) \quad \text{Eq.4-4}$$

Where U_b is the blow-out velocity and Re_H is Reynolds number based on dimensionless height, H_h , which is expressed as following:

$$H_h = \left[4 \frac{Y_0}{Y_{ST}} \left(\frac{\rho_e}{\rho_\infty} \right)^{0.5} + 5.8 \right] d_0 \quad \text{Eq.4-5}$$

Where Y_0 is the mass fraction at burner exit, Y_{ST} is the stoichiometric mass fraction and d_0 is the burner diameter.

Based on the large scale structural mixing model, Broadwell et al. (1983) proposed a correlation concerning blow-out velocity as a function of burner diameter and flame speed. The expression is shown as follow:

$$\varepsilon_B = \frac{d_0 S_L^2 \Psi^2 \left(\frac{\rho_e}{\rho_\infty} \right)^{0.5}}{\aleph U_b} \quad \text{Eq.4-6}$$

Where Ψ refers to the stoichiometric air to fuel ratio, \aleph represents the diffusivity and ε_B is a critical value calculated from large scale mixing time divided by the reaction time.

The predictions of blow-out velocity were agreed well with the data of Kalghatgi (1981).

4.4 Flame Stability of Hydrogen and Hydrocarbons

Wu et al. (2009) studied the liftoff, blowout and blow off stability limits of the jet flames of pure hydrogen and hydrogen-hydrocarbon mixtures, in which they experimentally tested the stability of hydrogen jet flame with addition of propane, methane, carbon dioxide and argon. It gave a view of the stability of hydrogen flame with addition of propane and methane. The experiment showed the characteristics of the visual flames stability for different blended hydrogen-hydrocarbon fuels. The study showed when the methane concentration was greater than 40% the H₂-CH₄ flame remain attached until blow-off state, while if the concentration was less than 40%, the flame reached blow-out condition after experiencing lifted state. For H₂-C₃H₈ flames, the addition of propane into hydrogen produced lifted flames and the lift-off height of the hydrogen flame increased. The paper also conducted the comparison of flame stability between pure H₂ and H₂-CH₄ and H₂-CH₈. They indicated that the liftoff velocity for pure hydrogen flame was 730 m/s and the height of liftoff increased linearly with liftoff velocity. The addition of C₃H₈ always produced lifted flames and increased the liftoff height. On the other hand, the flame stability of H₂-CH₄ depended on the concentration of the amount of the additional CH₄. For testing the flame stability of pure hydrogen flame, the study was compared with other studies (eg. Kalghatgi, 1984; Fu and Wu, 2001; Cheng and Chiou, 1998), in which

different imaging techniques were used.

The findings on flame stability by Wu et al. (2009) complemented the study by Schefer (2003) which determined the effects of hydrogen addition on flame stability of methane, for premixed and swirl-stabilised flame. It indicated that the addition of hydrogen caused an extension of the lean stability limit, depending on the concentration of the addition. Generally, the addition of up to 20% hydrogen increased the peak OH mole fractions about 20% and reduced the lean stability limit by about 15%. (Schefer, 2003).

Wu et al. (2007) used a straight concentric burner to produce co-axial flow and central flow jet flames. The study showed that both of propane and CO₂ had contributions on causing flame blowout, however, addition of propane was more sensitive in producing lifted flame. They also used the correlation proposed by Kalghatgi (1984) to correlate the laminar burning velocity and the flame lift-off height.

4.5 Summary

- The blowout velocity indicates the velocity at which the reaction cannot be sustained and the flame is extinguished.
- The lift-off velocity is defined as the inlet gas velocity at which the flame is lifted above the burner exit.
- The fame liftoff height is the height that the flame lifted from the exit of the burner due to high jet velocity.
- In the premixed flame propagation models, the premixing condition ahead of the flame front of lifted flame is considered. At the lifted flame base, the burning velocity is balanced with the local inlet jet velocity.
- In the laminar flamelet models, the flame lift-off is considered as the result of laminar flamelets quenching

- The large scale structural mixing model assumed the flame lift-off is caused by the flame extinction resulting from the large scale turbulent structures.
- The empirical correlations proposed by Kalghatgi show the relationship between burning velocity and flame lift-off height and blow-out velocity.

Chapter 5

Experimental Study of the Lift-off and Blow-out Stability of Hydrogen/hydrocarbon Flames

Chapter 4 has shown that the position of the flame base is determined by the result of the laminar burning velocity and the inlet jet velocity and the flame lift-off height can be correlated with the laminar burning velocity of the combustible mixture. An experimental programme is designed to determine the flame lift-off velocity, lift-off height and blow-out velocity. The aim of the experimental study is to examine the effect of hydrogen concentration and the presence of carbon dioxide on the flame stability characteristics of hydrogen-hydrocarbon and hydrogen-methane-carbon dioxide mixtures.

This chapter presents a brief explanation on the methodology of the experiment and the experimental rig employed. The data obtained and the flame images captured from the experiment is presented. The chapter also gives a discussion on the flame lift-off and blow-out characteristics of $\text{H}_2\text{-CH}_4$, $\text{H}_2\text{-C}_2\text{H}_6$, $\text{H}_2\text{-C}_3\text{H}_8$, $\text{H}_2\text{-CO}_2$ and $\text{H}_2\text{-CH}_4\text{-CO}_2$ gaseous mixtures.

5.1 Experimental Programme

5.1.1 Experimental Method

The jet diffusion flames were produced from a Bunsen burner with 2mm inner diameter and a settling chamber. $\text{H}_2\text{-CH}_4$, $\text{H}_2\text{-C}_2\text{H}_6$, $\text{H}_2\text{-C}_3\text{H}_8$, $\text{H}_2\text{-CO}_2$ and $\text{H}_2\text{-CH}_4\text{-CO}_2$ gaseous mixtures were used in order to simulate the flame stability characteristics of syngas. The hydrogen, hydrocarbons and carbon dioxide gases

were introduced from separated compressed gas cylinders. The gas mixture first entered a premixer and then went through the burner to produce jet diffusion flames. The attached flame, lifted flame and flame blow-out/off phenomenon were captured by using a commercial digital camera. The various compositions of the gas mixtures were achieved by adjusting the flowrate of each component in the mixture. The exit jet velocity was calculated from the overall flowrate of the gas mixture by using the equation below:

$$U_0 = \frac{F}{A_c} \quad \text{Eq.5-1}$$

Where U_0 is the exit jet velocity, F indicates the total flowrate of the gas mixture and A_c presents the cross-section area of the burner nozzle.

The flame lift-off height was measured from the flame images, which was the measurement of the distance from the flame base to the exit of the burner nozzle. The flame lift-off and blow-out data was then acquired at different H₂-Hydrocarbon ratios and H₂-CO₂ ratios to determine the effect of H₂ and CO₂ concentration on the flame stability mechanism of the gaseous mixtures. This approach of determining the flame stability parameters has been well documented and described in Kalghatgi (1984), Miake-Lye and Hammer (1989), Wu et al. (2007) and Wu, et al. (2009).

5.1.2 Experimental Rig

The experiment was conducted by employing a flame stability test rig, consisting of a gases preparing and mixing part and a flame producing and image capturing part. The former included a burner and a digital camera, the latter was composed by compressed gas cylinders, flowmeters and a premixer. As shown in Figure 5.1 (i), the gases were deposited in the compressed gas bottles. The flowrates of the

gases were controlled by the flowmeters shown in Figure 5.1 (ii). As shown in Figure 5.1 (iii), the premixed gaseous fuels were introduced into the burner from the bottom of the burner, which allows circulated and centralised flow. However, only centralised flow was applied in this study. A front view of the top of the burner is given in Figure 5.1 (iv). Figure 5.2 shows the geometry of the burner. The flow straight device in the settling chamber ensured the uniform and straight gas flow going through the burner. The use of 2mm inner diameter for the burner nozzle resulted in relatively high exit jet velocity. To make sure producing the lifted flame high gas jet velocity is required, since the lift-off velocity of pure H_2 flame is very high and over 800m/s.

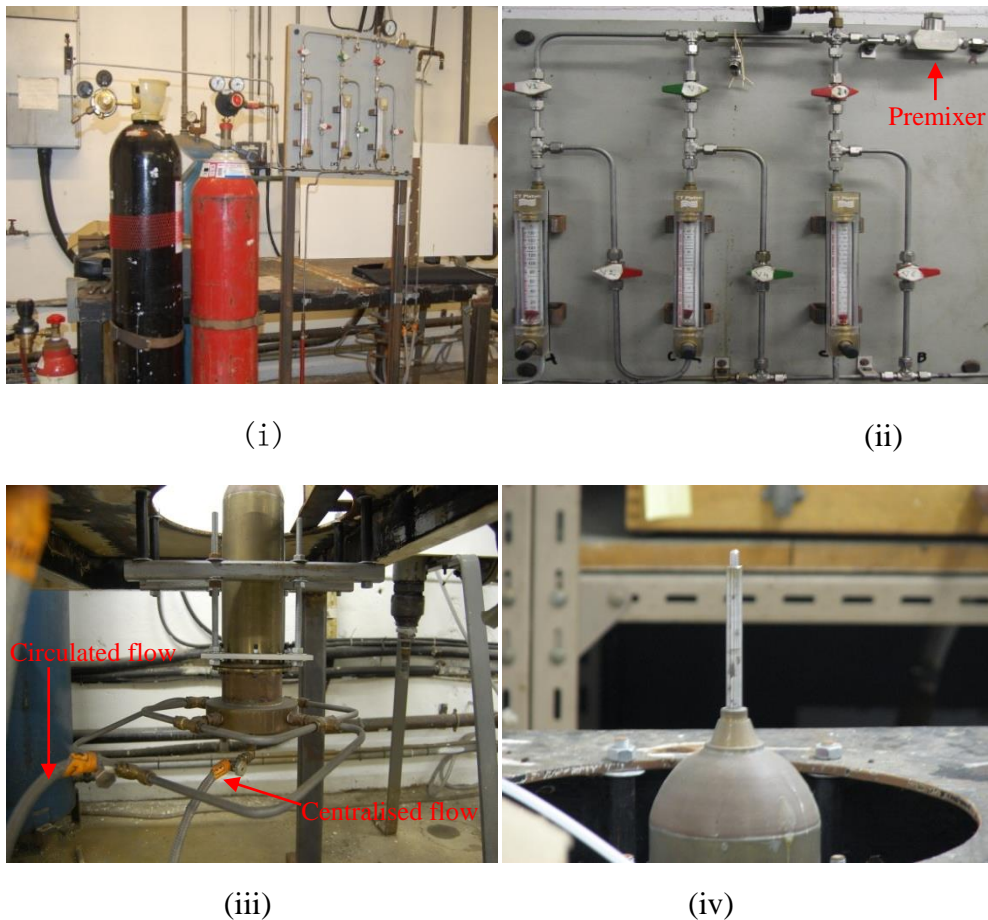


Figure 5.1: The rig employed in the flame stability experiment
(i) overview of the experiment rig (ii) control panel
(iii) the bottom part of the burner (iv) front view of the burner

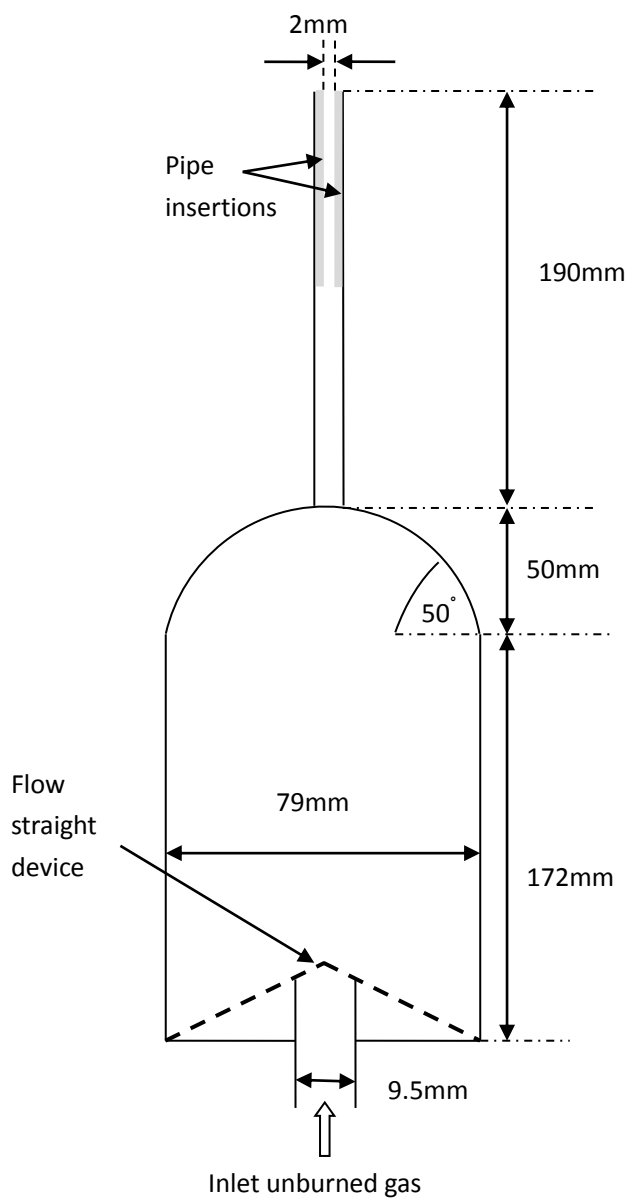


Figure 5.2: The schematic and geometry of the burner used in the experiment

The flame images were captured by a commercially digital camera. The model of the camera was Canon PowerShot S3IS. The resolution of the camera was up to 6.0 megapixels and the sensitivity range was up to ISO 800. The flame images were deposited as pictures and processed in a computer. The pictures had 2816×2112 pixels, with horizontal and vertical resolution of 180 dpi. The pictures were then analysed by employing CorelDRAW, which is an engineering graphic design software and capable of measuring the distance on a given picture. The lift-off height was measured as the distance between the flame base points and the burner nozzle exit. If the flame base points were not at the same horizontal level, an average value was then taken.

5.1.3 The Gaseous Mixtures Preparing and Mixing

Figure 5.3 illustrates the flowchart of the experiment programme. The components of the gaseous mixture came from the compressed gas cylinders which were capable of mixing up to three different gases. The compositions of gaseous mixtures were adjusted by the flowmeters, as indicated F1, F2 and F3 in Figure 5.3. The jet diffusion flame was then produced above burner. The experiments were carried out under room temperature and atmospheric pressure. The standard flowmeter tubes were calibrated for atmospheric pressure at the flowmeter outlet, however, if the operating pressure was different the reading required to be corrected to the actual flowrate at ATP condition. The equation for the correction is given below:

$$\text{Actual flow rate at ATP} = \sqrt{\frac{P(\text{Bar}_{abs})}{1.013}} \times \text{Scale reading} \quad \text{Eq.5-2}$$

Where P indicates the pressure reading from the piezometer.

As shown in Appendix F-H, methane, ethane and propane were added into hydrogen to produce $\text{H}_2\text{-CH}_4$, $\text{H}_2\text{-C}_2\text{H}_6$ and $\text{H}_2\text{-C}_3\text{H}_8$ flames. The flowrate of

hydrogen was fixed at 20 l/min and 40 l/min. The hydrocarbons flowrate increased systematically until the blow-out/off was observed. The readings of the pressure were recorded and the flowrates were corrected to the actual ATP flowrate with gauged pressure. This gave hydrogen concentration varied from 70-100 vol. % for H₂-CH₄ flames, 80-100 vol. % for H₂-C₂H₆ flames and 85-89 vol. % for H₂-C₃H₈ flames.

The compositions of the H₂-CH₄-CO₂ mixtures are shown in Appendix I and J. The flowrate of hydrogen was fixed at 20 l/min and 40 l/min. It was difficult to handle three components at the same time. Thus, for each set of the test the flowrates of hydrogen and CO₂ were fixed and increased the flowrate of methane systematically until the blow-out/off being observed. The flowrate of CO₂ then increased with fixed hydrogen flowrate. The experiment was then repeated in this manner until the flame reached its flammability. For hydrogen flowrate of 40 l/min, the hydrogen concentration in the mixture varied from 71-99%, the methane concentration varied from 0-28 % and the CO₂ concentration was in the range of 1-10 %. On the other hand, for hydrogen flowrate of 20 l/min, the hydrogen concentration in the mixture varied from 60-98%, the methane concentration varied from 0-39 % and the CO₂ concentration was in the range of 1-24 %.

As shown in Appendix K, H₂ was mixed with CO₂ to produce the H₂-CO₂ flames. The flowrate of CO₂ was fixed while H₂ flowrate was increased at each experimental set. The initial CO₂ flowrate increased from 0.4 l/min to 7 l/min. The volumetric concentration of CO₂ was in the range of 0.4%-24%. On the other hand, the hydrogen concentration varied from 76-99%.

To produce pure H₂ jet diffusion flames, the initial H₂ flowrate increased from 10 to 150 l/min. The flowrate increased by 10 l/min at each run. This is shown in Appendix L.

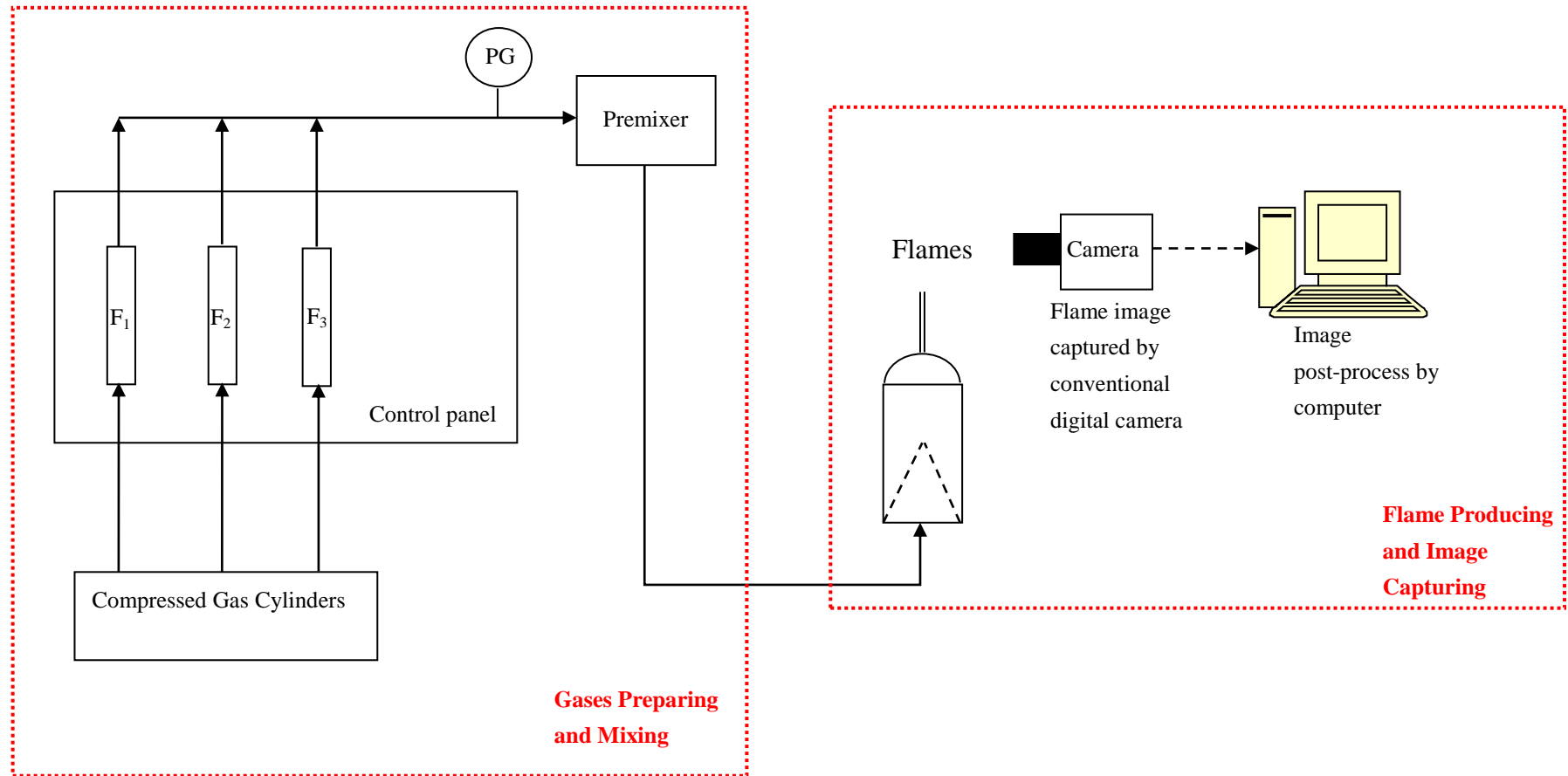


Figure 5.3: Schematic of the stability experimental set-up

5.2 Experimental Results

5.2.1 Experimental Results for Pure H₂ Flames

As shown in Table 5.1, the pure H₂ jet diffusion flame reaches lifted state at 803 m/s corresponding to the initial H₂ flowrate of 120 l/min. There is no blow-out observed until the jet velocity approaching 1094 m/s. The flames remain at attached state at the jet velocities in the range of 53 to 689 m/s. The lift-off heights of the flames are obtained from the flame images. They increase with the jet velocity.

Table 5.1: The lift-off heights and lift-off velocities for pure H₂ flames

Exit jet velocity [m/s]	Flame status	Flame Lift-off Height [mm]	Flame Images
803	Lift-off	24	Fig.5.1-1
897	Lift-off	26	Fig.5.1-2
993	Lift-off	28	Fig.5.1-3
1094	Lift-off	31	Fig.5.1-4

The lifted flame images corresponding to the jet velocities and lift-off heights are presented in Figure 5.4. It is clearly shown in the figure that the flames are lifted from the nozzle exit.

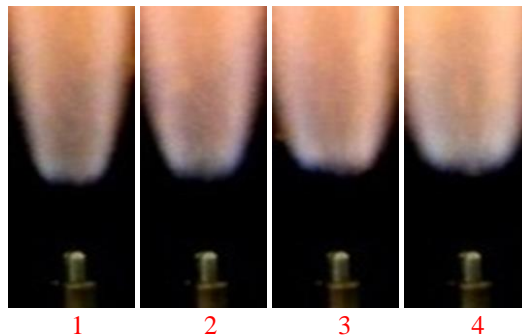


Figure 5.4: The images of lifted pure H₂ flames

5.2.2 Experimental Results for H₂-CH₄ Flames

As shown in Table 5.2, the jet velocities of lifted H₂-CH₄ flames are in the range of 167-192 m/s for initial H₂ flowrate of 20 l/min. On the other hand, for 40 l/min H₂, the lift-off velocities are in the range of 302-363 m/s. The flames remain at attached state at the jet velocities in the range of 106-154 m/s and 212-296 m/s, for 20 and 40 l/min initial H₂ flowrate respectively. For 20 l/min H₂, the flame blows out at 197 m/s. For 40 l/min initial H₂, the flame reaches blow-out condition at 370 m/s. At 20 l/min hydrogen flowrate, the hydrogen concentration in the mixture is from 59-67% from lift-off to blow-out state. On the other hand, at 40 l/min hydrogen flowrate condition, it is from 70-80%. It can be seen from the Table that the lift-off heights increase with the jet velocity for each H₂ flowrate level. The flame images correspond to the lifted flames are shown in Figure 5.5.

Table 5.2: The lift-off heights, lift-off velocities and blow-out velocities for H₂-CH₄ flames

H ₂ initial flow rate [l/min]	Exit velocity [m/s]	CH ₄ vol. %	Flame status	Flame lift-off height mm	Flame images
20	167	33	Lift-off	12	Fig. 5.2-1
	172	35	Lift-off	19	Fig. 5.2-2
	178	38	Lift-off	29	Fig. 5.2-3
	192	39	Lift-off	31	Fig. 5.2-4
	197	41	Blow-out	-	Fig. 5.2-5
40	302	20	Lift-off	17	Fig. 5.2-6
	320	22	Lift-off	22	Fig. 5.2-7
	326	23	Lift-off	29	Fig. 5.2-8
	332	25	Lift-off	41	Fig. 5.2-9
	338	26	Lift-off	49	Fig. 5.2-10
	345	27	Lift-off	51	Fig. 5.2-11
	363	29	Lift-off	61	Fig. 5.2-12
	370	30	Blow-out	-	Fig. 5.2-13

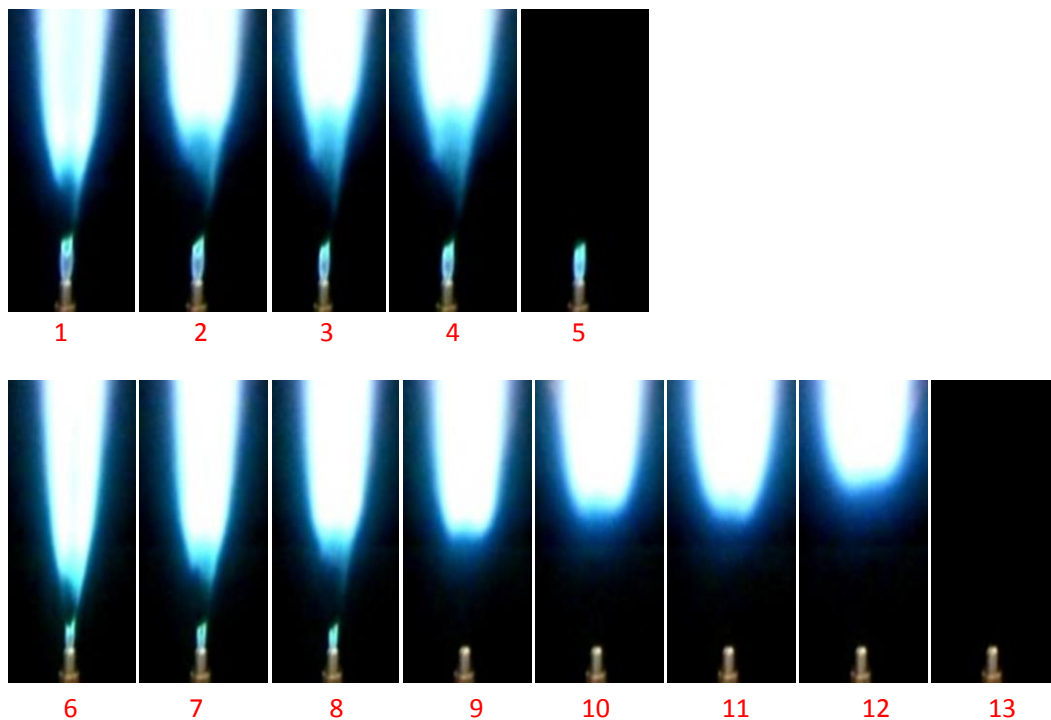


Figure 5.5: The flame images for $\text{H}_2\text{-CH}_4$ flames at lift-off and blow-out conditions

5.2.3 Experimental Results for $\text{H}_2\text{-C}_2\text{H}_6$ Flames

In terms of $\text{H}_2\text{-C}_2\text{H}_6$ flames, the flames reach lift-off state at 144 and 266 m/s for 20 l/min and 40 l/min initial H_2 flowrate respectively. The flames remain at attached state at the jet velocities in the range of 106-133 m/s and 212-262 m/s, for 20 and 40 l/min initial H_2 flowrate respectively. For 20 l/min H_2 , the flame blows out at 167 m/s. For 40 l/min initial H_2 , the flame reaches blow-out condition at 326 m/s. The lift-off heights of the flames increase with the jet velocities for each fixed H_2 flowrate. For H_2 flowrate fixed at 20 l/min, the flame reaches lifted state at 23% C_2H_6 and blows out at 30% C_2H_6 in the mixture. When H_2 flowrate is fixed at 40 l/min, the flame lifts off at 13% C_2H_6 and blows out at 20% C_2H_6 in the mixture. The experimentally determined lift-off and blow-out characteristics for $\text{H}_2\text{-C}_2\text{H}_6$ flames are summarised in Table 5.3. The flame images of $\text{H}_2\text{-C}_2\text{H}_6$ mixture corresponding to lift-off and blow-out state are shown in Figure 5.6.

Table 5.3: The lift-off heights, lift-off velocities and blow-out velocities for $H_2-C_2H_6$ flames

H_2 initial flow rate [l/min]	Exit velocity [m/s]	C_2H_6 vol. %	Flame status	Flame lift-off height mm	Flame images
20	144	23	Lift-off	9	Fig.5.2-1
	148	25	Lift-off	21	Fig.5.2-2
	159	27	Lift-off	43	Fig.5.2-3
	163	29	Lift-off	45	Fig.5.2-4
	167	30	Blow-out	/	Fig.5.2-5
40	266	13	Lift-off	24	Fig.5.2-6
	281	14	Lift-off	36	Fig.5.2-7
	286	15	Lift-off	40	Fig.5.2-8
	301	17	Lift-off	43	Fig.5.2-9
	306	18	Lift-off	45	Fig.5.2-10
	310	19	Lift-off	54	Fig.5.2-11
	326	20	Blow-out	/	Fig.5.2-12

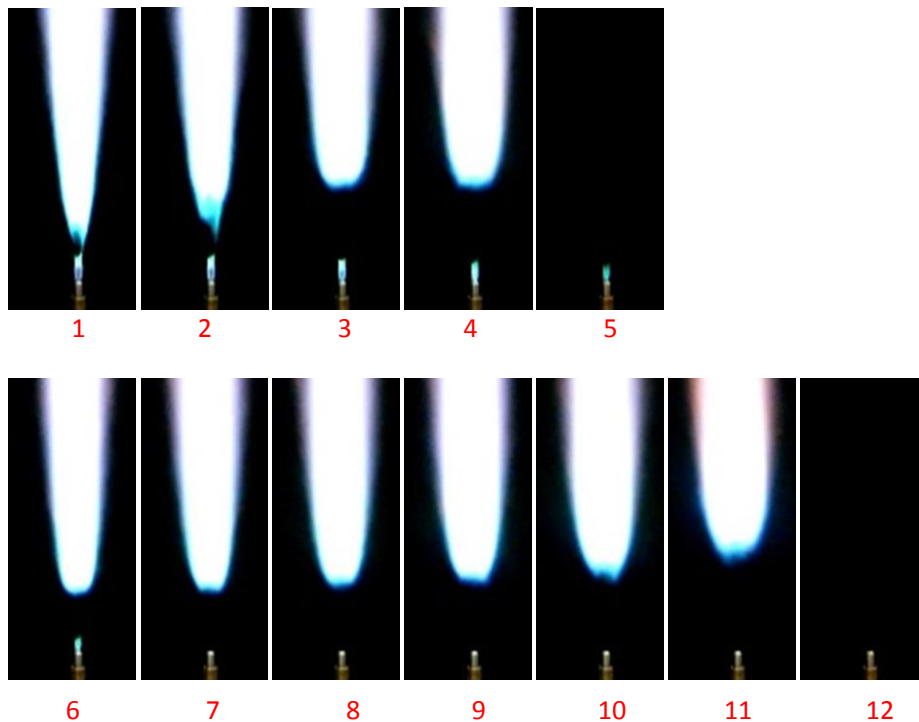


Figure 5.6: The flame images for $H_2-C_2H_6$ flames at lift-off and blow-out conditions

5.2.4 Experimental Results for H₂-C₃H₈ Flames

As shown in Table 5.4, in terms of H₂-C₃H₈ flames, the flames reach lift-off state at 148 and 257 m/s for 20 l/min and 40 l/min initial H₂ flowrate respectively. The flames remain at attached state at the jet velocities in the range of 119-144 m/s and 246-253 m/s, for 20 and 40 l/min initial H₂ flowrate respectively. For 20 l/min H₂, the flame blows out at 155 m/s. For 40 l/min initial H₂, the flame reaches blow-out condition at 274 m/s. The lift-off heights of the flames increase with the jet velocities for each fixed H₂ flowrate. For H₂ flowrate fixed at 20 l/min, the flame reaches lifted state at 21% C₃H₈ and blows out at 25% C₃H₈ in the mixture. When H₂ flowrate is fixed at 40 l/min, the flame lifts off at 10% C₃H₈ and blows out at 15% C₃H₈ in the mixture. The flame images of H₂-C₃H₈ mixture corresponding to lift-off and blow-out state are shown in Figure 5.7.

Table 5.4: The lift-off height, lift-off velocities and blow-out velocities for H₂-C₃H₈ flames

H ₂ initial flow rate [l/min]	Exit velocity [m/s]	C ₃ H ₈ vol. %	Flame status	Flame lift-off height mm	Flame images
20	148	21	Lift-off	55	Fig.5.4-1
	151	23	Lift-off	60	Fig.5.4-2
	155	25	Blow-out	-	Fig.5.4-3
40	257	10	Lift-off	21	Fig.5.4-4
	260	11	Lift-off	43	Fig.5.4-5
	267	13	Lift-off	48	Fig.5.4-6
	274	15	Blow-out	-	Fig.5.4-7

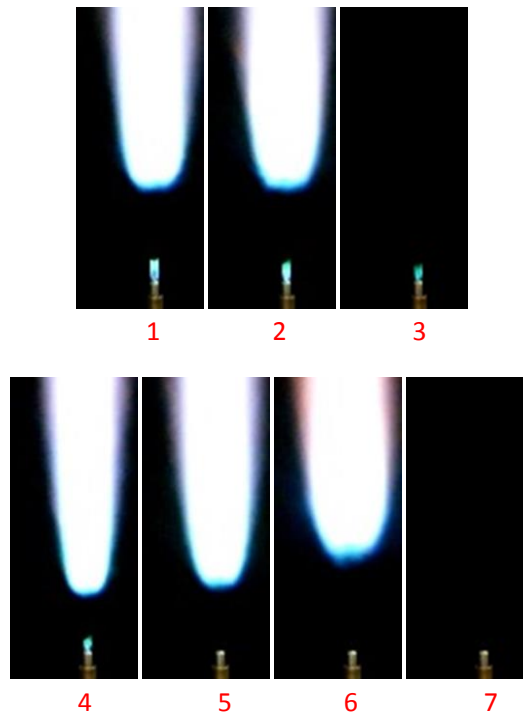


Figure 5.7: The flame images for $\text{H}_2\text{-C}_3\text{H}_8$ flames at lift-off and blow-out conditions

5.2.5 Experimental Results for $\text{H}_2\text{-CH}_4\text{-CO}_2$ Flames

As shown in Table 5.5, for 20 l/min initial hydrogen flowrate, the jet velocity at lifted state has the range of 160-194 m/s. The hydrogen concentration is in the range of 60-70% and the CO_2 concentration is from 1-7%. When the CO_2 concentration exceeds 8%, the flames reach blow-off condition without experiencing lift-off state. The CO_2 concentration in the mixture is up to 22%. Table 5.6 presents the experimental results for 40 l/min initial hydrogen flowrate. The jet velocity at lifted state has the range of 283-361 m/s. The hydrogen concentration is from 71-88% and the CO_2 concentration is from 1-10%. After 8% CO_2 , the flames reach blow-off conditions. The lift-off heights increases as the jet velocity for both 20 and 40 l/min hydrogen flowrate. For 20 l/min initial H_2 flowrate, there are some flames presenting fluctuation phenomenon, at which the flames reach critical condition just before approaching blow-out condition. Figure 5.8 shows the lifted and fluctuated flame images for the mixtures with 20 l/min H_2 . Figure 5.9 presents the lifted flame images for the mixtures with initial H_2 flowrate of 40 l/min.

Table 5.5: The lift-off heights, lift-off velocities and blow-out velocities for H₂-CH₄-CO₂ flames with initial hydrogen flowrate at 20 l/min

Jet Velocity [m/s]	H ₂ vol.%	CH ₄ vol.%	CO ₂ vol.%	Flame lift-off height [mm]	Flame status	Flame images
171	68	31	1	36.3		Fig.5.5-1
177	66	33	1	56		Fig.5.5-2
182	64	35	1	61.5		Fig.5.5-3
188	62	37	1	67.1		Fig.5.5-4
194	60	39	1		Blow-out	
160	69	28	3	27.9		Fig.5.5-5
173	67	30	3	44.7		Fig.5.5-6
179	65	32	3	58.9		Fig.5.5-7
185	63	35	3		Fluctuation	Fig.5.5-8
191	61	37	3		Blow-out	
170	68	27	4	33.7		Fig.5.5-9
176	66	30	4	72.9		Fig.5.5-10
181	64	32	4		Fluctuation	Fig.5.5-11
187	62	34	4		Blow-out	
167	70	24	6	27.9		Fig.5.5-12
172	67	27	6	36.3		Fig.5.5-13
178	65	29	6		Fluctuation	Fig.5.5-14
184	63	32	5		Blow-out	
169	69	24	7	30.8		Fig.5.5-15
175	66	27	7	39.5		Fig.5.5-16
181	64	29	7		Blow-out	
171	68	24	9		Fluctuation	Fig.5.5-17
177	65	26	8		Fluctuation	Fig.5.5-18
183	63	29	8		Fluctuation	Fig.5.5-19
189	61	31	8		Blow-off	
174	67	23	10		Fluctuation	Fig.5.5-20
180	65	26	10		Fluctuation	Fig.5.5-21
186	63	28	9		Blow-off	
171	68	20	12		Fluctuation	Fig.5.5-22
176	66	23	11		Fluctuation	Fig.5.5-23
182	64	26	11		Fluctuation	Fig.5.5-24
188	62	28	11		Blow-off	
173	67	20	13		Fluctuation	Fig.5.5-25
179	65	23	13		Blow-off	
176	66	20	14		Fluctuation	Fig.5.5-26

Jet Velocity	H ₂	CH ₄	CO ₂	Flame lift-off height	Flame status	Flame images
[m/s]	vol.%	vol.%	vol.%	[mm]		
181	64	22	14		Blow-off	
172	67	17	16		Fluctuation	Fig.5.5-27
178	65	20	15		Fluctuation	Fig.5.5-28
184	63	22	15		Blow-off	
175	66	17	17		Blow-off	
171	68	14	19		Blow-off	
180	65	16	19		Blow-off	
176	66	13	21		Blow-off	

Table 5.6: The lift-off heights, lift-off velocities and blow-out velocities for H₂-CH₄-CO₂ flames with hydrogen flowrate of 40 l/min

Jet Velocity	H ₂	CH ₄	CO ₂	Flame lift-off height	Flame Status	Flame images
[m/s]	vol.%	vol.%	vol.%	[mm]		
304	79	20	1	36.3	Lift-off	Fig.5.6-1
322	78	21	1	42.1	Lift-off	Fig.5.6-2
328	76	23	1	50.5	Lift-off	Fig.5.6-3
334	75	24	1	58.9	Lift-off	Fig.5.6-4
340	74	26	1	64.4	Lift-off	Fig.5.6-5
347	72	27	1	78.4	Lift-off	Fig.5.6-6
353	71	28	1		Blow-out	
312	80	18	2	36.3	Lift-off	Fig.5.6-7
318	79	20	2	42.1	Lift-off	Fig.5.6-8
324	77	21	2	42.1	Lift-off	Fig.5.6-9
330	76	23	2	47.6	Lift-off	Fig.5.6-10
337	74	24	2	58.9	Lift-off	Fig.5.6-11
355	73	26	2	64.4	Lift-off	Fig.5.6-12
361	72	27	2		Blow-out	
297	81	16	3	42.1	Lift-off	Fig.5.6-13
314	80	18	3	47.6	Lift-off	Fig.5.6-14
321	78	20	3	47.6	Lift-off	Fig.5.6-15
327	77	21	2	50.5	Lift-off	Fig.5.6-16

Jet Velocity [m/s]	H ₂ vol.%	CH ₄ vol.%	CO ₂ vol.%	Flame lift-off height [mm]	Flame Status	Flame images
333	75	23	2	56	Lift-off	Fig.5.6-17
351	74	24	2		Blow-out	
294	82	14	4	42.1	Lift-off	Fig.5.6-18
311	81	16	3	42.1	Lift-off	Fig.5.6-19
317	79	18	3	53.1	Lift-off	Fig.5.6-20
323	77	19	3	53.1	Lift-off	Fig.5.6-21
341	76	21	3	61.5	Lift-off	Fig.5.6-22
347	75	22	3		Blow-out	
307	81	14	4	39.23	Lift-off	Fig.5.6-23
313	80	16	4		LO & BO	
297	84	11	5	35.7	Lift-off	Fig.5.6-24
304	82	12	5	39.3	Lift-off	Fig.5.6-25
310	81	14	5		Blow-out	
300	83	10	6	39.3	Lift-off	Fig.5.6-26
306	82	12	6		Blow-out	
296	84	8	7		LO & BO	
293	85	6	8		Blow-off	
283	88	2	10		Blow-off	

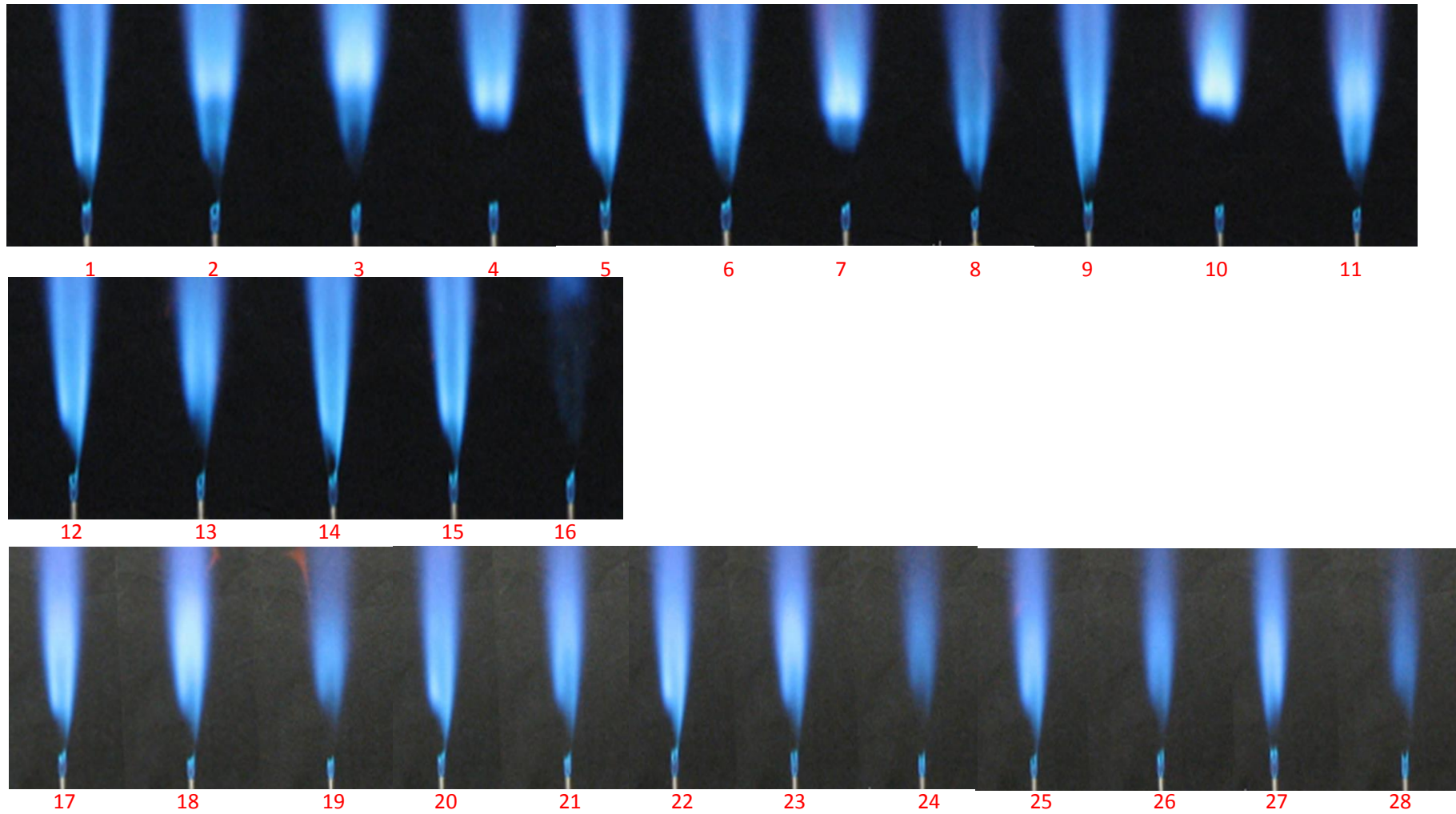


Figure 5.8: The flame images for $\text{H}_2\text{-CH}_4\text{-CO}_2$ mixtures at lift-off condition, for 20 l/min H_2 flowrate

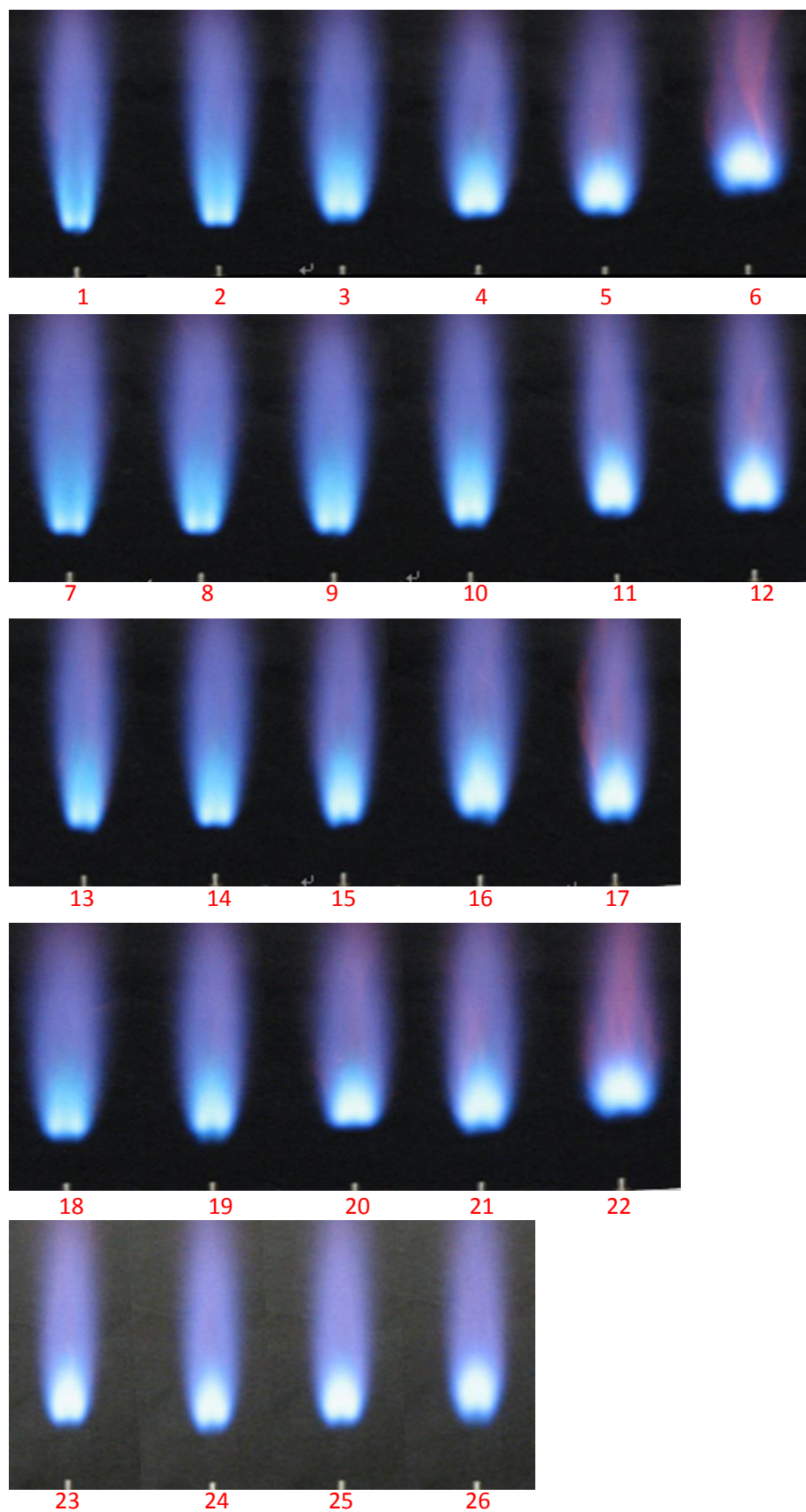


Figure 5.9: The flame images for H_2 - CH_4 - CO_2 flames at lift-off condition with hydrogen flowrate at 40 l/min

5.2.6 Experimental Results for H₂ -CO₂ Flames

Table 5.7 shows the lift-off heights, lift-off velocities and blow-out velocities data obtained from the experiment for H₂-CO₂ flames. The lift-off velocities have a range of 225-1004 m/s, which is obviously wider than that of H₂-CH₄-CO₂ flames. For lifted flames, the H₂ concentration of the mixture varies from 82% to over 99%. When CO₂ flowrate is less than 5 l/min, the flame blow-out status is not observed with up to 1000 m/s jet velocity. When CO₂ concentration is greater than 8%, the flames blow out without experiencing lift-off state. The maximum blow-out velocity is found at 1004 m/s. The flame lift-off heights increases with the jet velocities. The jet velocities resulting in attached flames reduce with the increasing CO₂ concentration in the mixture. The images of lifted H₂-CO₂ flames are shown in Figure 5.10 (a) and (b).

Table 5.7: The lift-off heights, lift-off velocities and blow-out velocities for H₂-CO₂ flames

Jet Exit Velocity	H ₂	CO ₂	Flame lift-off Height	Flame Status	Flame images
[m/s]	vol.%	vol.%	[mm]		
737	99.6	0.4	21.1	Lift-off	Fig.5.6-1
851	99.6	0.4	23.7	Lift-off	Fig.5.6-2
740	99.2	0.8	23.7	Lift-off	Fig.5.6-3
854	99.3	0.7	26.3	Lift-off	Fig.5.6-4
676	98.7	1.3	23.7	Lift-off	Fig.5.6-5
787	98.8	1.2	26.3	Lift-off	Fig.5.6-6
903	98.9	1.1	28.9	Lift-off	Fig.5.6-7
679	98.3	1.7	26.3	Lift-off	Fig.5.6-8
790	98.5	1.5	26.3	Lift-off	Fig.5.6-9
906	98.6	1.4	28.9	Lift-off	Fig.5.6-10
615	97.7	2.3	28.9	Lift-off	Fig.5.6-11
722	97.9	2.1	28.9	Lift-off	Fig.5.6-12
835	98.1	1.9	31.6	Lift-off	Fig.5.6-13
909	98.2	1.8	31.6	Lift-off	Fig.5.6-14
551	96.9	3.1	26.3	Lift-off	Fig.5.6-15
618	97.2	2.8	28.9	Lift-off	Fig.5.6-16
725	97.5	2.5	31.6	Lift-off	Fig.5.6-17
838	97.7	2.3	34.2	Lift-off	Fig.5.6-18
956	97.9	2.1	34.2	Lift-off	Fig.5.6-19
394	95.2	4.8	31.6	Lift-off	Fig.5.6-20
554	96.4	3.6	31.6	Lift-off	Fig.5.6-21
657	96.8	3.2	34.2	Lift-off	Fig.5.6-22

Jet Exit Velocity [m/s]	H ₂ vol	CO ₂ vol	Flame lift-off Height [mm]	Flame Status	Flame images
841	97.3	2.7	36.8	Lift-off	Fig.5.6-23
882	97.4	2.6	36.8	Lift-off	Fig.5.6-24
1002	97.6	2.4	36.8	Lift-off	Fig.5.6-25
396	94.6	5.4	34.2	Lift-off	Fig.5.6-26
557	95.9	4.1	34.2	Lift-off	Fig.5.6-27
844	97.0	3.0	36.8	Lift-off	Fig.5.6-28
1004	97.3	2.7		Blow-out	
274	91.2	8.8	32.1	Lift-off	Fig.5.6-29
426	94.0	6.0	35.7	Lift-off	Fig.5.6-30
560	95.4	4.6	39.3	Lift-off	Fig.5.6-31
848	96.6	3.4		Blow-out	
339	92.1	7.9		Blow-off	
280	89.5	10.5		Blow-off	
282	88.6	11.4		Blow-off	
285	87.8	12.2		Blow-off	
225	83.4	16.6		Blow-off	
228	82.4	17.6		Blow-off	

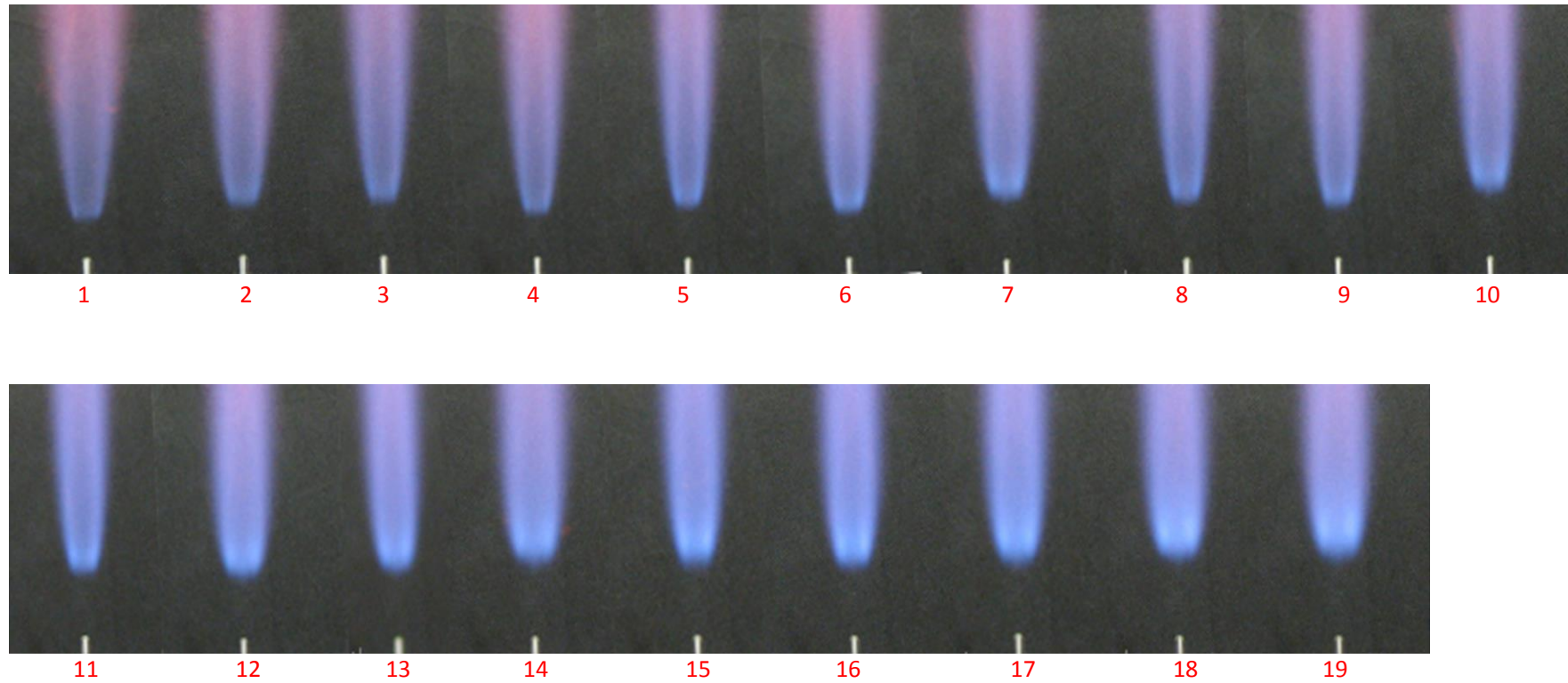


Figure 5.10 (a): The flame images for H_2 - CO_2 flames at lift-off condition

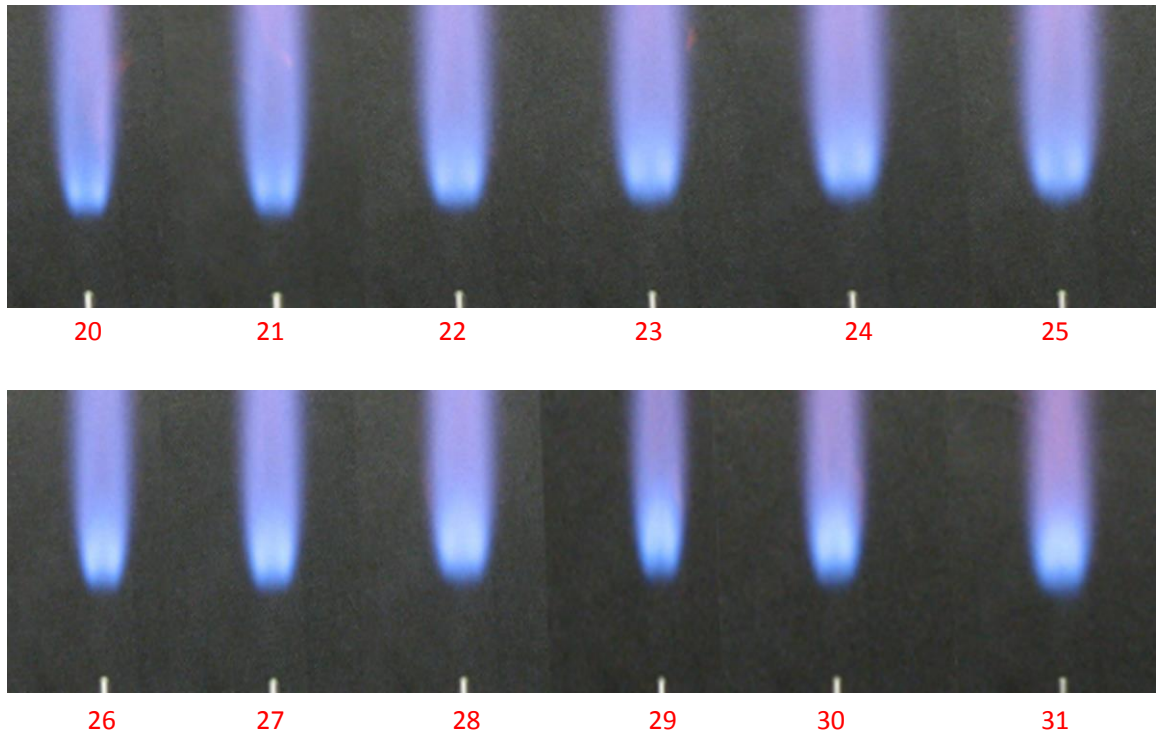


Figure 5.10 (b): The flame images for H₂- CO₂ flames at lift-off condition

5.3 Discussion

5.3.1 The Lift-Off Heights

As shown in Figure 5.11, the lift-off velocity of pure H₂ flame is over 800 m/s, which is far higher than that of H₂-hydrocarbon flames. The addition of CH₄, C₂H₆ and C₃H₈ into H₂ flames causes the flames reaching lift-off state at relatively low jet velocity. Compared with 20 l/min and 40 l/min initial H₂ flowrate, the high H₂ content in the H₂-hydrocarbon flames increases the lift-off velocities of the flames. At a specific H₂ jet velocity, the lift-off height of the flame has the order, H₂-C₃H₈ > H₂-C₂H₆ > H₂-CH₄. It also can be seen from the figure that the lift-off height increases linearly with the jet velocity.

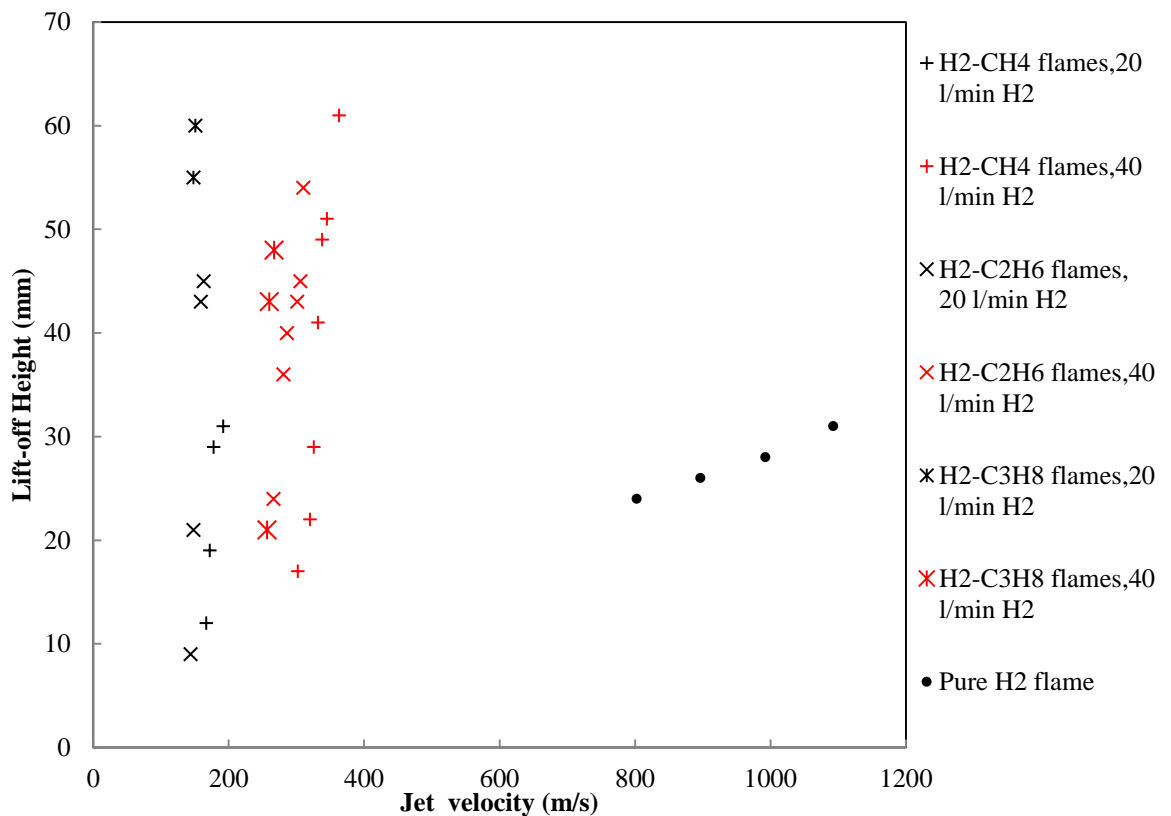


Figure 5.11: The lift-off height against exit jet velocity for pure H₂ and H₂-hydrocarbon flames

As shown in Figure 5.12, the increasing of H₂ concentration in H₂-CH₄, H₂-C₂H₆ and H₂-C₃H₈ mixtures results in a reduction in the lift-off height of the flames. To remain the flame at a specific lift-off height while increasing the jet velocity, it is required to increase the hydrogen concentration in the mixture.

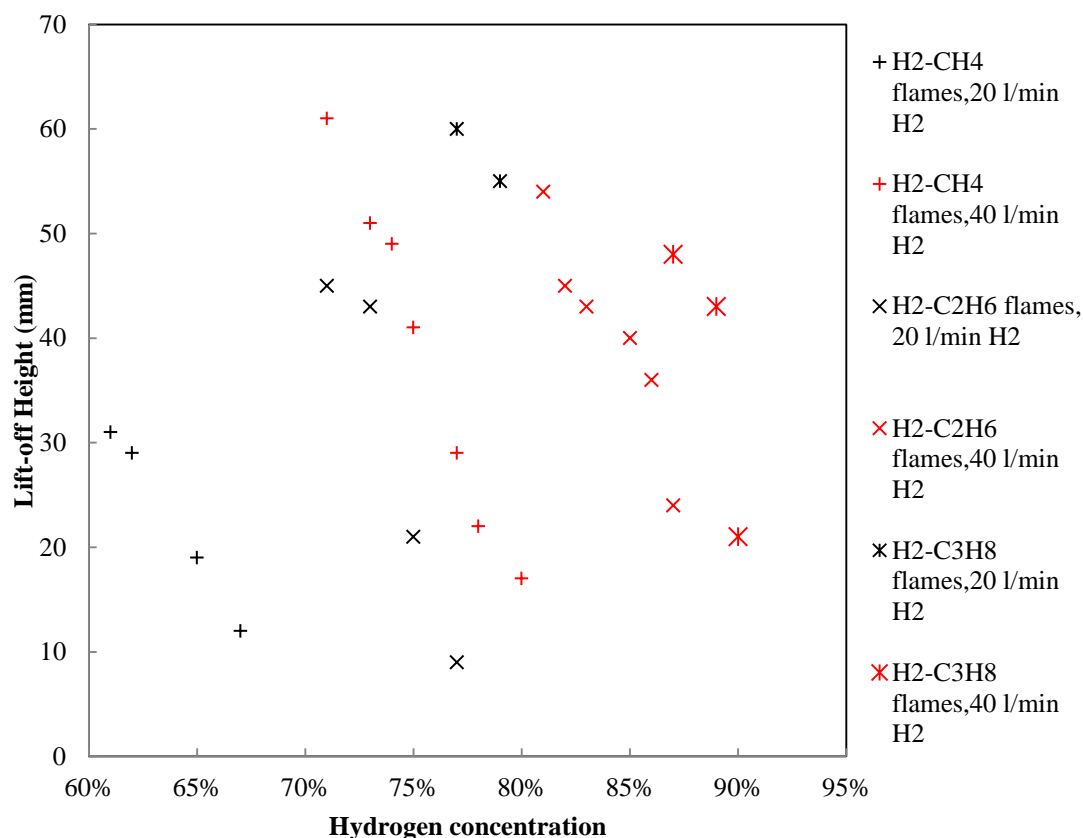


Figure 5.12: The flame lift-off height against hydrogen concentration for H₂-hydrocarbon flames

As shown in Figure 5.13, at same jet velocity, the lift-off height of the flame is proportional to the CO₂ concentration in the mixture. The higher CO₂ content results in greater lift-off height of the flame. In addition, at the same CO₂ concentration level, the lift-off height of the flame depends on the jet velocity of the inlet gas. Basically, increasing inlet gas velocity leads to relatively greater lift-off height.

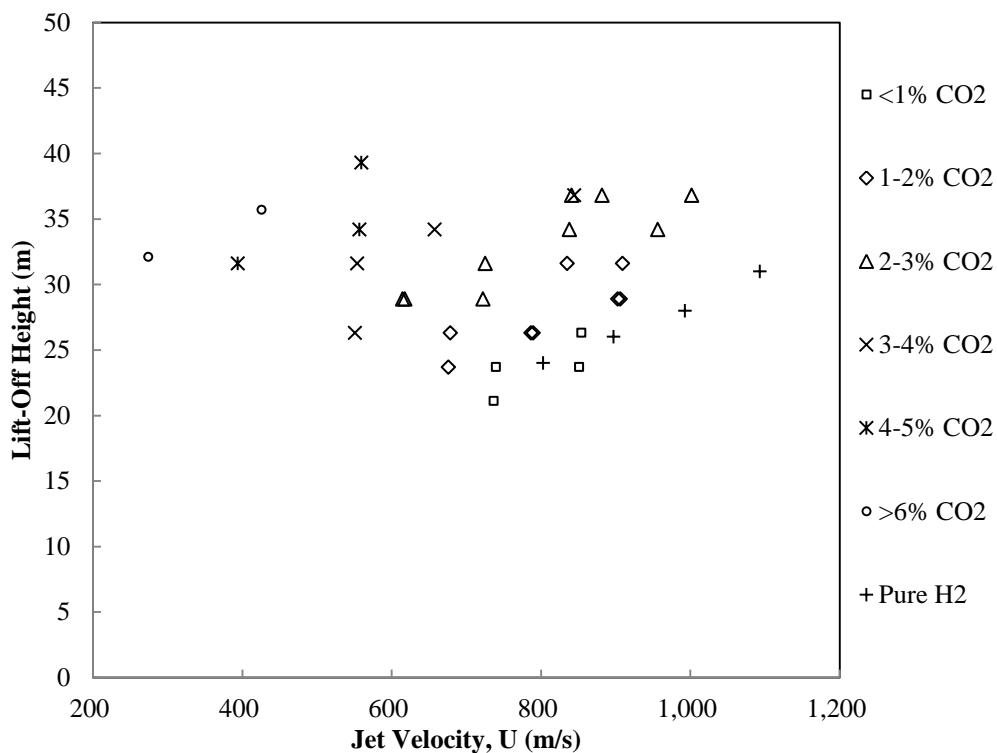


Figure 5.13: The lift-off velocity against jet velocity for pure H₂ and H₂-CO₂ flames

As shown in Figure 5.14, the lift-off height data of H₂-CH₄-CO₂ flames is in the region between that of H₂-CH₄ and H₂-C₂H₆ flames. Basically, the lift-off heights of H₂-CH₄-CO₂ flames are greater than that of H₂-CH₄ flames, and less than that of H₂-C₂H₆ and H₂-C₃H₈ flames. At the same CO₂ concentration level, the lift-off height increases linearly with the jet velocity of H₂-CH₄-CO₂ flames. Figure 5.15 shows the flame lift-off height data for these mixtures at 40 l/min initial H₂. They present similar phenomena with 20 l/min initial H₂. However, the increase in H₂ flowrate results in the flames approaching lifted state at relatively high jet velocity.

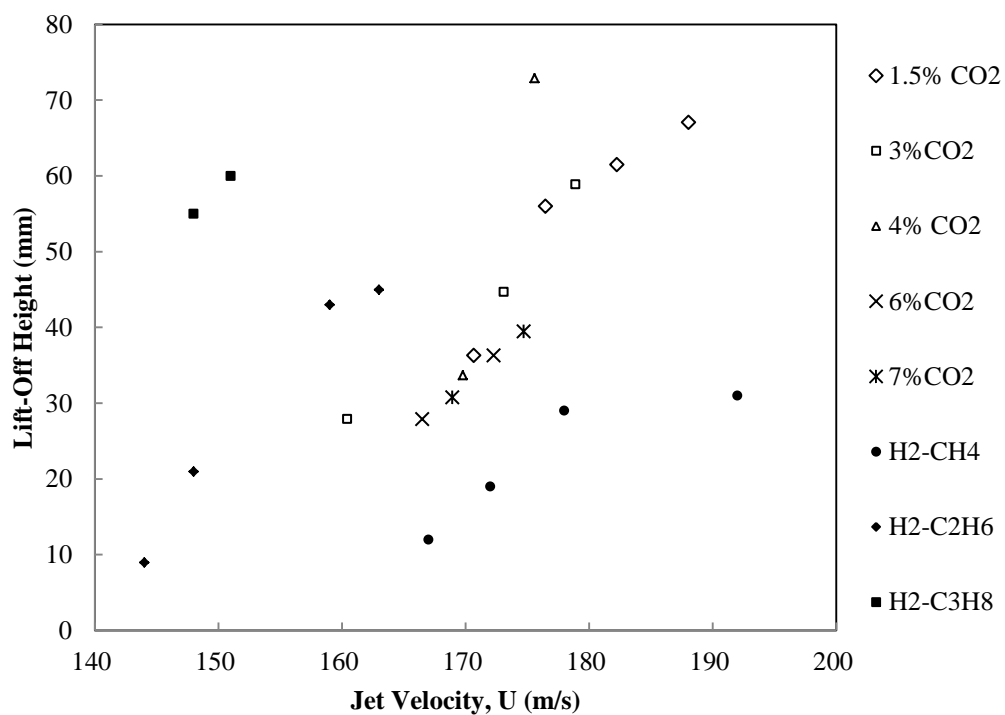


Figure 5.14: The lift-off height against jet velocity for H₂-CH₄, H₂-C₂H₆, H₂-C₃H₈ and H₂-CH₄-CO₂ flames, with initial H₂ flowrate of 20 l/min

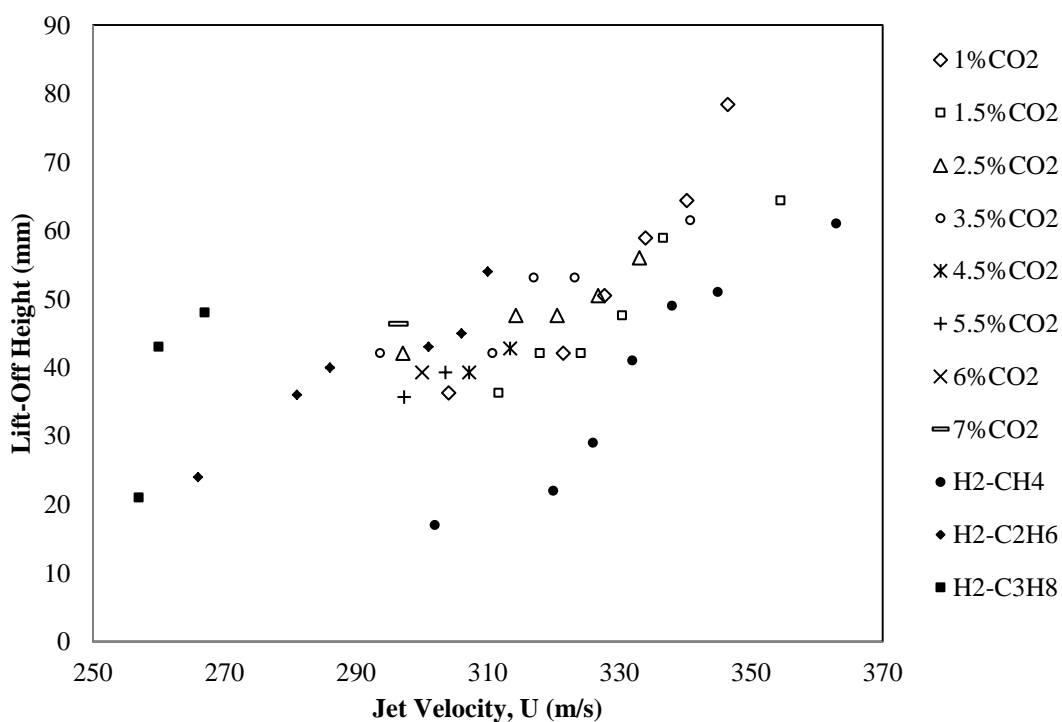


Figure 5.15: The lift-off height against jet velocity for H₂-CH₄, H₂-C₂H₆, H₂-C₃H₈ and H₂-CH₄-CO₂ flames, with initial H₂ flowrate of 40 l/min

Figure 5.16 summarise the lift-off height data against the jet velocity for H_2 - CH_4 - CO_2 flames at 20 l/min initial H_2 flowrate. Figure 5.17 illustrates the data for 40 l/min initial H_2 flowrate. At the same CO_2 concentration level, the increase of hydrogen concentration of the mixture leads to the reduction in the lift-off height. However, at the same CH_4 (H_2) concentration level, more CO_2 present in the mixture results in the increase in the lift-off height. Thus, the lift-off height is governed by both jet velocity and the composition of the mixture.

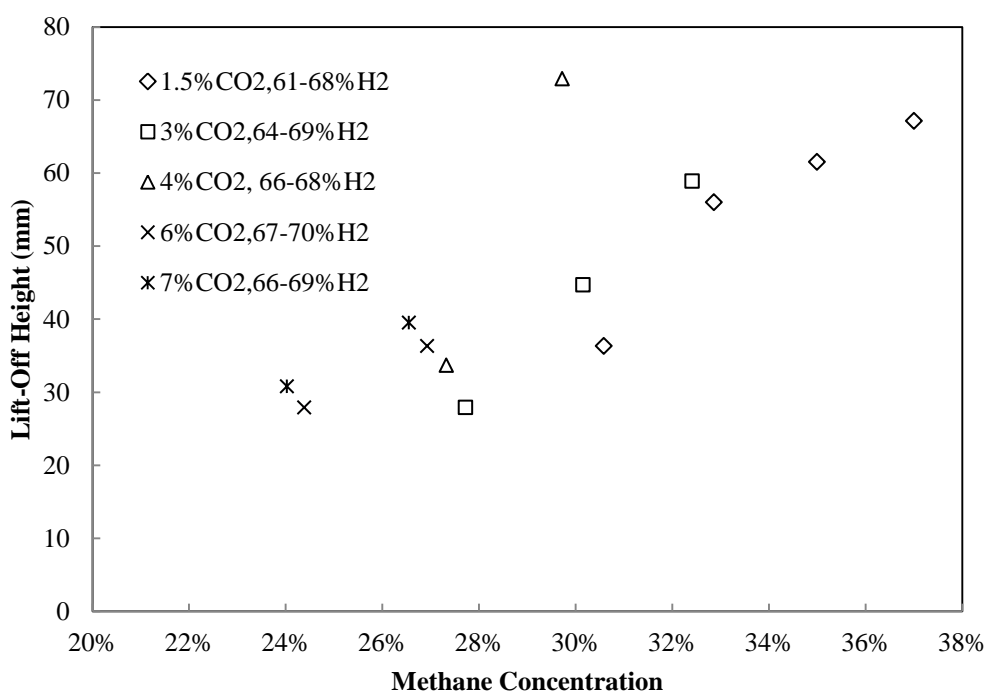


Figure 5.16: The lift-off height against CH_4 concentration of H_2 - CH_4 - CO_2 flames for 20 l/min initial H_2 flowrate

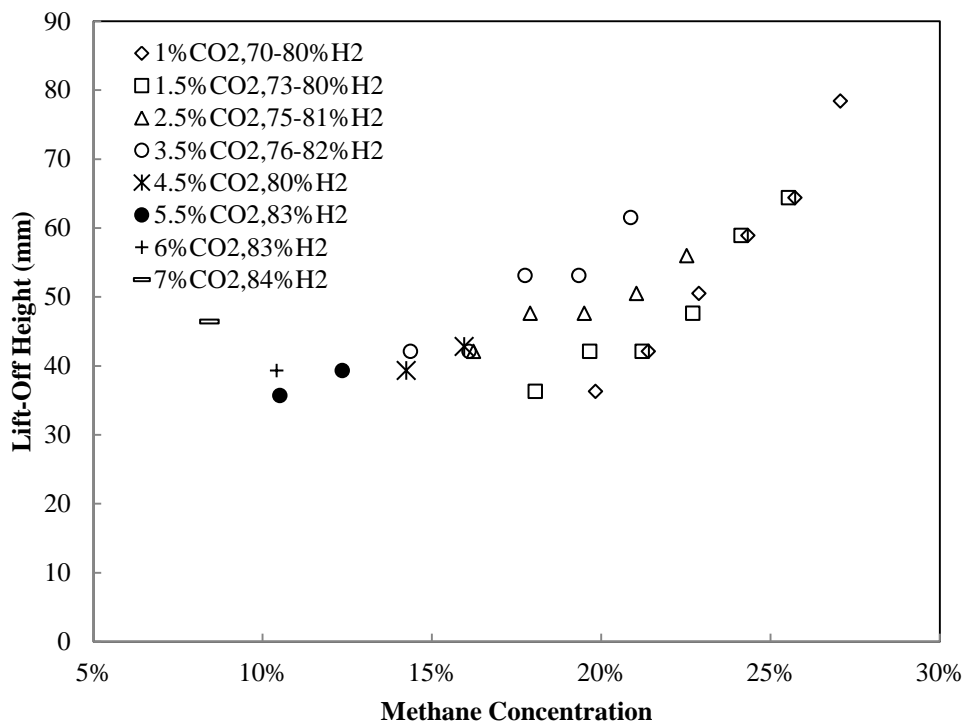


Figure 5.17: The lift-off height against CH_4 concentration of H_2 - CH_4 - CO_2 flames at 40 l/min initial H_2 flowrate

5.3.2 The Lift-Off Jet Velocities

As shown in Figure 5.18, at 20 and 40 l/min initial H_2 flowrate, the presence of CH_4 , C_2H_6 and CO_2 in H_2 flame slightly affect the lift-off jet velocities of the mixtures when H_2 concentration is over 60%. At the fixed initial H_2 flowrate, the H_2 - C_3H_8 flames are easier to reach lift-off state than H_2 - C_2H_6 flames, and followed by H_2 - CH_4 flames. Thus, when H_2 concentration is greater than 60%, the lift-off velocity of H_2 - CH_4 flame is higher than that of H_2 - C_2H_6 and H_2 - C_3H_8 flames. By comparing the 20 and 40 l/min initial H_2 flowrate, the flame lift-off velocity is dominated by the H_2 content in the mixture especially at high H_2 concentration. The lift-off height data points of H_2 - CH_4 and H_2 - CH_4 - CO_2 mixtures are emerged with each other. However, the addition of CO_2 into H_2 - CH_4 mixture causes the flame of the mixtures reach lift-off state more easily.

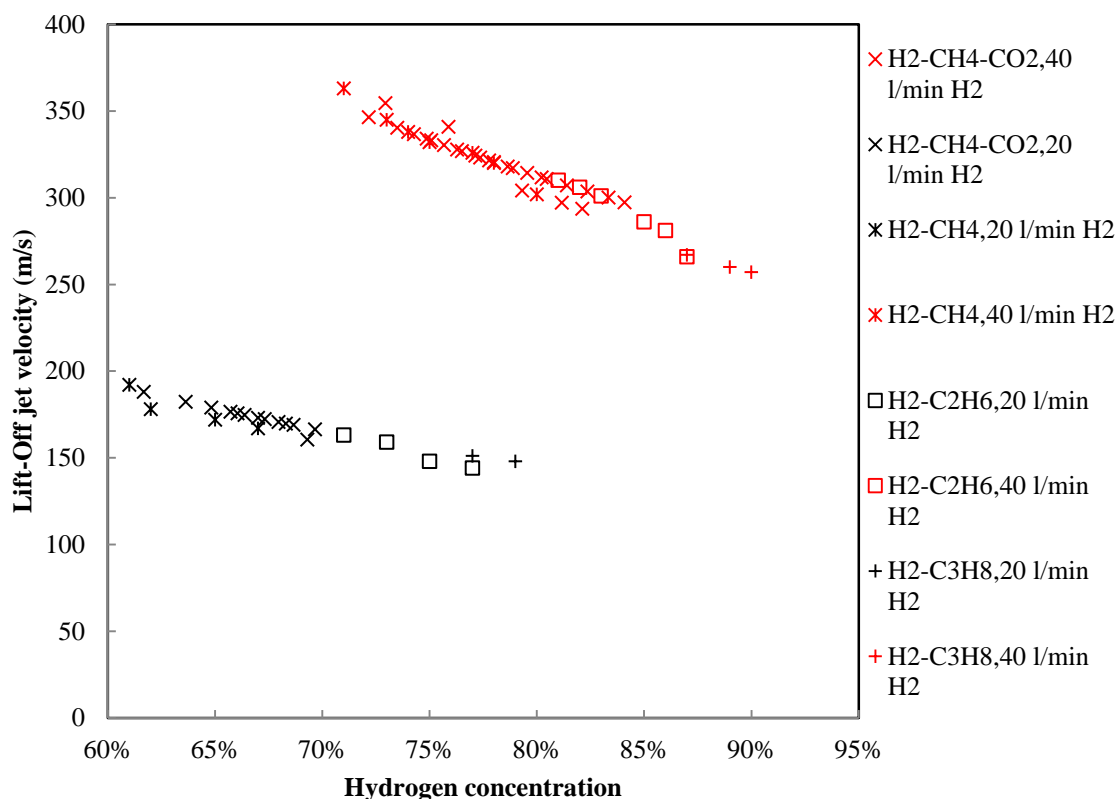


Figure 5.18: The lift-off jet velocity against the H₂ concentration for H₂-CH₄-CO₂ and H₂-hydrocarbon flames

5.3.3 The Blow-Out/Off Velocities

As shown in Figure 5.19, H₂-CH₄, H₂-C₂H₆ and H₂-C₃H₈ flames do not have blow-off status when H₂ concentration is greater than 50%. These flames blow out after experiencing the lift-off state. With H₂ concentration is higher than 50%, the H₂-CH₄ flames can sustain with more methane addition before reaching blow-out condition compared with H₂-C₂H₆ and H₂-C₃H₈ flames. The addition of C₃H₈ into H₂ results in the flame blows out more easily than adding C₂H₆ and CH₄. The blow-out velocity of these mixture has the order, H₂-CH₄ > H₂-C₂H₆ > H₂-C₃H₈ flames. By comparing 20 and 40 l/min initial H₂ flowrate it is realised that the blow-out velocity of the H₂-hydrocarbon mixtures strongly depend on the concentration and jet velocity of H₂ in the mixtures. The increasing of H₂ jet velocity of the mixtures raises the blow-out velocity.

In terms of H₂-CO₂ flames, the presence of CO₂ in H₂ flames causes the flame reaches blow-out state at the inlet jet velocity of 1004 m/s, when there is 3% CO₂

in H₂-CO₂ mixtures. When the CO₂ concentration reaches approximately 8%, the flame blows out at the inlet jet velocity of approximately 339 m/s. The increasing CO₂ concentration dramatically decreases the blow-out velocities. As the CO₂ concentration is greater than 8%, the flame reaches blow-off condition without experiencing lift-off state. When the inlet jet velocity is higher than 200 m/s, the CO₂ concentration can be tolerated up to 18% and the flame becomes very unstable.

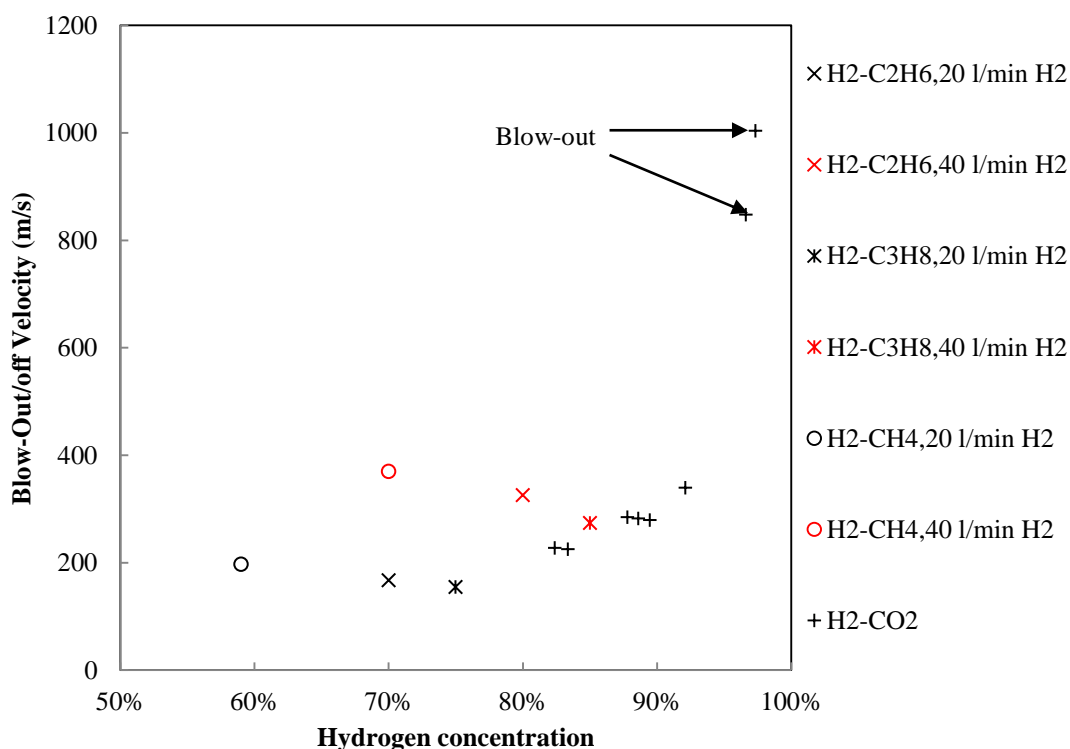


Figure 5.19: The blow-out velocity against hydrogen concentration for H₂-hydrocarbon and H₂-CO₂ flames

Figure 5.20 shows the comparison between H₂-CH₄-CO₂ and H₂-CH₄ mixtures upon the flame blow-out characteristics. The presence of CO₂ in H₂-CH₄ mixtures reduces the blow-out velocity of the mixtures. This reduction is proportional to the H₂ concentration in the mixture. At relatively higher H₂ concentration, the reduction is more obvious. For 20 l/min initial H₂ flowrate, the CO₂ concentration varies from 1.3%-21% with corresponding CH₄ concentration from 39%-13%. For 40 l/min initial H₂ flowrate, the CO₂ concentration varies from 0.8%-9.5%

with corresponding CH₄ concentration from 28.4%-2.2%. As illustrated in the figure, at a specific CH₄ concentration, the H₂-CH₄ mixture has the highest flame blow-out velocity followed by H₂(40 l/min)-CH₄-CO₂ and H₂(20 l/min)-CH₄-CO₂ mixtures. For H₂-CH₄ mixtures, reducing H₂ concentration dramatically decreases the blow-out velocity of the mixtures. When both of CH₄ and CO₂ are presented in H₂ flame, the flame blow-out velocity can be influenced by both of them. They contribute to the reduction in the blow-out velocity of the mixture. When the CO₂ concentration is greater than 8%, the flame reaches blow-off condition without experiencing lift-off state. However, at a fixed H₂ inlet velocity, the flame blow-out velocity is mainly determined by the H₂ concentration. The varying of the CH₄ and CO₂ composition only slightly influences the blow-out velocity of the mixture. When H₂ concentration is in the range of 60-68%, the flame will reach blow-out condition at the jet velocity approximately from 170-180 m/s. When H₂ concentration is in the range of 70 to 85% approximately, the flame will reach blow out condition at the jet velocity approximately from 300-350 m/s.

Therefore, the blow-out velocity is more sensitive and governed by the H₂ concentration of the mixture when H₂ concentration is greater than 60%. With fixed H₂ jet velocity, the flame blow-out velocity of the mixture does not change obviously as varying CO₂ and CH₄ composition. Thus when the gaseous mixture consists of hydrogen, hydrocarbon and carbon dioxide, the flame blow-out velocity can be increased by increasing the inlet H₂ velocity. The flame can be maintained through fixing the inlet H₂ velocity as long as H₂ concentration is higher than 60% in the mixture.

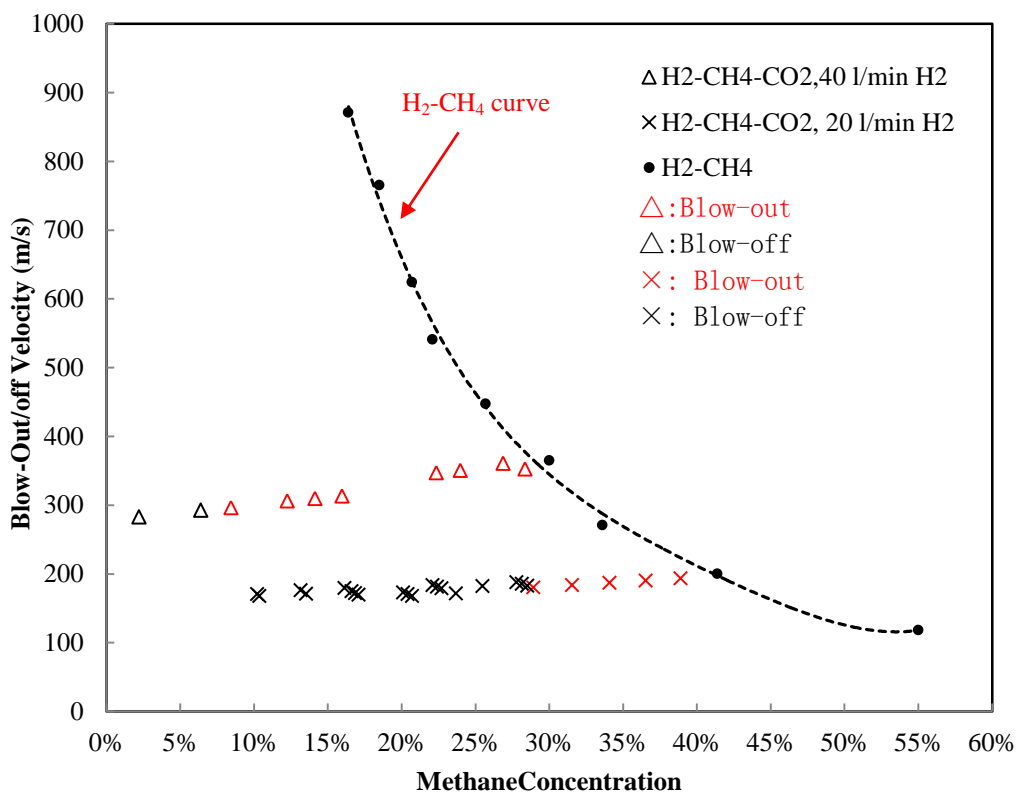


Figure 5.20: The blow-out/off velocity against CH₄ concentration for H₂-CH₄-CO₂ flames

5.4 Error Analysis

There are some errors occurred in the reading and measuring processes in the experiment. Firstly, the error is from the flowrates adjustments. The float of the flowmeter was fluctuated when fixing the flowrate at a specific value. This is especially for H₂ flowrate control, in which 20 l/min and 40 l/min were set as two fixed H₂ inlet flowrates. When fixing the flowrate at these values, slightly fluctuation of the float was observed. Secondly, the room temperature of the laboratory influenced the surrounding temperature of the flame. Thirdly, the flame fluctuations existed in the experiment, especially when the flame approached to a critical condition. The flames were not as stabilised as the idea condition, and moved up and down above the burner. This caused some challenges on measuring the flame lift-off heights from the images, since the high speed camera with very high resolution was not available in the experiment. Fourthly, the shape of the flame base was not ideal conical or plane front. This also caused the errors on

measuring the flame lift-off height. These errors can slightly influence the accuracy of the results from the experiment. Thus the data of the lift-off heights from the experiments can be considered having the error of $\pm 2\%$.

5.4 Summary

- A burner with 2mm inner diameter is employed to produce jet diffusion flames and the flame lift-off and blow-out characteristics of H_2 , $\text{H}_2\text{-CO}_2$, $\text{H}_2\text{-CH}_4\text{-CO}_2$, $\text{H}_2\text{-CH}_4$, $\text{H}_2\text{-C}_2\text{H}_6$ and $\text{H}_2\text{-C}_3\text{H}_8$ mixtures are determined experimentally.
- The lift-off velocity of pure H_2 flame is over 800 m/s. The blow-out velocity of the flame is not observed. The flame lift-off height increases linearly with the jet velocity.
- The addition of H_2 into CH_4 , C_2H_6 and C_3H_8 increases the flame lift-off and blow-out velocity of the mixtures. The increasing of H_2 concentration in the mixture reduces the flame lift-off height.
- At a fixed H_2 jet velocity, the flame lift-off height follows the order, $\text{H}_2\text{-C}_3\text{H}_8 > \text{H}_2\text{-C}_2\text{H}_6 > \text{H}_2\text{-CH}_4$.
- At a fixed H_2 jet velocity, the flame blow-out velocity follows the order, $\text{H}_2\text{-C}_3\text{H}_8 < \text{H}_2\text{-C}_2\text{H}_6 < \text{H}_2\text{-CH}_4$.
- At a fixed H_2 jet velocity, the flame lift-off velocity follows the order, $\text{H}_2\text{-C}_3\text{H}_8 < \text{H}_2\text{-C}_2\text{H}_6 < \text{H}_2\text{-CH}_4$.
- At a certain H_2 jet velocity, both of CO_2 and CH_4 addition are capable of increasing the lift-off height and reducing the blow-out velocity of $\text{H}_2\text{-CH}_4\text{-CO}_2$ mixtures.
- For $\text{H}_2\text{-CH}_4\text{-CO}_2$ mixtures, the flame blow-out velocity is dominated by the H_2 jet velocity of the mixture. At a fixed H_2 jet velocity, the flame blow-out velocity does not change obviously by adjusting the CO_2 and CH_4 concentration. The increasing of the H_2 flowrate of the mixture increases the flame blow-out velocity.

Chapter 6

Numerical Modelling of Reaction Kinetics

Literature review has shown that the laminar burning velocity of a gaseous mixture is determined by the reaction activity of the fuel. This chapter presents the numerical simulation of the reaction kinetics of H₂-CH₄, H₂-C₂H₆ and H₂-C₃H₈ mixtures. The species concentrations and reactions rates from beginning of the reactions to equilibrium state are presented in this chapter.

6.1 Computational Simulation Method

The chemical reaction kinetics simulation is conducted by applying CHEMKIN package. The gas phase reaction kinetics rates and species concentrations are simulated with applying a closed homogenous reactor model from reaction start to equilibrium state. All the reactions of H₂-CH₄, H₂-C₂H₆ and H₂-C₃H₈ are in stoichiometric conditions. It is assumed that all the gas species are thermally perfect and uniformly mixed in the reactor. The pressure was set to constant to 1 atm. A unit value of the initial volume of the gaseous mixture was given. However the volume will experience an expansion during the reaction. The initial temperature of 2500K was given. A relatively low initial temperature, such as room temperature, caused no reaction through the modelling. It was assumed that the flame was an adiabatic flame and there was no heat loss through the boundary.

Chapter 3 has shown the governing equations (*Eq. 3-14 to Eq. 3-20*) applied in CHEMKIN for solving the model. Arrhenius parameters used in the modified Arrhenius equation were supplied by the detailed reaction mechanism, in which each elementary reaction was given associated with the value of the Arrhenius parameters. A reaction mechanism developed by Warnatz and Heghes (2006) including the combustion of H₂, CO, CH₄, C₂H₆ and C₃H₈ was used to supply the Arrhenius parameters, A, n and E, as shown in Appendix A. The thermodynamic data was also required to solve the standard state entropy and enthalpy in the

governing equations. In addition, the transport properties were not required in this model.

6.1.1 Compositions of the Initial Reactants

Different ratios of H₂ to CH₄, C₂H₆ and C₃H₈ were given in order to estimate the effect of hydrogen concentration on the reaction kinetics of the mixture. Appendix M shows the initial compositions of H₂-CH₄, H₂-C₂H₆ and H₂-C₃H₈ mixtures. The initial combinations gave the H₂ concentration varying from 0-100% in the mixture. The required amount of air was calculated based on stoichiometric condition.

6.1.2 Apply Thermodynamic Data into Numerical Model

In CHEMKIN, the thermodynamic properties are presented in the form of polynomial fits as functions of temperature. It is assumed that the gas is thermally perfect for gas-phase species. There are 7 upper temperature range coefficients and 7 lower temperature range coefficients. Associated with the polynomial fitting coefficients the species name, elemental composition, electronic charge and the phase are also supplied by the thermodynamic data.

The specific heat, enthalpy of formation and entropy of formation, associated with A, n and E, are used to calculate equilibrium constant, K_c. The NASA polynomials used in CHEMKIN thermodynamic database have the form (Heghes, 2006):

$$\frac{C_p}{R} = a_1 + a_2T + a_3T^2 + a_4T^3 + a_5T^4,$$

$$\frac{H}{RT} = a_1 + a_2 \frac{T}{2} + a_3 \frac{T^2}{3} + a_4 \frac{T^3}{4} + a_5 \frac{T^4}{5} + \frac{a_6}{T},$$

$$\frac{S}{RT} = a_1 \ln T + a_2T + a_3 \frac{T^2}{2} + a_4 \frac{T^3}{3} + a_5 \frac{T^4}{4} + a_7$$

Where a₁, a₂,..., a₆ and a₇ are the numerical coefficients supplied in NASA thermodynamic files. An example of the NASA thermodynamic data used in the simulation is shown below:

CH4	L	8/88C	1H	4	G	200.000	3500.000	1000.000	1
7.48514950E-02	1.33909467E-02	-5.73285809E-06	1.22292535E-09	-1.01815230E-13					2
-9.46834459E+03	1.84373180E+01	5.14987613E+00	-1.36709788E-02	4.91800599E-05					3
-4.84743026E-08	1.66693956E-11	-1.02466476E+04	-4.64130376E+00						4

The data indicates the symbol of the species, the elements compose the species, the phase of the species and the range of the temperature. In the example, 200-1000 K indicates the lower temperature region and 1000-3500 K represents the upper temperature range.

6.1.3 Determine the Detailed Reaction Mechanism

The reaction mechanisms integrated hydrogen and hydrocarbons are relatively rare. There are two mechanism considered in the reaction kinetics equilibrium simulation, which are Gri-Mech 3.0 (Smith et al., 1999) and Warnatz and Heghes (2006). Both of them have been widely used upon kinetic modelling and analysis. Gri-Mech has been used on many studies for hydrogen, methane, ethane, propane and natural gas combustion reaction kinetics modelling. However, Warnatz supplied a more comprehensive mechanism for C₂ and C₃ compared with Gri-Mech. Both of them have a relatively complete reaction mechanism for CH₄ oxidation.

As shown in Figure 6.1 and 6.2, the changes in the concentrations of H₂ and CH₄ for oxidation of H₂-CH₄ mixture modelled by both mechanisms are well agreed with each other, although the molar fraction of H₂ modelled by Gri-Mech 3.0 mechanism is slightly higher than Warnatz mechanism. The $\frac{dT}{dt}$ profile is also tested for the two reaction mechanism. This is shown in Figure 6.3. As illustrated in Figure 6.3, the temperatures increase at the same rate for the two mechanisms. However, at the equilibrium state, the temperature profile obtained from the Warnatz reaction mechanism is slightly higher than that from the Gri-Mech 3.0.

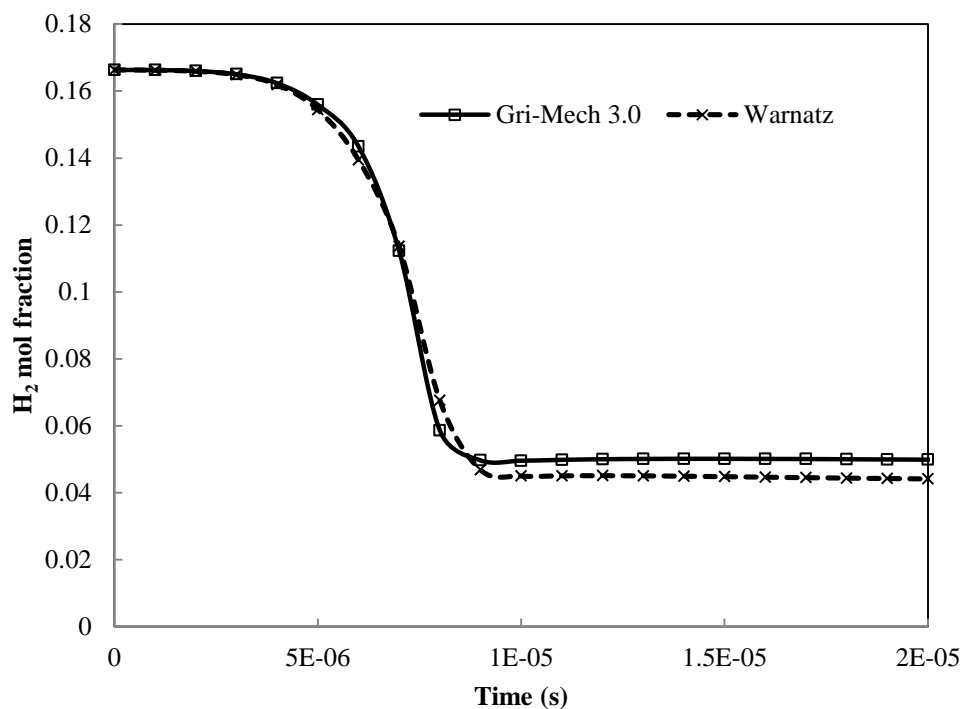


Figure 6.1: The comparison between Gri-Mech 3.0 and Warnatz reaction mechanisms for the oxidation of H₂-CH₄ mixture of 80% H₂

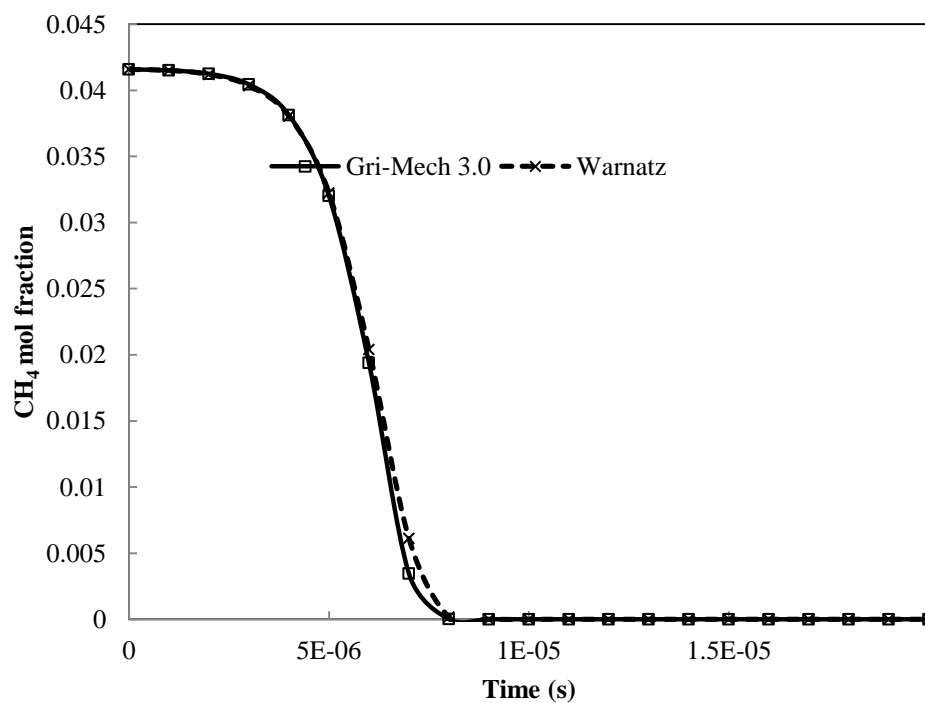


Figure 6.2: The comparison between Gri-Mech 3.0 and Warnatz reaction mechanisms for the oxidation of H₂-CH₄ mixture of 80% H₂

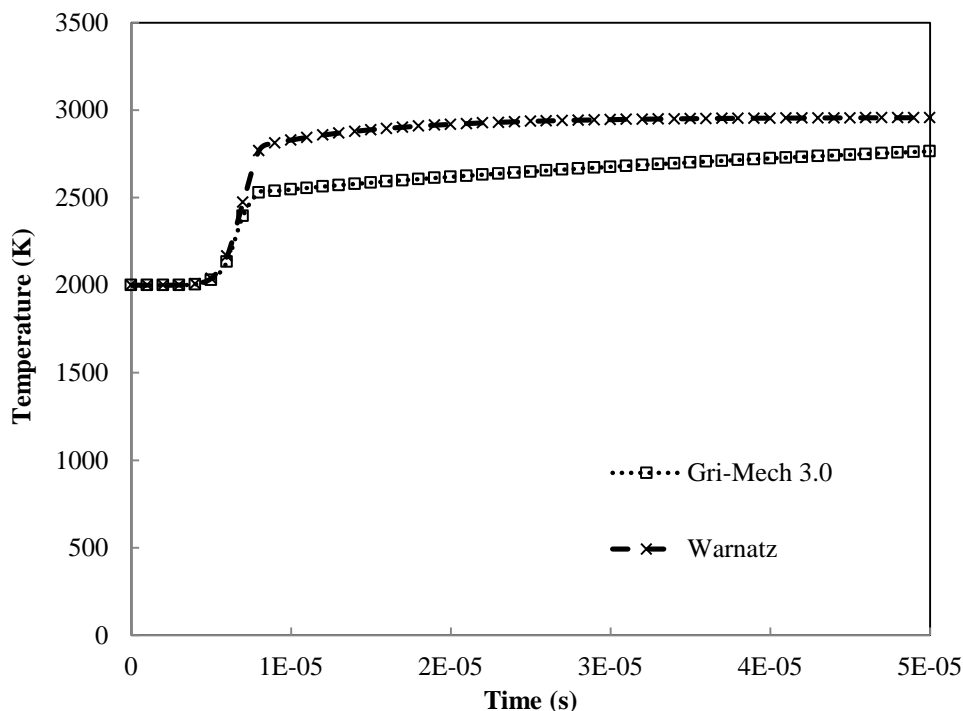


Figure 6.3: The comparison of the temperature profile between Gri-Mech 3.0 and Warnatz of the combustion of $\text{H}_2\text{-CH}_4$ mixture of 80% H_2

In terms of ethane and propane, these two reaction mechanisms consist of different elementary reactions. Table 6.1 shows the elementary reactions related to the primary decomposition of C_2H_6 in the two reaction mechanisms. The mechanism developed by Warnatz and Heghes (2006) covers nearly all of the primary C_2H_6 decomposition reactions in Gri-Mech 3.0. On the other hand, Gri-Mech 3.0 shortens 6 chain carrying reactions, compared with Warnatz and Heghes' mechanism. The decomposition of C_2H_6 through third body effect is given in Gri-Mech 3.0 but it is not presented by Warnatz and Heghes. Basically, both reaction mechanisms include the important chain initiating reactions for the primary decomposition of C_2H_6 . However, the reactions provided by Warnatz and Heghes are relatively more completed.

For the oxidation of C_3H_8 , both of the reaction mechanisms cover the critical initial steps for the primary decomposition of C_3H_8 . The elementary reactions for C_3H_8 oxidation in Gri-Mech 3.0 and Warnatz and Heghes are shown in Table 6.2. The initial decomposition of C_3H_8 into C_2H_5 and CH_3 is included in both reaction

mechanisms. However, Warnatz and Heghes' mechanism gives 10 more elementary reactions including the reaction of C_3H_8 with CH_3 . In this case, CH_3 is a very important radical since it is the primary decomposition product of CH_4 . Thus the reactions between C_3H_8 and CH_3 compete with the CH_3 generated from CH_4 decomposition. The CH_3 is further reacted with H and OH and decomposed to CH_2 and H. In addition, Warnatz and Heghes gives considerations on isotopic abnormality body of C_3H_7 in the reactions related to the attack by H, O and OH.

Table 6.1: The comparison between Gri-Mech 3.0 and Warnatz reaction mechanism for C_2H_6 oxidation

C ₂ H ₆ Decomposition	
Gri-Mech 3.0	Warnatz and Heghes
$O+C_2H_6 \rightleftharpoons OH+C_2H_5$	$C_2H_6 + O \rightleftharpoons C_2H_5 + OH$
$H+C_2H_5(+M) \rightleftharpoons C_2H_6(+M)$	-
$H+C_2H_6 \rightleftharpoons C_2H_5+H_2$	$C_2H_6 + H \rightleftharpoons C_2H_5 + H_2$
$OH+C_2H_6 \rightleftharpoons C_2H_5+H_2O$	$C_2H_6 + OH \rightleftharpoons C_2H_5 + H_2O$
$CH_2(S)+C_2H_6 \rightleftharpoons CH_3+C_2H_5$	$C_2H_6 + OH \rightleftharpoons C_2H_5 + H_2O$
$2CH_3(+M) \rightleftharpoons C_2H_6(+M)$	$CH_3 + CH_3 + M \rightleftharpoons C_2H_6 + M$
$CH_3+C_2H_6 \rightleftharpoons C_2H_5+CH_4$	$C_2H_6 + CH_3 \rightleftharpoons C_2H_5 + CH_4$
-	$C_2H_5 + C_2H_5 \rightleftharpoons C_2H_4 + C_2H_6$
-	$C_2H_6 + HO_2 \rightleftharpoons C_2H_5 + H_2O_2$
-	$C_2H_6 + O_2 \rightleftharpoons C_2H_5 + HO_2$
-	$C_2H_6 + H_2C \rightleftharpoons C_2H_5 + CH_3$
-	$C_2H_6 + CH \rightleftharpoons C_2H_4 + CH_3$
-	$C_3H_6 + C_2H_5 \rightleftharpoons C_3H_5 + C_2H_6$

Table 6.2: The comparison between Gri-Mech 3.0 and Warnatz reaction mechanism for C_3H_8 oxidation

C ₃ H ₈ Decomposition	
Gri-Mech 3.0	Warnatz and Heghes
$CH_3+C_2H_5(+M) \rightleftharpoons C_3H_8(+M)$	$C_3H_8 + M \rightleftharpoons CH_3 + C_2H_5 + M$
$O+C_3H_8 \rightleftharpoons OH+C_3H_7$	$C_3H_8 + O \rightleftharpoons n-C_3H_7 + OH$
	$C_3H_8 + O \rightleftharpoons i-C_3H_7 + OH$
$H+C_3H_8 \rightleftharpoons C_3H_7+H_2$	$C_3H_8 + H \rightleftharpoons H_2 + n-C_3H_7$
	$C_3H_8 + H \rightleftharpoons H_2 + i-C_3H_7$
$OH+C_3H_8 \rightleftharpoons C_3H_7+H_2O$	$C_3H_8 + OH \rightleftharpoons n-C_3H_7 + H_2O$
	$C_3H_8 + OH \rightleftharpoons i-C_3H_7 + H_2O$

Continue to Table 6.2

$C_3H_7 + H_2O_2 \rightleftharpoons HO_2 + C_3H_8$	$C_3H_8 + HO_2 \rightarrow n-C_3H_7 + H_2O_2$
	$n-C_3H_7 + H_2O_2 \rightarrow C_3H_8 + HO_2$
$CH_3 + C_3H_8 \rightleftharpoons C_3H_7 + CH_4$	$C_3H_8 + CH_3 \rightarrow CH_4 + i-C_3H_7$
	$C_3H_8 + CH_3 \rightarrow CH_4 + n-C_3H_7$
$H + C_3H_7(+M) \rightleftharpoons C_3H_8(+M)$	-
$HO_2 + C_3H_7 \rightleftharpoons O_2 + C_3H_8$	$C_3H_8 + O_2 \rightarrow n-C_3H_7 + HO_2$
	$C_3H_8 + O_2 \rightarrow i-C_3H_7 + HO_2$
-	$C_3H_8 + HO_2 \rightarrow i-C_3H_7 + H_2O_2$
-	$i-C_3H_7 + H_2O_2 \rightarrow C_3H_8 + HO_2$
-	$n-C_3H_7 + CH_4 \rightarrow CH_3 + C_3H_8$
-	$i-C_3H_7 + CH_4 \rightarrow CH_3 + C_3H_8$
-	$n-C_3H_7 + HO_2 \rightarrow C_3H_8 + O_2$
-	$i-C_3H_7 + HO_2 \rightarrow C_3H_8 + O_2$
-	$C_3H_8 + CH_3O \rightarrow n-C_3H_7 + CH_3OH$
-	$n-C_3H_7 + CH_3OH \rightarrow C_3H_8 + CH_3O$
-	$C_3H_8 + CH_3O \rightarrow i-C_3H_7 + CH_3OH$
-	$i-C_3H_7 + CH_3OH \rightarrow C_3H_8 + CH_3O$

In summary, both of the two reaction mechanisms can be used for the reaction kinetics simulation of H_2 , CH_4 , C_2H_6 and C_3H_8 . However, the Warnatz reaction mechanism gives more complete and detailed elementary reactions. It is suitable for the reaction kinetics simulation of oxidation of H_2 - CH_4 , H_2 - C_2H_6 and H_2 - C_3H_8 mixtures.

6.2 Reaction Kinetics Simulation of H_2 - CH_4 -Air Mixture

Figure 6.4 shows the molar fraction of H_2 changes over time. As shown in the Figure, when the hydrogen concentration in the mixture is below 50%, the molar fraction of H_2 in the gaseous mixture changes very slightly and reaches the equilibrium state at relatively late time point compared with the condition with high hydrogen concentration. From 50% hydrogen in the mixture, the hydrogen starts to be consumed moderately. However, when hydrogen concentration exceeds 60%, the molar fraction of hydrogen reduces more and more sharply with the increasing hydrogen concentration. As shown in the Figure, the most significant reduction is found for the fuel containing pure H_2 .

In terms of the time of reaching the equilibrium state, the time with high hydrogen concentration is shorter than that with relatively low hydrogen concentration in the mixture. For pure H₂ reactant, the reaction reaches the equilibrium state at about 2E-6 s, which is earlier than the H₂-CH₄ mixture reactants. This implies that when H₂ concentration is less than approximately 60%, the reaction rates increases very steady with the H₂ concentration in the mixture. In contrast, when H₂ concentration is greater than 60%, the increasing H₂ concentration strongly enhances the H₂ reaction rates of the mixture.

With considering the volume of gaseous mixture will expand during the reaction, the concentration of the species changing over time is also simulated in order to verify the plot of molar fraction versus time. Figure 6.5 shows the concentrations of H₂ of H₂-CH₄ mixture changing over time for different compositions of the H₂-CH₄ mixtures. Comparing Figure 6.4 with 6.5, the same phenomena is found that the presence of CH₄ in the reactant delays the consumption of H₂, in contrast, the increase of H₂ proportion in the H₂-CH₄ mixtures enhance the consumption of H₂. However, with the H₂ concentration below 40% the CH₄ oxidation mechanism dominates the reaction. As illustrated in Figures 6.4 and 6.5, the slight increase of H₂ during the reaction comes from the mechanism of the oxidation of CH₄. The addition of H₂ into H₂-CH₄ starts to effectively increase the reaction rates of H₂ when the H₂ concentration in the mixture is greater than 60%.

Figure 6.6 and Figure 6.7 illustrate the change of CH₄ over time. As shown in the Figures, the addition of H₂ into CH₄ increases the consumption efficiency of the CH₄. At 90% H₂ in the mixture, the consumption of CH₄ reaches equilibrium state at about 2E-6 s, which is approaching to that of pure H₂. By considering Figure 6.6 and Figure 6.7, it is realised that the behaviour of the reactant consumption becomes more and more similar to that of pure H₂ when the H₂ concentration is over 60%.

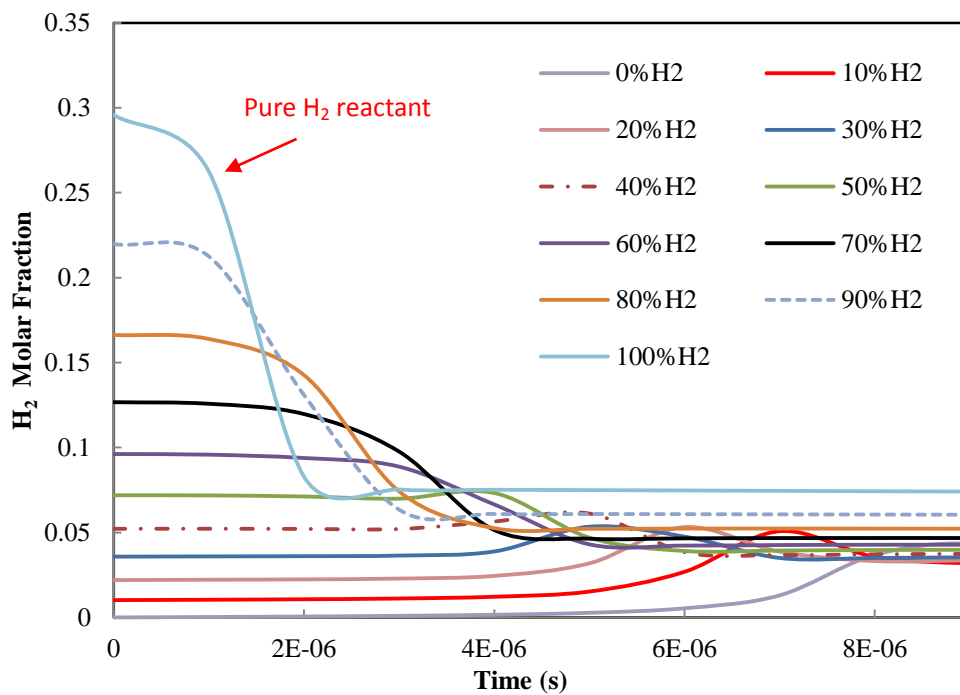


Figure 6.4: The change of H₂ molar fraction over time for H₂-CH₄ reactions, at 2500 K and 1 atm

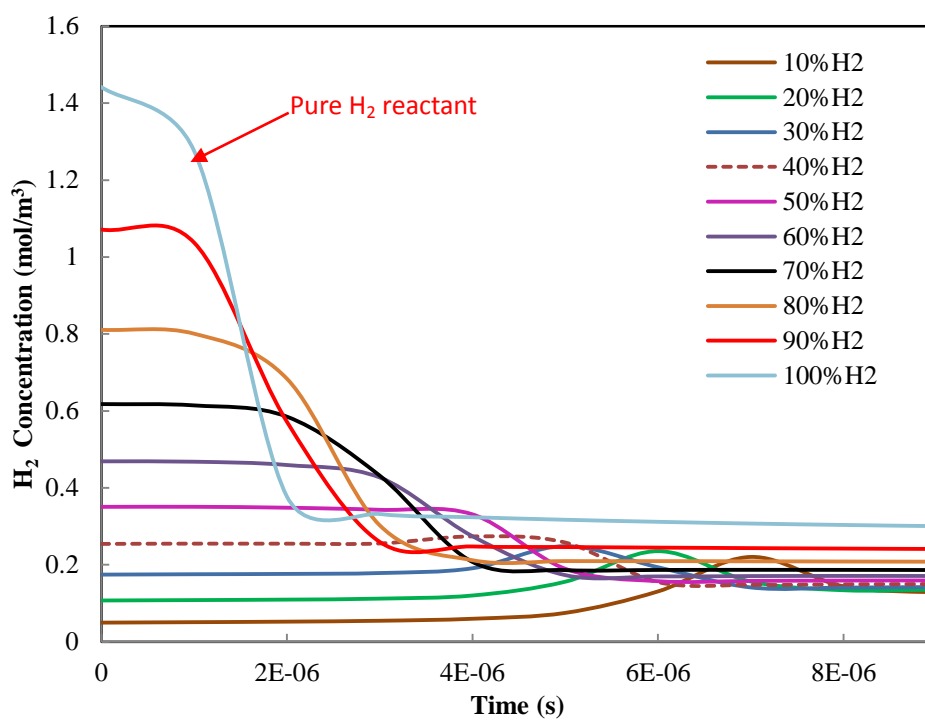


Figure 6.5: The H₂ concentration over time for H₂-CH₄, at 2500 K and 1 atm

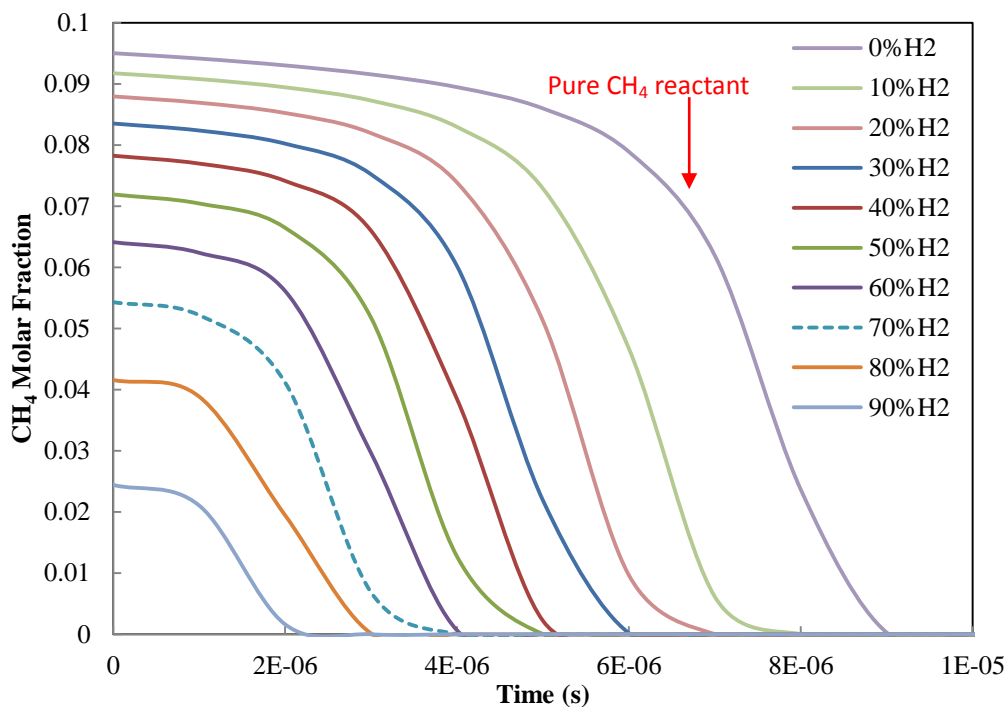


Figure 6.6: The change of CH₄ molar fraction over time for H₂-CH₄ reaction, at 2500K and 1 atm

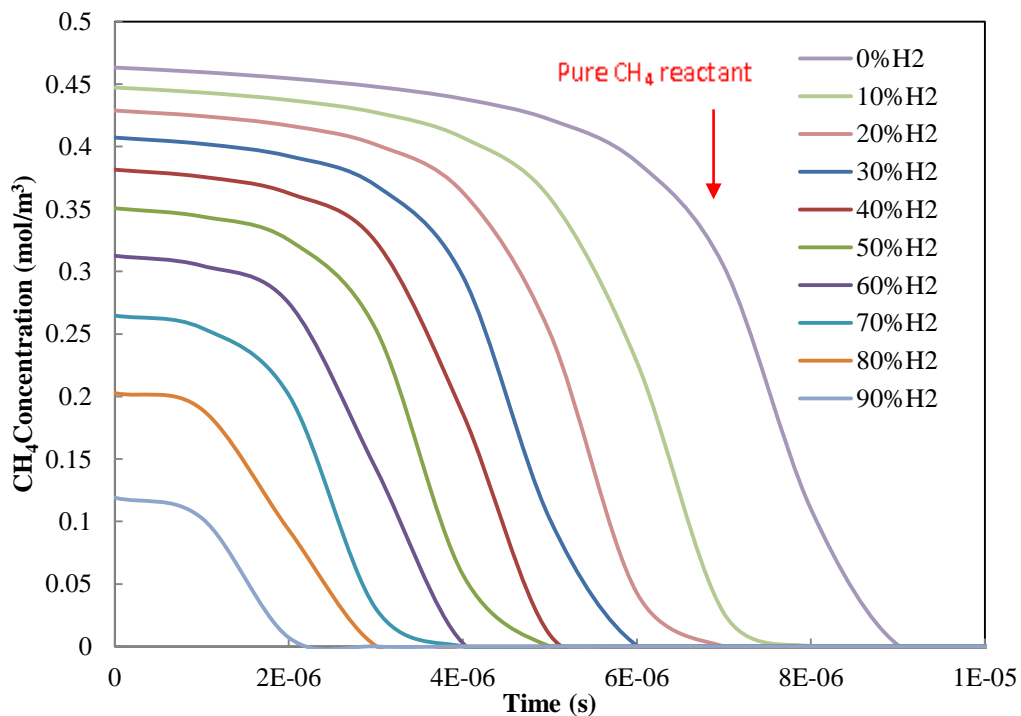


Figure 6.7: The CH₄ concentration over time for H₂-CH₄ reaction, at 2500K and 1 atm

Figure 6.8 and Figure 6.9 demonstrate the change of OH and H over the time for different H₂ concentration in H₂-CH₄ mixture. As shown in the Figures, the effect of H₂ addition on H and OH is significant and strongly dependent on the H₂ concentration. At relatively low H₂ concentration, the amount of H and OH at equilibrium state is low and they are generated at a relatively slow rate. At relatively high H₂ concentration in the mixture, the generation rate of the OH and H becomes faster. With H₂ concentration below 40%, the increase in OH and H generation is slight. However, with H₂ concentration over 60%, the enhancement on OH and H generation becomes more and more obvious.

Compared with H₂-CH₄ mixture, pure H₂ reaction has much higher production rates and peak values of concentrations for H and OH. When H₂ concentration is less than 60% and CH₄ dominates the overall reaction mechanism, the increase in the production rates and the equilibrium concentrations for H and OH is relatively slow. When H₂ concentration is greater than 60%, the influence of the addition of H₂ in the mixture on H and OH become stronger. This implies the H and OH in the reaction system are mainly contributed by the oxidation of H₂.

The temperatures of the H₂-CH₄ reaction simulation is shown in Figure 6.10. The reactions start from 2500 K and reach the equilibrium state at about 3100 K. Pure H₂ reaction has the highest equilibrium temperature which is just above 3100 K.

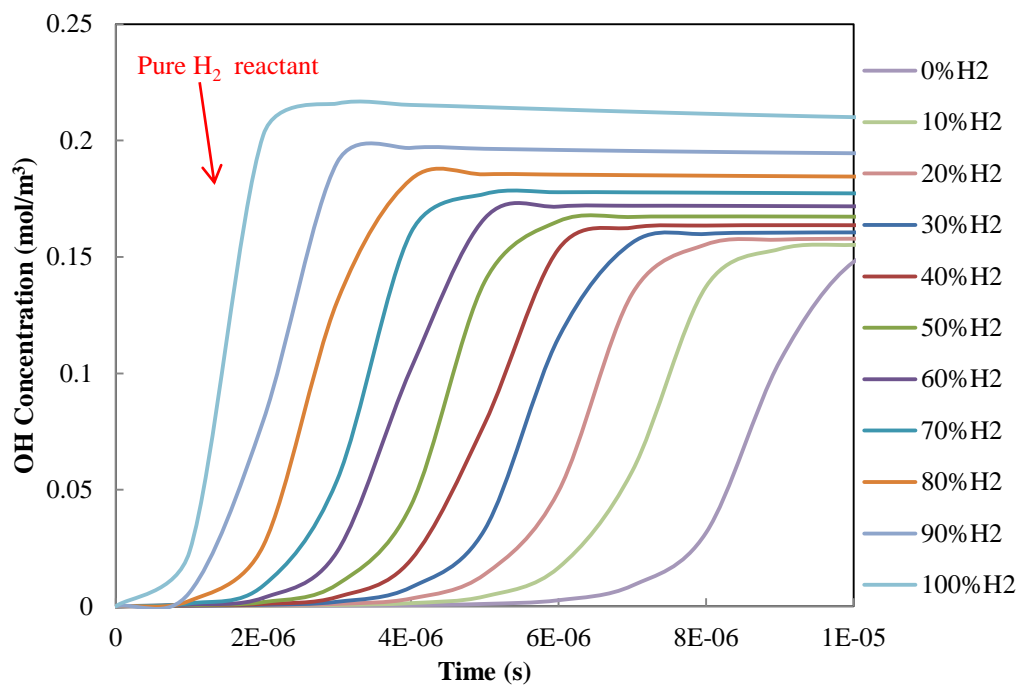


Figure 6.8: The OH concentration over time for H₂-CH₄ reaction, at 2500K and 1 atm

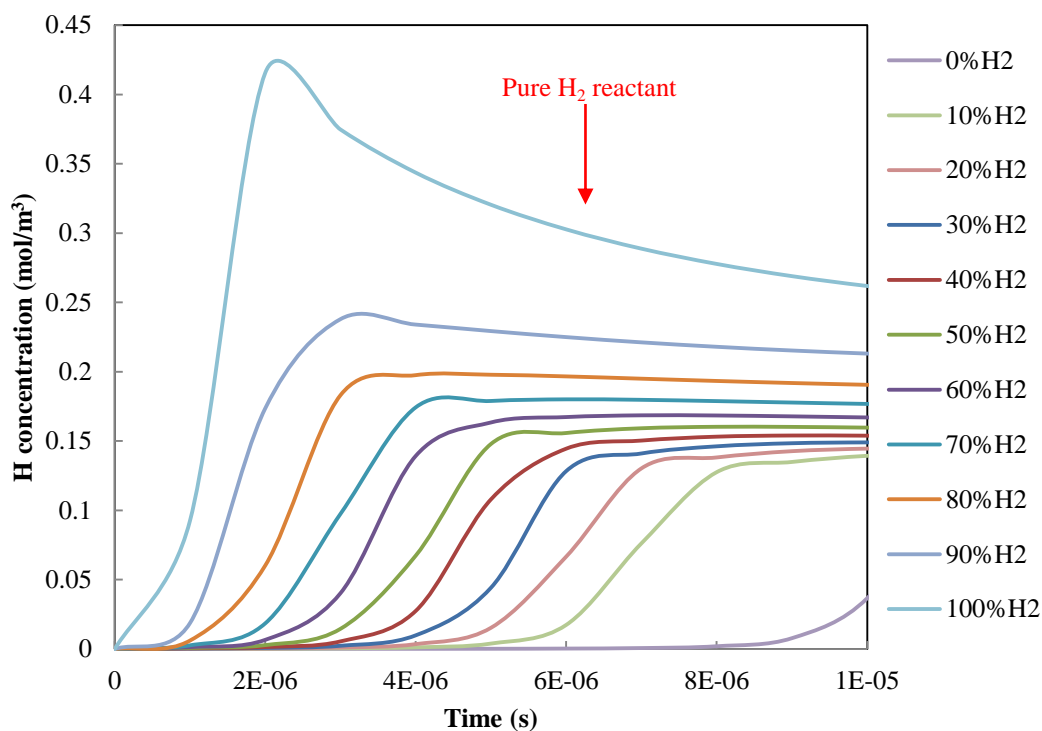


Figure 6.9: The H concentration over time for H₂-CH₄ reaction, at 2500K and 1 atm

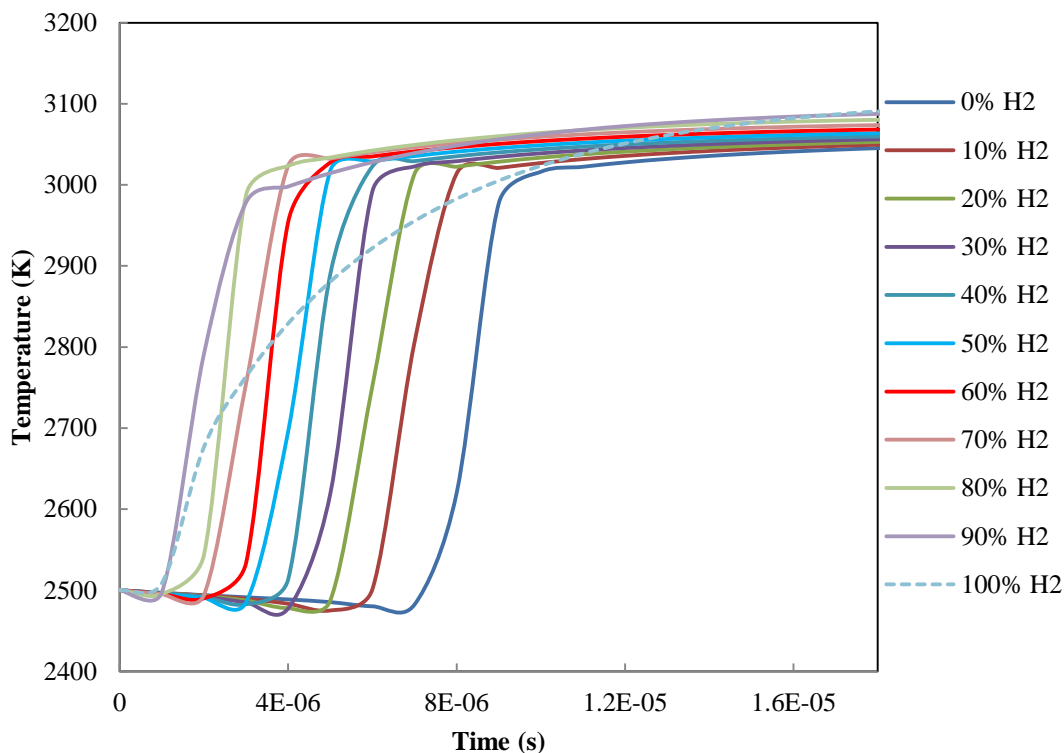


Figure 6.10: The Temperature profile of H₂-CH₄ reactions

6.3 Reaction Kinetics Simulation of H₂-C₂H₆-Air Mixture

The previous section has shown the effect of hydrogen addition in the reaction of H₂-CH₄ with air. The increasing concentration of hydrogen in the mixture results in an increase in the reaction rates for both of H₂ and CH₄. If the concentration of hydrogen addition has the similar effect on the reaction of H₂-C₂H₆ mixture will be discussed in this section.

The same initial temperature and pressure, 2500K and 1 atm respectively, were given and the same gas kinetics and thermodynamic files were supplied to make sure the comparison between H₂-CH₄ and H₂-C₂H₆ mixtures not being affected by the initial set up.

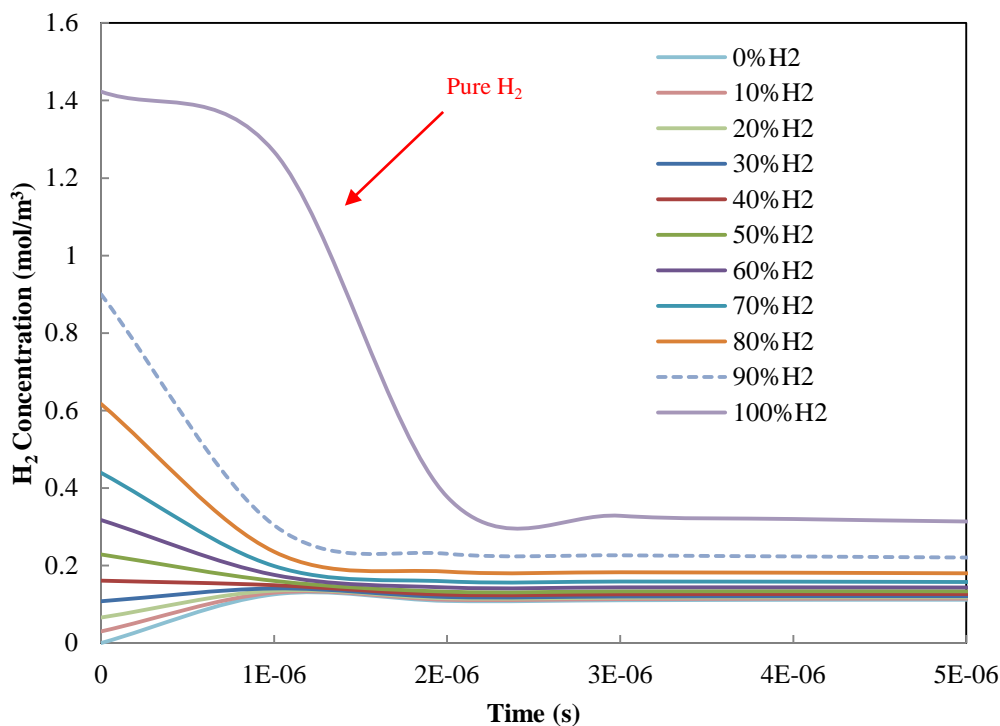


Figure 6.11: The H_2 concentration over time for H_2 - C_2H_6 reaction, at 2500K and 1 atm

Figure 6.11 shows the change in the H_2 concentration for the reaction of H_2 - C_2H_6 from initial state to equilibrium state. As illustrated in the Figure, when the H_2 addition concentration is below 50%, the change of the H_2 concentration over time experiences a slight increase before reaching equilibrium state. This slight increase is contributed by the oxidation of the hydrocarbon while the mechanism of the H_2 reaction is not at the dominant position in the overall reaction system.

When H_2 concentration is greater than 60%, H_2 is continuously consumed and then reaches equilibrium state. The consumption of H_2 becomes more and more sharply as increasing the H_2 addition concentration in the mixture. With continuously increasing H_2 concentration in the initial reactant, the reaction behaviour of the H_2 in H_2 - C_2H_6 mixture is approaching to that of pure H_2 . The effect of H_2 addition on the H_2 reaction rates of H_2 - C_2H_6 is same as that of H_2 - CH_4 mixture. However, differing with the oxidation of H_2 - CH_4 , the addition of H_2 in H_2 - C_2H_6 mixture does not affect the time at which the equilibrium state is reached.

The volume of the gas mixture, consisting of reactants and products, is changing over the reaction. It is expanded after the reaction starting. Thus, the total number of mole of the gas mixture changes at different time point. Figure 6.12 shows the total number of mole of H_2 changes over time corresponding to different reactant composition. It basically agrees with Figure 6.11. As shown in Figure 6.12, obviously, the line of 50% initial H_2 concentration can be considered as the separation line. Above 50%, the oxidation of H_2 mechanism starts to play a part in the overall reaction. The consumption rate of hydrogen increases as increasing initial H_2 addition in H_2 - C_2H_6 mixture, and approaching to that of pure H_2 .

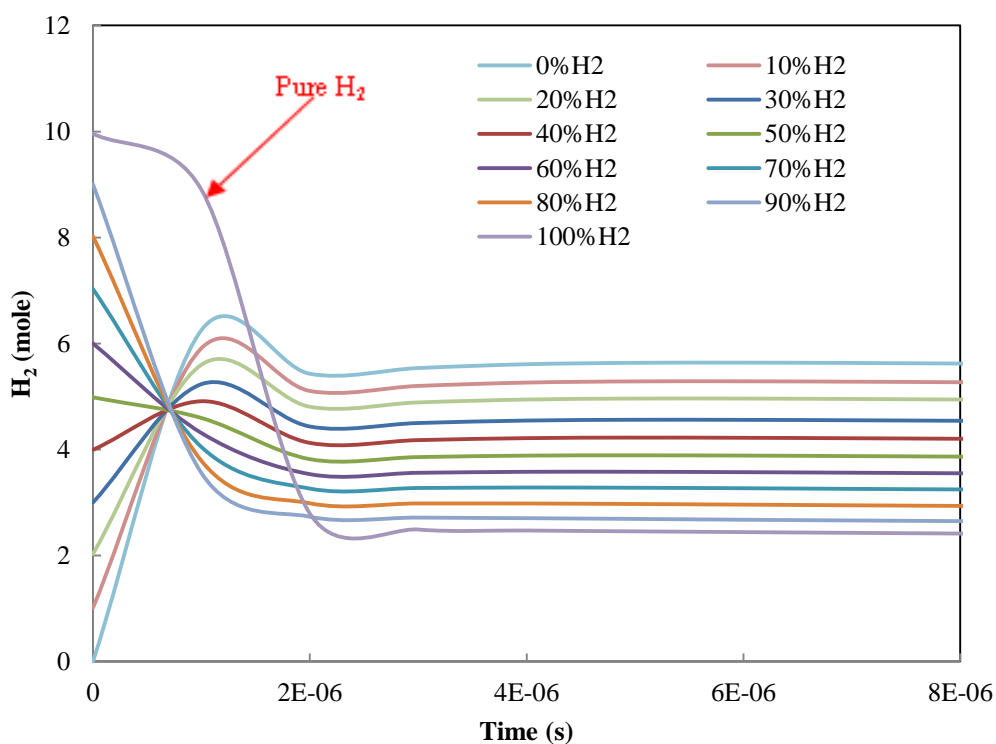


Figure 6.12: The number of mole of H_2 over time for H_2 - C_2H_6 reaction, at 2500K and 1 atm

However, the effect of the concentration of H_2 on the C_2H_6 consumption rate is not agreed with that on CH_4 . For the reaction of H_2 - CH_4 , the increasing concentration of the H_2 addition in the mixture results in the enhancement of the CH_4 decomposition. On the other hand, as illustrated in Figure 6.13, the reaction rate of C_2H_6 is independent with the H_2 addition concentration in the mixture. At

fixed initial system temperature and pressure, the decomposition rate of C_2H_6 is only relevant with the initial concentration of the C_2H_6 in the mixture. High initial C_2H_6 concentration in the reactant leads to high consumption rate of the C_2H_6 . In addition, with increasing the initial H_2 concentration in the reactant, the reactions of C_2H_6 reach the equilibrium state at the same time. The pure C_2H_6 as reactant has the highest decomposition rate compared with the others. Figure 6.14 shows the number of mole of the C_2H_6 during the reaction. It basically represents the same characteristics of C_2H_6 reaction kinetics as shown in Figure 6.13.

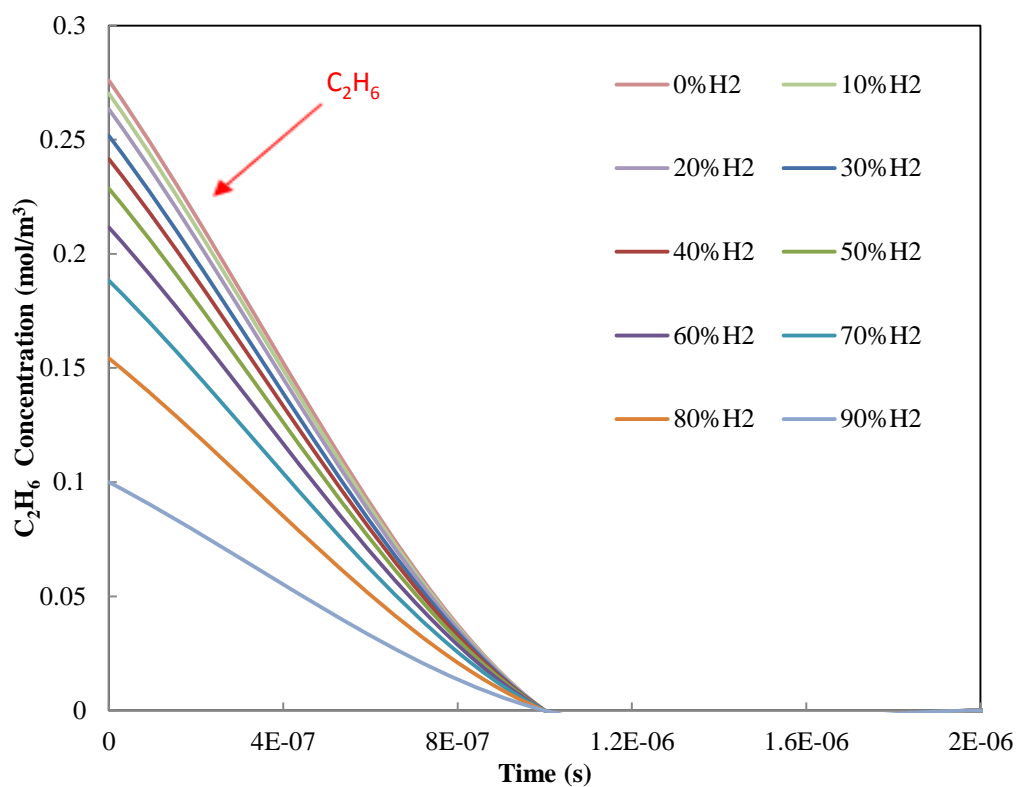


Figure 6.13: The C_2H_6 concentration over time for H_2 - C_2H_6 reaction, at 2500 K and 1 atm

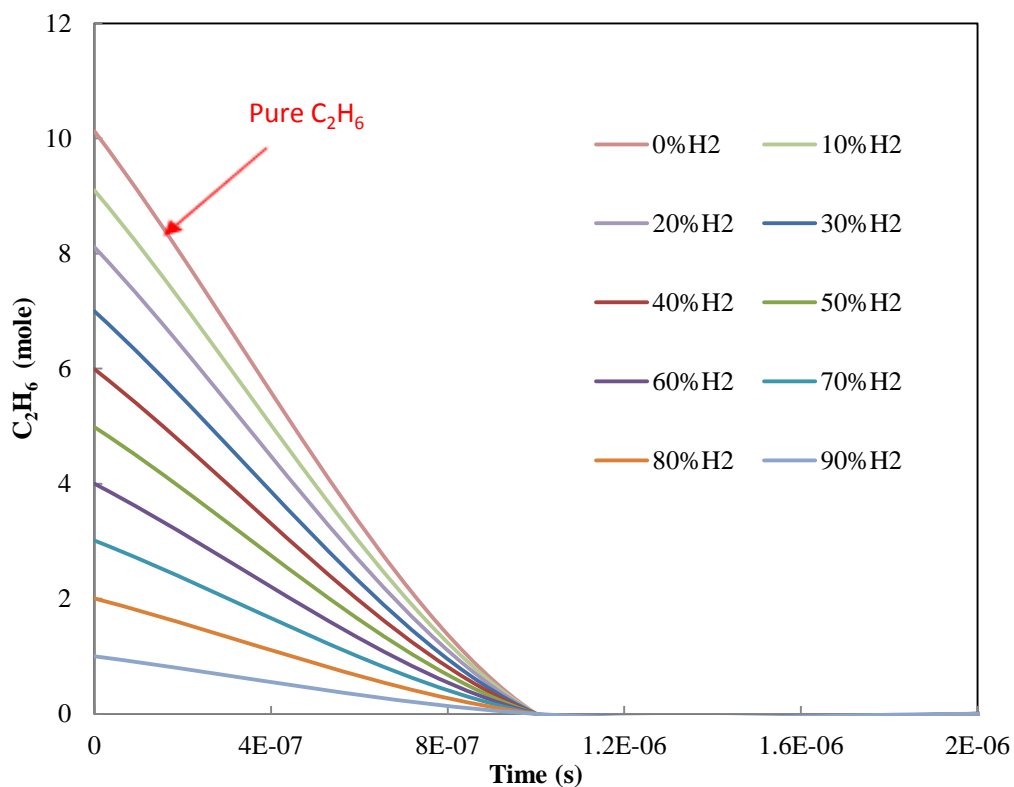


Figure 6.14: The number of mole of C_2H_6 over time for $H_2-C_2H_6$ reaction, at 2500 K and 1 atm

The correlation of OH and H concentration with the H_2 addition concentration in the reactant is shown in Figure 6.15 and Figure 6.16. It can be seen from the Figures that the main contributors of the OH and H in the reactions are from the oxidation of H_2 mechanism. The formation rate of H and OH increases with the initial H_2 concentration of the reactant. When H_2 concentration is greater than 60%, the increase in the concentrations and production rates of H and OH becomes more sensitive to the increase of H_2 addition concentration. Thus, the effect of H_2 addition on H and OH concentration for $H_2-C_2H_6$ is same as H_2-CH_4 mixture. When the fuel is consisting of pure hydrogen, the concentrations of H and OH at equilibrium state are higher than the other mixed $H_2-C_2H_6$ fuels. The pure H_2 fuel also gives the highest rate of formation of H and OH compared with the other $H_2-C_2H_6$ mixtures.

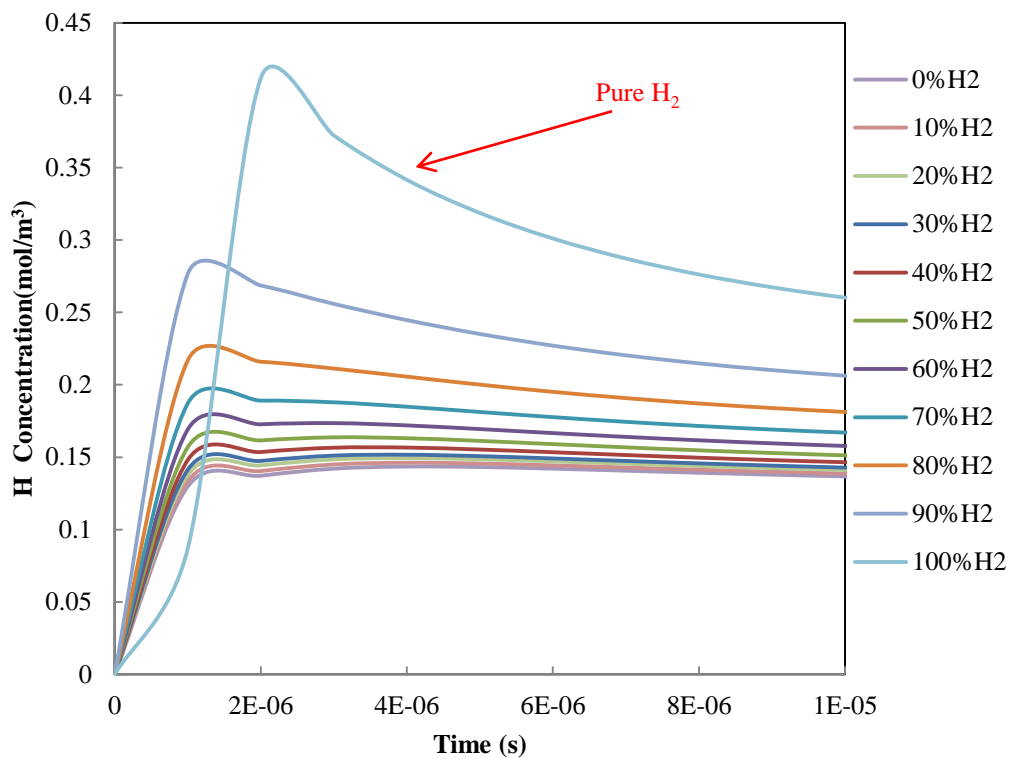


Figure 6.15: The H concentration over time for H₂-C₂H₆ reaction, at 2500 K and 1 atm

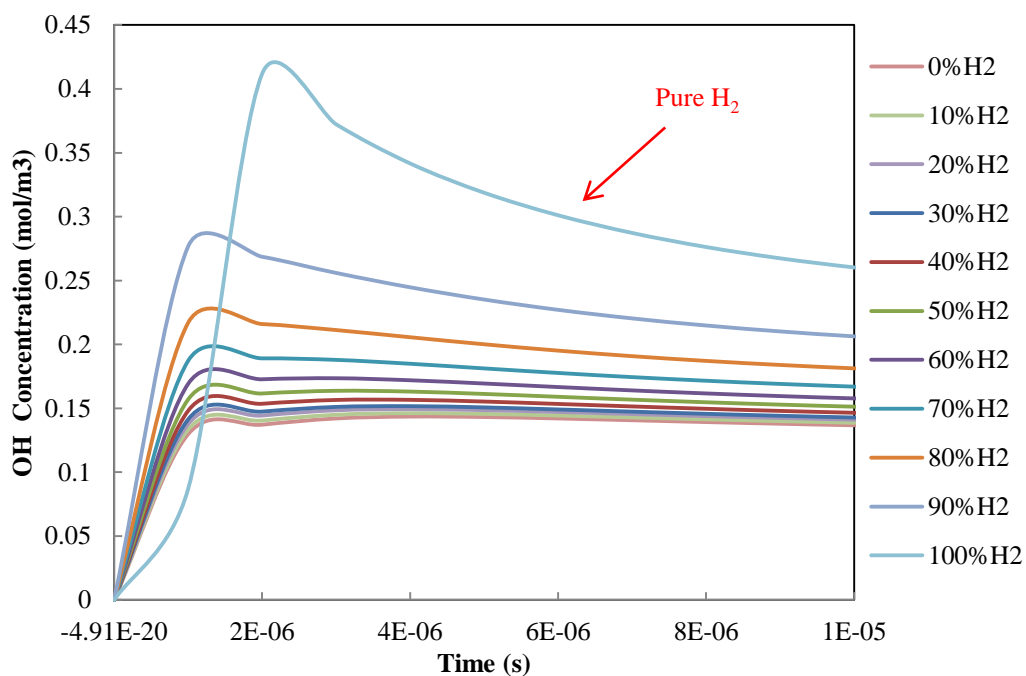


Figure 6.16: The OH concentration over time for H₂-C₂H₆ reaction, at 2500 K and 1 atm

The temperature characteristics of $\text{H}_2\text{-C}_2\text{H}_6$ reactions are shown in Figure 6.17. The reactions start from 2500 K and reach equilibrium state at approximately 3100 K. At equilibrium state, the reaction of pure H_2 has the highest temperature, which is just above 3100 K.

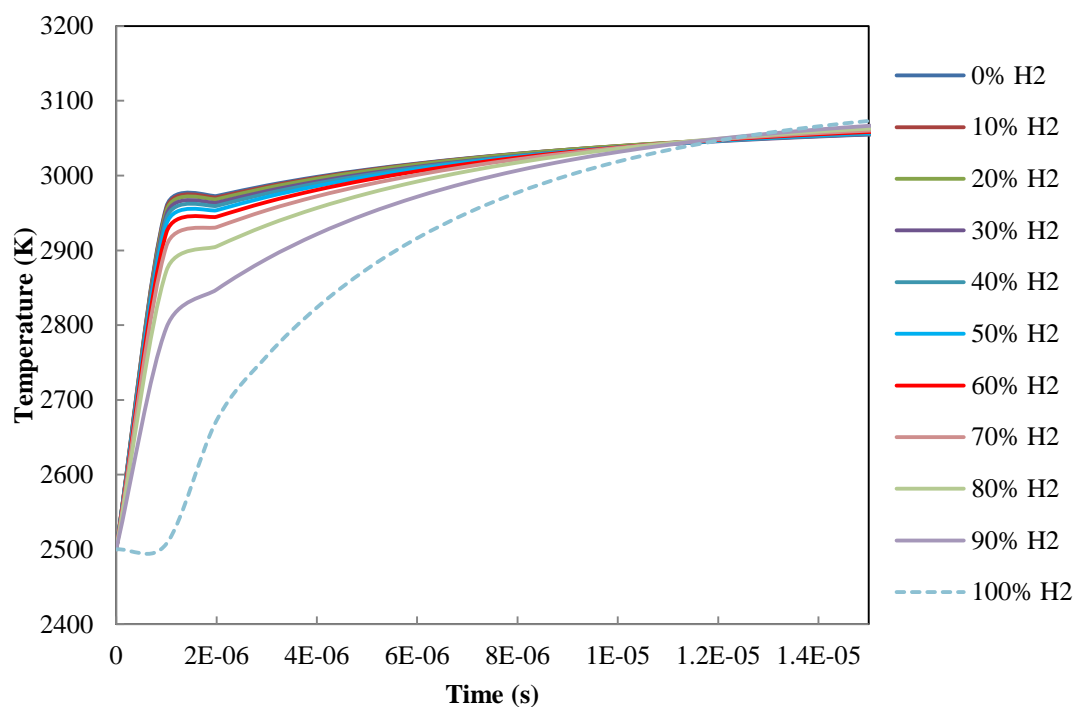


Figure 6.17: The Temperature profile of $\text{H}_2\text{-C}_2\text{H}_6$ reactions

6.4 Reaction Kinetics Simulation of $\text{H}_2\text{-C}_3\text{H}_8\text{-Air}$ Mixture

The effect of H_2 addition on the reaction of $\text{H}_2\text{-C}_3\text{H}_8$ mixture is similar to that of $\text{H}_2\text{-C}_2\text{H}_6$ mixture. The concentration and reaction rate of H_2 during the reaction is strongly dependent on the initial H_2 concentration in the mixture. However, the concentration and reaction rate of C_3H_8 is independent with the H_2 addition concentration but determined by the initial C_3H_8 concentration in the mixture. Figure 6.18 and Figure 6.19 present the concentration of H_2 and C_3H_8 changes over time at different H_2 addition concentration. Similar to $\text{H}_2\text{-CH}_4$ and $\text{H}_2\text{-C}_2\text{H}_6$ combustion, the H_2 addition starts to effectively influence the overall reaction mechanism when H_2 addition concentration is above 60%. On the other hand,

when the H_2 concentration is less than 60%, there is slight increase in H_2 concentration. This is caused by the H_2 generated from the oxidation of C_3H_8 . The oxidation of hydrocarbon mechanism is dominant the overall reaction. As the H_2 concentration is above 80%, the consumption rate of H_2 increases exponentially with the H_2 addition concentration. As the initial H_2 concentration of the reactant increasing, the consumption rate of H_2 is approaching to the curve of pure H_2 fuel.

As illustrated in Figure 6.19, the behaviour of the C_3H_8 is similar to C_2H_6 in the reaction of H_2 - C_2H_6 with air. High initial C_3H_8 concentration leads to high consumption rate of C_3H_8 during the reaction, rather than the concentration of H_2 addition. This is the main difference between H_2 - C_2H_6 / C_3H_8 mixture and H_2 - CH_4 mixture. The decomposition of the CH_4 strongly depends on the H_2 concentration in the fuel.

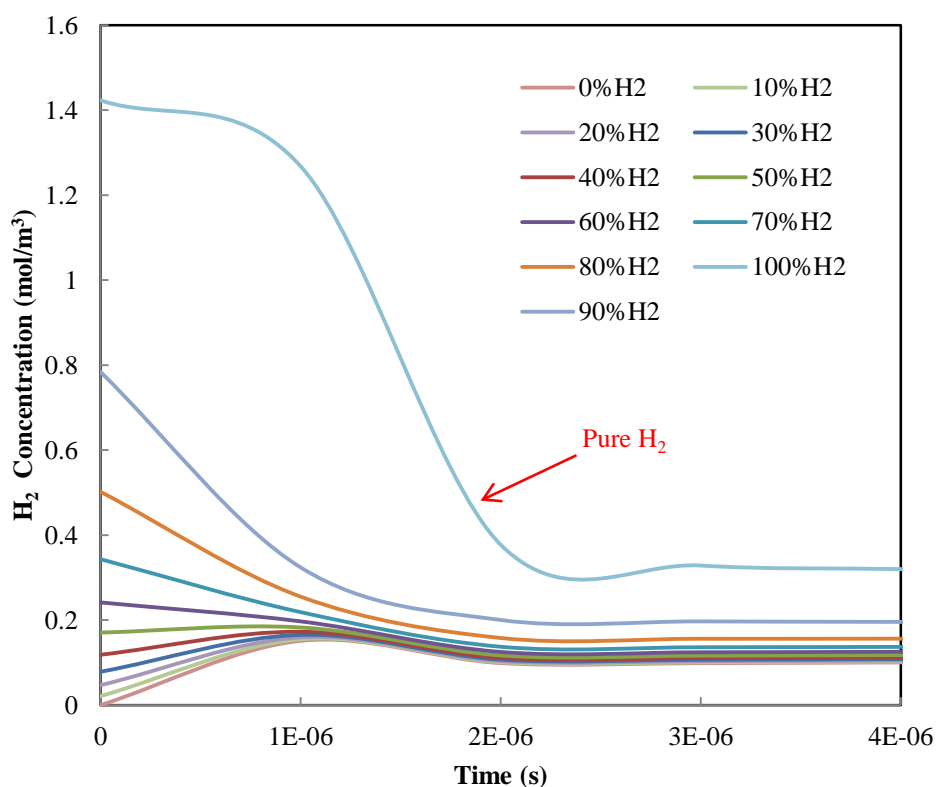


Figure 6.18: The H_2 concentration over time for H_2 - C_3H_8 reaction, at 2500 K and 1 atm

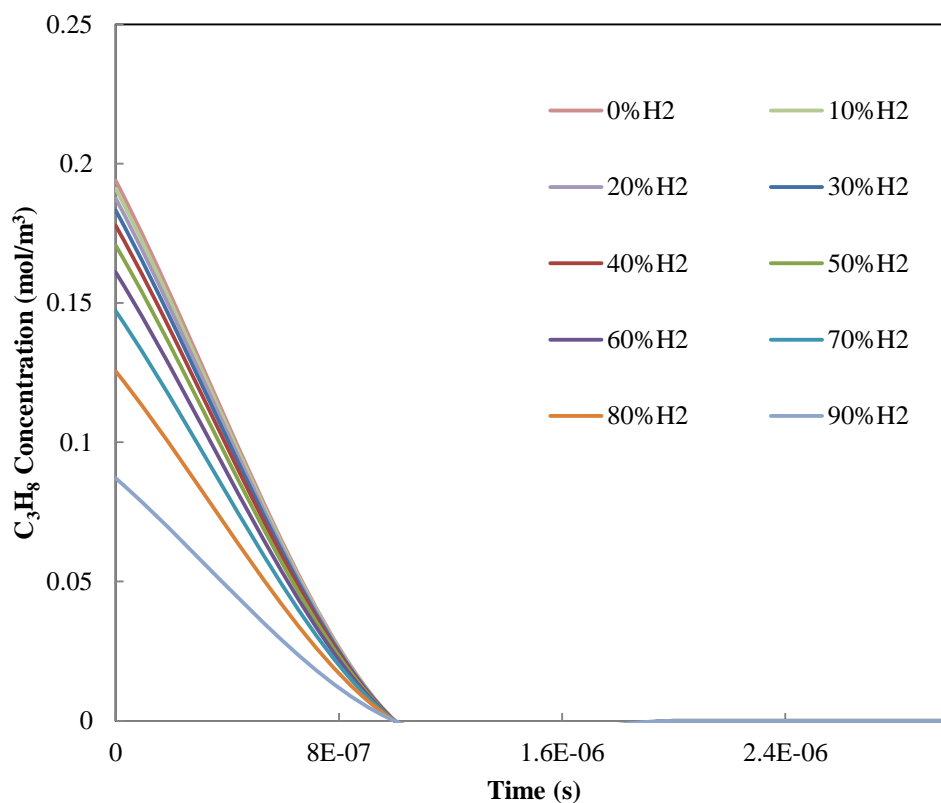


Figure 6.19: The C_3H_8 concentration over time for $H_2-C_3H_8$ reaction, at 2500 K and 1 atm

The concentration of the H and OH radicals are still strongly dependent on the concentration of the H_2 addition. This is one of the common points for H_2-CH_4 , $H_2-C_2H_6$ and $H_2-C_3H_8$ mixtures. This is shown in Figure 6.20 and Figure 6.21. The oxidation of pure H_2 has the much higher values of H and OH concentrations compared with that of H_2 -hydrocarbon.

The temperature gradients of $H_2-C_3H_8$ reactions are shown in Figure 6.22. The reactions start from 2500 K and reach equilibrium state at approximately 3100 K. At equilibrium state, the reaction of pure H_2 has the highest temperature, which is just above 3100 K.

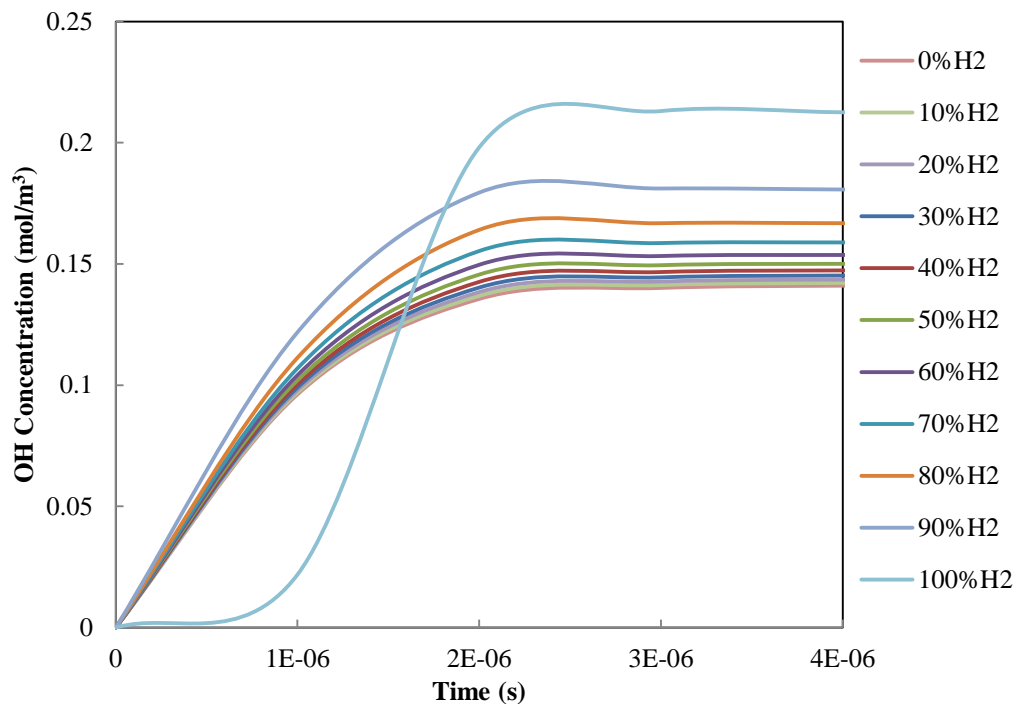


Figure 6.20: The OH concentration over time for $\text{H}_2\text{-C}_3\text{H}_8$ reaction, at 2500 K and 1 atm

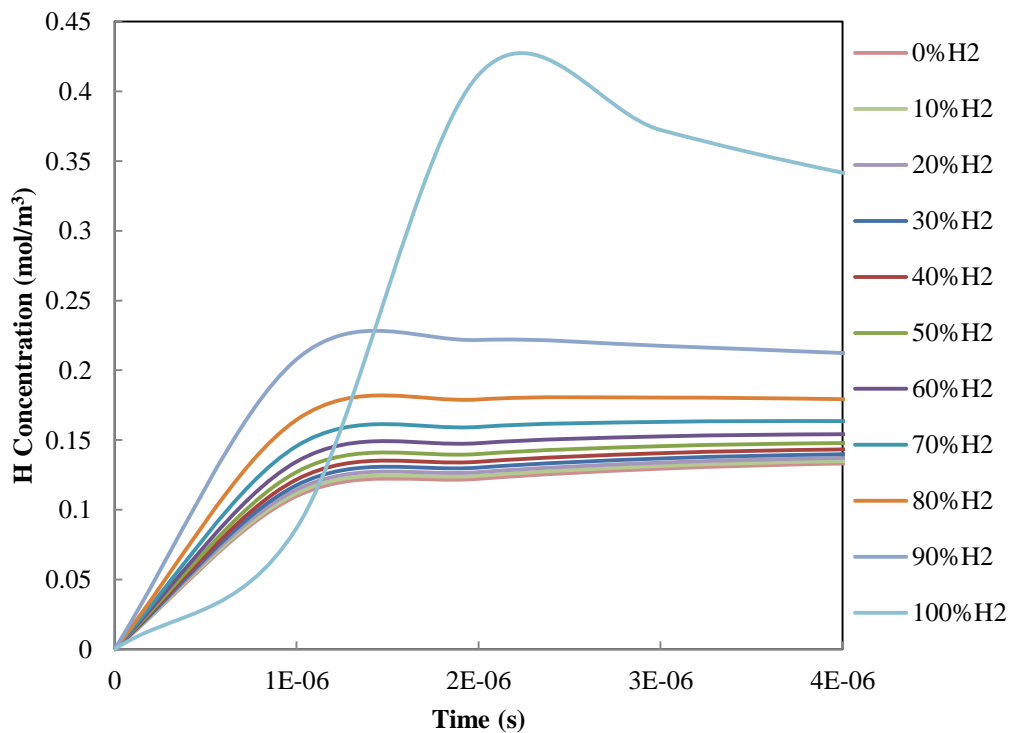


Figure 6.21: The H concentration over time for $\text{H}_2\text{-C}_3\text{H}_8$ reaction, at 2500 K and 1 atm

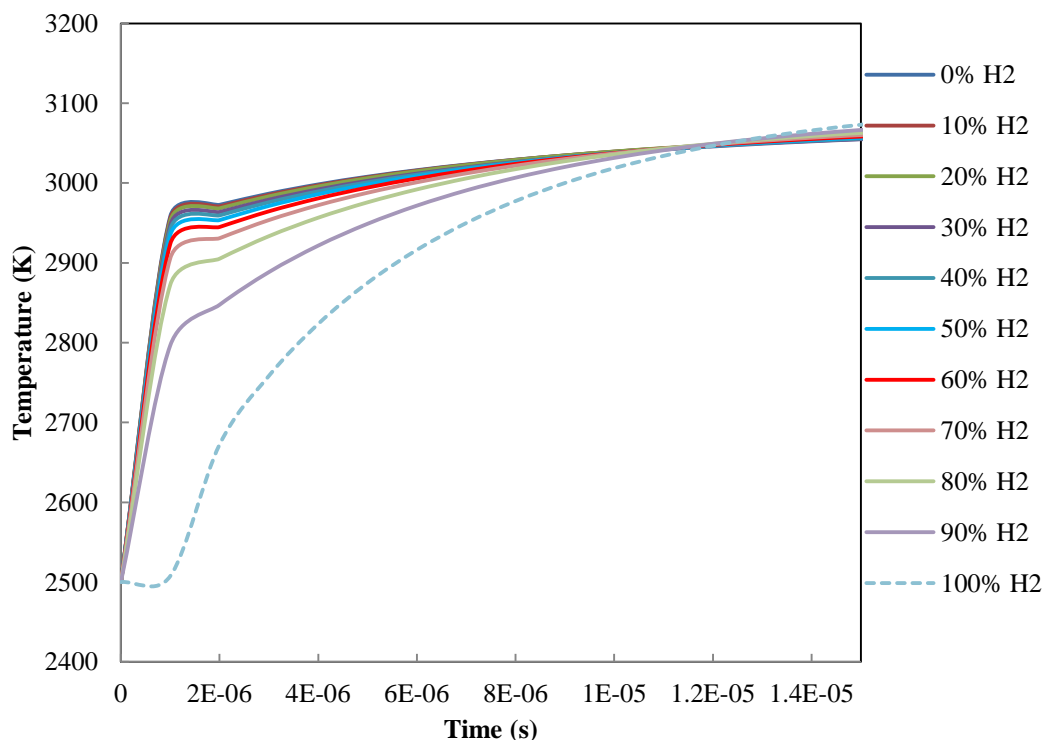


Figure 6.22: The temperature profile for $\text{H}_2\text{-C}_3\text{H}_8$ reactions

6.5 Summary

- Both of Gri-Mech 3.0 and Warnatz reaction mechanisms can be utilised for hydrogen, methane, ethane and propane combustion kinetics simulation. However, Warnatz is more suitable for the simulation of hydrogen-hydrocarbon mixtures, which provides relatively more detailed and comprehensive considerations for the reaction kinetics.
- The reaction kinetics equilibrium simulation is conducted in closed homogeneous reactor. The change in the concentration of CH_4 , C_2H_6 , C_3H_8 , H and OH is given.
- For $\text{H}_2\text{-CH}_4$ mixture, when initial H_2 in the mixture is lower than 50% the CH_4 oxidation mechanism governs the overall reaction mechanism. The consumption rate of CH_4 depends on the initial H_2 concentration in the mixture. The rate of decomposition of CH_4 increases as increasing the H_2 concentration.
- Compared with $\text{H}_2\text{-CH}_4$ mixture, the decomposition rate of C_3H_8 and C_2H_6 is

not quite sensitive to the initial H_2 concentration in the mixture. It is more dependent on the initial concentration of themselves.

- The main contributions of H and OH radicals are from the oxidation of H_2 . The concentration and formation rate of the radicals strongly depend on the initial H_2 concentration in the mixture.
- CH radical is an intermediate product and it does not present at the equilibrium state as a product.

Chapter 7

Species Pathway Analysis

The numerical modelling of the reaction kinetics has shown the effect of H₂ concentration on species concentrations and reaction rates of the reactions of H₂-hydrocarbon mixtures. This chapter presents the species pathway analysis which is capable of showing the paths of the species production and consumption

7.1 Introduction

The mechanism analysis for the oxidation of hydrocarbon-hydrogen mixtures concerns rate of production analysis and sensitivity analysis, in which the rate of production analysis can be used to determine the pathway of the selected species in the combustion process. The complementary information about the contributions of each individual reaction to a species' net rate can be obtained through the rate of production analysis. In this study, the hydrocarbon –hydrogen mixtures involved are CH₄-H₂, C₂H₆-H₂ and C₃H₈-H₂ mixtures. The mechanisms used in this study is the H₂, CO, C₁, C₂ and C₃ hydrocarbons oxidation mechanism developed by Warnatz and Heghes (2006), which is same as the one used for the reaction kinetics equilibrium simulation.

There are many elementary reactions and species involved in the oxidation of hydrocarbon-hydrogen mixtures. Both hydrocarbon and hydrogen contribute to the production and consumption of the free radicals in the reactions. Some of the radicals play very important roles in the combustion of such mixtures, such as OH, H and CH. These radicals determine the decomposition of the reactants, so that the movement of the flame front. Thus, it is valuable to understand the pathway of the important radicals involved in the reactions and which radicals are participated and influence the decomposition of the reactants. Furthermore, with the aim of

understanding the role of hydrogen in the hydrocarbon-hydrogen oxidations it is essential to develop the pathway net that links H₂ with CH₄, C₂H₆ and C₃H₈. This not only allows the study of the effect of hydrogen on the pathway of the hydrogen-hydrocarbon mixtures, but also the comparison of the reaction pathways for C1-C3 mixtures.

The rate of production analysis is carried out by using CHEMKIN 4.1 package. This analysis provides the data that determines the contributors of a selected species consumption and formation. Thus, it is allowed that the pathway of a species can be determined through the rate of production analysis. Since surface reaction is not considered, the rate of production of a species k from an elementary reaction i is given as below:

$$P_{ki} = v_{ki} q_i \quad \text{Eq. 7-1}$$

Where v_{ki} is the net stoichiometric coefficient for the gas reaction i and q_i indicates the rate of progress of the gas reaction i

$$q_i = k_{fi} \prod_{k=1}^K [X_k]^{v_{ki}'} - k_{ri} \prod_{k=1}^K [X_k]^{v_{ki}''} \quad \text{Eq. 7-2}$$

Where X_k is the molar concentration of the k th species k_{fi} and k_{ri} and are the forward and reverse rate constants of the i th reaction. In which the forward rate constants are associated with the modified Arrhenius equation as previously introduced in Chapter 3.

In addition, when the rate of production analysis is employed, the calculations will be performed at every time step that has been set up in the CHEMKIN control panel. Thus, the rate of production of a selected species from a specific elementary reaction associated with the Arrhenius parameters can be calculated in the unit of mol/cm³·s. In the species pathway analysis the rate of productions of the selected species from all relevant elementary reactions are calculated, so it is

able to determine the main contributor of the species and how many percentages of the species is generated or consumed through the path.

7.2 Pathway Analysis of the Reactions of CH₄-H₂ Mixtures

The species concerned in CH₄-H₂ reaction pathway analysis were H₂, CH₄, H, OH and CH. The rate of production calculations were performed for the elementary reactions related to those species. In which, H₂ and CH₄ are the main reactants and presents in initiating reactions, and the pathway analysis shows the approach of the decomposition of them and the radicals involved. The consumption rate of the reactants actually decides the rate of the reaction and thus the velocity of the movement of the flame front. As previously stated in literature review, OH and H basically are the crucial radicals in hydrogen oxidation reactions. They present in many dominant elementary reactions in H₂/O₂ system. In the CH₄-H₂ oxidation mechanism, OH and H act as chain carrier and participate in many chain branching reactions which may govern the overall reaction rate. CH indicates the decomposition extent of the hydrocarbon reactants, methane, ethane and propane in this case.

The pathway analysis started with low hydrogen concentration H₂-CH₄ mixtures and 30% hydrogen concentration was given. To compare with the low hydrogen content H₂-CH₄ mixture, 90% hydrogen was then given in order to show if there was any discrimination upon the species pathway between high and low hydrogen concentration in the H₂-CH₄ mixtures.

7.2.1 Pathway Analyses of H₂

There were 40 elementary reactions involved in this pathway analysis and they were contributing to the decomposition and formation of H₂ during the reaction.

Table 7.1 shows the main H₂ consumption pathways for 30% and 90% H₂ of H₂-CH₄ mixtures. As illustrated in the table, the major paths for the consumption of H₂ are H₂+OH \rightleftharpoons H₂O+H and H₂+O \rightleftharpoons OH+H in which both H and OH are involved. These reactions come from the hydrogen oxidation reaction system. This means that the CH₄ oxidation mechanism does not essentially contribute to

the consumption of H₂. In addition, the first reaction is considered as chain carrying reaction while the second is chain branching reaction. The chain carrier H is also responsible for attacking O₂ to form chain branching reaction, for example, O₂+H \rightleftharpoons OH+O, in which the produced chain carriers will participate WR3 and WR4 to develop a cycle. The increasing reaction rate of chain branching reactions results in large amount of activated radicals being produced, as activated complex, in a unit time and then the overall reaction rate increases. By comparing 30% H₂ and 90% H₂, it is realised that the major pathways of consuming H₂ do not change due to varying H₂ concentration of the mixtures. However, with increasing H₂ concentration, the consumption is more concentrated on the major pathways, which are H₂+OH \rightleftharpoons H₂O+H and H₂+O \rightleftharpoons OH+H. It can be seen from Table 7.1 that there is approximately 10% increase in the H₂ consumption through the major pathways. At 90% H₂, over 98% of the hydrogen is consumed through H₂+OH \rightleftharpoons H₂O+H and H₂+O \rightleftharpoons OH+H in which the former takes the responsibility for more than half of the hydrogen consumed. Furthermore, the results also show that the main products from the decomposition of H₂ oxidation are H and OH.

Table 7.1: H₂ consumption pathway of the oxidation of H₂-CH₄ mixtures

H ₂ consumption pathway for H ₂ -CH ₄ oxidation reactions			
30% H ₂		90% H ₂	
Reaction	%	Reaction	%
WR4: H ₂ +OH \rightleftharpoons H ₂ O+H	57.90	WR4: H ₂ +OH \rightleftharpoons H ₂ O+H	63.04
WR3: H ₂ +O \rightleftharpoons OH+H	31.71	WR3; H ₂ +O \rightleftharpoons OH+H	35.22
WR131: C ₂ H ₂ +H \rightleftharpoons C ₂ H+H ₂	5.73	WR2: H ₂ +O \rightleftharpoons OH+H	1.03
WR41: CH ₂ ¹ +H \rightleftharpoons CO+H+H	3.05		
WR2: H ₂ +O \rightleftharpoons OH+H	0.89		

CH₂¹: the isotope of normal CH₂

WR: indicating the reaction number in the Warnatz mechanism

7.2.2 Pathway Analysis of CH₄

The pathway analysis of CH₄ of reactions of H₂-CH₄ mixtures was achieved to

demonstrate the relationship of CH₄ consumption pathways with H₂ and the influence of H₂ present in the mixture on the consumption rate of CH₄. There were 28 elementary reactions associated with the decomposition of CH₄ and involved in the analysis. The CH₄ consumption rate of each of these elementary reactions was calculated in order to determine the main contributors of the consumption of CH₄.

Table 7.2 shows the pathways of CH₄ being consumed through. As illustrated in the Table, the main pathways of CH₄ decomposition are basically three elementary reactions, which are CH₄+H \rightleftharpoons H₂+CH₃, CH₄+OH \rightleftharpoons H₂O+CH₃ and CH₄+O \rightleftharpoons OH+CH₃. At the first place, the CH₄ is decomposed to CH₃ through reaction with H. There is approximate half of the amount of CH₄ is consumed through this path. The second approach of consuming CH₄ is through the reaction associated with OH. The third path accounts for about 18% of total CH₄ consumption. The first two paths are chain carrying reactions and the third one is a chain branching reaction. The three main paths of consuming CH₄ show that the way of CH₄ being consumed is through the attack of H, OH and O on C-H bond and CH₄ is decomposed to CH₃. By comparing different H₂ concentration, it is found that increasing H₂ concentration does not change the paths through which CH₄ is consumed. However, the first pathway, CH₄+H \rightleftharpoons H₂+CH₃, takes more responsibility with CH₄ consumption as increasing H₂ concentration. At 90% H₂ in the mixture, there is more than half of CH₄ consumption is achieved through the reaction between CH₄ and H.

It can be seen that H and OH play very important role in CH₄ decomposition. Thus, when more H and OH exist in the reaction zone the reaction will be pushed toward to consume CH₄ more quickly. As previously shown in H₂ pathway, the consumption of H₂ is capable of producing H and OH, so more H₂ present in the mixture causes more H and OH existing in the reservoir. This means that the reaction rate of CH₄ oxidation can be enhanced by increasing H₂ concentration in the mixture. This can be proved by examining OH and H pathways to see if the majority of H and OH come from the oxidation of H₂ and involve in the CH₄ consumption paths.

Table 7.2: CH₄ consumption pathway of the oxidation of H₂-CH₄ mixtures

CH ₄ consumption pathway for H ₂ -CH ₄ oxidation reactions			
30% H ₂		90% H ₂	
Reaction	%	Reaction	%
WR95:CH ₄ +H \rightleftharpoons H ₂ +CH ₃	44.45	WR95: CH ₄ +H \rightleftharpoons H ₂ +CH ₃	56.21
WR97:CH ₄ +OH \rightleftharpoons H ₂ O+CH ₃	34.24	WR97: CH ₄ +OH \rightleftharpoons H ₂ O+CH ₃	25.20
WR96:CH ₄ +O \rightleftharpoons OH+CH ₃	17.56	WR96: CH ₄ +O \rightleftharpoons OH+CH ₃	17.71
WR99:CH ₄ +O ₂ \rightleftharpoons CH ₃ +HO ₂	1.54	WR99:CH ₄ +O ₂ \rightleftharpoons CH ₃ +HO	0.68

WR: indicating the reaction number in the Warnatz mechanism

7.2.3 Pathway Analysis of H

The pathway analysis of H was implemented by calculating the rate of production of H for 88 elementary reactions concerning the generation and consumption of H.

Table 7.3 shows the pathway of H in the oxidation of CH₄-H₂ mixture. As indicated in Table 7.3, at 30% H₂ the paths listed in the Table cover near 75% of the total H production. There are also some other minor paths which are not shown in the Table. It can be seen that the paths of generating H are relatively disperse, however, the major paths, WR4 and WR3, are from the direct decomposition of H₂. They are also the main pathways of consuming H₂ as discussed previously. The other noticeable paths, such as CH₃+O \rightleftharpoons CH₂O+H, CHO+M \rightleftharpoons CO+H+M and CH₂+O₂ \rightleftharpoons CO+OH+H, account for approximate 30% of the H generation in the reaction. These elementary reactions produce H through the breakdown of CH₃, CHO and CH₂, which are essentially the intermediate products of the decomposition of CH₄. These results show that at low H₂ concentration in the mixture both CH₄ and H₂ oxidation supply the paths for H generation and contribute to a large amount of H production. On the other hand, when the mixture having 90% H₂ present in, the pathways of generating H seem more concentrated compared with low H₂ concentration. There are more than 70% of the H produced through WR4 and WR3, in which the reaction, H₂+OH \rightleftharpoons H₂O+H, is the path for more than 50% of the H generation during the reaction while H₂+O \rightleftharpoons OH+H is responsible for almost 30% of the total H

produced. The proportion for the other paths is relatively reduced. In addition, as previously discussed in CH₄ consumption pathway, one of the major pathways for CH₄ decomposition is CH₄+H \rightleftharpoons H₂+CH₃, in which CH₄ is attacked by H to form CH₃. This claims that H is one of the main carriers for decomposing CH₄. With 90% H₂ concentration, over 80% of the total H production comes from the primary decomposition of H₂ and is directly related to the H₂ concentration in the mixture. This implies that the decomposition rate of CH₄ is dependent on H₂, rather than methane itself, when very high H₂ concentration existing in CH₄-H₂ mixture. This can be concluded as that when H₂ concentration of the CH₄-H₂ mixture is high enough the H₂ oxidation mechanism starts to govern the production of H and dominate the overall reaction mechanism as well as the overall reaction rate.

Table 7.3 also illustrates the consumption pathways for H. This analysis is capable of showing if H is essentially associated with the decomposition of CH₄ as previously discussed, and also, of course, is able to determine the paths through which the H is consumed. As shown in Table 7.3, the most distinct pathway is WR1, O₂+H \rightleftharpoons OH+O. For both 30% and 90% hydrogen, there is about half of the H consumed through this elementary reaction. By comparing the pathways of 30% with 90% hydrogen, although the main pathways of H consumption do not change due to varying H₂ concentration, the proportion of each path accounted for is slightly different.

WR95 is appeared as one of the main paths for H consumption, and which is also as the major path for the decomposition of CH₄. As shown in Table 7.3, at 30% H₂ concentration it accounts for approximate 23% of the total H consumption and is the second path through which H is consumed. WR50, CH₃+H \rightleftharpoons CH₂+H₂, is at the third place and accounts for about 8% of the H consumption. CH₃ is actually produced through the breaking down of CH₄, in which C-H is attacked by H, OH and O. However, when H₂ concentration reaching 90%, H consumption through WR95 is reduced and distributed to other paths. The second place is taken by WR130, C₂H+H+M \rightleftharpoons C₂H₂+O, in which H is consumed through reacting with C₂H.

The main source of C₂H in the reaction mechanism is from the decomposition of

C_2H_2 via H and OH. Basically, C_2H_2 is produced in three paths, which are the combination of CH_2 , the reaction between C_2H and H and the decomposition of C_2H_4 . This interaction is illustrated in Figure 7.1. When H content increases as increasing H_2 concentration in H_2 - CH_4 mixture, more CH_3 and CH_2 will be generated through the decomposition of CH_4 . This results in the production of C_2H and C_2H_2 in the system. C_2H and C_2H_2 are taken account as the products that are resulted from the decomposition of CH_4 . Thus, H not only participates in the primary decomposition of CH_4 , but also is employed to decompose the products risen from the decomposition of CH_4 .

Table 7.3 also introduces some other paths which are responsible for the consumption of H. These paths include the reaction of H with CHO, CH_2O , HO_2 , CH_3 and CH, in which the reaction between H and HO_2 belongs to the H_2 oxidation system and the others are relevant to the decomposition of CH_4 . And these paths account for approximate 20% of the H consumption. The relationship between CHO, CH_2O and CH_3 and the decomposition of CH_4 is shown in Figure 7.2. As shown in the Figure, the CHO, CH_2O and CH_3 are essentially the products resulting from the decomposition of CH_4 same as C_2H and C_2H_2 . Apart from WR1, WR10 and WR11, the other paths that the H is consumed through are all concerning the primary decomposition of CH_4 and the products produced from the decomposition of CH_4 . Thus, the presence of H in the system strongly influences the decomposition rate of CH_4 . In addition, as H is consumed by CH_4 and its decomposed products, the consumption rate of H_2 in WR4 and WR3 will be increased. The pathway of CH is not discussed here yet, but it will be introduced later in this Chapter. The other important radical which links CH_4 with H_2 is OH.

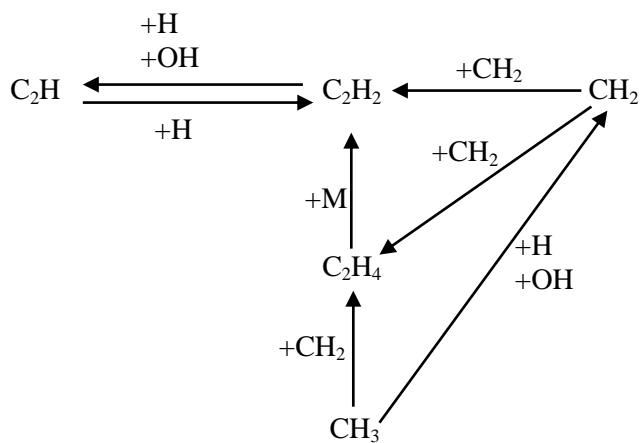


Figure 7.1: The production paths of C_2H and C_2H_2

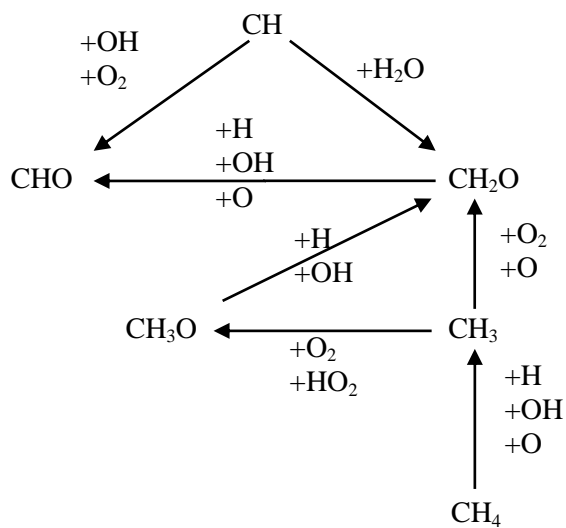


Figure 7.2: The production paths of CHO , CH_2O and CH_3

Table 7.3: H consumption and generation pathways of the oxidation of H₂-CH₄ mixtures

H pathways for H ₂ -CH ₄ oxidation reactions			
Generation			
30% H ₂		90% H ₂	
Reaction	%	Reaction	%
WR4:H ₂ +OH<=>H ₂ O+H	24.52	WR4:H ₂ +OH<=>H ₂ O+H	53.63
WR3:H ₂ +O<=>OH+H	13.43	WR3:H ₂ +O<=>OH+H	29.97
WR67:CH ₃ +O<=>CH ₂ O+H	10.21	WR67:CH ₃ +O<=>CH ₂ O+H	3.67
WR34:CHO+M<=>CO+H+M	9.34	WR51:CH ₂ +O ₂ <=>CO+OH+H	3.04
WR51:CH ₂ +O ₂ <=>CO+OH+H	9.11	WR34:CHO+M<=>CO+H+M	2.66
WR118:CO+OH<=>CO ₂ +H	4.88	WR118:CO+OH<=>CO ₂ +H	1.07
WR119:CO+OH<=>CO ₂ +H	3.02	WR42:CH ₂ ¹ +O=>CO+H+H	1.04
Consumption			
30% H ₂		90% H ₂	
Reaction	%	Reaction	%
WR1:O ₂ +H<=>OH+O	48.86	WR1:O ₂ +H<=>OH+O	54.96
WR95:CH ₄ +H<=>H ₂ +CH ₃	23.18	WR130:C ₂ H ₂ +O<=>C ₂ H+H+M	9.33
WR50:CH ₂ +H ₂ <=>CH ₃ +H	8.06	WR131:C ₂ H ₂ +H<=>C ₂ H+H ₂	6.16
WR54:CH ₂ O+H<=>CHO+H ₂	5.39	WR95:CH ₄ +H<=>H ₂ +CH ₃	5.71
WR130:C ₂ H ₂ +O<=>C ₂ H+H+M	4.52	WR10:H+O ₂ +M<=>HO ₂ +M	5.71
WR25:CH+H<=>C+H ₂	2.33	WR50:CH ₂ +H ₂ <=>CH ₃ +H	4.20
WR35:CHO+H<=>CO+H ₂	2.05	WR54:CH ₂ O+H<=>CHO+H ₂	4.06
WR11:HO ₂ +H<=>OH+OH	1.55	WR11:HO ₂ +H<=>OH+OH	3.36
WR10:H+O ₂ +M<=>HO ₂ +M	1.53	WR35:CHO+H<=>CO+H ₂	1.76

WR: indicating the reaction number in the Warnatz mechanism

7.2.4 Pathway Analysis of OH

As shown in Tables 7.1 and 7.2, OH is the chain carrier in the paths for both CH₄ and H₂ consumption. WR4, H₂+OH<=>H₂O+H, accounts for about 60% of the H₂ consumption, on the other hand, WR97, CH₄+OH<=>H₂O+CH₃, is the path through which over 20% of the CH₄ in the mixture is decomposed. In the pathway analysis of the OH of the H₂-CH₄ mixtures oxidation reaction, there were 80 elementary reactions concerned for generation and consumption of OH in the

reaction mechanism. The rate of production for each of the elementary reactions was calculated and simulated to determine the paths in which OH is produced and consumed.

Table 7.4 shows the consumption and production paths for OH of H₂-CH₄ oxidation reaction. Firstly, the generation paths of OH are discussed. For 30% H₂ concentration, the paths listed in the table occupy about 95% of the total OH generation. There are 4 out of 8 paths coming from the hydrogen oxidation system, which are WR1, WR3, WR11 and WR5. At the first place, O₂+H \rightleftharpoons OH+O is the path through which approximate 47% OH is produced. As shown in Table 7.3, the major path of producing H is WR4 in which H is produced through the reaction between H₂ and OH. Thus, in terms of generation, H and OH have impact on each other. The other crucial path for OH generation is WR3 which also is one of the main paths for H generation. In fact, OH not only is from the H₂-O₂ system, but also the decomposition of CH₄ and its sub-decomposed products. As listed in Table 7.4, paths WR51, WR96, WR135 and WR55 are from CH₄ oxidation mechanism. These paths account for 28% of the OH generation, while the paths from the H₂-O₂ system occupy about 68%. This shows that though CH₄ decomposition mechanism produces OH, the main contributors for OH generation are from H₂-O₂ system. This phenomenon is same as that of H.

The paths for OH generation at 90% H₂ concentration are listed in Table 7.4. As shown in the Table the two major pathways of OH generation still are WR1 and WR3. As increasing hydrogen concentration of the mixture, the proportion of each path accounts for is increasing. Over 50% of the OH generated comes through WR1, O₂+H \rightleftharpoons OH+O. There also is a dramatic increase in WR3 from 15% to 35%. It can be seen from Table 7.4 that there is about 85% of the OH generated through WR1 and WR3. Compared with this value, the amount of OH generation through CH₄ oxidation mechanism is far more less. With increasing H₂ concentration, the increase of the OH production rate in the paths from hydrogen oxidation mechanism causes the reduction in the paths from methane oxidation mechanism.

Table 7.4 also introduces the paths for the consumption of OH. For 30% and 90% hydrogen, the path through which OH is consumed the most is WR4. It means that the majority of the OH in the system is consumed through the decomposition of hydrogen. This is slightly different with H, most of which is employed to react with oxygen to form OH and O. These two radicals are then used to decompose H₂. At relatively lower hydrogen concentration, WR97(CH₄+OH<=>H₂O+CH₃) is the second path for OH consumption and which is one of the main path through which CH₄ is primarily decomposed.

Table 7.4: OH consumption and generation pathways of the oxidation of H₂-CH₄ mixtures

OH pathways for H ₂ -CH ₄ oxidation reactions			
Generation			
30% H ₂		90% H ₂	
Reaction	%	Reaction	%
WR1:O ₂ +H<=>OH+O	47.42	WR1:O ₂ +H<=>OH+O	50.42
WR3:H ₂ +O<=>OH+H	15.42	WR3:H ₂ +O<=>OH+H	34.78
WR51:CH ₂ +O ₂ <=>CO+OH+H	10.47	WR11:HO ₂ +H<=>OH+OH	6.17
WR96:CH ₄ +O<=>OH+CH ₃	8.89	WR51:CH ₂ +O ₂ <=>CO+OH+H	3.53
WR135:C ₂ H ₂ +O ₂ <=>HCCO	7.25	WR96:CH ₄ +O<=>OH+CH ₃	1.65
WR11:HO ₂ +H<=>OH+OH	3.02	WR2:H ₂ +O<=>OH+H	1.02
WR5:OH+OH<=>H ₂ O+O	1.92	WR135:C ₂ H ₂ +O ₂ <=>HCCO	0.90
WR55:CH ₂ O+O<=>CHO+OH	1.26		
Consumption			
30% H ₂		90% H ₂	
Reaction	%	Reaction	%
WR4:H ₂ +OH<=>H ₂ O+H	35.69	WR4:H ₂ +OH<=>H ₂ O+H	78.22
WR97:CH ₄ +OH<=>H ₂ O+CH ₃	21.97	WR134:C ₂ H ₂ +OH<=>H ₂ O+C ₂ H	3.82
WR69:CH ₃ +OH<=>CH ₂ +H ₂ O	11.95	WR69:CH ₃ +OH<=>CH ₂ +H ₂ O	3.31
WR134:C ₂ H ₂ +OH<=>H ₂ O+C ₂ H	7.24	WR97:CH ₄ +OH<=>H ₂ O+CH ₃	2.95
WR118:CO+OH<=>CO ₂ +H	7.10	WR15:HO ₂ +OH<=>H ₂ O+O ₂	2.85
WR119:CO+OH<=>CO ₂ +H	4.40	WR5: OH+OH<=>H ₂ O+O	2.34
WR38:CHO+OH<=>CO+H ₂ O	2.47	WR118:CO+OH<=>CO ₂ +H	1.55
WR5:OH+OH<=>H ₂ O+O	2.44	WR38:CHO+OH<=>CO+H ₂ O	1.12

Continue to Table 7.4

WR56:CH ₂ O+OH<=>CHO+H ₂ O	2.22	WR119:CO+OH<=>CO ₂ +H	0.99
--	------	----------------------------------	------

The third path of OH consumption is WR69(CH₃+OH<=>CH₂+H₂O), in which OH is used to decompose CH₃, the product from the primary decomposition of CH₄, into CH₂. Basically, at 90% hydrogen, the crucial path of OH consumption is WR4. The rest of the OH consumption is approximately evenly distributed to the other paths.

Table 7.4 also illustrates some other paths that are relevant to the decomposition of methane. In these paths, OH is employed to decompose C₂H₂, CH₂O and CHO. The sources of these radicals have already been shown in Figure 7.1 and Figure 7.2. Thus, the role of OH is similar to H, involving in the decomposition of CH₄. WR4 and WR97 are the main paths for decomposition of hydrogen and methane respectively, and both of them are the paths through which OH is consumed. This indicates that OH plays important role in both hydrogen and methane decomposition in the oxidation reaction of H₂-CH₄ mixtures. Apart from H and OH, CH is selected as the other important radical. It indicates the decomposition degree of CH₄.

7.2.5 Pathway Analysis of CH

CH is the product resulting from breaking down of CH₂. Figure 7.1 shows that CH₂ is produced from the decomposition of CH₃ through H and OH. Therefore, it can be considered that CH₄ is the root of CH. In addition, some other sub-products from the primary decomposition of CH₄, such as HCCO and C₂H, also lead to the generation of CH. There were 14 elementary reactions concerned for determining the paths of CH production and consumption.

The elementary reactions providing the pathways for generating and consuming CH are shown in Table 7.5. It can be realised from the Table that three paths of the CH generation are distinguished from the others, which are reaction WR30, WR41 and WR125. At 30% H₂ concentration, WR30 (CH+CO<=>HCCO) is at a dominant position over the other paths for generating CH. This path is performed

through the decomposition of HCCO into CH and CO and it accounts for near 77% of the CH generation in the mixture. However, with increasing hydrogen concentration to 90%, WR30 no longer is the first path for CH generation. Instead, WR41 ($\text{CH}_2^1 + \text{H} \rightleftharpoons \text{CH} + \text{H}_2$) takes the first place with a dramatic increase in the percentage. As indicated in Table 7.5, more than half of the CH is generated through WR41, in which the CH is produced through the oxidation of CH₂. At 90% hydrogen, WR30 is the second path as near 40% of the CH is produced through it. The proportion taken by the path, WR125 ($\text{C}_2\text{H} + \text{O}_2 \rightleftharpoons \text{CO}_2 + \text{CH}$), is reduced from 12.7% to 4.4% with increasing hydrogen concentration from 30% to 90%. So the main sources of CH production are from CH₂ and HCCO.

Table 7.5: CH consumption and generation pathways of the oxidation of H₂-CH₄ mixtures

CH pathways for H ₂ -CH ₄ oxidation reactions			
Generation			
30% H ₂		90% H ₂	
Reaction	%	Reaction	%
WR30: $\text{CH} + \text{CO} \rightleftharpoons \text{HCCO}$	76.92	WR41: $\text{CH}_2^1 + \text{H} \rightleftharpoons \text{CH} + \text{H}_2$	52.55
WR125: $\text{C}_2\text{H} + \text{O}_2 \rightleftharpoons \text{CO}_2 + \text{CH}$	11.66	WR30: $\text{CH} + \text{CO} \rightleftharpoons \text{HCCO}$	39.48
WR41: $\text{CH}_2^1 + \text{H} \rightleftharpoons \text{CH} + \text{H}_2$	8.90	WR125: $\text{C}_2\text{H} + \text{O}_2 \rightleftharpoons \text{CO}_2 + \text{CH}$	4.44
WR66: $\text{CH}_3 + \text{M} \rightleftharpoons \text{CH} + \text{H}_2 + \text{M}$	1.57	WR33: $\text{CH} + \text{H}_2\text{O} \rightleftharpoons \text{CH}_2^1 + \text{OH}$	2.20
WR33: $\text{CH} + \text{H}_2\text{O} \rightleftharpoons \text{CH}_2^1 + \text{OH}$	0.81	WR66: $\text{CH}_3 + \text{M} \rightleftharpoons \text{CH} + \text{H}_2 + \text{M}$	1.23
Consumption			
30% H ₂		90% H ₂	
Reaction	%	Reaction	%
WR29: $\text{CH} + \text{O}_2 \rightleftharpoons \text{CHO} + \text{O}$	42.38	WR25: $\text{CH} + \text{H} \rightleftharpoons \text{C} + \text{H}_2$	62.73
WR25: $\text{CH} + \text{H} \rightleftharpoons \text{C} + \text{H}_2$	26.52	WR29: $\text{CH} + \text{O}_2 \rightleftharpoons \text{CHO} + \text{O}$	23.22
WR41: $\text{CH}_2^1 + \text{H} \rightleftharpoons \text{CH} + \text{H}_2$	17.42	WR28: $\text{CH} + \text{OH} \rightleftharpoons \text{CHO} + \text{H}$	8.33
WR28: $\text{CH} + \text{OH} \rightleftharpoons \text{CHO} + \text{H}$	5.81	WR27: $\text{CH} + \text{O} \rightleftharpoons \text{CO} + \text{H}$	4.31
WR100: $\text{CH}_4 + \text{CH} \rightleftharpoons \text{C}_2\text{H}_4 + \text{H}$	3.80		
WR27: $\text{CH} + \text{O} \rightleftharpoons \text{CO} + \text{H}$	2.93		

CH₂¹: the isotope of normal CH₂, WR: indicating the reaction number in the Warnatz mechanism

CH_2 is a product resulting from the decomposition of CH_4 . With increasing hydrogen concentration in the mixture, the amount of H in the radical reservoir increases due to relatively high reaction rate of H_2 . WR41 comes up to the first path at 90% hydrogen meaning the decomposition rate of CH_2 is increased as increasing H_2 concentration.

The sources that HCCO is produced from are shown in Figure 7.3. It is essentially an intermediate product as the result of the decomposition of CH_3 into CH. And in this process, H_2 and O_2 play very important role, as they either directly take part in the reactions involved in the process or supply H, OH and O.

The role of H_2 in the decomposition of CH can be testified by conducting the pathway analysis for CH consumption. The main paths are determined and listed in Table 7.5. Hydrogen not only contributes to the formation of CH from a complex decomposition process of CH_3 , but also participates in the paths which are responsible for consuming CH. For both high and low hydrogen concentration, WR29 and WR25 are the two major paths through which CH is consumed. These two reactions are carried out in the way that CH radical is oxidised by O_2 and H. At high hydrogen concentration, as shown in Table 7.5, WR25 ($\text{CH} + \text{H} \rightleftharpoons \text{C} + \text{H}_2$) becomes the first path for CH consumption due to high H production rate in the system. As indicated in Table 7.5, over half of the CH in the system is consumed through the reaction with H. The other radicals directly contributing to the CH consumption are OH and O.

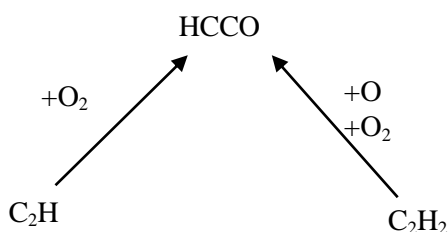


Figure 7.3: The production paths of HCCO

7.2.6 The Main Reaction Pathways

As previously discussed, when the combustion concerns the reaction of CH₄-H₂ mixture with air, the concentration of H and OH increases due to the presence of H₂ in the mixture. The primary paths of CH₄ consumption are WR95 (CH₄+H \rightleftharpoons H₂+CH₃) and WR97 (CH₄+OH \rightleftharpoons H₂O+CH₃). This shows that CH₄ is decomposed through the attack from H and OH. And CH₃ is formed through the primary decomposition of CH₄, it then derives to formation other sub-products. H and OH also participate in the paths of decomposition of the sub-products.

H and OH are mainly from the decomposition of H₂. Thus, it is realised that the presence of H₂ provides the radicals, H and OH, which are capable of enhancing the decomposition of the CH₄ in the mixture. As shown in Figure 7.4, primarily CH₄ is decomposed associated with H and OH to CH₃, and H₂ is oxidised to form H and OH. CH₃ is then decomposed to CHO and CH. In the complicated process of the decomposition of CH₄, O₂, O, OH and H play important role. As illustrated in Figure 7.5, both CH₄ and H₂ can provide H and OH radicals, however, the production from H₂ decomposition is far higher than that from CH₄ decomposition. Thus, the main contributors of H and OH are from the oxidation of H₂. The decomposition rates of both CH₄ and H₂ are strongly dependent on H and OH.

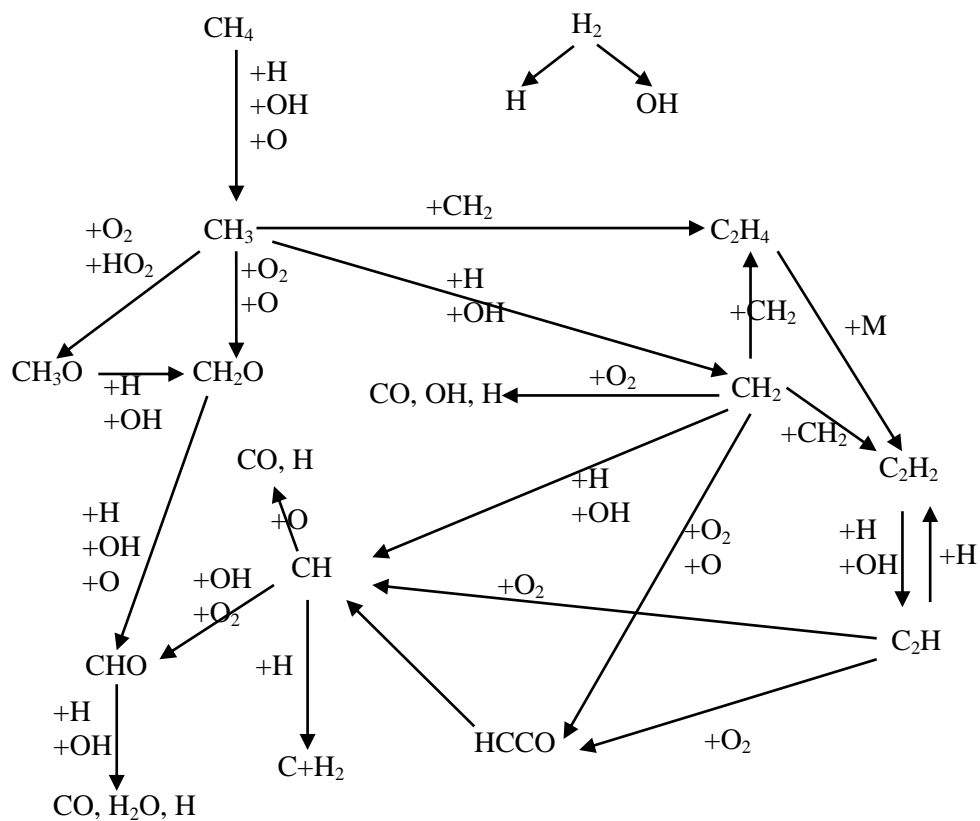
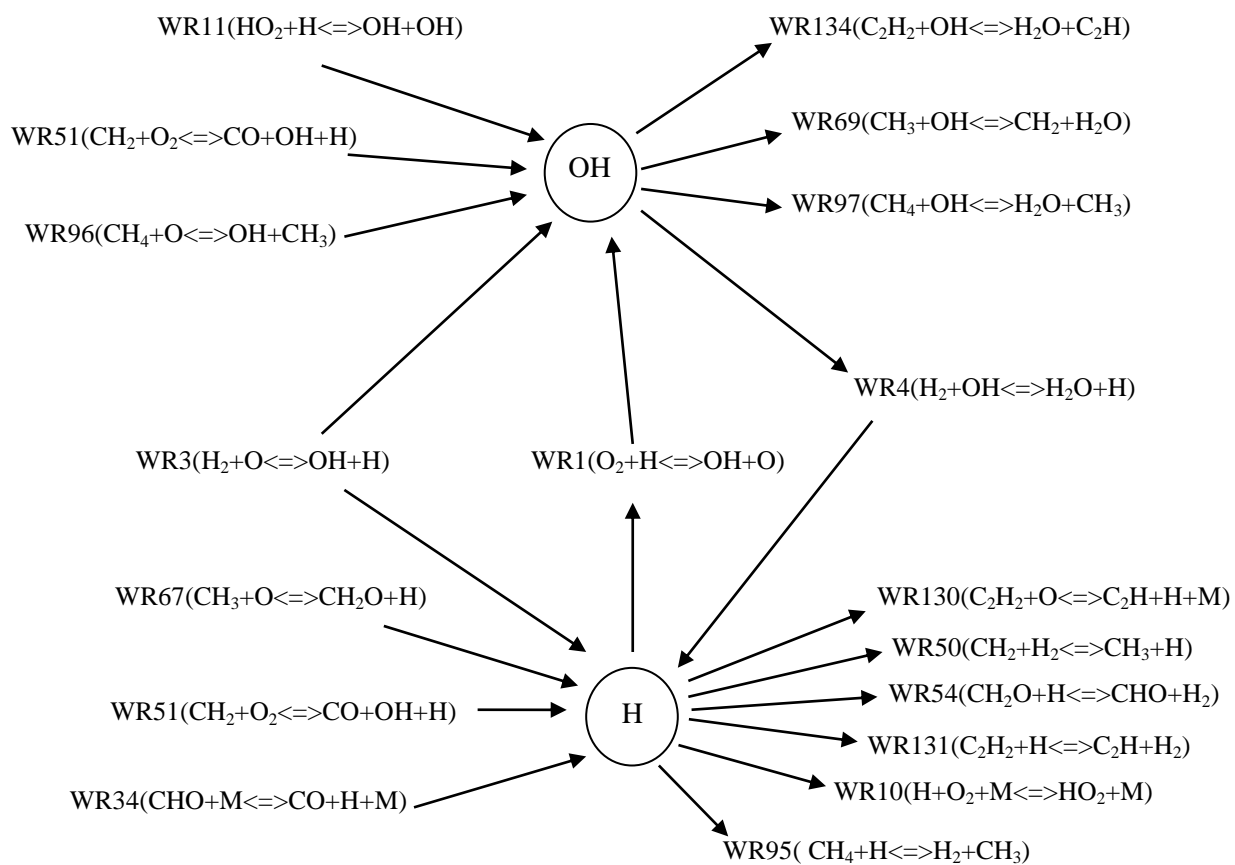


Figure 7.4: The main paths for CH₄ and H₂ in the oxidation of CH₄-H₂

Figure 7.5: The formation and consumption of H and OH in the oxidation of CH₄-H₂

7.3 Pathway Analysis of the Reactions of C₂H₆-H₂ Mixtures

The reaction pathways of the reactions of H₂-CH₄ mixtures have been discussed in the previous section. This section includes the pathway analysis of H₂-C₂H₆ mixture to compare the decomposition pathways of CH₄-H₂ mixtures.

7.3.1 Pathway Analysis of H₂

In the combustion of C₂H₆-H₂ mixtures, the major paths for consuming H₂ are basically same as those of CH₄-H₂ mixtures. WR4, WR3 and WR2 are the main elementary reactions through which the hydrogen is consumed. Thus, it can be realised that the paths of H₂ oxidation is not influenced by mixing hydrogen with different hydrocarbons. Hydrogen is still oxidised through $\text{H}_2 + \text{OH} \rightleftharpoons \text{H}_2\text{O} + \text{H}$ and $\text{H}_2 + \text{O} \rightleftharpoons \text{OH} + \text{H}$. Differing with CH₄-H₂ mixtures, WR131 and WR41 do not appear as the paths for H₂ consumption at low H₂ concentration in C₂H₆-H₂ mixtures. At low hydrogen concentration in the C₂H₆-H₂ mixtures, more H₂ is oxidised by O rather than OH. This is different from the paths of H₂-CH₄ mixture. However, with high hydrogen concentration, C₂H₆-H₂ and CH₄-H₂ mixtures have the same paths to for H₂ consumption.

7.3.2 Pathway Analysis of C₂H₆

Table 7.7 shows the paths through which C₂H₆ is consumed in the oxidation reaction of C₂H₆-H₂ mixtures. It is distinctly indicated in the Table that the primary pathway of consuming C₂H₆ is literally WR220 for both low and high hydrogen concentration conditions, in which C₂H₆ is directly oxidised by oxygen molecule. This shows the difference from the CH₄ decomposition pathways of CH₄-H₂ mixtures, in which the CH₄ decomposition is carried out through reacting with H and OH to form CH₃. However, in the reaction of H₂-C₂H₆ mixtures, H and OH do not present in the primary pathways and the primary product from the decomposition of C₂H₆ is C₂H₅.

Table 7.6: C₂H₆ consumption pathways of the oxidation of H₂-C₂H₆ mixtures

C ₂ H ₆ consumption pathways			
30% H ₂		90% H ₂	
Reaction	%	Reaction	%
WR220:C ₂ H ₆ +O ₂ <=>C ₂ H ₅ +HO ₂	99.997	WR220:C ₂ H ₆ +O ₂ <=>C ₂ H ₅ +HO ₂	99.997
WR77:C ₂ H ₆ +M<=>CH ₃ +CH ₃ +M	0.003	WR77:C ₂ H ₆ +M<=>CH ₃ +CH ₃ +M	0.003

WR: indicating the reaction number in the Warnatz mechanism

7.3.3 Pathway Analysis of H

When comparing the formation and consumption of H, the pathways for C₂H₆-H₂ and CH₄-H₂ mixtures are different especially in terms of consumption paths. As shown in Table 7.7, WR3(H₂+O<=>OH+H) and WR4(H₂+OH<=>H₂O+H) are still present in the main paths for H formation and this is similar to that of CH₄-H₂ mixture. However, the percentage taken by the path, CO+OH<=>CO₂+H, is dramatic increased. The relatively high carbon content in the reactant mixture results in more carbon dioxide formation as well as H. However, when hydrogen concentration is at 90%, WR4 and WR3 are still the dominant paths contributing for the formation of H. In the reaction of CH₄-H₂ mixture, there is relatively small amount of H come from CH₂, CH₃ and CHO, which are the products from the decomposition of CH₄. This is not found in the case of C₂H₆-H₂ mixture.

In terms of H consumption paths, basically all paths are from the oxidation of H₂. H is consumed through neither the decomposition of C₂H₆ nor the decomposition of its further decomposed products. For instance, C₂H₆+H<=>C₂H₅+H₂ does not appear in the pathway list as a path for H consumption. However, the first path of H being consumed is still O₂+H<=>OH+O and this is same as the circumstance in the reaction of CH₄-H₂ mixture.

Table 7.7: H formation and consumption pathways of the oxidation of H₂-C₂H₆ mixtures

H pathways for H ₂ -C ₂ H ₆ oxidation reactions			
Generation			
30% H ₂		90% H ₂	
Reaction	%	Reaction	%
WR118:CO+OH<=>CO ₂ +H	28.34	WR4:H ₂ +OH<=>H ₂ O+H	49.57
WR3:H ₂ +O<=>OH+H	24.80	WR3:H ₂ +O<=>OH+H	33.86
WR4:H ₂ +OH<=>H ₂ O+H	21.86	WR118:CO+OH<=>CO ₂ +H	6.01
WR119:CO+OH<=>CO ₂ +H	17.90	WR119:CO+OH<=>CO ₂ +H	4.13
WR120: CO+OH<=>CO ₂ +H	4.32	WR1:O ₂ +H<=>OH+O	3.34
WR1:O ₂ +H<=>OH+O	1.16	WR120: CO+OH<=>CO ₂ +H	1.03
Consumption			
30% H ₂		90% H ₂	
Reaction	%	Reaction	%
WR1:O ₂ +H<=>OH+O	64.73	WR1:O ₂ +H<=>OH+O	56.62
WR10:H=O ₂ +M<=>HO ₂ +M	18.59	WR10:H=O ₂ +M<=>HO ₂ +M	25.07
WR11:HO ₂ +H<=>OH+OH	7.41	WR11:HO ₂ +H<=>OH+OH	11.62
WR4:H ₂ +OH<=>H ₂ O+H	4.65	WR8:H+OH+M<=>H ₂ O+M	2.53
WR8:H+OH+M<=>H ₂ O+M	1.74	WR12:HO ₂ +H<=>H ₂ +O ₂	2.33
WR12:HO ₂ +H<=>H ₂ +O ₂	1.37		

WR: indicating the reaction number in the Warnatz mechanism

7.3.4 Pathway Analysis of OH

Table 7.8 shows that the major paths of OH formation are WR1 and WR3, accounting for more than 70% of the OH formation. This is same as the reaction of H₂-CH₄ mixture. But in the oxidation of H₂-CH₄ mixture the system of methane oxidation also contributes to the formation of OH as main paths, such as WR51, WR96 and WR135. However, this phenomenon is not found in the case of C₂H₆-H₂ mixture. The amount of OH produced from the oxidation of hydrocarbon compounds is extremely small, so that they are not listed in Table 7.8. Basically, all the paths contributing to more than 1% of OH formation come from the hydrogen oxidation mechanism.

As indicated in Table 7.8, in terms of OH consumption, at 30% hydrogen in the mixture, WR118 is the first path through which OH is consumed rather than WR4. When H₂ concentration is 90% in the mixture, WR4 becomes the first path through which OH is consumed. Apart from WR118, WR119 and WR120, the other paths are from the hydrogen oxidation mechanism. This is distinguished from the paths of H₂-CH₄ mixture, in which CH₄ decomposition mechanism also provides the paths for OH consumption

Table 7.8: OH formation and consumption pathways of the oxidation of H₂-C₂H₆ mixtures

OH pathways for H ₂ -C ₂ H ₆ oxidation reactions			
Generation			
30% H ₂		90% H ₂	
Reaction	%	Reaction	%
WR1:O ₂ +H<=>OH+O	53.07	WR1:O ₂ +H<=>OH+O	49.76
WR3:H ₂ +O<=>OH+H	20.69	WR3:H ₂ +O<=>OH+H	27.25
WR11:HO ₂ +H<=>OH+OH	12.15	WR11:HO ₂ +H<=>OH+OH	20.43
WR5:OH+OH<=>H ₂ O+O	9.19	WR5:OH+OH<=>H ₂ O+O	1.40
WR4:H ₂ +OH<=>H ₂ O+H	3.81	WR2:H ₂ +O<=>OH+H	0.76
Consumption			
30% H ₂		90% H ₂	
Reaction	%	Reaction	%
WR118:CO+OH<=>CO ₂ +H	31.54	WR4:H ₂ +OH<=>H ₂ O+H	54.82
WR4:H ₂ +OH<=>H ₂ O+H	24.33	WR15:HO ₂ +OH<=>H ₂ O+O ₂	13.08
WR119:CO+OH<=>CO ₂ +H	19.92	WR5:OH+OH<=>H ₂ O+O	12.69
WR15:HO ₂ +OH<=>H ₂ O+O ₂	10.32	WR118:CO+OH<=>CO ₂ +H	6.65
WR5:OH+OH<=>H ₂ O+O	5.40	WR119:CO+OH<=>CO ₂ +H	4.57
WR120:CO+OH<=>CO ₂ +H	4.80	WR1:O ₂ +H<=>OH+O	3.69
WR8:H+OH+M<=>H ₂ O+M	1.90	WR8:H+OH+M<=>H ₂ O+M	3.05
WR1:O ₂ +H<=>OH+O	1.29	WR120:CO+OH<=>CO ₂ +H	1.14

WR: indicating the reaction number in the Warnatz mechanism

7.3.5 Pathway Analysis of CH

Table 7.9 shows the paths for CH formation and consumption. In terms of formation, the major paths are same as those in the CH₄-H₂ reaction. For both 90% and 30% H₂ concentration in the mixture, the major paths of CH formation are through WR41, WR30, WR125 and WR33. However, as illustrated in Table 7.9, at low hydrogen concentration, WR41 is the first path for CH production. In the reaction of CH₄-H₂ mixture at 30% H₂ concentration, the dominant path of CH formation is WR30.

In terms of CH consumption, C₂H₆-H₂ and CH₄-H₂ reaction mechanisms have the same main paths, which are WR25, WR27, WR28 and WR29. However, at 30% hydrogen concentration, CH is mainly consumed to form C in C₂H₆-H₂ reaction mechanism but the first path of CH consumption is to form CHO in CH₄-H₂ reaction mechanism. In addition, at 90% hydrogen concentration, WR29 in C₂H₆-H₂ reaction mechanism also accounts for more percentage than that in CH₄-H₂ reaction mechanism.

Table 7.9: CH formation and consumption pathways of the oxidation of H₂-C₂H₆ mixtures

CH pathways for H ₂ -C ₂ H ₆ oxidation reactions			
Generation			
30% H ₂		90% H ₂	
Reaction	%	Reaction	%
WR41:CH ₂ ¹ +H<=>CH+H ₂	74.22	WR41:CH ₂ ¹ +H<=>CH+H ₂	52.55
WR30:CH+CO<=>HCCO	17	WR30:CH+CO<=>HCCO	39.48
WR125:C ₂ H+O ₂ <=>CO ₂ +CH	4.57	WR33:CH+H ₂ O<=>CH ₂ ¹ +OH	4.44
WR33:CH+H ₂ O<=>CH ₂ ¹ +OH	2.61	-	-
WR66:CH ₃ +M<=>CH+H ₂ +M	0.92	-	-
Consumption			
30% H ₂		90% H ₂	
Reaction	%	Reaction	%
WR25:CH+H<=>C+H ₂	53.06	WR25:CH+H<=>C+H ₂	62.73
WR28:CH+OH<=>CHO+H	16.13	WR28:CH+OH<=>CHO+H	23.22
WR27:CH+O<=>CO+H	14.47	WR27:CH+O<=>CO+H	8.33

Continue to Table 7.9

WR29:CH+O ₂ <=>CHO+O	13.81	WR29:CH+O ₂ <=>CHO+O	4.31
WR31:CH+CO ₂ <=>CHO+CO	1.72	-	-

CH₂¹: the isotope of normal CH₂

WR: indicating the reaction number in the Warnatz mechanism

7.3.6 The Main Reaction Pathways

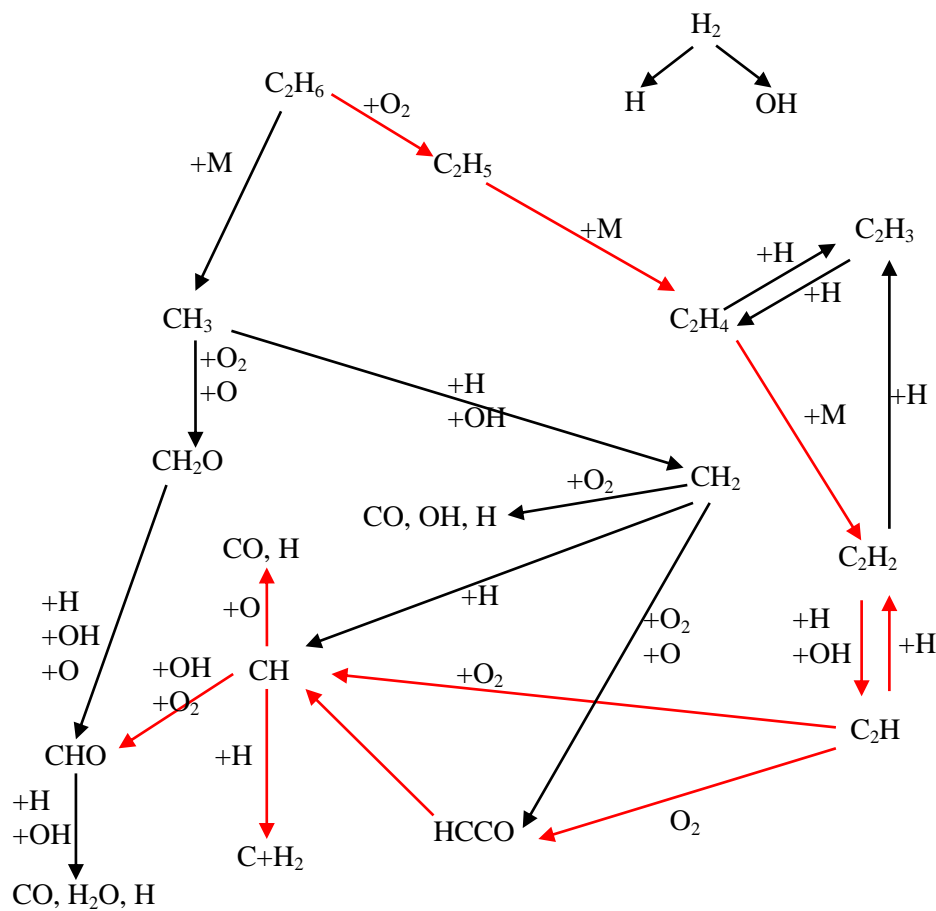
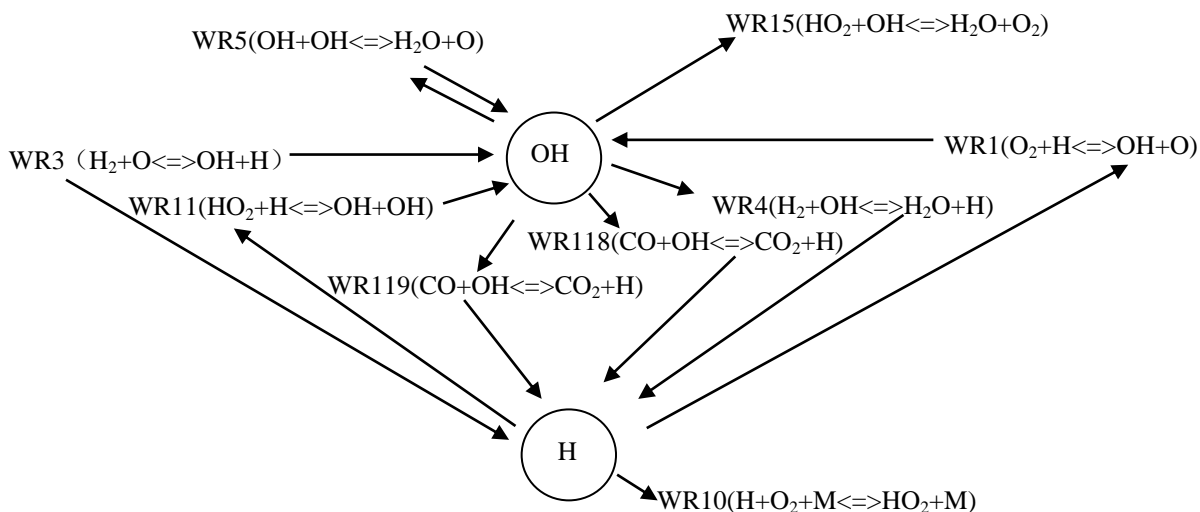
Figure 7.6 shows the main paths through which the C₂H₆ and H₂ are decomposed. C₂H₆ is primarily decomposed into C₂H₅ through the direct oxidation with oxygen. This step is different from CH₄-H₂ mixture as shown in Figure 7.4. There is no OH and H involved in the primary decomposition and basically all of the C₂H₆ is decomposed through the oxidation with oxygen as indicated in Table 7.6. The red lines in Figure 7.6 highlight the dominant path for the decomposition of C₂H₆.

The C₂H₅ is then decomposed to C₂H₄ through third body effect, and which is then decomposed to C₂H₂. These first three decomposition steps, from C₂H₆ to C₂H₂, are achieved through oxygen oxidation and third body effect and both of OH and H are not participated in the three paths. Compared with the paths from CH₄ to C₂H₂, CH₄ is primarily decomposed to CH₃, which is then decomposed to CH₂ and C₂H₄, and therefore producing C₂H₂. In addition, in the processes of CH₄ to CH₃ and CH₃ to CH₂, OH and H play very important role in the decompositions.

Furthermore, the decomposition of C₂H₆ is strongly preferred the path of oxidising C₂H₆ to C₂H₅ rather than decomposing to CH₃, so that the amount of CH₃ and CH₂ decomposed in C₂H₆-H₂ mechanism is less than that in CH₄-H₂ mechanism. Consequently, the amount of OH and H involved in CH₄ decomposition is far more than that in C₂H₆ decomposition. Thus, the effect of OH and H on the decomposition of CH₄ is more efficient than that of C₂H₆. However, from C₂H₂ to CH, the paths are same between CH₄-H₂ and C₂H₆-H₂ mixtures.

On the other hand, the main paths of OH and H formation and production are different between CH₄-H₂ and C₂H₆-H₂ reaction mechanisms. There are some

elementary reactions, belonging to CH_4 decomposition mechanism, contributing to the formation of OH and H. But, in $\text{C}_2\text{H}_6\text{-H}_2$ reaction mechanism, basically all paths are from hydrogen oxidation system for the formation of OH and H. In addition, OH and H are not very active in the paths of decomposing hydrocarbons in $\text{C}_2\text{H}_6\text{-H}_2$ reaction mechanism. The consumption paths are basically from the hydrogen oxidation system.

Figure 7.6: The main paths for C_2H_6 and H_2 in the oxidation of $C_2H_6-H_2$ Figure 7.7: The main contributors of the formation and consumption of H and OH in the oxidation of $C_2H_6-H_2$

7.4 Pathway Analysis of the Reactions of C₃H₈-H₂ Mixtures

As previously discussed, it has been demonstrated the differences between CH₄-H₂ and C₂H₆-H₂ mixtures upon the reaction pathways. The approaches of the decomposition of the CH₄ and C₂H₆ are different.

This section introduces the reaction paths of the oxidation of C₃H₈-H₂ mixtures. The pathways, formation and consumption, of the reactants and the same radicals are illustrated to carry out the comparison among CH₄-H₂, C₂H₆-H₂ and C₃H₈-H₂ mixtures.

7.4.1 Pathway Analysis of H₂

The major paths of consuming H₂ are WR4, WR3 and WR2 in the oxidation of C₃H₈-H₂ mixture. This is indicated in Table 7.10. The dominant paths through which H₂ is consumed are carried out through the reaction with OH and O. This is same as the paths for CH₄-H₂ and C₂H₆-H₂ mixtures.

Table 7.10: H₂ consumption pathway of the oxidation of H₂-C₃H₈ mixtures

H ₂ consumption pathway for H ₂ -C ₃ H ₈ oxidation reactions			
30% H ₂		90% H ₂	
Reaction	%	Reaction	%
WR4: H ₂ +OH<=>H ₂ O+H	53.37	WR4: H ₂ +OH<=>H ₂ O+H	58.41
WR3: H ₂ +O<=>OH+H	45.33	WR3; H ₂ +O<=>OH+H	40.04
WR2: H ₂ +O<=>OH+H	1.15	WR2: H ₂ +O<=>OH+H	1.07

WR: indicating the reaction number in the Warnatz mechanism

7.4.2 Pathway Analysis of C₃H₈

The primary decomposition of CH₄ is through the reaction with H, OH and O and that of C₂H₆ is completed through the reaction with O₂. However, the path through which C₃H₈ is decomposed is different and illustrated in Table 7.11. As shown in the Table, the decomposition of C₃H₈ in the mixture is achieved through the third body effect for both low and high hydrogen concentration. Pressure dependency is

greater in such reaction. However, the concentration of the effective third body influences the reaction rate. Similar to $C_2H_6-H_2$ mixtures, the OH and H are not involved in the primary path of the decomposition of C_3H_8 .

Table 7.11: C_3H_8 consumption pathways of the oxidation of $H_2-C_3H_8$ mixtures

C_3H_8 consumption pathways			
30% H_2		90% H_2	
Reaction	%	Reaction	%
WR263: $C_3H_8(+M) \rightleftharpoons CH_3 + C_2H_5(+M)$	99.99996	WR263: $C_3H_8(+M) \rightleftharpoons CH_3 + C_2H_5(+M)$	99.99997
WR278: $C_3H_8 + O_2 \rightleftharpoons C_3H_7 + HO_2$	0.00002	WR278: $C_3H_8 + O_2 \rightleftharpoons C_3H_7 + HO_2$	0.00002

WR: indicating the reaction number in the Warnatz mechanism

7.4.3 Pathway Analysis of H

The formation and consumption paths of H are listed in Table 7.12. Similar to C_2H_6 , the main paths of H generation are WR4, WR3, WR118 and WR119 for both low and high H_2 concentration in the reactant mixture. And for all C_1 , C_2 and C_3 mixed hydrogen mixtures, WR4 and WR3 are the main contributors to H formation. However, as shown in Table 7.12, WR34 and WR67 also are the paths for relatively very few percentage of the H formation and they are from the hydrocarbon decomposition mechanism. This is similar to CH_4-H_2 although the percentage taken is low compared to the paths in CH_4-H_2 mechanism.

In terms of H consumption, WR1, WR10 and WR11 are the major paths which are responsible for the H consumption. This phenomenon is same as $C_2H_6-H_2$ mixtures. The majority of the H is consumed through the hydrogen oxidation system. Compared with $C_2H_6-H_2$ paths, however, more H is used to react with CH_2O , C_2H , C_2H_2 , CH_3 and CHO , even though the percentage taken account by these paths are low. These paths are also given in Table 7.3 as H consumption

paths for CH₄-H₂ mixtures but with higher percentage. In addition, when hydrogen concentration is at 90%, the percentages of paths WR130 and WR131 increase dramatically. This is similar to what happens on the H consumption paths in CH₄-H₂ mixture reaction mechanism.

Table 7.12: H formation and consumption pathways of the oxidation of H₂-C₃H₈ mixtures

H pathways for H ₂ -C ₃ H ₈ oxidation reactions			
Generation			
30% H ₂		90% H ₂	
Reaction	%	Reaction	%
WR4:H ₂ +OH<=>H ₂ O+H	28.87	WR4:H ₂ +OH<=>H ₂ O+H	48.72
WR3:H ₂ +O<=>OH+H	24.52	WR3:H ₂ +O<=>OH+H	33.40
WR118:CO+OH<=>CO ₂ +H	16.93	WR118:CO+OH<=>CO ₂ +H	5.31
WR119:CO+OH<=>CO ₂ +H	10.52	WR119:CO+OH<=>CO ₂ +H	3.45
WR34:CHO+M<=>CO+H+M	5.81	WR34:CHO+M<=>CO+H+M	1.81
WR67:CH ₃ +O<=>CH ₂ O+H	3.88	WR67:CH ₃ +O<=>CH ₂ O+H	1.67
WR120:CO+OH<=>CO ₂ +H	2.52	WR1:O ₂ +H<=>OH+O	0.97
WR51:CH ₂ +O ₂ <=>CO+OH+H	2.05		
Consumption			
30% H ₂		90% H ₂	
Reaction	%	Reaction	%
WR1:O ₂ +H<=>OH+O	69.29	WR1:O ₂ +H<=>OH+O	64.94
WR10:H+O ₂ +M<=>HO ₂ +M	7.84	WR10:H+O ₂ +M<=>HO ₂ +M	13.10
WR54:CH ₂ O+H<=>CHO+H ₂	6.19	WR11:HO ₂ +H<=>OH+OH	6.11
WR11:HO ₂ +H<=>OH+OH	3.64	WR130:C ₂ H ₂ +O<=>C ₂ H+H+M	3.13
WR4:H ₂ +OH<=>H ₂ O+H	2.35	WR54:CH ₂ O+H<=>CHO+H ₂	2.62
WR35:CHO+H<=>CO+H ₂	2.21	WR131:C ₂ H ₂ +H<=>C ₂ H+H ₂	2.14
WR50:CH ₂ +H ₂ <=>CH ₃ +H	1.97	WR8:H+OH+M<=>H ₂ O+M	1.27
WR25:CH+H<=>C+H ₂	1.64	WR35:CHO+H<=>CO+H ₂	1.26

Continue to Table 7.12

Consumption			
30% H ₂		90% H ₂	
Reaction	%	Reaction	%
WR41:CH ₂ ¹ +H<=>CH+H ₂	1.58	WR50:CH ₂ +H ₂ <=>CH ₃ +H	1.08
		WR41: CH ₂ ¹ +H<=>CH+H ₂	1.05

WR: indicating the reaction number in the Warnatz mechanism

CH₂¹: the isotope of normal CH₂

7.4.4 Pathway Analysis of OH

As illustrated in Table 7.13, in the oxidation reaction of C₃H₈-H₂ mixture, the major paths of generating OH are WR1, WR3, WR5 and WR11. The major sources of OH formation are same between C₃H₈-H₂ and C₂H₆-H₂ mixtures. On the other hand, elementary reactions, WR4, WR5, WR15, WR118 and WR119, provide the paths for the consumption of OH. However the amount of OH consumed in the paths from the decomposition of hydrocarbon products is higher than that of C₂H₆-H₂ oxidation reaction mechanism, but it is lower than that of CH₄-H₂ oxidation reaction mechanism.

Table 7.13: OH formation and consumption pathways of the oxidation of H₂-C₃H₈ mixtures

OH pathways for H ₂ -C ₃ H ₈ oxidation reactions			
Generation			
30% H ₂		90% H ₂	
Reaction	%	Reaction	%
WR1:O ₂ +H<=>OH+O	56.86	WR1:O ₂ +H<=>OH+O	53.70
WR3:H ₂ +O<=>OH+H	23.41	WR3:H ₂ +O<=>OH+H	31.58
WR5:OH+OH<=>H ₂ O+O	6.16	WR11:HO ₂ +H<=>OH+OH	10.11
WR11:HO ₂ +H<=>OH+OH	5.97	WR5:OH+OH<=>H ₂ O+O	1.52
WR51:CH ₂ +O ₂ <=>CO+OH+H	1.95		
WR4:H ₂ +OH<=>H ₂ O+H	1.93		
WR55:CH ₂ O+O<=>CHO+OH	1.75		

Continue to Table 7.13

Consumption			
30% H ₂		90% H ₂	
Reaction	%	Reaction	%
WR4:H ₂ +OH<=>H ₂ O+H	38.21	WR4:H ₂ +OH<=>H ₂ O+H	64.79
WR118:CO+OH<=>CO ₂ +H	22.4	WR5:OH+OH<=>H ₂ O+O	8.38
WR119:CO+OH<=>CO ₂ +H	13.93	WR118:CO+OH<=>CO ₂ +H	7.06
WR5:OH+OH<=>H ₂ O+O	7.26	WR15:HO ₂ +OH<=>H ₂ O+O ₂	6.89
WR15:HO ₂ +OH<=>H ₂ O+O ₂	4.56	WR119:CO+OH<=>CO ₂ +H	4.59
WR120:CO+OH<=>CO ₂ +H	3.34	WR8:H+OH+M<=>H ₂ O+M	1.48
WR38:CHO+OH<=>CO+H ₂ O	2.56	WR1:O ₂ +H<=>OH+O	1.28
WR56:CH ₂ O+OH<=>CHO+H ₂ O	2.19	WR134:C ₂ H ₂ +OH<=>H ₂ O+C ₂ H	1.18
WR69:CH ₃ +OH<=>CH ₂ +H ₂ O	2.19	WR120:CO+OH<=>CO ₂ +H	1.12
		WR38:CHO+OH<=>CO+H ₂ O	1.04

WR: indicating the reaction number in the Warnatz mechanism

7.4.5 Pathway Analysis of CH

Table 7.14 shows the pathways of the formation and consumption of CH in the oxidation reaction of C₃H₈-H₂ mixture. For both 30% and 90% H₂ concentration in the mixture, the main paths for the consumption and formation of CH are same as those for CH₄-H₂ and C₂H₆-H₂ mixtures. The reactions, WR41, WR30, WR33 and WR125 are for the formation of CH, on the other hand, the reactions, WR25, WR29, WR29 and WR27 act as the paths through which CH are consumed.

Table 7.14: CH formation and consumption pathways of the oxidation of H₂-C₃H₈ mixtures

CH pathways for H ₂ -C ₂ H ₆ oxidation reactions			
Generation			
30% H ₂		90% H ₂	
Reaction	%	Reaction	%
WR41:CH ₂ ¹ +H<=>CH+H ₂	68.71	WR41:CH ₂ ¹ +H<=>CH+H ₂	80.42
WR30:CH+CO<=>HCCO	18.64	WR30:CH+CO<=>HCCO	14.32
WR125:C ₂ H+O ₂ <=>CO ₂ +CH	7.80	WR33:CH+H ₂ O<=>CH ₂ ¹ +OH	2.28
WR33:CH+H ₂ O<=>CH ₂ ¹ +OH	2.41	WR125:C ₂ H+O ₂ <=>CO ₂ +CH	2.06

Continue to Table 7.14

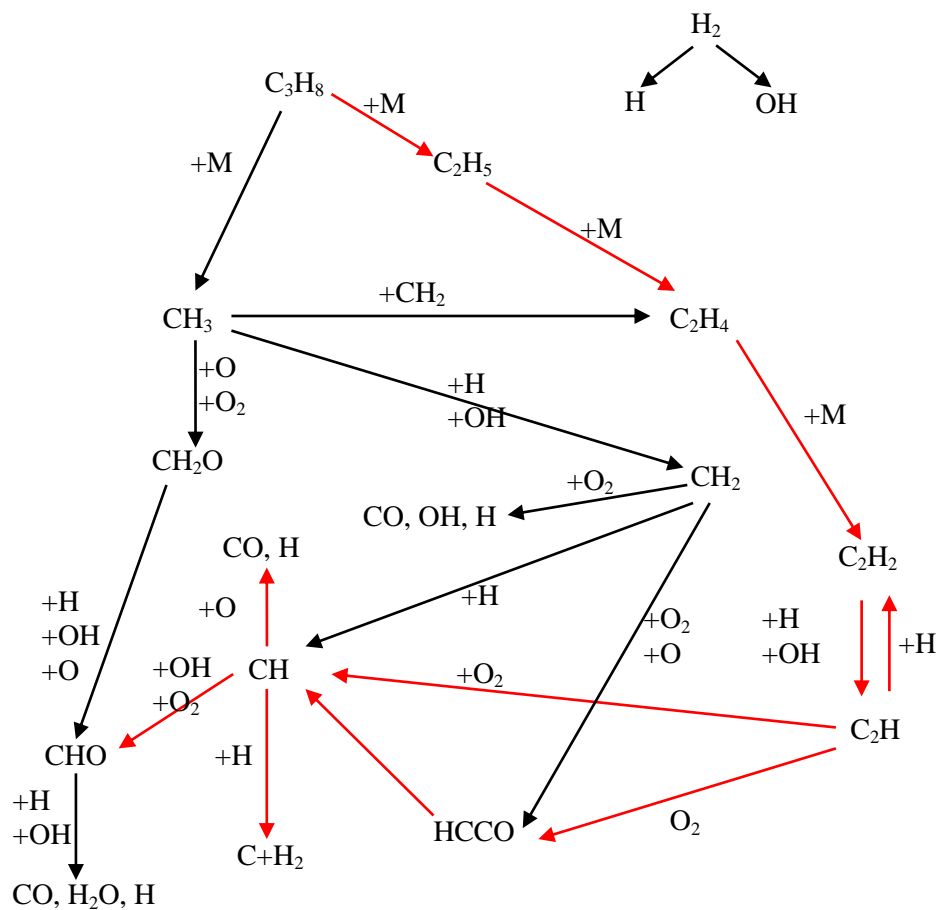
Generation			
30% H ₂		90% H ₂	
Reaction	%	Reaction	%
WR66:CH ₃ +M<=>CH+H ₂ +M	1.88		
Consumption			
30% H ₂		90% H ₂	
Reaction	%	Reaction	%
WR25:CH+H<=>C+H ₂	55.51	WR25:CH+H<=>C+H ₂	65.45
WR29:CH+O ₂ <=>CHO+O	19.29	WR29:CH+O ₂ <=>CHO+O	13.53
WR28:CH+OH<=>CHO+H	13.21	WR28:CH+OH<=>CHO+H	11.64
WR27:CH+O<=>CO+H	9.89	WR27:CH+O<=>CO+H	8.14
WR31:CH+CO ₂ <=>CHO+CO	1.35		

WR: indicating the reaction number in the Warnatz mechanism

CH₂¹: the isotope of normal CH₂

7.4.6 The Main Reaction Pathways

As illustrated in Figure 7.8, C₃H₈ is primarily decomposed into CH₃ and C₂H₅, however, this process is not involved with H and OH. The C₂H₅ is then decomposed to C₂H₄ and then C₂H₂, and ultimately to CH. Differing with C₂ but similar to C₁, CH₃ is produced at the primary decomposition step. This results in more CH₃ and CH₂ are generated in the middle of the decomposition process so that more H and OH are involved in the process, CH₃ → CH₂ → CH. Thus, the paths from CH₃ to CH is similar to the paths of the oxidation of CH₄-H₂ mechanism. However, the dominant paths, as highlighted in red, are through C₂H₄ to C₂H₂, and to CH. H₂-C₂H₆ and H₂-C₃H₈ mixtures have the similar paths, and which are different from that of H₂-CH₄.

Figure 7.8: The main paths for C_3H_8 and H_2 in the oxidation of $C_3H_8-H_2$

7.5 Summary

- For H₂-CH₄, H₂-C₂H₆ and H₂-C₃H₈ mixtures, H₂ is mainly consumed through H₂+OH \rightleftharpoons H₂O+H and H₂+O \rightleftharpoons OH+H.
- For H₂-CH₄ mixtures, CH₄ is mainly consumed through CH₄+H \rightleftharpoons H₂+CH₃, CH₄+OH \rightleftharpoons H₂O+CH₃ and CH₄+O \rightleftharpoons OH+CH₃.
- For H₂-C₂H₆ mixtures, C₂H₆ is mainly consumed through C₂H₆+O₂ \rightleftharpoons C₂H₅+HO₂.
- For H₂-C₃H₈ mixtures, C₃H₈ is mainly consumed through C₃H₈(+M) \rightleftharpoons CH₃+C₂H₅(+M).
- Compared with C₂H₆ and C₃H₈, the CH₄ consumption paths is more sensitive to the H and OH concentrations in the reaction.
- The main contributors of H are H₂+OH \rightleftharpoons H₂O+H and H₂+O \rightleftharpoons OH+H.
- The main contributors of OH are O₂+H \rightleftharpoons OH+O and H₂+O \rightleftharpoons OH+H.
- The decomposition of CH₄, C₂H₆ and C₃H₈ also contributes to H and OH production, though the main sources of H and OH in the reactions are from the H₂ oxidation system.

Chapter 8

Numerical Modeling of the Laminar Burning Velocity

Literature review from previous chapters has shown that the experimental measurements of the laminar burning velocity are influenced by the distorted flame front and heat losses through the boundaries. This chapter presents the numerical modelling method to simulate the laminar burning velocity of methane, ethane and propane, and the effect of hydrogen addition on the laminar burning velocity of the mixtures.

8.1 The Laminar Burning Velocity Modeling Method

The numerical modeling of the laminar burning velocity is conducted by employing the One-dimensional Flame Speed Calculation model in CHEKIN, in which the boundary value method of calculating adiabatic flame speed is employed. The configuration is used to determine the characteristics of the burning velocity of a given gaseous mixture at a specified pressure and given inlet temperature. It is assumed the heat losses are not considered in the modeling. The gas phase reaction mechanism, thermodynamic files and transport properties are required to supply as inputs. The reaction mechanism used in the simulation is Gri-mech 3.0 which contains the essential steps for C₁-C₃ oxidation. The detail of the Gri-mech 3.0 is given in Appendix E.

The initial gas pressure was set at 1 atm. The heat loss and thermal expansion were not considered in the simulation, so that the pressure was constant throughout the calculation. A fixed temperature value was introduced to constrain the flame position. The temperature was just above the inlet cold gas temperature. A value of 300K was given for the fixed temperature. In addition to the fixed temperature input, a temperature profile was also supplied as initial guess of the temperature distribution corresponding to the distance, x , above the burner. The

first value of the temperature profile input indicated the initial temperature of the gaseous mixture with a corresponding grid point. The initial gas temperature was set at 298K. The reaction zone above the burner was also estimated. The starting point of 0 cm was given, meaning the start position being just above the burner. The ending axial position was set at 20cm, which basically covers the reaction zone for H₂ and H₂-C₁-C₃ flames. An initial number for grid points was required to be given for initially solving the problem. The number of the grid points was then added according to the degree of the gradient and curve between the initial grid points. The initial number of the grid points was given and adjusted between 9-11, depending on if the solution could be found. The inlet velocity of the inlet gaseous mixture was also supplied. However, the final solution is not sensitive to the value of the inlet velocity as long as the equivalence ratio of the mixture is not close to the flammability. In addition to this data, the composition of the reactants and the expected composition of the products were also introduced as input before running the model.

The energy and species governing equations are given in *Eq. 3-21* to *Eq. 3-25*. The governing equations for gas transport are given as *Eq. 3-26* to *Eq. 3-28*. To solve the laminar burning velocity of a specified mixture requires situating the flame to a coordinate system. In freely propagation flame model, the mass flow rate, \dot{M} , is the eigenvalue associated with the flame burning velocity. The problem becomes solving the mass flow rate, M , and the laminar burning velocity, u . Thus, it is necessary to constrain the flame position by specifying the flame front position to establish a flame fixed coordinate system. Figure 8.1 shows the temperature over the flame front. At flame front, the unburned gas is heated and converted to intermediate radicals or products. The flame front is taken account as the indication of the propagation of the flame. Flame is generally considered as consisting of preheat zone and reaction zone (Rallis and Garforth, 1980; Heravi et al., 2007). The preheat zone and reaction zone exist between the cold boundary at the temperature of the unburned gas and the hot boundary at the temperature approaching to flame temperature (equilibrium temperature) (Rallis and Garforth, 1980). As shown in Figure 8.1, the temperature increases as a convex shape due to very low chemical reaction rate in the preheat zone. The heat being accumulated

in this zone mainly results from the conduction and convection from the reaction zone. The temperature rises as a concave shape while entering the reaction zone. The reaction rate is relatively fast in this region. As temperature continuously growing and reaching the flame temperature at equilibrium state, both of temperature and concentration gradients level off. Ideally, the thickness of a flame front is between the cold boundary and the hot boundary.

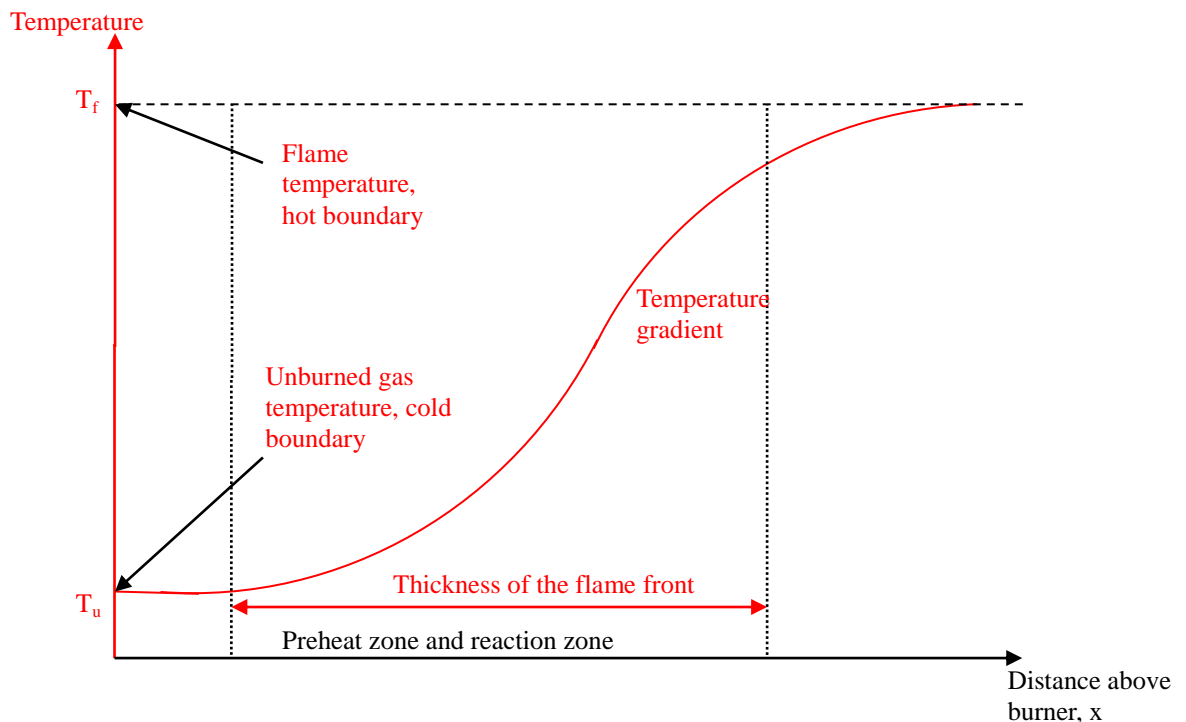


Figure 8.1: The temperature gradients through a flame front, adapted from Rallis and Garforth, 1980

Therefore, the specified flame temperature should be just above the inlet flame temperature and far lower than the equilibrium temperature. Since the position of the flame is fixed in the coordinate system and the laminar burning velocity is the relative velocity between the flame front and the unburned gas, the solution of the laminar burning velocity is the velocity at the point where the temperature and species molar fraction are nearly as same as them of unburned gas. In addition, the temperature and species gradients should be close to zero at the hot boundary either to make sure there is no heat loose and mass diffusive flux through the

boundary. Thus, the solution of the laminar burning velocity should satisfy the temperature and species gradients being close to zero at both cold and hot boundaries. The equations for cold boundary are given as *Eq. 3-29 and Eq. 3-30*, while the hot boundary equations are presented as *Eq. 3-31 and Eq. 3-32*.

8.2 Transport Coefficients

Differing from the reaction kinetic equilibrium modeling, the one-dimensional laminar burning velocity simulation needs to consider both of the thermodynamic data and the transport properties for the flame. The thermodynamic fitting approach has been introduced in Chapter 6. By considering the transport equations given in Chapter 3, for mixture average transport properties, the required transport coefficients required are dynamic viscosity, the thermal conductivity and the mixture-average diffusion coefficients. These parameters are used in the transport equations to solve the laminar burning velocity, u , in the continuity equation associated with the energy and species equations. For gas phase mixture-average transport properties, these parameters can be calculated from the coefficients of polynomial fits of the logarithm of the property versus the logarithm temperature, which are supplied in the CHMKIN transport data file (CHEMKIN theory manual, 2005). The expressions for the fitting procedure are shown as below:

For dynamic viscosity,

$$\ln \eta = \sum_{n=1}^N a_n (\ln T)^{n-1} \quad \text{Eq. 8-1}$$

For the thermal conductivity,

$$\ln \lambda = \sum_{n=1}^N b_n (\ln T)^{n-1} \quad \text{Eq. 8-2}$$

And for the binary diffusion coefficients,

$$\ln D = \sum_{n=1}^N d_n (\ln T)^{n-1} \quad \text{Eq. 8-3}$$

Where N is the number of coefficients in polynomial fits for C_p/R and a_n , b_n and

d_n are the coefficients of fits to thermodynamic data.

8.3 1-D Laminar Burning Velocity Simulations

In this section the laminar burning velocity simulations for pure H_2 , pure CH_4 , pure C_2H_6 and pure C_3H_8 are analysed and discussed. The change of flame laminar burning velocity with equivalence ratio is not considered in the simulations.

8.3.1 Laminar Burning Velocity of CH_4

In the simulation, the reaction of methane with air carries out under stoichiometric condition. The composition of the reactant and the expected product is shown in Table 8.1. As shown in the Table, nitrogen is both the reactant and product in the CH_4 -air flame.

Table 8.1: The reactants and products mol fractions for the laminar burning velocity calculation of the combustion of CH_4 -air mixture

Reactants	Mol Fraction
N_2	0.715
H_2	0.000
O_2	0.190
CH_4	0.095
Products	Mol Fraction
N_2	0.715
H_2O	0.190
CO_2	0.095

The solution of the simulation in the CHEMKIN output text format is shown in Appendix N. The result shows the number of grid point has grown from the initial value of 10 to 48 in the final solution. The solution makes sure that the temperature and species gradients are close to zero. The axial velocity at the cold boundary is the relative velocity of the unburned gas to the flame front, so that the laminar burning velocity for CH_4 -air combustion is gained to be approximate 41.6 cm/s from the simulation. Figure 8.2 and Figure 8.3 show the temperature profile

and the axial velocity characteristics correlated to the distance above burner. The comparison of the laminar burning velocity evaluated from this simulation with previous published studies is illustrated in Figure 8.4. It can be seen from the Figure that 41.6 cm/s falls into the reasonable range.

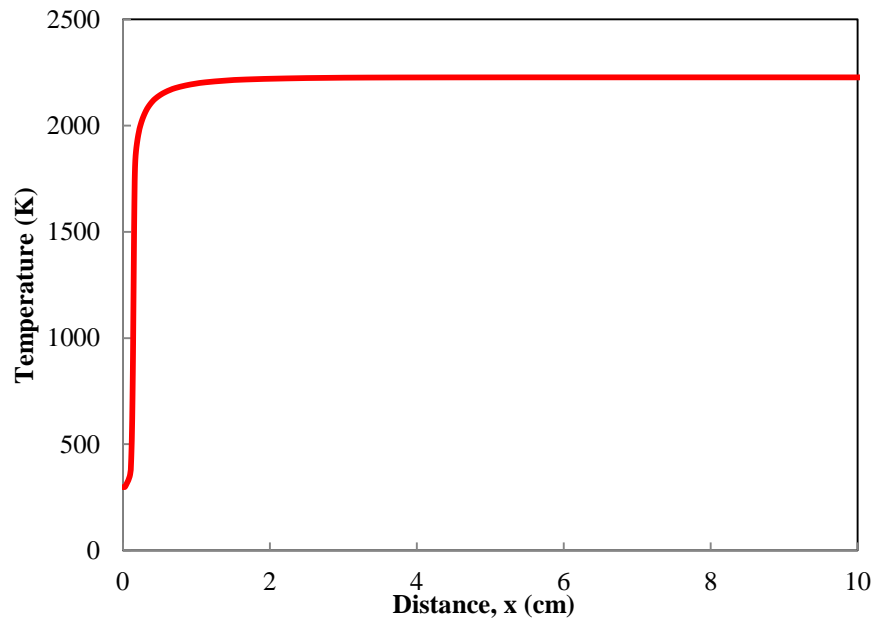


Figure 8.2: The gas temperature above burner for the CH₄-air flame

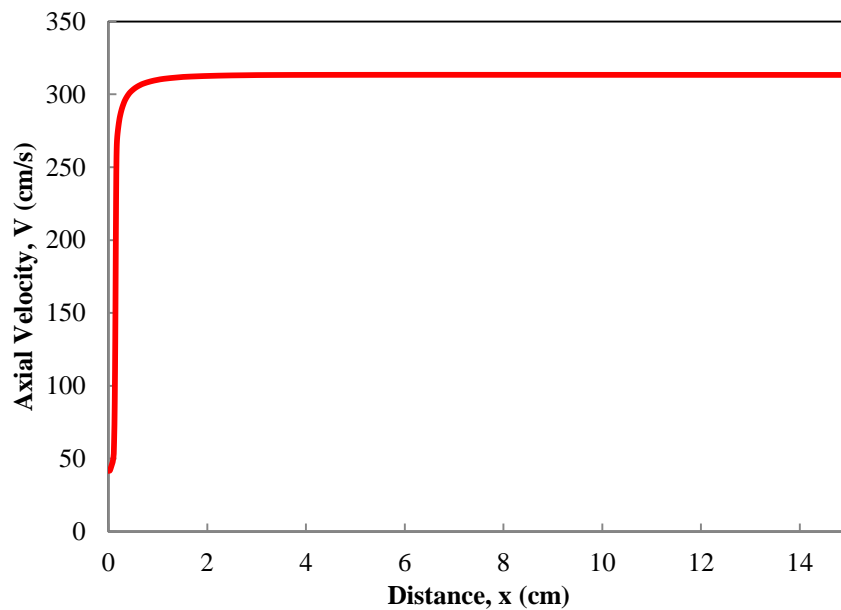


Figure 8.3: The axial velocity profile above burner for the CH₄-air flame

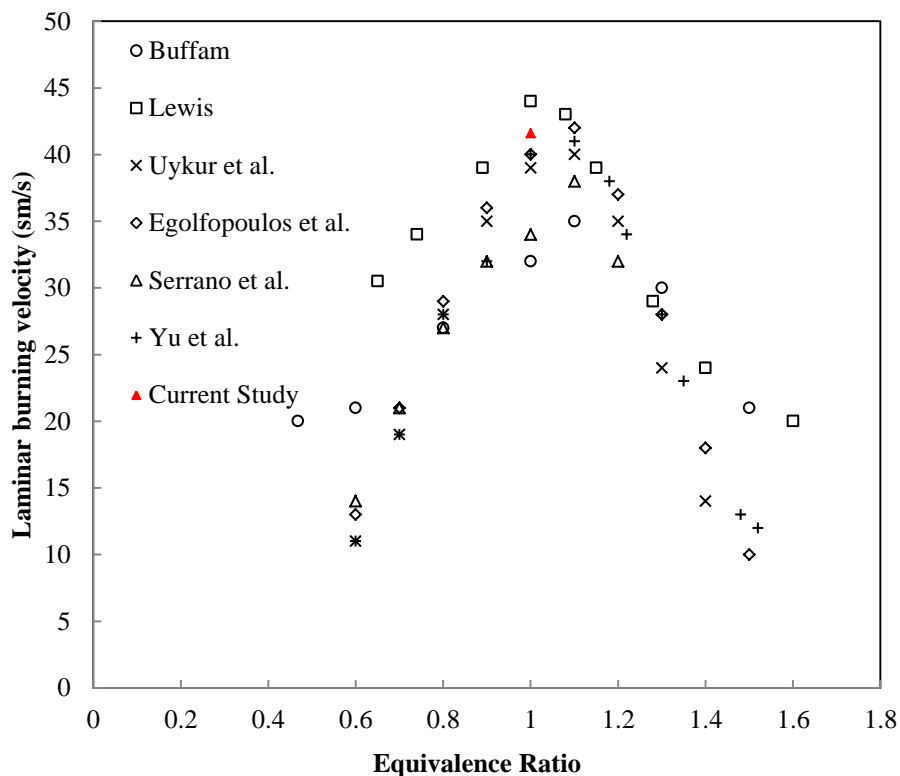


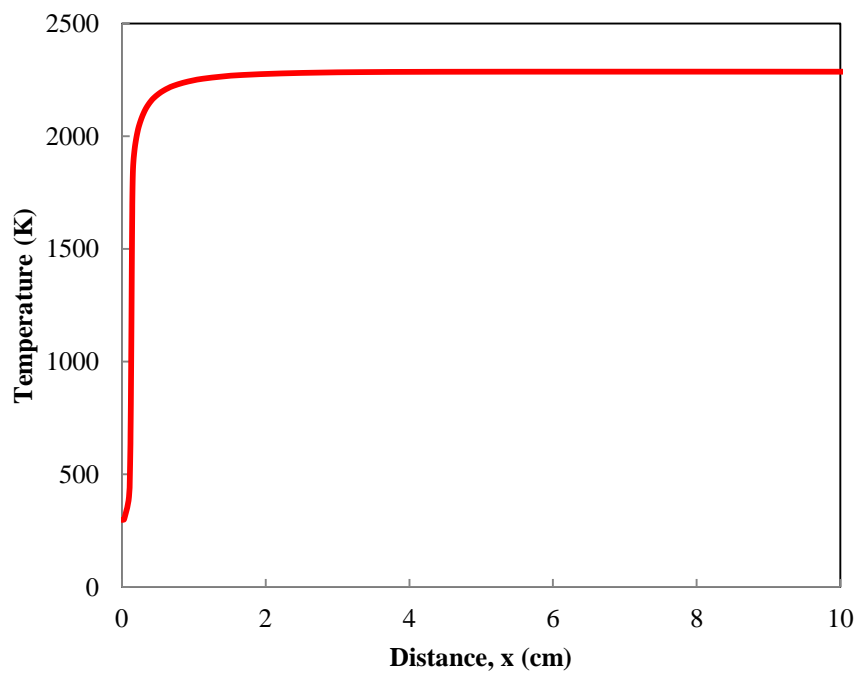
Figure 8.4: The comparison of the laminar burning velocity of CH₄-air of current study with previous studies

8.3.2 Laminar Burning Velocity of Pure C₂H₆

Table 8.2 shows the mol fraction of the reactants and the expected products. The number of mole of C₂H₆ used in the simulation is same as that of CH₄, which is 1 mole. However, the requirement of the oxygen grows up as the carbon content increases in the mixture. Thus the initial reactants molar fraction of C₂H₆ oxidation is different with that of CH₄. The other critical inputs are same as those employed in the simulation of CH₄-air oxidation. The CHEMKIN solution output file is shown in Appendix O. It is illustrated in the result that the temperature gradients at both boundaries are close to zero enough. It ensures that the axial velocity of the fluid is the relative velocity between the unburned and the flame front, so that the solution is the laminar burning velocity. It indicates that the laminar burning velocity of C₂H₆-air flame is approximate 49.2 cm/s. Figure 8.5 and Figure 8.6 present the gas temperature and axial velocity profiles of the flame of C₂H₆-air correlated to the distance above burner.

Table 8.2: The reactants and products mol fractions for the laminar burning velocity calculation of the combustion of C_2H_6 -air mixture

Reactants	Mol Fraction
N_2	0.745
H_2	0.000
O_2	0.198
C_2H_6	0.057
Products	Mol Fraction
N_2	0.725
H_2O	0.165
CO_2	0.110

Figure 8.5: The gas temperature above burner for the C_2H_6 -air flame

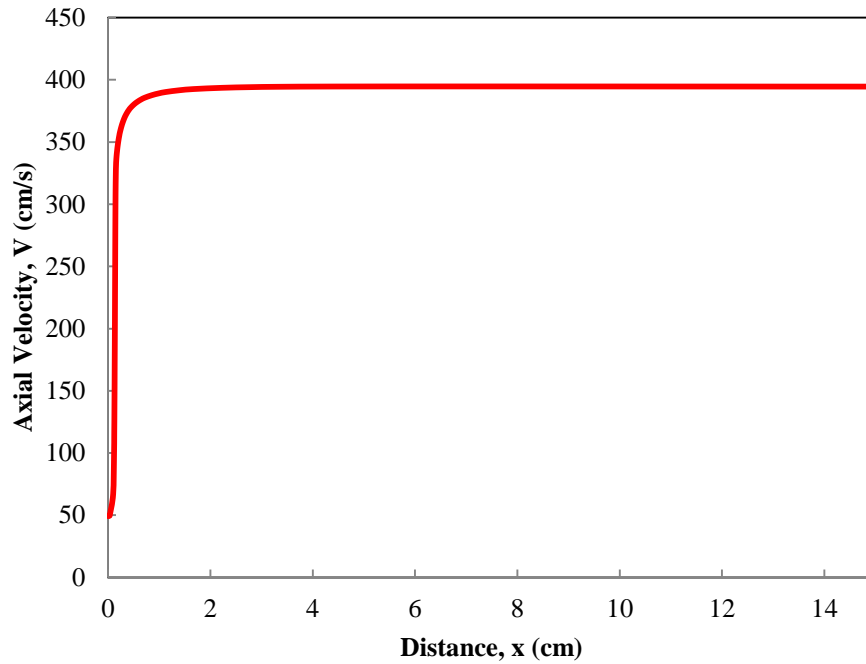


Figure 8.6: The axial velocity profile above burner for the C_2H_6 -air flame

Figure 8.7 shows the simulation of the laminar burning velocity of C_2H_6 -air being compared with the previous studies. As illustrated in the Figure, the current calculation is slightly higher than the previous studies for the flame at equivalence ratio of 1. The heat loose is not considered in the current simulation, so that adiabatic flame is one of the main reasons for the higher value of the laminar burning velocity.

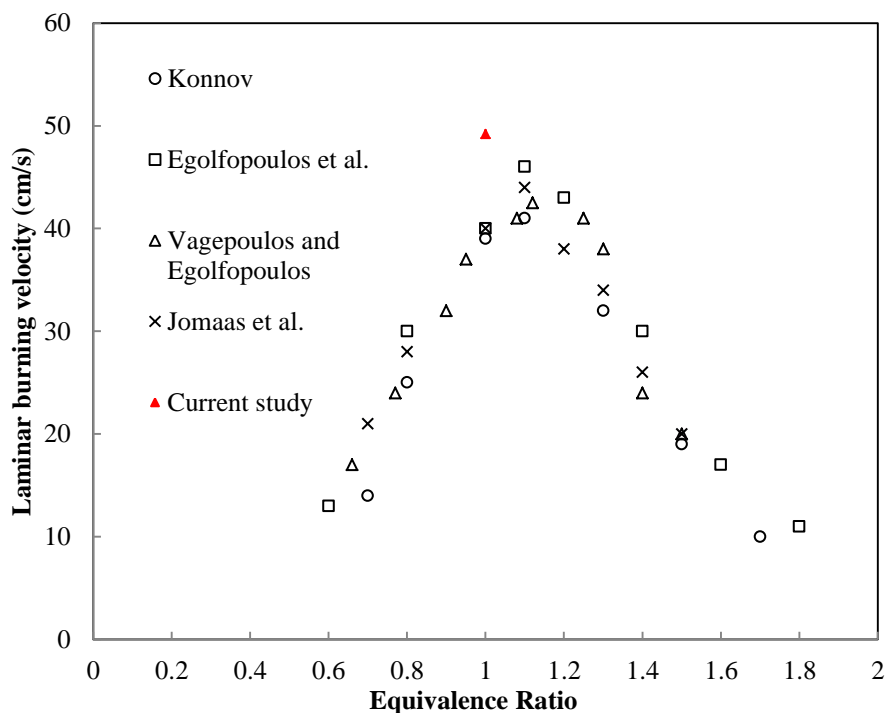


Figure 8.7: The comparison of the laminar burning velocity of C_2H_6 -air of current study with previous studies

8.3.3 Laminar Burning Velocity of Pure C_3H_8

The requirement of oxygen from C_3H_8 is higher than that of the oxidation of CH_4 and C_2H_6 due to the highest carbon content. The initial composition of the reactants is 1 mole C_3H_8 mixing with 23.8 mole air (18.8 mole N_2 and 5 mole O_2). The other critical inputs remain the same. The initial composition of the mixture is shown in Table 8.3.

Table 8.3: The reactants and products mol fractions for the laminar burning velocity calculation of the combustion of C_3H_8 -air mixture

Reactants	Mol Fraction
N_2	0.758
H_2	0.000
O_2	0.202
C_3H_8	0.040
Products	Mol Fraction
N_2	0.710

Continue to Table 8.3

H ₂ O	0.166
CO ₂	0.124

The solution for the laminar burning velocity is found at the cold boundary of the flame, which is approximate 55.7 cm/s. The CHEMKIN output text file is presented in Appendix P. Figure 8.8 and Figure 8.9 show the temperature and axial velocity characteristics of the flame above burner.

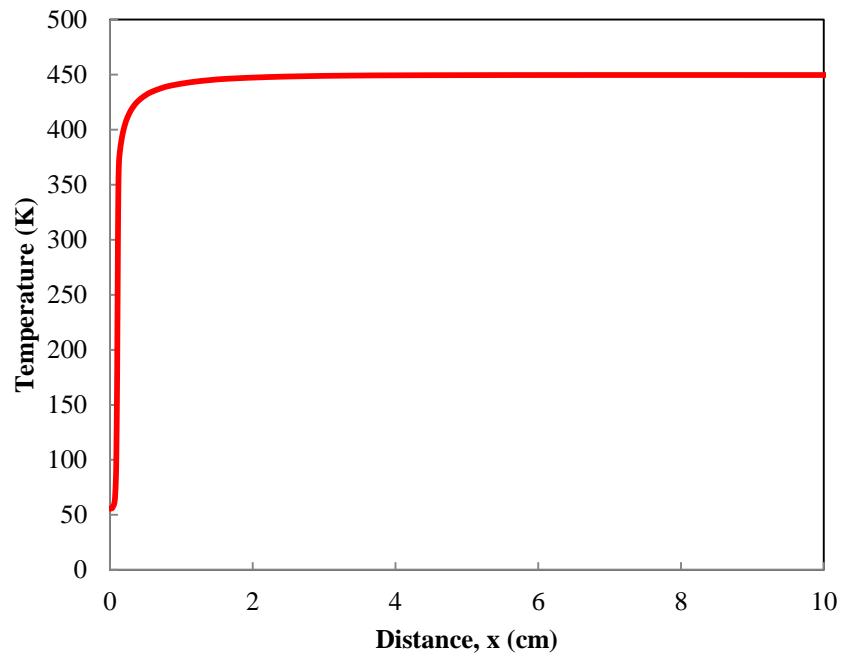


Figure 8.8: The gas temperature above burner for the C₃H₈-air flame

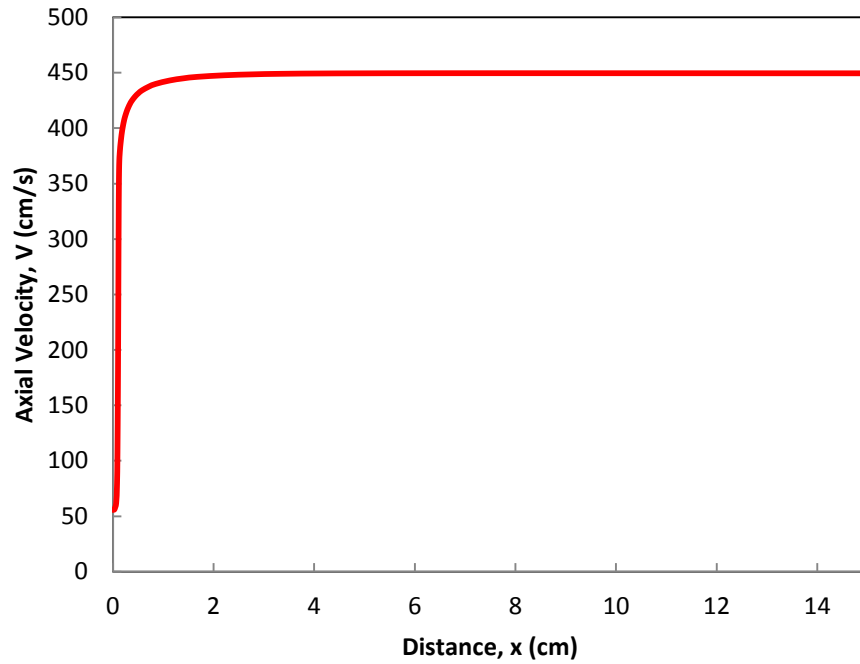


Figure 8.9: The axial velocity profile above burner for the C_3H_8 -air flame

The comparison of the current simulation with the previous studies is shown in Figure 8.10. The simulated value of 55.7 cm/s of the laminar burning velocity of C_3H_8 -air is higher than the previous studies. The main reasons for this can be the considerations on heat losses and the temperature distribution profile which is not from an experimental measurement.

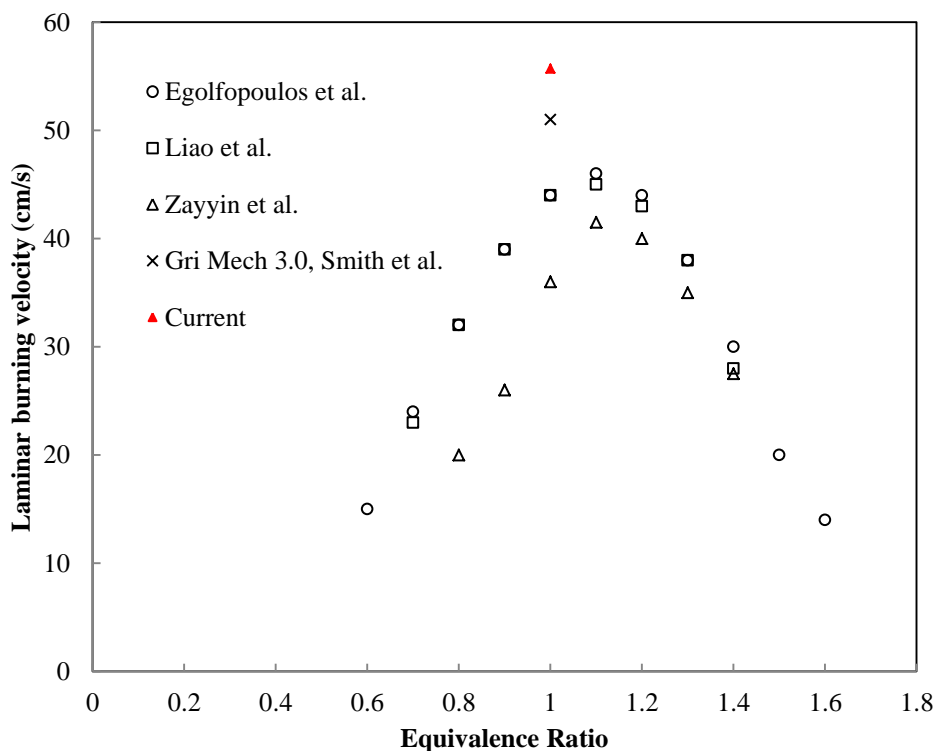


Figure 8.10: The comparison of the laminar burning velocity of C_3H_8 -air of current study with previous studies

8.3.4 The Comparison for the Laminar Burning Velocity of H_2 with CH_4 , C_2H_6 and C_3H_8 Flames

For the simulation of H_2 -air, the initial H_2 in the mixture is 1 mole. However, H_2 consumes less oxygen in the combustion compared with CH_4 , C_2H_6 and C_3H_8 oxidations. Thus the initial molar fraction of hydrogen in the inlet gaseous mixture is relative higher compared with the hydrocarbons. The CHEMKIN output result for the laminar burning velocity of H_2 -air at stoichiometric condition, shown in Appendix Q, shows the first 10 and last 5 grid points of the final solution. At the could boundary, the solution for the laminar burning velocity of H_2 flame is found to be approximately 248 cm/s, which is far higher than that of CH_4 , C_2H_6 and C_3H_8 oxidation. Figure 8.11 shows the laminar burning velocity of H_2 -air against the equivalence ratio. In the Figure, the current simulation is compared with previous studies. It can be seen from that the result from the simulation agrees well with Liu and MacFarlane. It is in a reasonable range with the data from previous studies. It has been shown that the laminar burning velocity has the feature, H_2 -air > C_3H_8 -air > C_2H_6 -air > CH_4 -air.

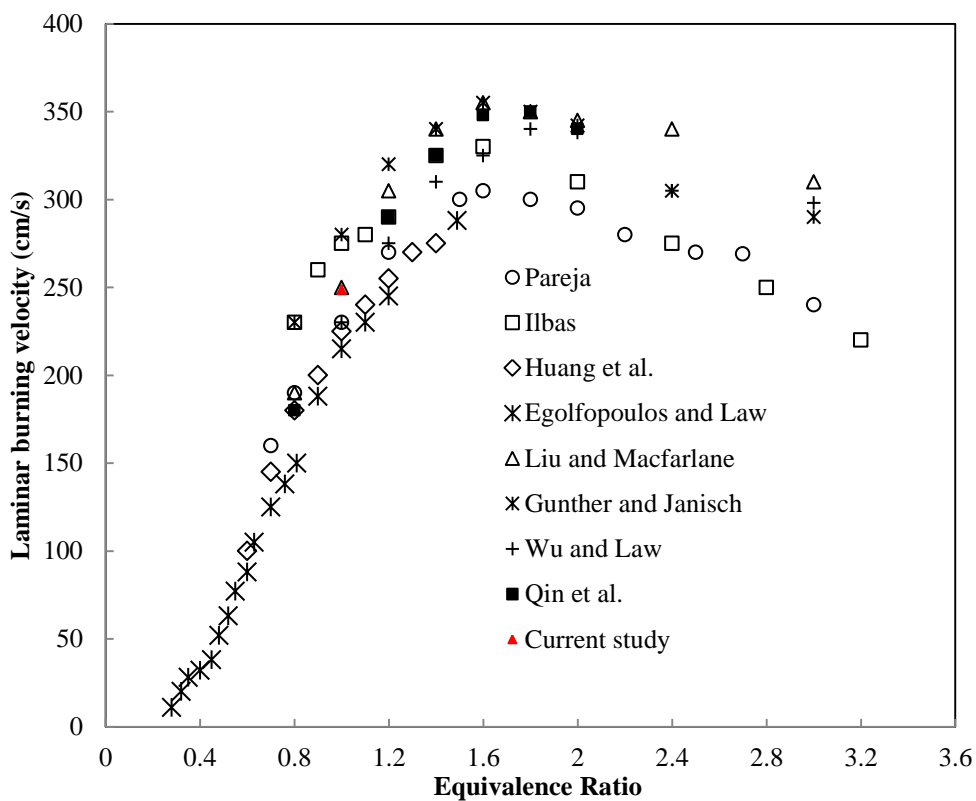


Figure 8.11: The comparison of the laminar burning velocity of H₂-air of current study with previous studies

Figure 8.12 illustrates the molar fraction of H above the burner for H₂, H₂-CH₄, H₂-C₂H₆ and H₂-C₃H₈. As shown in the Figure, at the position near the flame front H₂-air flame has the outstanding H formation compared with the other H₂-hydrocarbon mixtures. In terms of the H₂-hydrocarbon mixtures, the H formations in the flame front are basically same. The positions of the formation of the H are same for H₂, H₂-CH₄, H₂-C₂H₆ and H₂-C₃H₈.

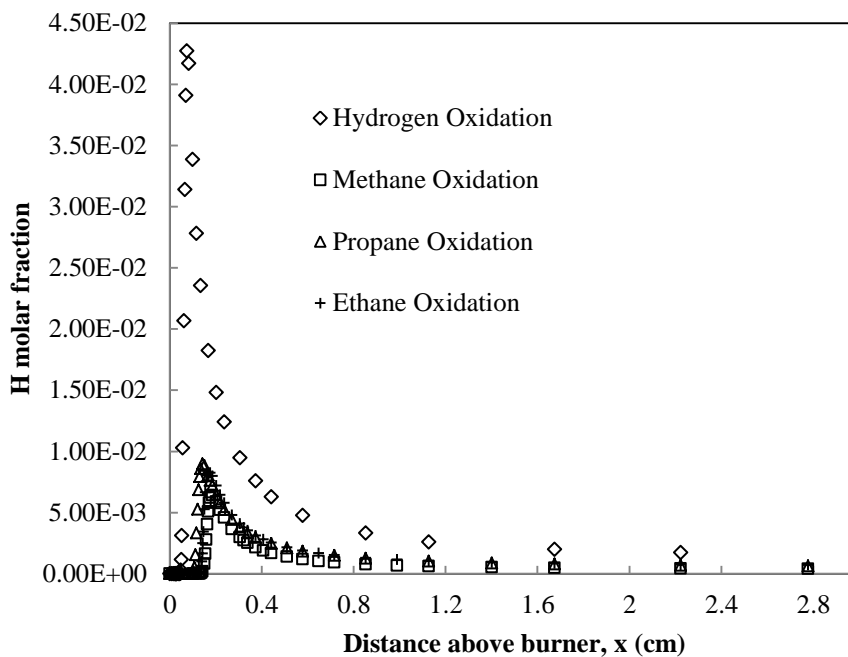


Figure 8.12: The distribution of the molar fraction of H above burner for the flames of H_2 , CH_4 , C_2H_6 and C_3H_8 oxidation

In Figure 8.13, the profile of the OH molar fraction above burner is presented. Differing with H, the generated OH is not vanished at the hot boundary of the flames. The other characteristics are basically same with that of H. Thus, it can be realised by considering Figure 8.12 and Figure 8.13 that H_2 flame has the much higher value on OH and H molar fraction, comparing with $\text{H}_2\text{-CH}_4$, $\text{H}_2\text{-C}_2\text{H}_6$ and $\text{H}_2\text{-C}_3\text{H}_8$ mixtures. Figure 8.14 demonstrates the molar fraction of the CH radical above burner for the H_2 -hydrocarbon flames. The decomposition of CH_4 , C_2H_6 and C_3H_8 results in the formation of CH radical at the flame front zone.

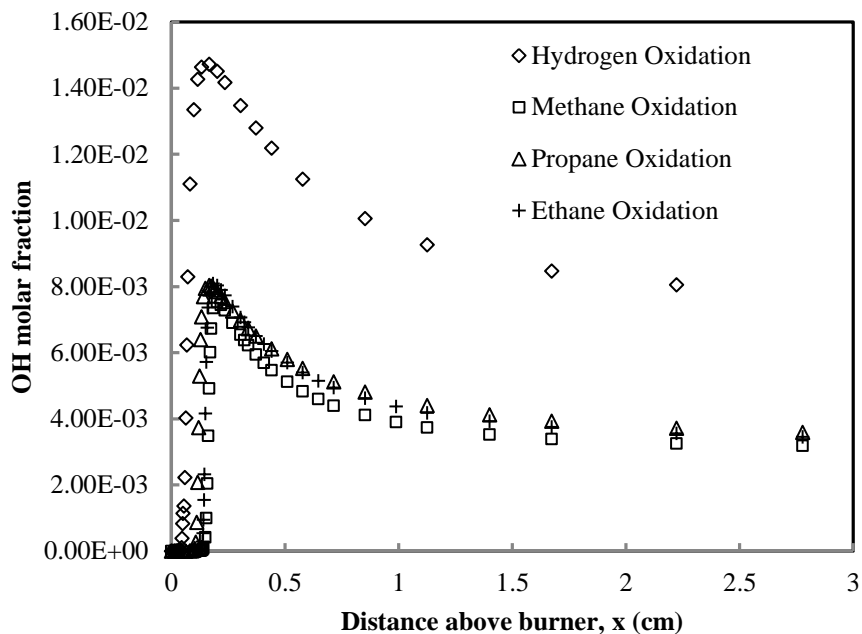


Figure 8.13: The distribution of the molar fraction of OH above burner for the flames of H₂, CH₄, C₂H₆ and C₃H₈ oxidation

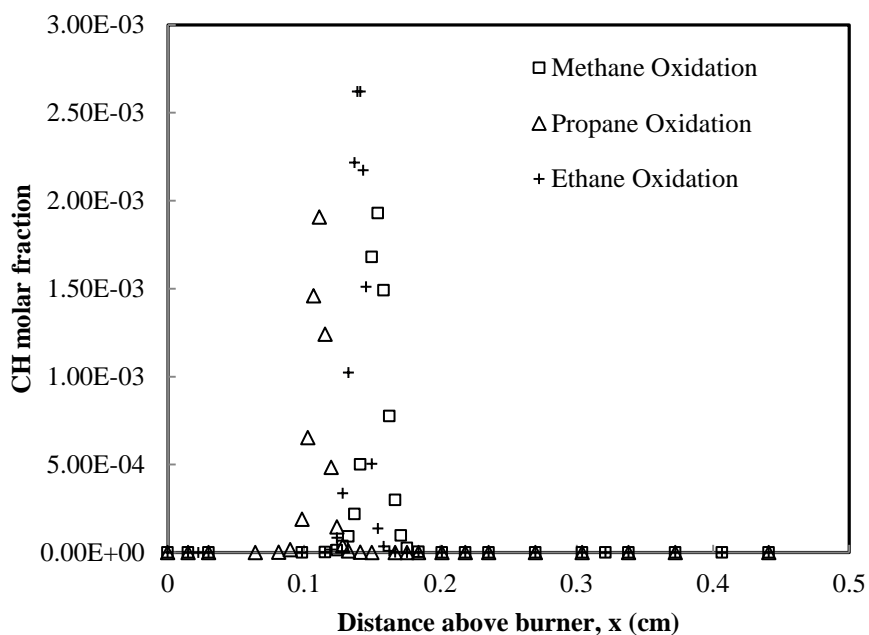


Figure 8.14: The distribution of the molar fraction of CH above burner for the flames of CH₄, C₂H₆ and C₃H₈ oxidation

Figure 8.15 and Figure 8.16 illustrate distribution of the CH_3 , C_2H_4 and C_2H_5 radicals in C_2H_6 and C_3H_8 flames above burner. On the other hand, the distribution of these radicals in CH_4 -air flame is shown in Figure 8.17. These radicals, CH_3 , C_2H_4 and C_2H_5 , are considered as the intermediate products from the primary decomposition of the hydrocarbons. Comparing the flames of C_2H_6 -air and C_3H_8 -air with CH_4 -air, it is realised that CH_3 is the major intermediate products as the primary decomposition of CH_4 at the flame front. However, the molar fraction of C_2H_4 is higher than CH_3 in the C_2H_6 -air and C_3H_8 -air flames. This situation is different with CH_4 -air oxidation. The primary decomposition of the hydrocarbon reactants, C_2H_6 and C_3H_8 , result in more C_2H_4 radicals generation rather than CH_3 .

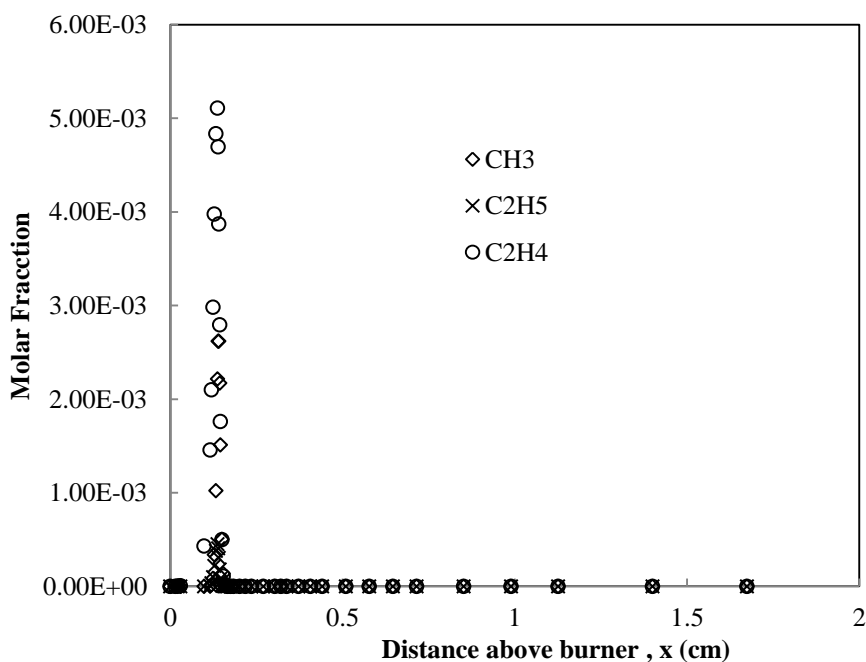


Figure 8.15: The distribution of the molar fraction of CH_3 , C_2H_4 and C_2H_5 radicals above burner for the C_2H_6 -air flame

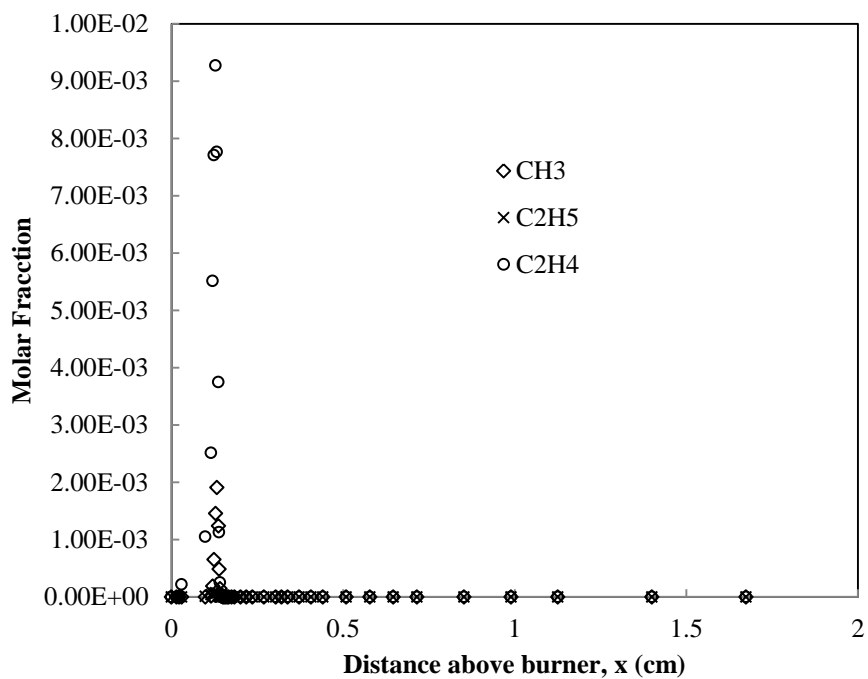


Figure 8.16: The distribution of the molar fraction of CH_3 , C_2H_4 and C_2H_5 radicals above burner for the C_3H_8 -air flame

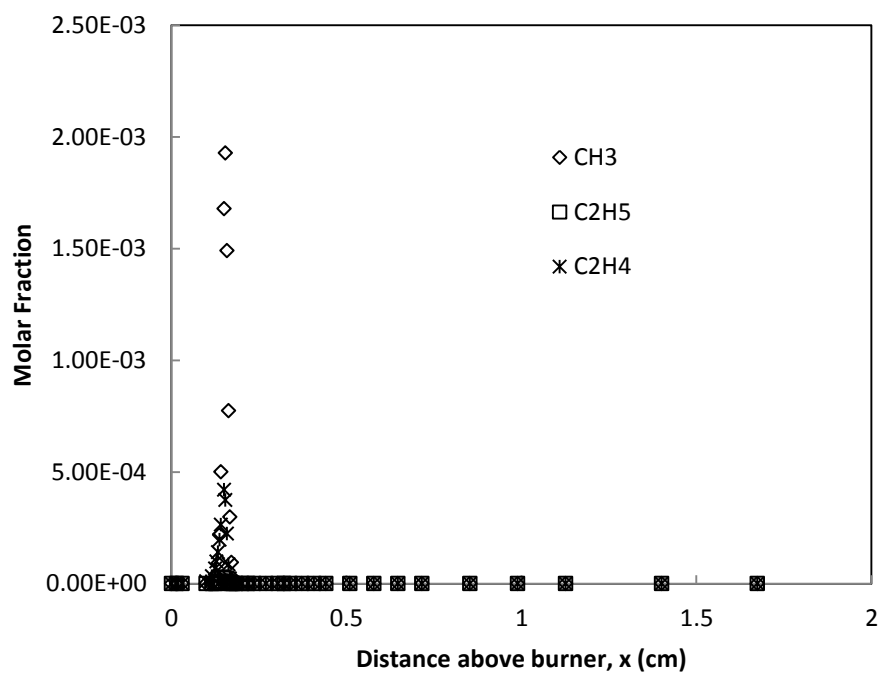


Figure 8.17: The distribution of the molar fraction of CH_3 , C_2H_4 and C_2H_5 radicals above burner for the CH_4 -air flame

8.4 The Laminar Burning Velocity Simulation of the CH₄-H₂, C₂H₆-H₂ and C₃H₈-H₂ Mixtures

This section includes the discussions of the simulations of the laminar burning velocity for mixtures. Methane, ethane and propane are mixed with hydrogen as fuel and reacting with air at stoichiometric condition. As previously introduced, laminar burning velocity is essentially related with the reaction kinetics of the combustion. With the aim of determining the effect of hydrogen concentration on the laminar burning velocity of hydrogen-hydrocarbon mixtures, the concentration of hydrogen in the mixture is verified from 0-100% and then the laminar burning velocity of the mixture is simulated. The set up of the simulation is basically same as the simulation for the oxidations of pure H₂, CH₄, C₂H₆ and C₃H₈.

Figure 8.18 illustrates the results from the simulations of the laminar burning velocity of CH₄-H₂, C₂H₆-H₂ and C₃H₈-H₂ mixtures. As shown in the Figure, when the hydrogen concentration is less than 60%, the laminar burning velocities of the mixtures obey the sequence, CH₄-H₂<C₂H₆-H₂<C₃H₈-H₂, which is same as the characteristics of the laminar flame velocities for the pure reactants. When the hydrogen concentration is higher than 60%, the laminar burning velocity of CH₄-H₂ increases more steeply compared with that of H₂-C₂H₆ and H₂-C₃H₈. At high hydrogen addition concentration (>90%), the laminar burning velocity of C₂H₆-H₂ becomes a bit larger than that of C₃H₈-H₂ mixture. The laminar burning velocity of the mixtures starts to approach the value for pure H₂ as the increasing H₂ concentration in the mixtures, when H₂ concentration is greater than 60%. It also can be seen from the Figure that the addition of hydrogen into CH₄, C₂H₆ and C₃H₈ increases the laminar burning velocity, but the increase strongly depends on the H₂ concentration. When H₂ concentration is less than 60%, the increase is very slow and steady. When H₂ concentration is greater than 60%, the effect of H₂ concentration becomes stronger and the laminar burning velocity of the mixtures increases with H₂ concentration. When H₂ concentration is greater than 80%, the laminar burning velocities of the mixtures increase exponentially and approach to that of pure H₂.

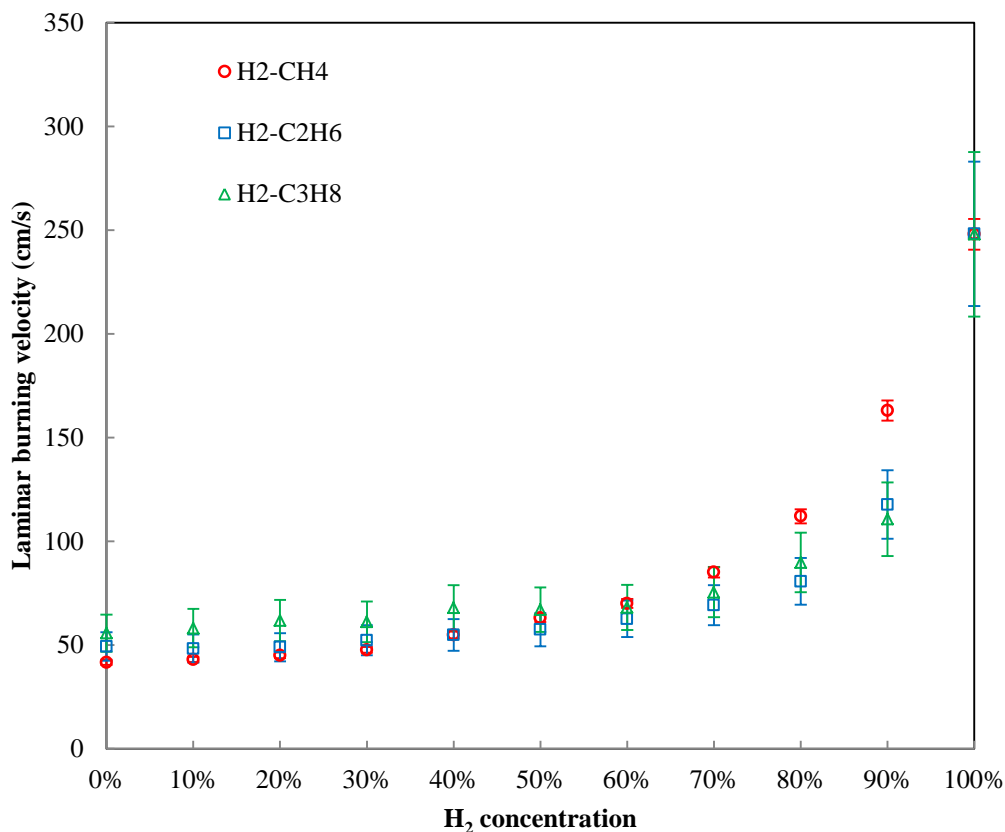


Figure 8.18: The laminar burning velocity of CH₄/ H₂, C₂H₆/ H₂ and C₃H₈/H₂ mixtures, at 1 atm and stoichiometric condition

It is shown that the effect of the hydrogen addition concentration on the laminar burning velocity of H₂-CH₄ is more effective and sensitive compared with the other two mixtures when H₂ concentration is over 60%. It has been shown that pure H₂ has the far higher H and OH molar fraction at the flame front compared with CH₄, C₂H₆ and C₃H₈. On the other hand, the oxidations of C₂H₆ and C₃H₈ produce more C₂H₄ at the flame front while CH₄-air flame has more CH₃ at its flame front. It has been shown in the species path way analysis that H and OH are the major agent in the decomposition of CH₃ and CH₄. The decomposition of C₂H₆ and C₃H₈ is majorly accomplished through the formation of C₂H₄ without the participation of H and OH. The increase in H₂ concentration results in increasing H and OH concentration at the flame front. This can be the reason for the laminar burning velocity of H₂-CH₄ mixture is more sensitive to the hydrogen addition.

Although the factors influencing the accuracy of experimentally measuring laminar burning velocity are not considered in computational simulation, the reaction mechanisms used in the computational calculation include experimentally determined reaction kinetics parameters. Figure 8.18 also presents the error analysis of the data obtained from computational simulation. The data is compared with previous experimentally and computationally studies in order to give a deviation. The data for H₂ and CH₄ has approximate $\pm 3\%$ deviation compared with other studies, on the other hand, C₂H₆ and C₃H₈ have $\pm 14\%$ and $\pm 16\%$ respectively.

Figure 8.19 shows the comparison of the current study with the previous study for the laminar burning velocity of H₂-CH₄. As shown in the Figure, the study conducted by Ilbas basically shows the same trend as the simulation in current study. At high hydrogen concentration (>80%), the increase in the laminar burning velocity is exponentially. At low H₂ concentration, the result from current study is agreed well with the previous study. However, when H₂ addition is over 60%, the data of current study is lower than the results obtained by Ilbas (2006).

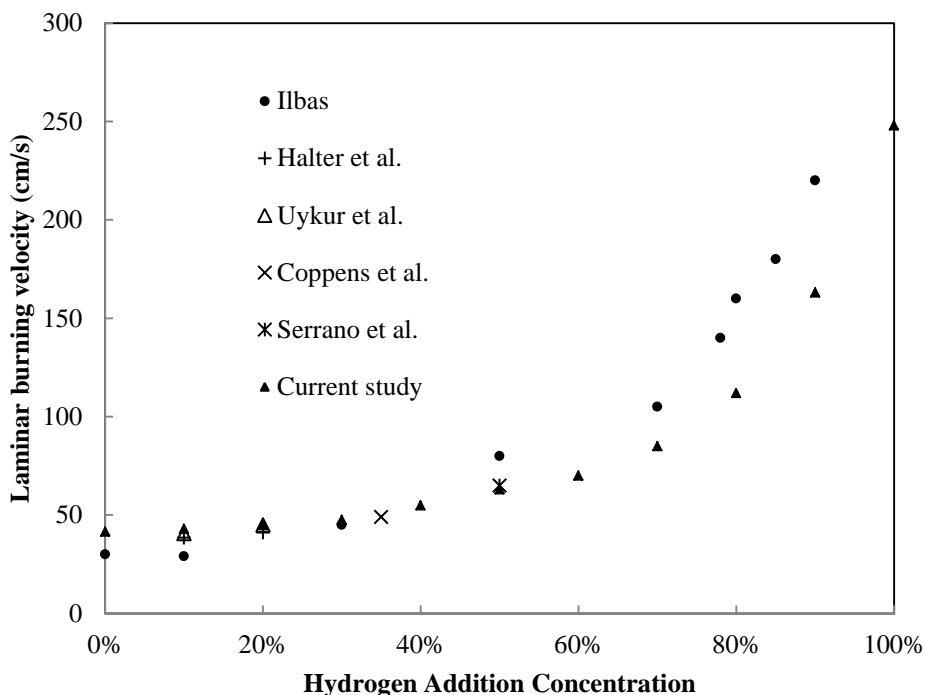


Figure 8.19: The comparison of the laminar burning velocity of methane-hydrogen mixture of current study with previous study

8.5 Summary

- The laminar burning velocity of H₂-air from the numerical modelling is 248.6 cm/s.
- The laminar burning velocity of CH₄-air from the numerical modelling is 41.6 cm/s.
- The laminar burning velocity of C₂H₆-air from the numerical modelling is 49 cm/s.
- The laminar burning velocity of C₃H₈-air from the numerical modelling is 55.7 cm/s.
- The addition of H₂ into CH₄, C₂H₆ and C₃H₈ increases the laminar burning velocity of the mixtures. However, the increase strongly depends on the H₂ concentration. With H₂ addition is below 50%, the increase is very slight. With H₂ addition is over 80%, the laminar burning velocity of the mixtures increases exponentially with the H₂ concentration
- When H₂ concentration is below 60%, the laminar burning velocity of the

H₂-hydrocarbon mixtures has the following order:
CH₄-H₂<C₂H₆-H₂<C₃H₈-H₂.

- When H₂ concentration is higher than 60%, the order is reversed.
- When H₂ concentration is over 90%, the value of the laminar burning velocity of the mixture approaches to the value of pure H₂.

Chapter 9

Discussions

The laminar burning velocity of a combustible gas mixture is determined by the reaction activity of the flame front. The flame lift-off and blow-out characteristics are also influenced by the laminar burning velocity. The effect of H₂ concentration on the laminar burning velocity and flame stability mechanism has already been briefly discussed in previous chapters.

This chapter is aimed at giving a detailed discussion on the relation of laminar burning velocity of H₂-hydrocarbon mixtures associated with the reaction kinetics and the flame stability mechanism. The results from species pathway analysis are applied in the discussion to explain the effect of hydrogen concentration on the reaction rate and the laminar burning velocity of H₂-hydrocarbon mixtures. The correlation developed by Kalghatgi (1984) is also discussed in this chapter.

9.1 Laminar Burning Velocity and Reaction Kinetics

9.1.1 Laminar Burning Velocity

The numerical simulation of the laminar burning velocity has shown that the laminar burning velocity of H₂ is 248 cm/s, and is far higher than that of H₂-CH₄, H₂-C₂H₆ and H₂-C₃H₈ mixtures. Figure 9.1 illustrates the ratio of the laminar burning velocity of H₂-CH₄, H₂-C₂H₆ and H₂-C₃H₈ to that of H₂-air against the H₂ concentration of the mixtures at stoichiometric condition. As shown in Figure 9.3, when H₂ concentration is less than 60%, the laminar burning velocity increase very slowly with the H₂ concentration. The increase of H₂-CH₄ is higher than that of C₂H₆ and C₃H₈. However, the influence of H₂ on the laminar burning velocity for is limited for all the three mixtures as the value of laminar burning velocities of the mixtures are less than 30% of that of pure H₂. When H₂ concentration is greater than 60%, the increase in the laminar burning velocities of

all the three mixtures becomes sharply with the increase of H_2 concentration in the mixtures. The ratio of $S_{L,\text{methane}}$ to $S_{L,\text{hydrogen}}$ becomes greater than that of C_2H_6 and C_3H_8 . When H_2 concentration exceeds 80%, the laminar burning velocities of the three mixtures increase exponentially with H_2 concentration, and the ratios exponentially approach to 1.

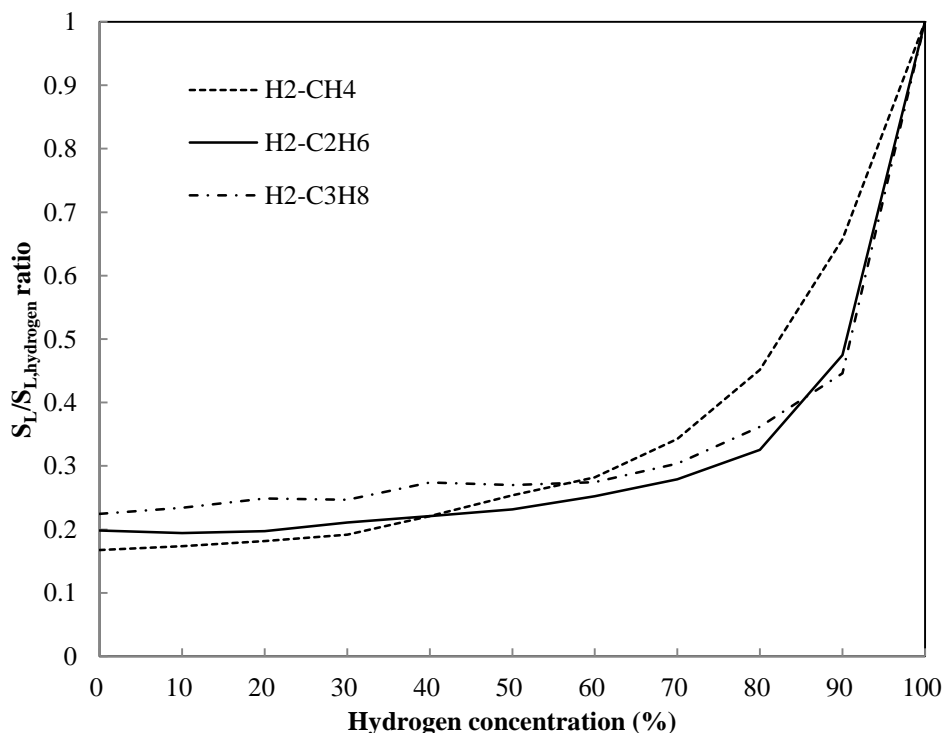


Figure 9.1: The laminar burning velocity ratio of CH_4-H_2 , $C_2H_6-H_2$ and $C_3H_8-H_2$ to pure H_2 over a range of H_2 concentration, at 1 atm and stoichiometric condition

9.1.2 The Effect of H_2 on Reaction Rates

The laminar burning velocities of the mixtures are related and determined by the reaction rates of the reactants. Figure 9.2 illustrates the average reaction rates of H_2 , C_2H_6 and C_3H_8 in the corresponding H_2 -hydrocarbon mixtures against the H_2 concentration. The average reaction rate indicates the average production rate of the reactants from reaction beginning to equilibrium state. It is calculated by dividing the concentration difference between initial state and equilibrium state by the time period from initial state to equilibrium state. As shown in Figure 9.2, the reaction rates of H_2 of the mixtures start with positive production rates, since the

hydrocarbon oxidation mechanism dominates the overall reaction mechanism at low H_2 addition concentration. The reaction kinetics simulation in Chapter 6 has shown that the hydrocarbon oxidation mechanism governs the overall reaction mechanism when H_2 concentration is less than 60%. As illustrated in Figure 9.2, the average consumption rates of H_2 increase slowly with H_2 concentration when hydrogen is less than 60%. The average reaction rate of C_3H_8 is greater than that of C_2H_6 and following by CH_4 . The consumption rates of C_3H_8 and C_2H_6 continuously decrease due to the reduction in the initial concentrations. However, different from C_3H_8 and C_2H_6 , the consumption rate of CH_4 experiences an increase with H_2 concentration. The laminar burning velocities of the mixtures are more determined by the reaction rates of the hydrocarbons. The laminar burning velocity of H_2 - C_3H_8 is higher than that of H_2 - C_2H_6 and H_2 - CH_4 .

When hydrogen concentration in the mixtures is greater than 60%, the H_2 reaction rates begin to dominate the overall reaction mechanism. The average reaction rates of H_2 increase relatively sharply with the H_2 concentration. The increase of the H_2 consumption rates of H_2 - CH_4 is faster than H_2 - C_2H_6 and H_2 - C_3H_8 mixtures, and exceeding the others at approximately 70% H_2 concentration. Furthermore, when H_2 concentration is greater than 80%, the H_2 average reaction rates rises up exponentially as continuously increasing H_2 concentration. The laminar burning velocities are dominated by the H_2 reaction rates and become very sensitive to the H_2 concentration. The laminar burning velocity of H_2 - CH_4 exceeds that of H_2 - C_2H_6 and H_2 - C_3H_8 .

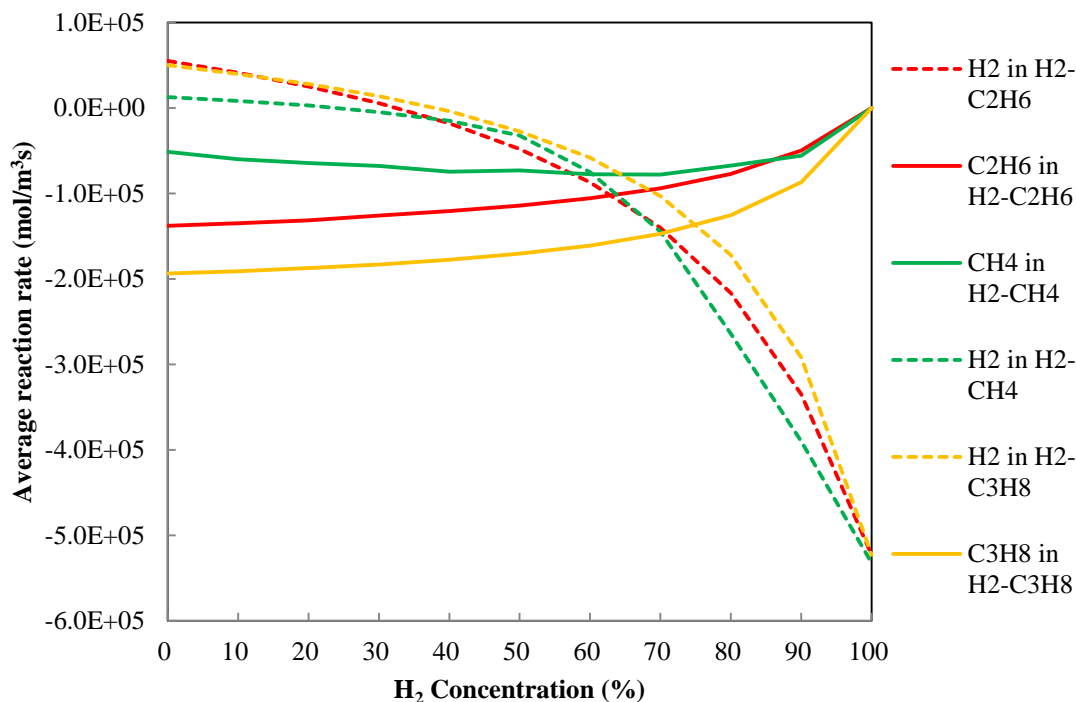


Figure 9.2: The average reaction rate of CH_4 , C_2H_6 , C_3H_8 and H_2 over the time of the combustion reaction of H_2 - CH_4 / C_2H_6 / C_3H_8 with air, at 2500 K and 1 atm

9.1.3 The Reaction Pathways

The species pathway analysis of H_2 - CH_4 , H_2 - C_2H_6 and H_2 - C_3H_8 in chapter 7 has concluded that the decomposition of H_2 in all the three mixtures is mainly through the reactions $\text{H}_2 + \text{OH} \rightleftharpoons \text{H}_2\text{O} + \text{H}$ and $\text{H}_2 + \text{O} \rightleftharpoons \text{OH} + \text{H}$ and the main contributors of H and OH in the reactions are from the oxidation of H_2 . Figure 9.3 shows that the concentration of H of the mixtures against the H_2 concentration at equilibrium state while Figure 9.4 presents the concentration of OH of the mixtures with the corresponding H_2 concentration. As shown in Figure 9.3 and Figure 9.4, the production of H and OH grows up due to the increase in the initial hydrogen concentration in the mixtures. At equilibrium state, the H and OH concentration of H_2 - CH_4 is greater than that of H_2 - C_2H_6 and followed by H_2 - C_3H_8 mixture. Compared with H_2 -hydrocarbon mixtures, pure H_2 reaction has much higher values of H and OH concentrations.

The pathway analysis shows that the presence of H and OH in H_2 - CH_4 mixtures contributes to the reaction paths of CH_4 . The decomposition of CH_4 is mainly through the reactions, $\text{CH}_4 + \text{H} \rightleftharpoons \text{H}_2 + \text{CH}_3$, $\text{CH}_4 + \text{OH} \rightleftharpoons \text{H}_2\text{O} + \text{CH}_3$ and

$\text{CH}_4 + \text{O} \rightleftharpoons \text{OH} + \text{CH}_3$. The primary decomposition of CH_4 forms CH_3 , which is further decomposed to CH with the presence of H and OH . Therefore, these radicals, OH , H and O , enhance the decomposition of the CH_4 and cause a slight increase in the CH_4 decomposition rate. As the hydrogen content increasing, the decomposition rates of the hydrocarbons reduce due to the decrease in the initial concentration in the mixture. However, the presence of H and OH contributes to a relatively slow reduction in CH_4 decomposition rate compared with C_3H_8 and C_2H_6 .

The species pathway analysis also indicates that the primary decomposition of C_2H_6 is through the attack of O_2 , and that of C_3H_8 is through third body effect. The primary decomposition product of C_2H_6 and C_3H_8 is C_2H_4 , which is further decomposed to C_2H_2 . The conversion from C_2H_2 to CH is accomplished with the presence of H and OH . Therefore, the addition of H_2 supplies H and OH for the decompositions of CH_4 and CH_3 . However, H and OH do not directly influence the primary decompositions of C_2H_6 and C_3H_8 .

Thus, the decomposition of CH_4 and H_2 are more sensitive to the H_2 concentration, compared with C_2H_6 and C_3H_8 . When H_2 concentration is greater than 60%, the influence of H_2 on the reaction pathways of $\text{H}_2\text{-CH}_4$ becomes strong. It results in the development of H_2 reaction rates of $\text{H}_2\text{-CH}_4$ is faster than that of $\text{H}_2\text{-C}_2\text{H}_6$ and $\text{H}_2\text{-C}_3\text{H}_8$, and the decline of CH_4 reaction rates is slower than that of C_2H_6 and C_3H_8 . Consequently, the laminar burning velocity of $\text{H}_2\text{-CH}_4$ exceeds that of $\text{H}_2\text{-C}_2\text{H}_6$ and $\text{H}_2\text{-C}_3\text{H}_8$. When H_2 concentration is less than 60%, the effect of H_2 on the reaction pathways of $\text{H}_2\text{-CH}_4$ mixtures is weak, the reaction rates of both H_2 and CH_4 in $\text{H}_2\text{-CH}_4$ mixture are slower than that of $\text{H}_2\text{-C}_2\text{H}_6$ and $\text{H}_2\text{-C}_3\text{H}_8$. Therefore, the laminar burning velocity of $\text{H}_2\text{-C}_3\text{H}_8$ is higher than that of $\text{H}_2\text{-CH}_4$ and $\text{H}_2\text{-C}_2\text{H}_6$ mixtures.

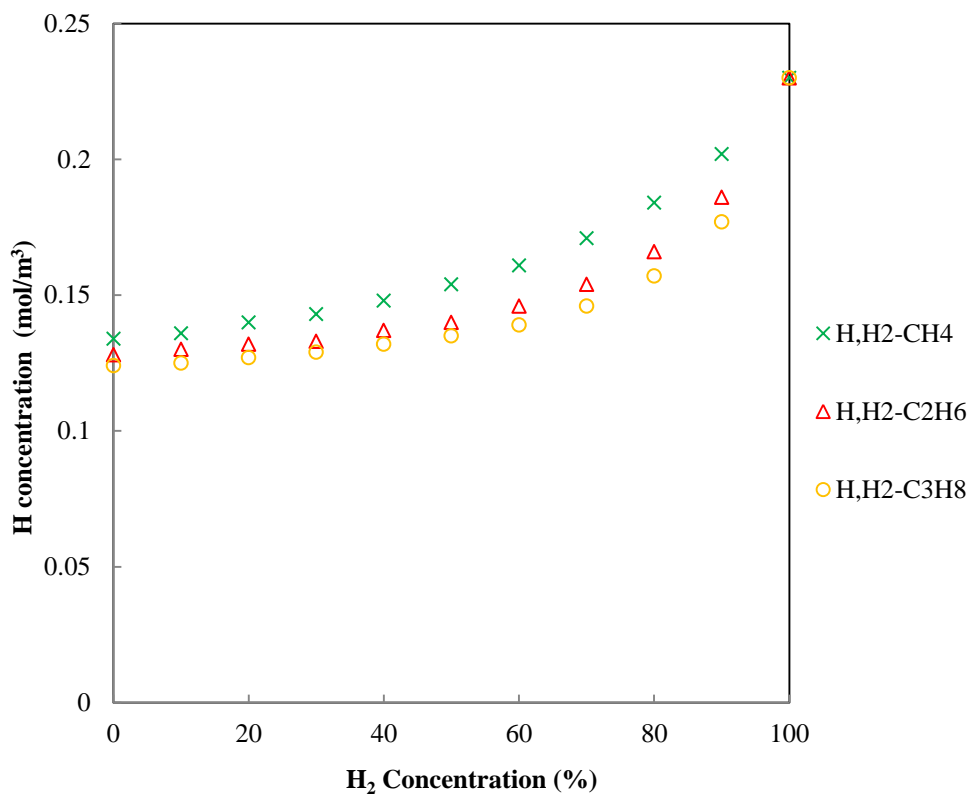


Figure 9.3: The H concentration against the H₂ addition concentration for H₂-CH₄, H₂-C₂H₆ and H₂-C₃H₈ mixtures

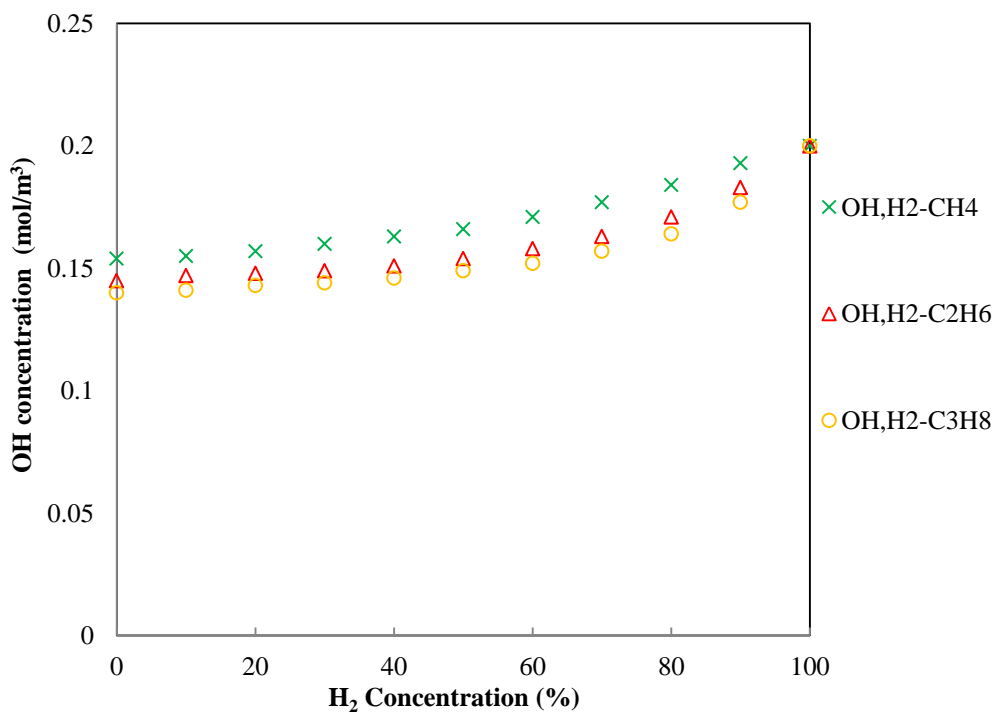


Figure 9.4: The OH concentration against the H₂ addition concentration for H₂-CH₄, H₂-C₂H₆ and H₂-C₃H₈ mixtures

9.2 Laminar Burning Velocity and the Flame Stability Parameters

Chapter 5 has shown that the flame lift-off height increases linearly with the inlet jet velocity. When H₂ concentration is greater than 60%, at a fixed inlet velocity, the flame lift-off heights of H₂-CH₄ have the lowest value while those of H₂-C₃H₈ have the highest value. Based on the premixed flame stabilisation model, the lifted flame base is balanced by the result of inlet gas velocity and the local burning velocity. This indicates that H₂-CH₄ has the highest laminar burning velocity compared with H₂-C₂H₆ and H₂-C₃H₈ mixtures when H₂ concentration is greater than 60%. This section presents the discussions on the correlation of computationally simulated laminar burning velocity data with the experimentally determined flame lift-off height data. The correlation is examined by using the correlation proposed by Kalghatgi (1984).

Figure 9.5 shows the correlation of the laminar burning velocities with the flame lift-off heights. At a fixed H₂ inlet velocity, the flame lift-off heights decrease approximately linearly with the laminar burning velocities. With increasing inlet gas velocity, the flame lift-off heights are stabilised by increasing the corresponding laminar burning velocities. Therefore, if a high inlet gas velocity is required, increasing the laminar burning velocity can stabilise the flame lift-off height at a desirable value and avoid flame blow-out.

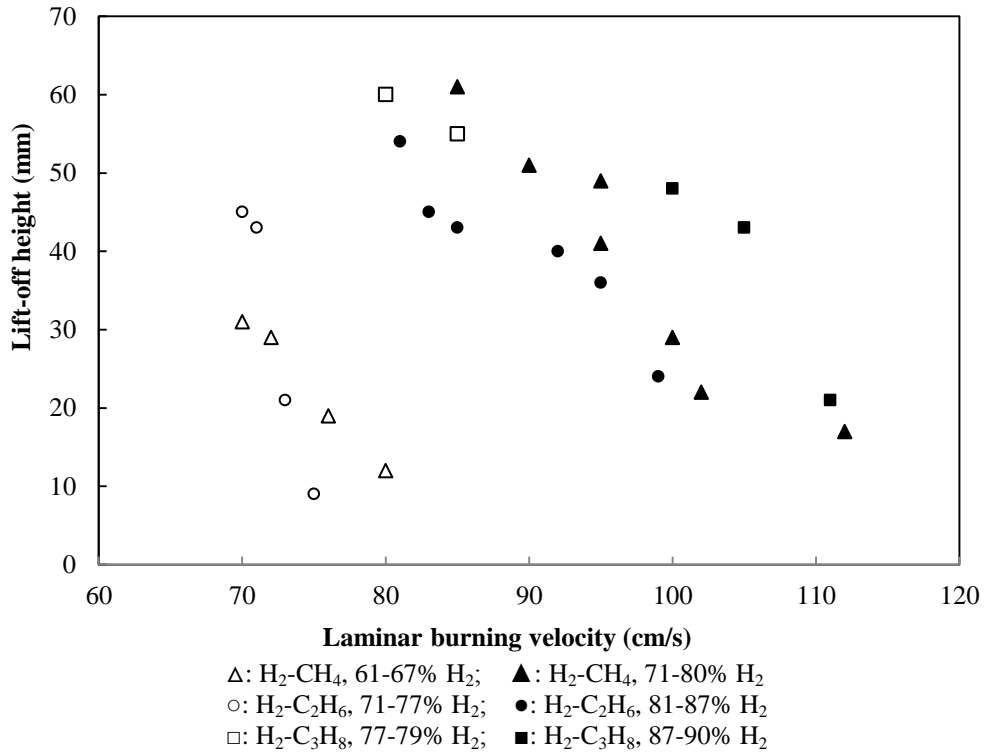


Figure 9.5: The flame lift-off height against the laminar burning velocity for H₂-CH₄, H₂-C₂H₆ and H₂-C₃H₈ lifted flames

The correlations introduced in Chapter 4 (*Eq. 4-2 and Eq. 4-3*) showed the correlation between the laminar burning velocity, S_L , and the flame lift-off height, h . This correlation is specified for the flame base as the flame is at a stabilised state. From these two proposed expressions, a linear equation concerning the flame lift-off height and laminar burning velocity can be obtained, shown as:

$$h = k \left(\frac{U_0}{S_L^2} \right) \quad \text{Eq.9-1}$$

According to Kalghatgi's correlation, k represents the slope of the plot of h with U_0/S_L^2 . As the lamina burning velocity profile has been computational modelled in Chapter 8 and the flame stability experimental data collected from Chapter 5, for H₂-CH₄, H₂-C₂H₆ and H₂-C₃H₈ flames the correlation between the laminar burning velocity and the corresponding flame lift-off height can be established and testified by the correlation proposed by Kalghatgi (1984).

$$h = C_2 \left(\frac{U_o}{S_L^2} \right) (\rho)^{1.5} v_e \quad \text{Eq. 9-2}$$

The values of the laminar burning velocity are obtained from the correlation between H₂ concentration and laminar burning velocity.

As shown in Figure 9.6, the plot of the h against the $\frac{U_o}{S_L^2}$ for CH₄-H₂ flames show a linear relationship. The flame lift-off height is proportional to the inlet gas velocity and the inverse of the square of the laminar burning velocity. The slope of the linear relation is determined to be 0.0002.

Figure 9.7 shows the relation for C₂H₆-H₂ lifted flames. It also shows a linear relation with a slope of 0.0002. Figure 9.8 shows this relation for lifted C₃H₈-H₂ flames. However, it behaves as different with H₂-CH₄ and H₂-C₂H₆ mixtures. It is difficult to conclude there is a linear relation between h and $\frac{U_o}{S_L^2}$.

The plot of pure H₂ flames is shown in Figure 9.9. The result is same as H₂-CH₄ and H₂-C₂H₆. There is linear relation between h and $\frac{U_o}{S_L^2}$. The slope is determined as 0.0001. To verify if the correlation developed by Kalghatgi (1984) can be applied to the H₂-hydrocarbon mixtures and if the experimentally and numerically measured data can fit to the Kalghatgi's correlation, it is required to calculate the slope term based on Eq. 9-2.

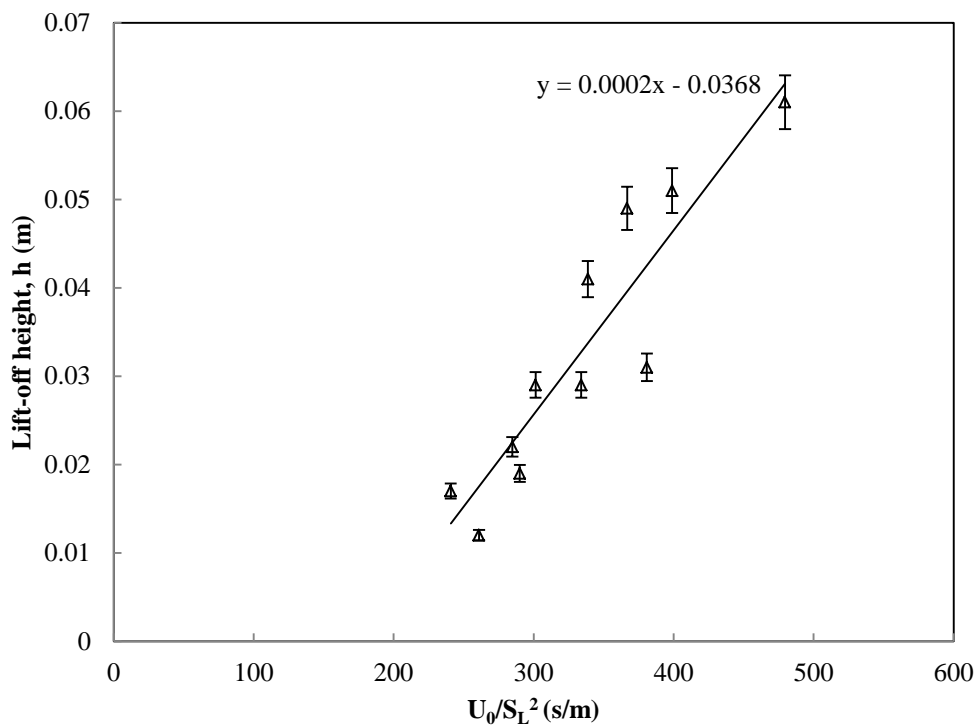


Figure 9.6: The correlation between h and U_0/S_L^2 for lifted H_2-CH_4 flames

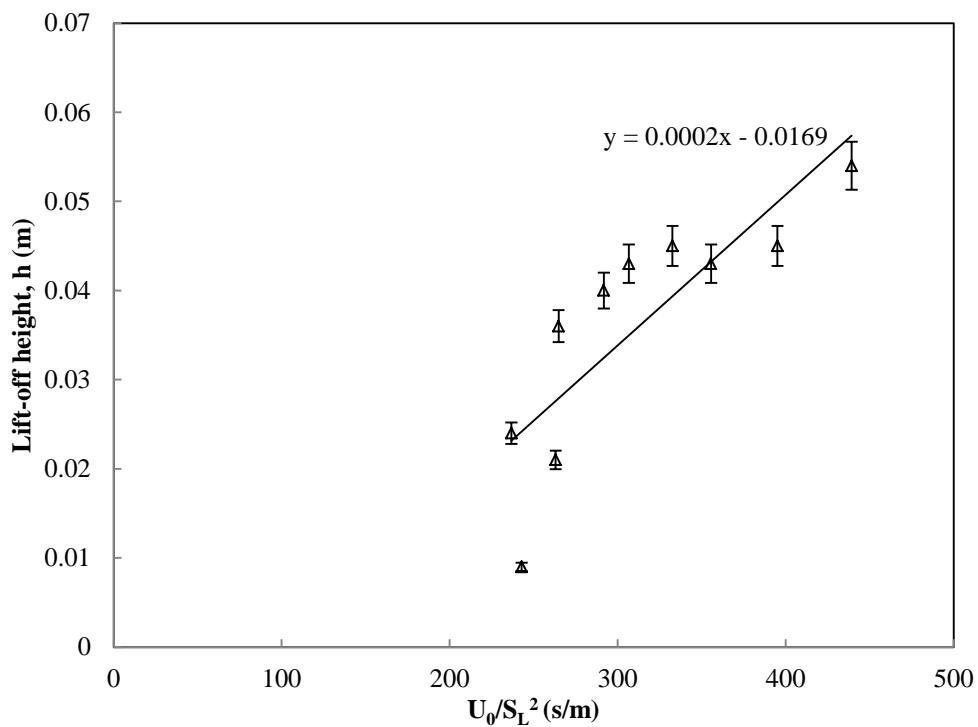


Figure 9.7: The correlation between h and U_0/S_L^2 for lifted $H_2-C_2H_6$ flames

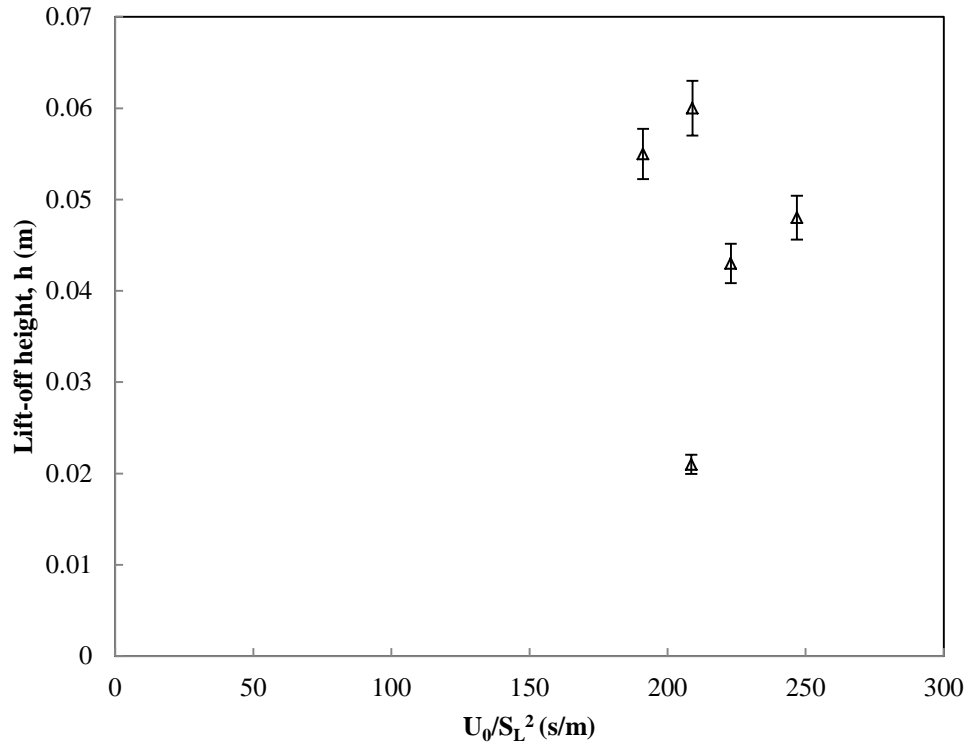


Figure 9.8: The correlation between h and U_0/S_L^2 for lifted $H_2-C_3H_8$ flames

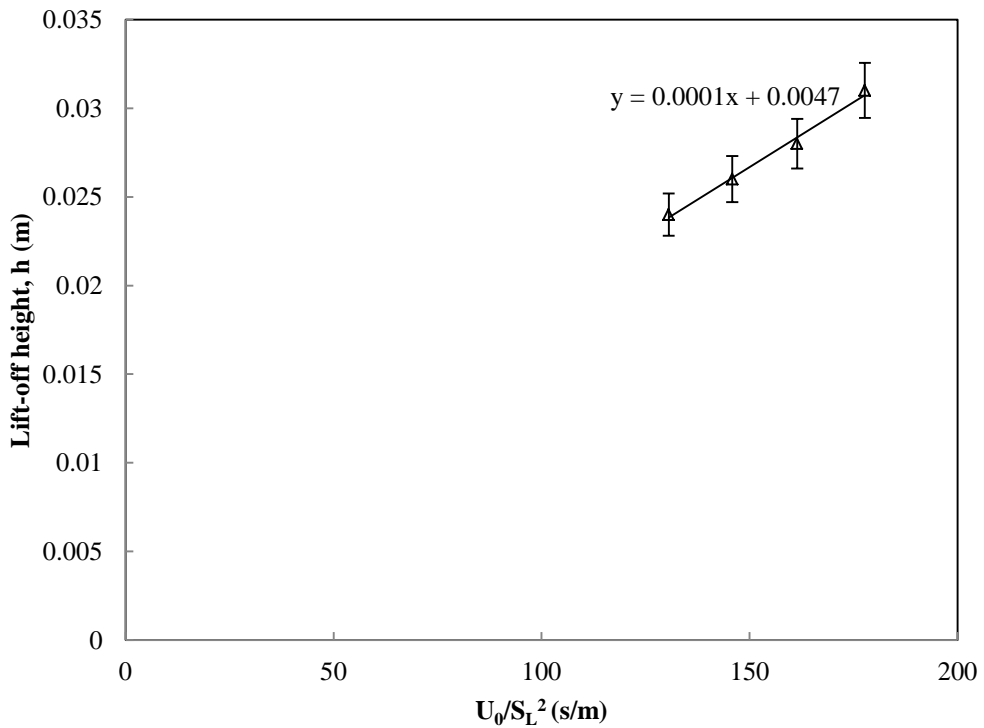


Figure 9.9: The correlation between h and U_0/S_L^2 for pure H_2 lifted flames

Table 9.1 shows densities and dynamic viscosities, μ , used to calculate the kinematic viscosity and density ratio expressed in Kalghatgi's correlation. The data is obtained from Younglove and Ely (1987).

Table 9.1: The physical and thermodynamic properties of H₂, CH₄, C₂H₆ and C₃H₈ at 1 atm and 300 K

	Density [kg/m ³]	Density of Air [kg/m ³]	Dynamic Viscosity [kg/ms]
CH ₄	0.6443	1.2	1.12E-05
C ₂ H ₆	1.215	1.2	9.48E-06
C ₃ H ₈	1.796	1.2	8.29E-06
H ₂	0.0899	1.2	8.80E-06

The calculations for the term, $C_2 (\bar{\rho})^{1.5} \nu_e$, are shown in Table 9.2. This represents the slope, k , of the plots shown in Figure 9.6, Figure 9.7, Figure 9.8 and Figure 9.9. The dynamic viscosity and density of the gaseous mixtures are calculated by using the equations given below.

Density of the mixtures, ρ_{mixture} (Perry, 2008):

$$\rho_{\text{mix}} = \frac{\sum_i \rho_i V_{f_i}}{\sum_i V_{f_i}} \quad \text{Eq.9-3}$$

Where ρ_i is the density of i^{th} component and V_{f_i} is the volumetric flow rate of i^{th} component.

Dynamic viscosity of the mixtures, μ_{mix} (Perry, 2008):

$$\mu_{\text{mix}} = \frac{\sum_i x_i \mu_i \sqrt{M_i}}{\sum_i x_i \sqrt{M_i}} \quad \text{Eq.9-4}$$

Where x_i is the mole fraction of the i^{th} component, M_i is the molecular weight of the i^{th} component and μ_i is the viscosity of the i^{th} component.

As indicated in Table 9.2, the calculated $C_2(\bar{\rho})^{1.5} v_e$ values are agreed well with the slopes of the plots for H₂, H₂-CH₄ and H₂-C₂H₆. This demonstrates that correlation developed by Kalghatgi (1984) can be applied well for H₂, H₂-CH₄ and H₂-C₂H₆. The computationally simulated correlation of the laminar burning velocity can fit into Kalghatgi's equation. However, the behavior of H₂-C₃H₈ is different from H₂, H₂-CH₄ and H₂-C₂H₆ and the plot does not match the calculations. This can be caused by the accuracy of the measurements in the experiments, or the Kalghatgi's correlation can not be well applied for H₂-C₃H₈ mixtures.

Table 9.2: The calculations of $C_2(\bar{\rho})^{1.5} v_e$ based on Kalghatgi's correlation

U ₀ [m/s]	H ₂ %	h [m]	S _L [m/s]	ρ_{mix} kg/m ³	$\bar{\rho}$	μ_{mix} [kg/ms]	v_e [m ² /s]	$C_2(\bar{\rho})^{1.5} v_e$
H ₂ -CH ₄								
167	67	0.012	0.8	0.269	0.224	1.02E-05	3.79E-05	2.01E-04
172	65	0.019	0.77	0.292	0.243	1.02E-05	3.52E-05	2.10E-04
178	62	0.029	0.73	0.302	0.252	1.03E-05	3.42E-05	2.16E-04
192	61	0.031	0.71	0.306	0.255	1.03E-05	3.39E-05	2.17E-04
302	80	0.017	1.12	0.197	0.164	9.79E-06	4.97E-05	1.65E-04
320	78	0.022	1.06	0.21	0.175	9.87E-06	4.70E-05	1.72E-04
326	77	0.029	1.04	0.217	0.181	9.90E-06	4.56E-05	1.75E-04
332	75	0.041	0.99	0.224	0.187	9.96E-06	4.45E-05	1.79E-04
338	74	0.049	0.96	0.237	0.198	1.00E-05	4.21E-05	1.85E-04
345	73	0.051	0.93	0.243	0.203	1.00E-05	4.12E-05	1.88E-04
363	71	0.061	0.87	0.251	0.209	1.01E-05	4.02E-05	1.92E-04
H ₂ -C ₂ H ₆								
144	77	0.009	0.77	0.34	0.283	9.16E-06	2.70E-05	2.03E-04
148	75	0.021	0.75	0.371	0.309	9.18E-06	2.47E-05	2.13E-04
159	73	0.043	0.72	0.39	0.325	9.20E-06	2.36E-05	2.19E-04
163	71	0.045	0.7	0.417	0.347	9.22E-06	2.21E-05	2.26E-04
266	87	0.024	1.06	0.225	0.187	9.05E-06	4.02E-05	1.63E-04
281	86	0.036	1.03	0.238	0.199	9.06E-06	3.80E-05	1.68E-04
286	85	0.04	0.99	0.257	0.214	9.08E-06	3.54E-05	1.75E-04
301	83	0.043	0.92	0.271	0.226	9.10E-06	3.36E-05	1.80E-04
306	82	0.045	0.88	0.287	0.239	9.11E-06	3.17E-05	1.86E-04

U_0 [m/s]	H_2 %	h [m]	S_L [m/s]	ρ_{mix} kg/m ³	$\bar{\rho}$	μ_{mix} [kg/ms]	v_e [m ² /s]	$C_2(\bar{\rho})^{1.5} v_e$
H ₂ -C ₂ H ₆								
310	81	0.054	0.84	0.303	0.253	9.12E-06	3.01E-05	1.91E-04
H ₂ -C ₃ H ₈								
148	79	0.055	0.88	0.455	0.38	8.52E-06	1.87E-05	2.19E-04
151	77	0.06	0.85	0.502	0.418	8.50E-06	1.69E-05	2.29E-04
257	90	0.021	1.11	0.264	0.22	8.63E-06	3.27E-05	1.69E-04
260	89	0.043	1.08	0.264	0.22	8.61E-06	3.26E-05	1.68E-04
267	87	0.048	1.04	0.324	0.27	8.59E-06	2.65E-05	1.86E-04
H ₂								
803	100	0.024	2.48	0.089	-	8.80E-06	9.79E-05	1.00E-04
897	100	0.026	2.48	0.089	-	8.80E-06	9.79E-05	1.00E-04
993	100	0.028	2.48	0.089	-	8.80E-06	9.79E-05	1.00E-04
1093	100	0.031	2.48	0.089	-	8.80E-06	9.79E-05	1.00E-04

Chapter 8 has shown the comparison between the experimental study conducted by Ilbas (2006) and current study on the laminar burning velocity of H₂-CH₄. The study predicted a stoichiometric correlation of the laminar burning velocity and H₂ concentration at ambient temperature (298 K) and 1 atm. The data of Ilbas' correlation is higher than current study when H₂ concentration is greater than 50%. The laminar burning velocity data from Ilbas is tested by applying the Kalghatgi's correlation and compared with current study. Figure 9.10 shows the plots of h against $\frac{U_o}{S_L^2}$ by using the laminar burning velocity data of Ilbas (2006) and current study. As shown in Figure 9.10, the plot of Ilbas's data also shows a linear relation. The slope is obtained as 0.0005, which is slightly higher than current study. However, it is higher than the calculated value of $C_2(\bar{\rho})^{1.5} v_e$. Therefore, the laminar burning velocity data from current study is more matching the Kalghatgi's correlation.

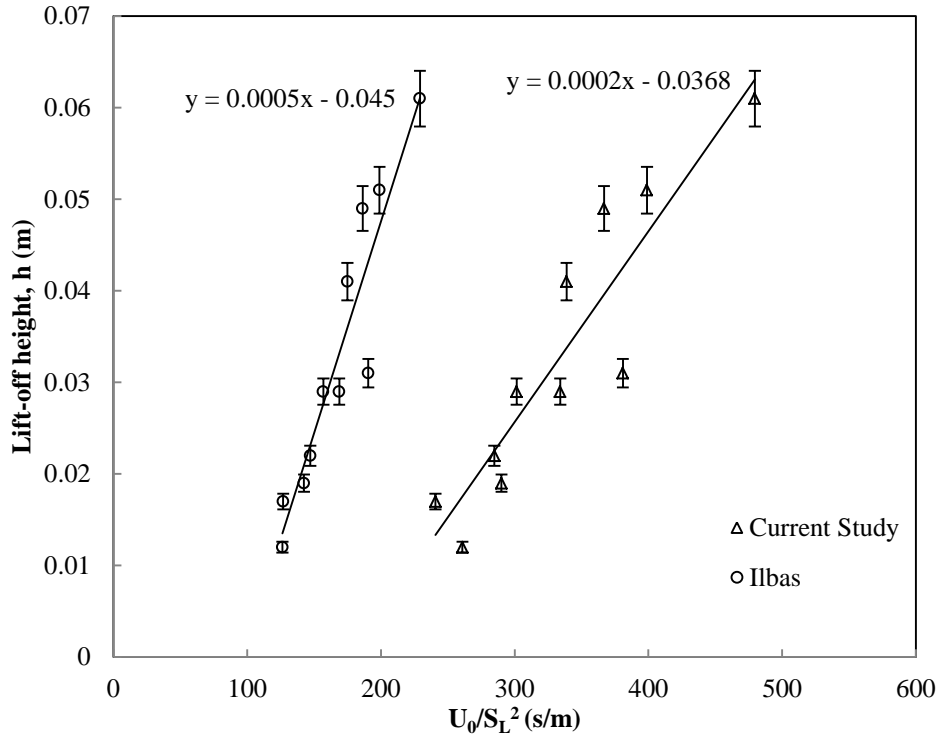


Figure 9.10: The comparison of the laminar burning velocity correlation between Ilbas and current study based on Kalghatgi's correlation

As discussed previously, the laminar burning velocity profiles of H_2-CH_4 and $H_2-C_2H_6$ mixtures are presented well in the Kalghatgi's correlation. The empirical expressions of correlation of the laminar burning velocity with H_2 concentration can be obtained from the plot illustrated in Figure 8.18 and shown below:

For H_2-CH_4 mixtures,

$$S_L = 0.0098x^2 - 0.075x + 42.071, (x < 60\%) \quad \text{Eq. 9-5}$$

and

$$S_L = 0.002x^3 - 0.3624x^2 + 23.541x - 466.79, (x \geq 60\%) \quad \text{Eq. 9-6}$$

For $H_2-C_2H_6$ mixtures,

$$S_L = 0.0045x^2 + 0.0431x + 48.722, (x < 60\%) \quad \text{Eq. 9-7}$$

and

$$S_L = 0.0002x^4 - 0.0626x^3 + 6.8154x^2 - 329.59x + 6016.5, (x \geq 60\%) \quad \text{Eq. 9-8}$$

Where x indicates the H_2 concentration in the mixtures.

Figures 9.11 and 9.12 illustrate the fits of the expressions of the laminar burning velocity of H_2 - CH_4 mixtures. As shown in the Figures, the laminar burning velocity data fits the expressions, *Eq. 9-5* and *Eq. 9-6*, very well.

The expressions of the laminar burning velocity of H_2 - C_2H_6 mixtures are shown in Figures 9.13 and 9.14. It can be seen from the Figures that the data fits well into the expressions, *Eq. 9-7* and *Eq. 9-8*.

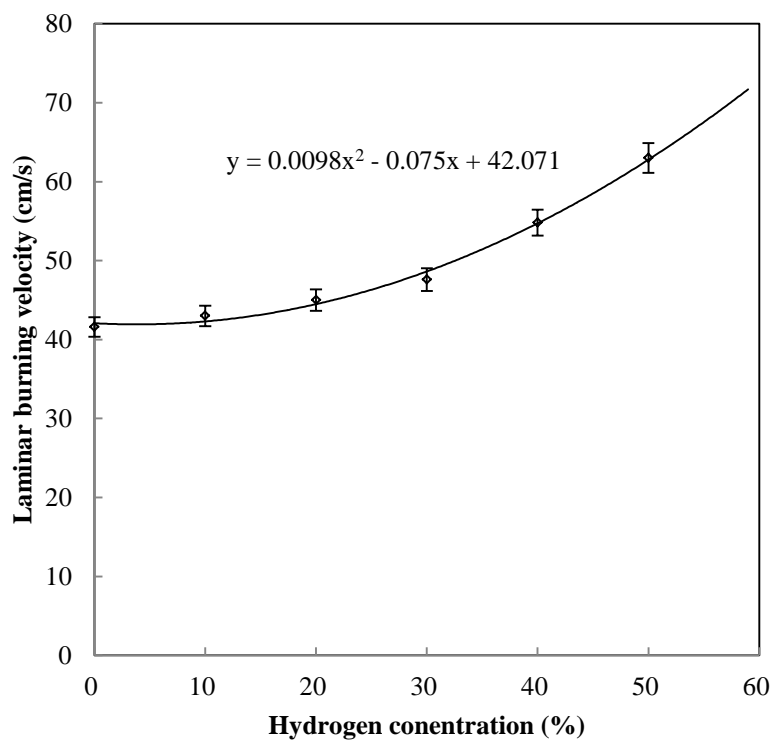


Figure 9.11: The laminar burning velocity correlation of H_2 - CH_4 at stoichiometric condition and $H_2 < 60\%$

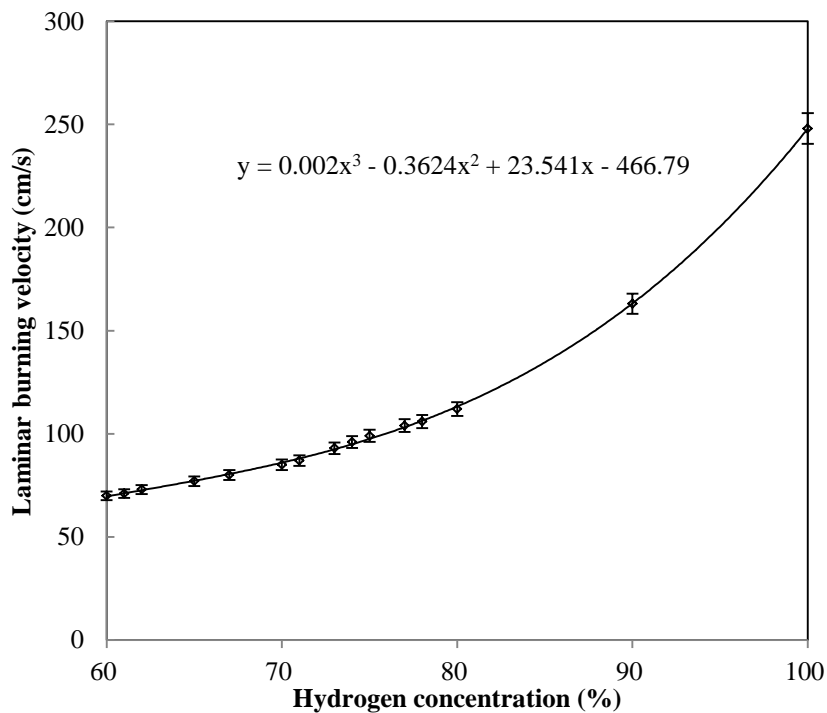


Figure 9.12: The laminar burning velocity correlation of H₂-CH₄ at stoichiometric condition and H₂ ≥ 60%

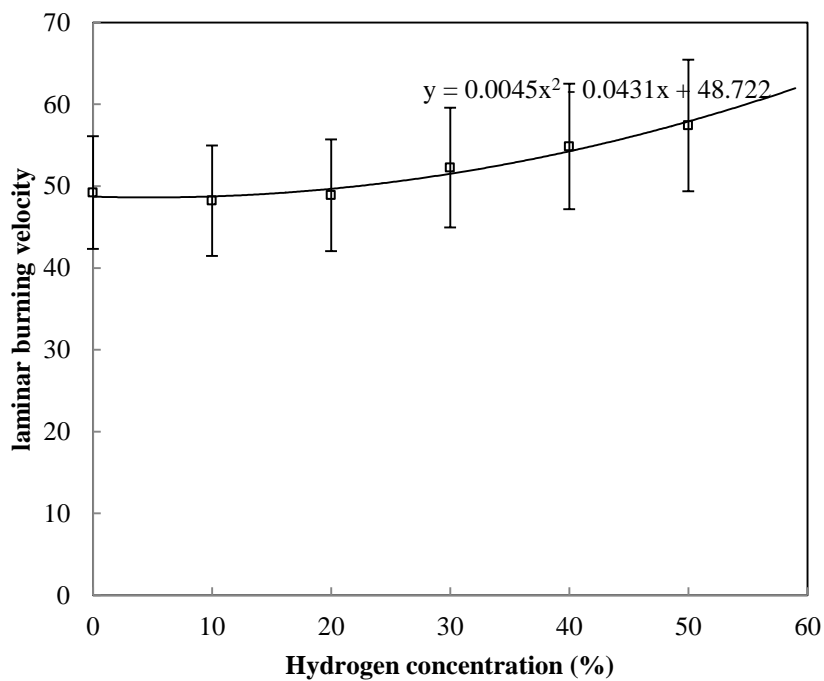


Figure 9.13: The laminar burning velocity correlation of H₂-C₂H₆ at stoichiometric condition and H₂ < 60%

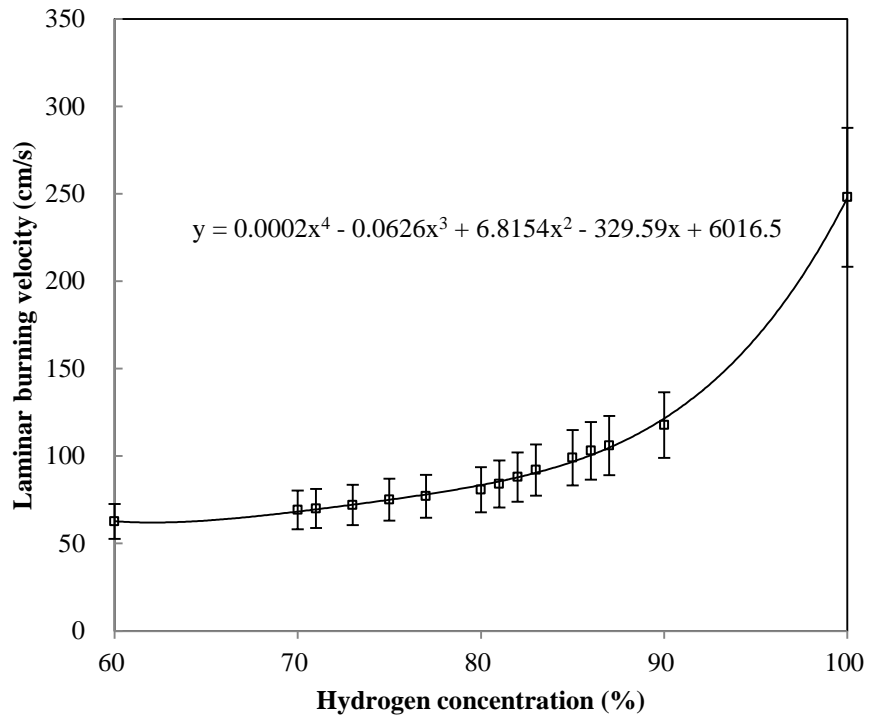


Figure 9.14: The laminar burning velocity correlation of $\text{H}_2\text{-C}_2\text{H}_6$ at stoichiometric condition and $\text{H}_2 \geq 60\%$

Chapter 10

Conclusions and Further Considerations

Conclusions

This study experimentally determines the lift-off and blow-out characteristics of H_2 , H_2 - CH_4 , H_2 - C_2H_6 , H_2 - C_3H_8 , H_2 - CO_2 and H_2 - CH_4 - CO_2 flames. The effect of H_2 and CO_2 concentration on the flame lift-off height, lift-off velocity and blow-out velocity is analysed based on the experiment data. The laminar burning velocities of H_2 , H_2 - CH_4 , H_2 - C_2H_6 and H_2 - C_3H_8 mixtures are determined through numerically modelling. The correlation of the laminar burning velocity with H_2 concentration is simulated. The experimentally determined flame stability data and computationally simulated lamina burning velocity data are related to present the relationship between laminar burning velocity and flame stability parameters. The conclusions of the study are:

- For H_2 - CH_4 , H_2 - C_2H_6 and H_2 - C_3H_8 mixtures, at fixed inlet H_2 velocity the flame lift-off height increases linearly with increasing inlet jet velocity and H_2 concentration. When H_2 concentration is greater than 60%, the flame lift-off height of H_2 - CH_4 is higher than H_2 - C_2H_6 and following by H_2 - C_3H_8 . For H_2 - CO_2 and H_2 - CH_4 - CO_2 mixtures, at a fixed jet velocity the addition of CH_4 and CO_2 composition increases the flame lift-off height. When the CO_2 concentration is over 8%, the flame reaches blow-out state without experiencing lift-off state. To increase the inlet jet velocity without increasing the flame lift-off height, it is required to increase the hydrogen concentration in the mixture.
- The lift-off velocity of H_2 -air flame is over 800 m/s, which is far higher than the mixture of H_2 , hydrocarbon and CO_2 . With a fixed exit diameter and inlet H_2 velocity, the lift-off velocity decreases with increasing H_2 concentration.

- The addition of CO₂ in H₂ flames results in the flame reaches blow-out state at the jet velocity of 1004 m/s, when there is 3% CO₂ in H₂-CO₂ mixtures. When the CO₂ concentration reaches approximately 8%, the flame blows out at the inlet jet velocity of approximately 339 m/s. When the inlet jet velocity is higher than 200 m/s, the CO₂ concentration can be tolerated up to 18%. For H₂-CH₄-CO₂ mixtures, at fixed inlet H₂ velocity, the varying of the CH₄ and CO₂ composition only slightly influences the blow-out velocity of the mixture. When H₂ concentration is in the range of 60-68%, the flame will reach blow-out condition at the jet velocity approximately from 170-180 m/s. When H₂ concentration is in the range of 70 to 85% approximately, the flame will reach blow out condition at the jet velocity approximately from 300-350 m/s. The effect of CH₄ and CO₂ on flame blow-out velocity can be minimised by fixing the inlet H₂ velocity, and the blow-out velocity of the mixture can be predicted through maintaining the inlet H₂ velocity.
- The numerically modelling of the homogenous reaction kinetics has been done for H₂-CH₄, H₂-C₂H₆ and H₂-C₃H₈ mixtures. It demonstrates that when H₂ concentration is less than 60% the overall reaction mechanism is governed by hydrocarbon reactions while H₂ reactions dominate the overall reaction mechanism when H₂ concentration is greater than 60%. With increasing H₂ concentration, the consumption rates of CH₄ increases. Compared with CH₄, the reaction rates of C₂H₆ and C₃H₈ are relatively independent of H₂ concentration. When H₂ addition is less than 60%, the reaction rates of H₂ increase slowly. The consumption rate of C₃H₈ is greater than C₂H₆ and following by CH₄. When the addition is greater than 60%, the increase in the H₂ reaction rate becomes relatively faster. The consumption rate of H₂ of H₂-CH₄ increases more sharply compared with H₂-C₂H₆ and H₂-C₃H₈.
- The production rates of H and OH increase with the increasing of H₂ concentration of the mixtures.
- The species pathway analysis has been implemented to study the reaction pathways of H₂-CH₄, H₂-C₂H₆ and H₂-C₃H₈ mixtures. The primary decomposition of CH₄ is mainly through the reactions, CH₄+H<=>H₂+CH₃,

$\text{CH}_4 + \text{OH} \rightleftharpoons \text{H}_2\text{O} + \text{CH}_3$ and $\text{CH}_4 + \text{O} \rightleftharpoons \text{OH} + \text{CH}_3$ to form CH_3 . The primary decomposition of C_2H_6 is through $\text{C}_2\text{H}_6 + \text{O}_2 \rightleftharpoons \text{C}_2\text{H}_5 + \text{HO}_2$ and C_3H_8 is primarily consumed through $\text{C}_3\text{H}_8(+\text{M}) \rightleftharpoons \text{CH}_3 + \text{C}_2\text{H}_5(+\text{M})$. C_2H_5 is then converted into C_2H_4 . The main pathways of H_2 reaction are $\text{H}_2 + \text{OH} \rightleftharpoons \text{H}_2\text{O} + \text{H}$ and $\text{H}_2 + \text{O} \rightleftharpoons \text{OH} + \text{H}$.

- H and OH play important role in the decomposition processes of CH_4 and CH_3 . However, they are not strongly involved in the primary decomposition of C_2H_6 , C_3H_8 and C_2H_4 . The main contributors of H and OH are from the H_2 oxidation mechanism.
- The laminar burning velocity of H_2 -air at stoichiometric condition is 248.6 cm/s. That of H_2 - CH_4 is 41.6 cm/s. H_2 - C_2H_6 and H_2 - C_3H_8 have the value of 49.2 cm/s and 55.7 cm/s respectively.
- When H_2 concentration is less than 60%, the laminar burning velocity of H_2 - C_3H_8 is higher than H_2 - C_2H_6 and H_2 - CH_4 at stoichiometric condition. However, when H_2 concentration is greater than 60%, the order is inversed and the increase in the laminar burning velocity of CH_4 - H_2 is more sensitive to H_2 concentration than the other two mixtures. A correlation of the laminar burning velocity with H_2 concentration is established for H_2 - CH_4 , H_2 - C_2H_6 and H_2 - C_3H_8 mixtures.
- The experimentally measured flame lift-off heights data and computationally modeled laminar burning velocity correlation are verified by applying Kalghatgi's correlation. For H_2 - CH_4 and H_2 - C_2H_6 mixtures, the plots show linear relation with slope of 0.0002. For pure H_2 , the plot also shows a linear relation with slope of 0.0001. The calculated value of the slopes from Kalghatgi's correlation of H_2 , H_2 - CH_4 and H_2 - C_2H_6 well match the value from the plots. For pure H_2 , H_2 - CH_4 and H_2 - C_2H_6 mixtures, the experimentally determined flame stability data and numerically simulated laminar burning velocity data are well presented in the Kalghatgi's correlation. However, the data for H_2 - C_3H_8 is not well verified.

- The laminar burning velocity is determined by the reaction rates of $\text{H}_2\text{-C}_3\text{H}_8$, $\text{H}_2\text{-C}_2\text{H}_6$ and $\text{H}_2\text{-CH}_4$ mixture. When H_2 concentration is less than 60%, the laminar burning velocity is determined by hydrocarbon reaction rates, while it is governed by H_2 reaction rates when H_2 concentration is greater than 60%.
- The addition of H_2 supplies H and OH for the decompositions of CH_4 and CH_3 . The increase in H_2 concentration enhances the reaction rates of H_2 and CH_4 . However, H and OH do not directly influence the primary decompositions of C_2H_6 and C_3H_8 . They participate in the later paths of decomposing of C_2H_4 , C_2H_2 and CH. This results in that the increase of the laminar burning velocity of $\text{H}_2\text{-CH}_4$ is more sensitive to the increase in H_2 concentration. Therefore, when H_2 begins to govern the overall reaction rates at 60% and the increase of H_2 reaction rate of $\text{H}_2\text{-CH}_4$ starts to exceed that of $\text{H}_2\text{-C}_2\text{H}_6$ and $\text{H}_2\text{-C}_3\text{H}_8$ at approximately 60%, then the laminar burning velocity of $\text{H}_2\text{-CH}_4$ exceeds that of $\text{H}_2\text{-C}_2\text{H}_6$ and $\text{H}_2\text{-C}_3\text{H}_8$.

The outcomes from this study are capable of providing a guideline for industries to utilise hydrogen to either enhance combustion performance or achieve any specific purposes in various combustion processes, such as in gas turbine. When using hydrogen addition to increase the burning velocity of gaseous mixtures, the effect is strongly dependent on the addition concentration. The change is very steady when hydrogen addition is less than 60% while the increase is exponential as hydrogen addition is over 80%. The established correlation of hydrogen concentration with laminar burning velocity will provide a basic reference for predicting the burning velocity of hydrogen-hydrocarbon (up to C_3) mixtures. It also can be used by ant future studies as a comparison to conduct the modelling of the laminar burning velocity of hydrogen-hydrocarbon mixtures.

The analysis of the flame stability associated with the laminar burning velocity will help industrial utilisation of hydrogen based syngas. The understanding of the flame stability characteristics will ensure the utilisation of such syngas gives optimised performance with safe handling. To predict the blow-out velocity of $\text{H}_2\text{-CH}_4\text{-CO}_2$ gaseous mixtures can be implemented through adjusting the inlet hydrogen velocity. In industrial processes, with various CH_4 and CO_2

compositions, the blow-out limit of the gaseous mixture can be predicted and maintained through manipulating the inlet hydrogen velocity. In addition, to achieve high jet velocity without causing high lift-off height and blow-out, it is required to increase the hydrogen concentration and the hydrogen inlet velocity of the gaseous mixtures when using such gaseous mixtures in gas turbine.

Further Considerations

In the computational reaction kinetics modelling, the radicals concentration gradients, such as OH and CH, are simulated in CHEMKIN package. It is valuable to design an experimental programme to test the radicals consumption and production in the reactions. A spectrum based experiment can be employed to capture the light emitted from the flame and then to detect the intensity of the radicals, such as OH and CH. Figure 10.1 shows the Spectrograph system that will be applied to testify the emission intensity of OH and CH. The spectrum-based analysis will focus on the flame base, for the emission intensity of OH and CH radicals from the reaction of hydrogen-hydrocarbon mixtures. For obtaining spectrometry-based results, detailed spectrum of the flame radiation can be acquired from a spectrometer included in the spectrograph system, as shown in Figure 10.1. The polychromatic light emitted from the flame will be projected on the optical probe of the spectrograph system. It then will pass through the fiber optical cable to enter the spectrometer (imaging Czerny-Turner).

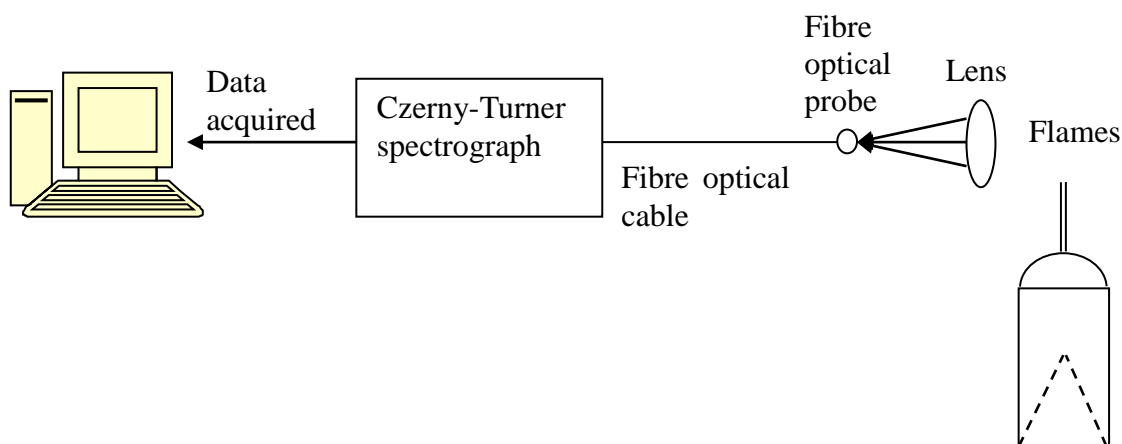


Figure 10.1: Schematic of the setup of the spectral analysis system

Fig. 10.2 shows the internal structure of the spectrometer. The two concave mirrors form the images of the source and the grating is responsible for dispersing the light or making an angular deflection of the light as a function of the wavelength. The flame radiation which enters the entrance slit of the spectrometer is collected by the collimating mirror. The collimated light is then reflected onto the diffraction grating and is dispersed into individual wavelengths. As shown in the Figure, each individual wavelength leaves the grating plane at different angle, and through the focusing mirror it is imaged onto a CCD detector at the exit plane on which each position represents a different wavelength. As each wavelength images at a different horizontal position, the spectrum of the input light is spread across the CCD. The radiation from different species has different wavelength and it is unique. The light emitted from CH and OH will be centred at different horizontal position on the spectrum. Rotating the diffraction grating scans wavelengths across the CCD, allowing the intensity at individual wavelengths to be readily measured.

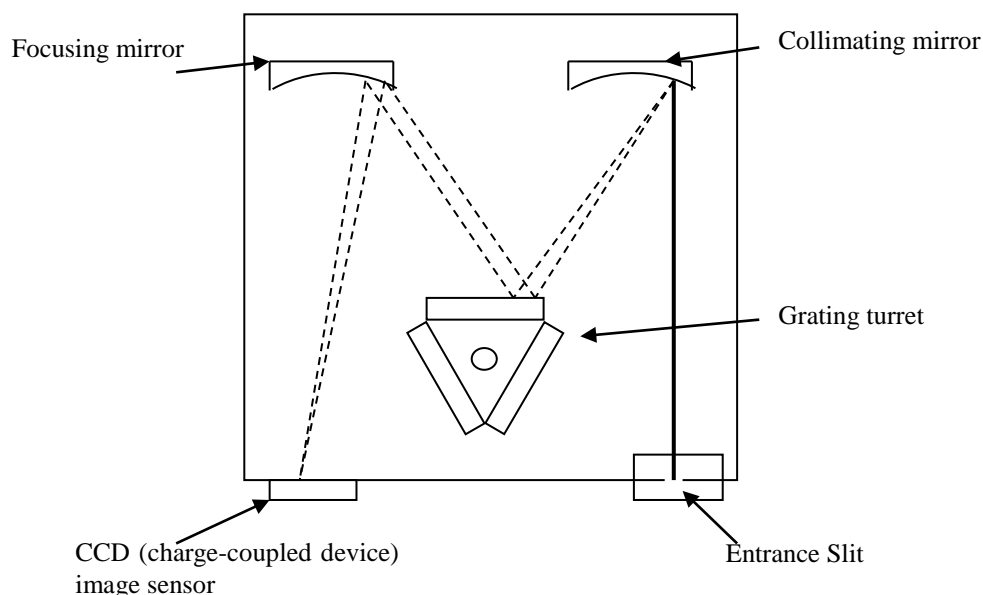


Figure 10.2: The internal structure of the spectrometer

The emission intensity data obtained from the spectrum based experiment can then be used to compare and verify with the results from the computational simulations in order to valid the results.

Another consideration for the future studies is the effect of the presence of CO₂ on the laminar burning velocity of hydrogen-hydrocarbon-CO₂ mixtures. The reaction kinetics simulation has also been conducted for H₂-CH₄-CO₂ mixtures. The results show that the addition of CO₂ does not influence the reaction kinetics. However, it is considered that the presence of CO₂ in the mixture will reduce the laminar burning velocity and the flame temperature of the mixture. The simulation data obtained so far shows that the reduction in the flame temperature is very slight with increasing CO₂ concentration in the mixture. Further computational kinetics modelling is required to establish a more comprehensive analysis for the effect of CO₂ concentration on the flame temperature and the laminar burning velocity of hydrogen-hydrocarbon mixtures.

A dimensionless plot according to Kalghatgi's correlation is shown as Figure 10.3. The data for H₂, H₂-CH₄, H₂-C₂H₆ and H₂-C₃H₈ is expected to collapse into a straight line. However, as shown in the Figure, the data is not presented in the expected way. As previously discussed in Chapter 9, the deviation of the lift-off height and laminar burning velocity of H₂-C₃H₈ mixtures is more significant than that of H₂, H₂-CH₄ and H₂-C₂H₆ mixtures. The laminar burning velocity values are obtained from the correlation established in Chapter 8. The lift-off height values are measured from the flame stability experiment. More experimental data is required to fit into the data to testify if the experimental and computational results can be plot in the form of the Kalghatgi's dimensionless plot to produce a straight line.

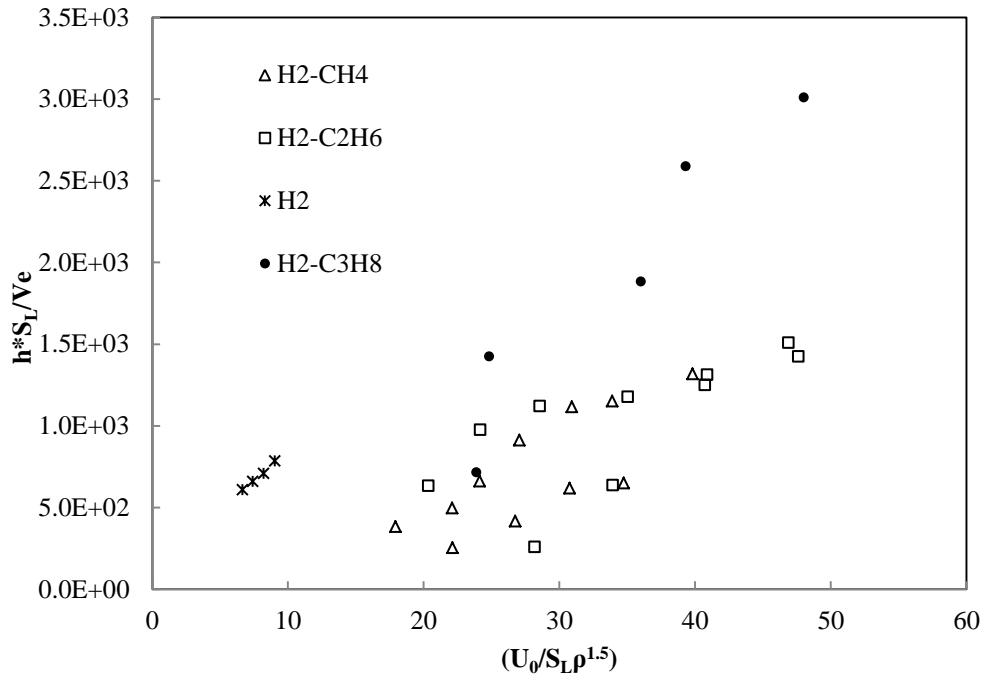


Figure 10.3: The dimensionless plot of lift-off height with laminar burning velocity based on Kalghatgi's correlation

References

- Andrews, G.E. and Bradley, D. (1972) 'Determination of Burning Velocities: A critical Review', *Combustion and Flame*, 18:133-53.
- Agrawal, D.D. (1981) 'Experimental determination of burning velocity of methane-air mixtures in a constant volume vessel', *Combustion and Flame*, 42:243-52.
- Anderson, David M., Kottke, Peter A., Fedorov, Andrei G. (2014) 'Thermodynamic analysis of hydrogen production via sorption-enhanced steam methane reforming in a new class of variable volume batch-membrane reactor', *International Journal of Hydrogen Energy*, 39:17985-97.
- Aung, K.T., Hassan, M.I. and Faeth, G.M. (1998) 'Effects of pressure and nitrogen dilution on flame stretch interactions of laminar premixed H₂-O₂-N₂ flames', *Combustion and Flame*, 112(1-2):1-15.
- Berman, M.R. and Lin M.C. (1983) 'Kinetics and mechanisms of the reactions of CH with CH₄, C₂H₆ and n-C₄H₁₀', *Chemical Physics*, 82:435-442.
- Bilgen, S. (2014) 'Structure and environmental impact of global energy consumption', *Renewable and Sustainable Energy Reviews*, 38:890-902.
- Botha, J.P. and Spalding, D.B. (1954) 'The laminar flame speed of propane/air mixtures with heat extraction from the flame', *Proc. Roy. Soc. A* 225:71-96
- Bruzzi, L., Boragno, V. and Verita, S. (2007) 'Sostenibilità ambientale dei sistemi energetici', *Tecnologie e Normative*, ENEA report
- Buffam, J., Cox, K. and Schiess, H. (2008) 'Measurement of laminar burning velocity of methane-air mixtures using a Slot and Bunsen burner', Faculty of the Worcester Polytechnic Institute.
- Chhiti, Younes. And Kemiha, Mohammed. (2013) 'Thermal conversion of biomass, pyrolysis and gasification: A review', *The International Journal of Engineering and Science (IJES)*, 2(3):75-85.
- Connaire, M.O., Curran, H.J., Simmie, J.M., Pitz, W.J. and Westbrook, C.K., 'A comprehensive modelling study of hydrogen oxidation', *International Journal of Chemical Kinetics*, 36:603-22
- Contribution of Working Group I to the Fourth Assessment Report of the Intergovernmental Panel on Climate Change, Working Group I: The Physical Basis for Climate Change, edited by Susan Solomon IPCC; 2007.
- Coppens, F. H. V., De Ruyck, J. and Konnov, A. A. (2007) 'Effects of hydrogen enrichment on adiabatic burning velocity and NO formation in methane + air flames', *Experimental Thermal and Fluid Science*, 31:437-444

- Chacategui, R., [Sánchez](#), D., [Muñoz de Escalona](#), J.M., [Muñoz](#), A. and [Sánchez](#), T. (2013) 'Gas and steam combined cycles for low calorific syngas fuels utilisation', *Applied Energy*, 101:81-92.
- Cheng, T.S. and Chiou, C.R. (1998) 'Experimental investigation on the characteristics of turbulent hydrogen jet flames', *Combustion Science and Technology*, 136(1-6): 81-94
- Chiesa, P., Consonni, S., Kreutz, T. and Williams, R. (2005) 'Co-production of hydrogen, electricity and CO₂ from coal with commercially ready technology. Part A: performance and emissions' *International Hydrogen Energy*, 30:747-67
- Cormos, Calin-Cristian., Cormos, Ana-Maria. and Agachi, Serban. (2009) 'Heat and power integration for hydrogen-fuelled Combined Cycle Gas Turbine (CCGT)', *Computer Aided Chemical Engineering*, 26:1239-44
- Dagaut, P. and Nicolle, A. (2005) 'Experimental and detailed kinetic modelling study of hydrogen-enriched natural gas blend oxidation over extended temperature and equivalence ratio ranges, Proceedings of the 13th symposium (international) on combustion', pp.2631-2638
- Dimitrov, V.I. and Azatyan, V.V. (1975), 'Maximum kinetic mechanism of oxidation of H₂', in *Problems of gas dynamics*, Inst. Theor. Appl. Mech., Sib. Div., Acad. Of Sci. of the USSR, Novosibirsk, pp. 69-73
- Di Sarli, V. and Benedetto, A.D. (2007) 'laminar burning velocity of hydrogen-methane-air premixed flames', *International Journal of Hydrogen Energy*, 32:637-46
- Dixon-Lewis, G. and Williams, A. (1967) 'Some observations on the combustion of methane in premixed flames', *Eleventh (International) Symposium on Combustion*, pp.951-958, The Combustion Institute, Pittsburgh.
- Dixon-Lewis, G. and Islam, S.M. (1982) 'Flame modeling and burning velocity measurement' *Symposium (International) on Combustion*, 19(1):283-291
- Dougherty, E.P. and Rabitz, H. (1980) 'Computational kinetics and sensitivity analysis of hydrogen-oxygen combustion', *J. Chem. Phys.* 72(12)
- Dowdy, D.R., Smith, D.B., Taylor, S.C. and Williams, A. (1990) 'The use of expanding spherical flames to determine burning velocity and stretch effects in hydrogen/air mixtures', *Twenty-third symposium (International) on Combustion*, The Combustion Institute, 325:332
- Edmondson, H. and Heap, M.P. (1970) *Combustion and Flame* 14:195
- Egolfopoulos, F.N., Cho, P. and Law, C.K. (1989) 'Laminar flame speeds of methane-air mixtures under reduced and elevated pressures', *Combustion and Flame*, 76:375-91.

- Egerton, A.C. and Thabet, S.K. (1952) 'Flame propagation: the measurement of burning velocities of slow flames and the determination of the limits of combustion', Proc. Roy. Soc. 211A:445-471.
- EI-Sherif, S.A. (2000) 'Control of emission by gaseous additives in methane-air and carbon monoxide-air flames', Fuel, 79, pp. 567-575
- Eickhoff, H., Lenze, B. and Leckel, W. (1984) 'Experimental investigation on the stabilization mechanism of jet diffusion flames', Symposium (International) on Combustion, 20, pp. 311-318.
- Eickhoff, H., Lenze, B. and Leckel, W. (1985) Twentieth Symposium (International) on Combustion, The Combustion Institute p.311.
- Everest, D.A., Feikema, D.A. and Driscoll, J.F. (1996) 'Images of the strained flammable layer used to study the liftoff of turbulent jet flames', Symposium (International) on Combustion, 26, pp. 129-136.
- Fires and Explosions (2010) Fire and Explosions, Lecture handouts, Sheffield University
- Foat, T., Yao, K.P. and Zhang, Y. (2001) 'The visualization and mapping of turbulent premixed impinging flames', Combust Flame, 125:839-51
- Fristrom, R.M. (1956) Flame zone studies, II. Applicability of one-dimensional models to three-dimensional laminar Bunsen flame fronts, J. Chem. Phys. 24:888-94
- Fu, S. and Wu, Y. (2001) 'Detection of velocity distribution of a flow field using sequences of schlieren images', Optical engineering, 40 (Part 4): 1661-6
- Fuller, L.E., Parks, D.J. and Fletcher, E.A. (1969) Combustion and Flame 13:455.
- Gaforth, A.M. (1974) 'Measurement of rapidly varying density, and hence temperatures, by laser interferometry in the unburnt gas region of a spherical constant volume vessel during flame propagation', University of the Witwatersrand, School of Mechanical Engineering, Research Report No.57
- Gaforth, A.M. and Rallis, C.J. (1975) 'The spherical bomb method for laminar burning velocity determination: Equations for thick flame propagation' University of the Witwatersrand, School of Mechanical Engineering, Research Report No.59; Also presented at The Second European Symposium on Combustion, Orleans, France
- Gauducheau, J.L., Denet, B. and Searby, G. (1998) 'A numerical study of lean CH₄/H₂/air premixed flames at high pressure', Combustion Science Technology, 137:81-99
- Gibbs, G.J. and Calcote, H.F. (1959) 'Effect of molecular structure on burning velocity', J.Chem.Eng. Data, 4:226-37

- Goncalves, R.F.B., Ferrao, L.F.A., Rocha, R.J., Machado, F.B.C., Iha, K. and Rocco, A.F.F. (2010) 'Kinetic simulation of hydrogen combustion in a homogeneous reactor', AIAA 2010-6655
- Gontkovskaya, V.T., Gordopolova, I.S. and Basevich, V.Ya. (1981) 'Kinetics of hydrogen oxidation over a wide pressure and temperature range', Translated from *Fizika Goreniya I Vzryva*, Vol.17 No. 1, pp. 64-68
- Gottgen, J., Mauss, F. and Peter, N. (1992) 'Analytic Approximations of Burning Velocities and Flame Thickness of Lean Hydrogen, Methane, Ethylene, Ethane, Acetylene and Propane Flames', 24th Symposium (international) on Combustion, 129.
- Groff, E.G. (1982) *Combustion Flame*, 48:51-62.
- Gunther, R. and Janisch, G. (1972) 'Measurements of burning velocity in a flat flame front', *Combustion Flame*, 19(1):49-53
- Gunther, R. Horch, K. and Lenze, B. (1981) First Specialist Meeting (International) of the Combustion Institute, Combustion Institute, p.117.
- Hall, L., Horch, K. and Gonther, R. (1980) *Brennst-Warme-Kraft*, 32, 26
- Halter, F., Chauveau, N.D-C. and Gokalp, I. (2004) 'Characterization of the effects of pressure and hydrogen concentration on laminar burning velocities of methane-hydrogen-air mixtures', *Proceedings of the Combustion Institute*, 30:201-8
- Haniff, M.S., Melvin, A., Smith, D.B. and Williams, A. (1989) 'The burning velocities of methane and SNG mixtures with air', *J.Inst.E.* 229.
- Heghes, C.I. (2006) 'C1-C4 Hydrocarbon oxidation mechanism' Faculty of Chemistry of the Rupertus Carola University of Heidelberg, Germany
- Heravi., H.M., Azarinfar, A., Kwon, S.I., Bowen, P.J. and Syred, N. (2007) 'Determination of Laminar Flame Thickness and Burning Velocity of Methane-Air Mixture', 3rd European Combustion Meeting ECM 2007.
- Herdem, Munur Sacit., Farhad, Siamak., Dincer, Ibrahim. and Hamdullahpur, Ferdun. (2014) 'Thermodynamic modelling and assessment of a combined coal gasification and alkaline water electrolysis system for hydrogen production', *International Journal of Hydrogen Energy*, 39:3061-71.
- Herout, M., Malatak, J., Kucera, L. and Dlabaja, T. (2011) 'Biogas composition depending on the type of plant biomass used', *Res. Agr. Eng.*, 57(4):137-43.
- Hinshelwood, C. N. (1940) *The kinetics of Chemical Change*, Clarendon Press, Oxford
- Hirschfelder, J.O. and Curtiss, C.F. (1954) *Molecular Theory of Gases and Liquids*, John Wiley and Sons, New York, p.76

- Hu, E., Huang, Z., He, J., Jin, C. and Zheng, J. (2009) 'Experimental and numerical study on laminar burning characteristics of premixed methane-hydrogen-air flames', *International Journal of Hydrogen Energy*, 34:4876-88
- Hu, Erjang, Fu, Jin., Pan, Lun., Jiang, Xue., Huang, Zuohua. and Zhang, Yang. (2012) 'Experimental and numerical study on the effect of composition on laminar burning velocities of H₂/CO/N₂/CO₂/air mixtures', *International Journal of Hydrogen Energy*, 37(23):18509-19.
- Huang, Z., Zhang, Y., Zeng, K., Liu, B., Wang, Q. and Jiang, D. (2006) 'Measurements of laminar burning velocities for natural gas-hydrogen-air mixtures', *Combustion and Flame*, 146:302-11
- Huang, H. and Zhang, Y. (2008) 'Flame colour characterisation in the visible and infrared spectrum using a digital camera and image processing', *Measurement Science and Technology*, 19, 085406 (9pp)
- Huang, H. and Zhang, Y. (2010) 'Digital colour image processing based measurement of premixed CH₄+air and C₂H₄+air flame chemiluminescence', *Fuel*, 90:48-53
- Hung, J. (1986) 'Effects of propane or ethane additives on laminar burning velocity of methane-air mixtures', *Energy, Mines and Resources Canada*
- Huzayyin, A. S., Moneib, H. A., Shehatta, M. S. and Attia, A. M. A. (2008) 'Laminar burning velocity and explosion index of LPG-air and propane-air mixtures', *Fuel*, 87:39-57.
- Ilbas, M., Crayford, A.P., Yilmaz, I., Bowen, P.J. and Syred, N. (2006) 'Laminar-burning velocities of hydrogen-air and hydrogen-methane-air mixtures: An experimental study', *International Journal of Hydrogen Energy*, 34:1768-79
- Isidoro Martinez (2010) *Combustion kinetics*, Isidoro Martinez
- Jachimowski, Casimir J. (1984) 'Chemical kinetic reaction mechanism for the combustion of propane', *Combustion and Flame*, 55:213-24.
- Jomaas, G., Zheng, X. L., Zhu, D. L. and Law, C. K. (2005) 'Experimental determination of counterflow ignition temperatures and laminar flame speeds of C₂-C₃ hydrocarbons at atmospheric and elevated pressures', *Proceedings of the Combustion Institute*, 30:193-200.
- Kalghatgi, G.T. (1984) 'Lift-off heights and visible lengths of vertical turbulent jet diffusion flames in still air', *Combustion Science and Technology*, 41:17-29
- Karlovitz, B., Denniston, D.W. and Wells, F.E. (1951) 'Investigation of Turbulent Flames', *The Journal of Chemical Physics*, 19(5), pp. 541-7.
- Kassel, L.S. (1937) 'The mechanism of the combustion of hydrogen', *Universal Oil Products Company, Chicago, Illinois*

- Kassel, L.S. and Storch, H.H. (1935) *J. Am. Chem. Soc.* 57,672
- Kaufmann, D. and Roth, P. (1990) 'Numerical Simulation of One-dimensional Laminar Flames Propagating into Reacting Premixed Gases', *Combustion and Flame*, 80:385-94.
- Kee, R.J., Grcar, J.F., Smooke, M.D. and Miller, J.A. (1985) 'A FORTRAN program for modeling steady laminar one-dimensional premixed flames;', Sandia National Laboratories report, SAND 85-8240
- Kee, R.J., Grcar, J.F., smoke, M.D., Miller, J.A. and Meeks, E. (1998) 'PREMIX: A Fortran Program for Modelling Steady Laminar One-Dimensional Premixed Flames' Reaction Design, 11436 Sorrento Valley Road, San Diego, CA 92121.
- Kido, H., Huang, S., Tanoue, K., and Nitta, T. (1994) 'Improving the combustion performance of lean hydrocarbon mixtures by hydrogen addition', *JSAE Review*, 15:165-170.
- Konnov, A.A., Dyakov, I.V. and Ruyck, J.D. (2003) 'Measurement of Adiabatic burning velocity in ethane-oxygen-nitrogen and in ethane-oxygen-argon mixtures', *Experimental Thermal and Fluid Science*, 27(4):379-384
- Kreutz, T., Williams, R., Consonni, S. and Chiesa, P. (2005) 'Co-production of hydrogen, electricity and CO₂ from coal with commercially ready technology. Part B: economic analysis', *International Hydrogen Energy*, 30:769-84
- Kumar, Praveen and Meyer, Terrence R. (2013) 'Experimental and modelling study of chemical kinetics mechanisms for H₂-NH₃-air mixture in laminar premixed jet flames', *Fuel*, 108:166-176.
- Kunioshi, N. and Fukutani, S. (1992) 'Fuel mixing effects on propagation of premixed flames. II. Hydrogen + methane flames', *Bull Chem Soc Japan*, 65:2573-2577
- Kuo, K.K. and Acharya, R. (2012) *Fundamentals of turbulent and multiphase combustion*, John Wiley & Sons, Inc., Hoboken, New Jersey, p.296.
- Kuo, Kenneth K. (2005) *Principles of Combustion*, second edition, John Wiley & Sons, Inc., Canada, p. 484-5
- Kwon, O.C. and Faeth, G.M. (2001) 'Flame stretch interactions of premixed hydrogen-fueled flames: measurements and predictions' *Combustion and Flame*, 124(4):590-610
- Kwon, S., Tseng, L.L. and Faeth, G.M. (1992) *Combustion and Flame*, 90:230-246
- Lamoureux, N., Djebaili-Chaumeix, N. and Paillard C.E. (2003) 'Laminar flame velocity determination for H₂-air-He-CO₂ mixture using bomb method', *Experimental Thermal and Fluid Science*, 27:385-93

- Law, C.K. 'Compilation of experimental data on laminar burning velocities', in Peters, N. and Rogg, B. (ed.) (1993) *Reduced Kinetic Mechanism for Applications in Combustion Systems*, p15-26, Berlin: Springer-Verlag
- Law, C.K. (2006) *Combustion Physics*, Cambridge University Press, New York
- Lee, J.H., Lee, S.I. and Kwon, O.C. (2010) 'Effects of ammonia substitution on hydrogen/air flame propagation and emissions', *International Journal of Hydrogen Energy*, 35(20):11332-341
- Levenspiel, O. (1999) *Chemical Reaction Engineering*, 3rd edition, pp. 1-4, 13-32, USA: John Wiley & Sons, Inc.
- Levy, A. and Weinberg, F.J. (1959) 'Optical flame structure studies: some conclusions concerning the propagation of flat flames', *Seventh (International) Symposium on Combustion*, pp. 296-3-3, Butterworths, London
- Lewis, B. and von Elbe, G. (1951) 'Combustion, Flames and Explosions of Gases', Academic Press Inc., New York.
- Lewis, B. and von Elbe, G. (1961) 'Combustion, Flames and Explosions of Gases', 2nd edition, Chapter V, Academic Press, New York.
- Li J., Zhao, Y., Kazakov, A. and Dryer, F.L. (2004) 'An updated comprehensive kinetic model of hydrogen combustion', *International Journal of Chemical Kinetics*, Vol. 36 pp. 566-575.
- Liao, S. Y., Jiang, D. M., Huang, Z. H., Shen, W. D., Yuan, C., and Cheng, Q. (2007) 'Laminar burning velocities for mixtures of methanol and air at elevated temperatures', *Energy Conversion and Management*, 48:857-863.
- Liu, D.D.S. and MacFarlane, R. (1983) 'Laminar burning velocities of hydrogen-air and hydrogen-air-steam flames', *Combustion and Flame*, 49:59-71.
- Matveev, V.G. (2001) 'Reduction of the combustion mechanism of hydrogen', *Combustion, Explosion, and Shock Waves*, Vol. 37, NO.1, pp. 1-3.
- Markstein, G.H. 'Non-steady Flame propagation', Pergamon, New York, 1964, p.22.
- Meng, Ming. and Niu, Dongxiao. (2011) 'Modeling CO₂ emission from fossil fuel combustion using the logistic equation', *Energy*, 36:3355-59
- Metghalchi, M. and Keck, J.C. (1980) 'Laminar burning velocity of propane-air mixtures at high temperature and pressure', *Combustion and Flame*, 38:143-54
- Methling, T., Armbrust, N., Haitz, T., Speidel, M., Poboss, N., Braun-Unkhoff, M., Dieter, H., Kempter-Regel, B., Kraaij, G., Schliessman, U., Sterr, Y., Worner, A., Hirth, T., Riedel, U. and Scheffknecht, G. (2014) 'Power generation based on biomass by combined fermentation and gasification- A new concept derived from experiments and modeling' *Bioresource Technology*, 169:510-17.

- Miake-Lye, R. C., and Hammer, J. A. (1989) 'Lifted turbulent jet flames: A stability criterion based on the jet large-scale structure', Symposium (International) on Combustion, 22:817-824.
- Milton, B.E., Keck, J.C. (1984) 'Laminar burning velocity in stoichiometric hydrogen and hydrogen-hydrocarbon gas mixtures', Combustion and Flame, 49:59-71
- Mueller, M.A., Yetter, R.A. and Dryer, F.L. (1999), International Journal of Chemical Kinetics, 31:113-125
- Namazian, M., Kelly, J. and Schefer, R.W. (1988) 'Near field instantaneous flame and fuel concentration structures', 22nd (International) Symposium on Combustion.
- Nicoletti Gi, Alitto G, Anile F. Il Controllo della CO₂: Misure e Strategie. In: Proceedings of Italian conference ATI, L'Aquila (ITALY); 2009.
- Nicoletti Giovanni., Arcuri, Natale., Nicoletti, Gerardo. and Bruno. Roberto., (2014) 'A technical and environmental comparison between hydrogen and some fossil fuels', Energy Conversion and Management, 89:205-213
- O'Donovan, K.H. and Rallis, C.J.A. (1959) 'Modified analysis for the determination of the burning velocity of a gas mixture in a spherical constant volume combustion vessel', Combustion and Flame, 5(2):201-214
- Olaleye, Akeem K., Adedayo. Kunle J., Wu, Chunfei., Nahil, Mohamad A., Wang, Meihong and Williams, Paul T. (2014) 'Experimental study, dynamic modelling, validation and analysis of hydrogen production from biomass pyrolysis/gasification of biomass in a two-stage fixed bed reaction system' Fuel, 137:364-74.
- Pantano, C. (2004) 'Direct simulation of non-premixed flame extinction in a methane-air jet with reduced chemistry', J. Fluid Mech. 514:231-70
- Pareja, J., Burbano, Hugo J. and Ogami, Y. (2010) 'Measurements of the laminar burning velocity of hydrogen-air premixed flames', International Journal of Hydrogen Energy, 35:1812-18
- Perry, R. H., and Green, D.W. (2008) Perry's Chemical Engineers' Handbook, (8th Edition). McGraw-Hill.
- Peters, N. (1985) 'Numerical and asymptotic analysis of systematically reduced reaction schemes for hydrocarbon flames', Lecture Notes in Physics, 241:90-109
- Peters, N. (1986) 'Laminar flame concepts in turbulent combustion', Symposium (International) on Combustion, 21:1231-1250
- Peters, N. and Williams, F.A. (1983) 'Lift-off characteristics of turbulent jet diffusion flames', J. Am. Inst. Aeronaut. Astronaut, 21(3):423-429. Research

- Powling, J. (1961) 'The flat flame burner', *Experimental Methods in Combustion* (Ed. Surugue, J.), Section 2.2.1, AGARD, Pergamon Press, London.
- Qin, X., Kobayashi, H. and Niioka, T. (2000) 'Laminar burning velocity of hydrogen-air premixed flames at elevated pressure', *Exp Thermal Fluid Sci*, 12(1-3):58-63
- Qin, Z., Lissianski, V.V., Yang, H., Gardiner, W.C., Davis, S.G. and Wang, H. (2000) 'Combustion chemistry of propane: A case study of detailed reaction mechanism optimisation', *Proceedings of the Combustion Institute*, 28:1663-9
- Raezer, S.D. and Olsen, H.L. (1962) 'Measurement of laminar flame speeds of ethylene-air and propane-air mixtures by the double kernel method', *Combustion and Flame*, 6:227-232
- Rallis, C.J. and Tremeer, G.E.B. (1963) 'Equations for the determination of burning velocity in a spherical constant volume vessel', *Combustion and Flame*, 7(1):51-61
- Rallis, C.J., Garforth, A.M. and Stenz, J.A. (1965) 'Laminar burning velocity of acetylene/air mixtures by constant volume method: dependence on mixture composition, pressure and temperature', *Combustion and Flame*, 9:345-356
- Rallis, C.J. and Garforth, A.M. (1980) 'The Determination of Laminar Burning Velocity', *Prog. Energy Combustion. Sci.*, Vol. 6, p.302-329
- Razus, D., Brinzea, V., Mitu, M. and Oancea, D. (2010) 'Burning velocity of liquefied petroleum gas (LPG)-air mixtures in the presence of exhaust gas', *Energy Fuels*, 24 (3):1487-94, DOI: 10.1021/ef901209q
- Refael, S. and Sher, E. (1989) 'Reaction kinetics of hydrogen-enriched methane-air and propane-air flames', *Combust Flame*, 78, pp. 326-338
- REN21, (2014) 'Renewables 2014 global status report', REN21 Secretariat, Paris, France
- Report Kyoto Protocol: Status of Ratification, United Nations Framework Convention on Climate Change; January 2009.
- Santoro, R.J., Dryer, F., Ju, Y., Burke, M. and Santner, J. (2010) 'An experimental and chemical kinetics study of combustion of syngas and high hydrogen content fuels', U.S. Department of Energy, National Energy Technology Laboratory, FY10 Advanced Turbines Peer Review.
- Savas, O. and Gollahalli, S.R. (1986) *AIAA J.* 24:1137
- Schefer, R.W. (2003) 'Hydrogen enrichment for improved lean flame stability', *International Journal of Hydrogen Energy*, 28:P1131-41
- Schefer, R.W., Namazian, M. and Kelly, J. (1988) 'Structural characteristics of lifted turbulent-jet flames', 22nd Symposium (International) on Combustion, The Combustion Institute, pp. 833-842

- Scholefield, D.A. and Garside, J.E. (1949) Third Symposium on Combustion, Flame, and Explosion Phenomena, Williams and Willkins, p.102
- Scholte, T.G. and Vaags, P.B. (1959) *Combust. Flame*, 3:495.
- Semenov, N. N. (1935) *Chemical Kinetics and Chain Reactions*, Oxford University Press, Oxford.
- Serrano, C., Hernández, J. J., Mandilas, C., Sheppard, C. G. W., and Woolley, R. (2008) 'Laminar burning behaviour of biomass gasification-derived producer gas', *International Journal of Hydrogen Energy*, 33:851-862.
- Sher, E. and Refael, S. (1988) 'A simplified reaction scheme for the combustion of hydrogen enriched methane/air flame', *Combust Sci Technol*, 59, pp. 371-389.
- Silva, Aline Lima da., and Muller, Iduvirges Lourdes. (2011) 'Hydrogen production by sorption enhanced steam reforming of oxygenated hydrocarbons (ethanol, glycerol, n-butanol and methanol) thermodynamic modelling' *International Journal of Hydrogen Energy*, 36:2057-75.
- Smooke, Mitchell D. (2013) 'The computation of laminar flames', *Proceedings of the Combustion Institute*, 34(1):65-98.
- Spalding, D.B. (1956) 'The theory of flame phenomena with a chain reaction' *Phil. Trans. R. Soc. Lond. A*, 249 (957), pp. 1–25
- Stiegel, G.J. and Ramezan, M. (2006) 'Hydrogen from coal gasification: an economical pathway to a sustainable energy future' *International Coal Geol*, 65:173-90
- Sun, C.J., Sung, C.J., He, L. and Law, C.K. (1999) 'Dynamics of Weakly Stretched Flames: Quantitative Description and Extraction of Global Flame Parameters', *Combustion and Flame*, 118, 108.
- Tang, C., Huang, Z., Jin, C., He, J., Wang, J., Wang, X., and Miao, H. (2008) 'Laminar burning velocities and combustion characteristics of propane-hydrogen-air premixed flames', *International Journal of Hydrogen Energy*, 33:4906-4914.
- Titova, N. S., Kuleshov, P. S. and Starik, A. M. (2010) 'Kinetic mechanism of propane ignition and combustion in air', *Combustion, Explosion, and Shock Waves*, Vol. 47, No. 3, pp. 249-64
- Tripathi, A., Chandra, H. and Agrawal, M. (2010) 'Effect of mixture constituents on the laminar burning velocity of LPG-CO₂-air mixtures', *ARPN Journal of Engineering and Applied Sciences*, Vol. 5 No. 3, ISSN 1819-6608
- Tse, S.D., Zhu, D.L. and Law G.K. (2000) 'Morphology and burning rates of expanding spherical flames in H₂/O₂/inert mixtures up to 60 atmospheres' *Proceedings of the Combustion Institute*, 28:1793-1800

- Ulinski, M., Moore, P., Elia, M. and Metghalchi, M. (1998) 'Laminar burning velocity of methane-air-diluent mixtures', Proceedings of the ASME Internal Combustion Engine Division, Port Lauderdale, Florida, ICE-Vol 30-2
- Uykur, C., Henshaw, P. F., Ting, D. S. K., and Barron, R. M. (2001) 'Effects of addition of electrolysis products on methane/air premixed laminar combustion', International Journal of Hydrogen Energy, 26:265-273.
- Vanquickenborne, L. and van Tiggelen, A. (1966) 'The stabilization mechanism of lifted diffusion flames', Combustion and Flame, 10:59-69
- Van Oostendorp, D.L. and Levinsky, H.B. (1990) 'The effects of fuel and non-fuel gases on the laminar burning velocity of methane-air flames', Journal of the Institute of Energy, 63:160-6.
- Von Elbe, G. and Lewis, B. (1937) J. Am. Chem. Soc. 59, 656
- Warnatz, J. (1985) 'Chemistry of high temperature combustion of alkanes up to octane', Symposium (International) on Combustion, 20, 845-56
- Waston, K.A., Lyond, K.M., Donbar, J.M. and Carter, C.D. (1999) 'Scalar and velocity field measurements in a lifted CH₄-air diffusion flame', Combustion and Flame, 117(1-2):257-71
- Weimer, T., (1997) 'Comparison of CO₂ sources for fuel synthesis', Fuel Energy, 38, p.118
- Westbrook, C.K., Creighton, I., Lund, C. and Dryer, F.L. (1977) J. Phys. Chem. 81, 2542
- Westbrook, C. K. (2000) 'Chemical kinetics of hydrocarbon ignition in practical combustion systems', Proceedings of the Combustion Institute, 28:1563-77
- Williams, F. and Grcar, J.F. (2009) 'A hypothetical burning-velocity formula for very lean hydrogen-air mixtures', Proceedings of the Combustion Institute, 32:1351-57
- Wohl, K., Kapp, N.M. and Gazley, C. (1949) Third Symposium on Combustion, Flame, and Explosion Phenomena, Williams and Wilkins, p.3
- Wu, K.C. and Law C.K. (1985) 'On the determination of laminar flame speeds from stretched flames' Symposium (International) on Combustion, 20(1):1941-49.
- Wu, Y., Al-Rahbi, I. S., Lu, Y., and Kalghatgi, G. T. (2007) 'The stability of turbulent hydrogen jet flames with carbon dioxide and propane addition', Fuel, 86:1840-1848.
- Wu, Y., Lu, Y., Al-Rahbi, I.S. and Kalghatgi, G.T. (2009) 'prediction of the liftoff, blowout and blowoff stability limits of pure hydrogen and hydrogen/hydrocarbon mixture jet flames', International Journal of Hydrogen Energy, 34:5940-5

Yeh, Fang-YU., Hu, Jin-Li. and Lin, Cheng-Hsun. (2012) 'Asymmetric impacts of international energy shocks on macroeconomic activities', Energy Policy, 44:10-22

Younglove, B.A. and Ely, J.F. (1987) 'Thermophysical Properties of Fluids.II. Methane, Ethane, Propane, Isobutane and Normal Butane', J.Phys.Chem.Ref.Data, Vol.16, NO.4.

Yu, G., Law, C. K., and Wu, C. K. (1986) 'Laminar flame speeds of hydrocarbon + air mixtures with hydrogen addition', Combustion and Flame, 63:339-347

Appendix A: Warnatz and Heghes (2006) C₁-C₃ Hydrocarbon Oxidation

Mechanism

ELEMENTS

O C H N

END

SPECIES

O₂ OH O H H₂ HO₂ H₂O H₂O₂ HCCO C CH CO CO₂ CHO CH₂O CH₂

H₂C C₂H₂ CH₃ C₂H₄ CH₄ CH₂OH CH₃O

CH₃O₂ CH₃CO C₂H₆ CH₃OH CH₃O₂H N₂

C₂H CH₂CO C₂H₃ CH₂CHO CH₃CHO C₂H₅ C₄H₂ C₃H₄ C₂H₅O CH₃CHOH

CH₂CH₂OH C₂H₅OH C₃H₂ C₃H₃

C₃H₄ C₃H₅ C₃H₆ C₃H₇ C₃H₈ H₇C₃

END

REACTIONS

Reactions	A	n	E _a (cal/mol)
1. O ₂ + H <=> OH + O	2.06E+14	-0.097	15084
2. H ₂ + O <=> OH + H	3.82E+12	0.0	7982.4
DUPLICATE			
3. H ₂ + O <=> OH + H	1.02E+15	0.0	19255.2
DUPLICATE			
4. H ₂ + OH <=> H ₂ O + H	2.17E+8	1.52	3472.8
5. OH + OH <=> H ₂ O + O	3.35E+4	2.42	-1934.4
6. H + H + M <=> H ₂ + M	1.02E+17	-0.6	0.0
H ₂ /1/H ₂ O/6.5/O ₂ /0.4/N ₂ /0.4/CO/0.75/CO ₂ /1.5/CH ₄ /3.0/AR/0.35/			
7. O + O + M <=> O ₂ + M	5.40E+13	0.0	-1776
H ₂ /1/H ₂ O/6.5/O ₂ /0.4/N ₂ /0.4/CO/0.75/CO ₂ /1.5/CH ₄ /3.0/AR/0.35/			
8. H + OH + M <=> H ₂ O + M	5.56E+22	-2.0	0.0
H ₂ /1/H ₂ O/2.5/O ₂ /0.4/N ₂ /0.4/CO/0.75/CO ₂ /1.5/CH ₄ /3.0/AR/0.15/			
9. H + O ₂ + M <=> HO ₂ + M	1.30E+12	0.56	0.0
DUPLICATE			
H ₂ /1/H ₂ O/6.5/O ₂ /0.4/N ₂ /0.4/CO/0.75/CO ₂ /1.5/CH ₄ /3.0/AR/0.29/			
10. H + O ₂ + M <=> HO ₂ + M	1.75E+17	0.0	0.0
DUPLICATE			
H ₂ /1/H ₂ O/6.5/O ₂ /0.4/N ₂ /0.4/CO/0.75/CO ₂ /1.5/CH ₄ /3.0/AR/0.29/			
11. HO ₂ + H <=> OH + OH	4.46E+14	0.0	1396.8
12. HO ₂ + H <=> H ₂ + O ₂	1.05E+14	0.0	2054.4
13. HO ₂ + H <=> H ₂ O + O	1.44E+12	0.0	0.0
14. HO ₂ + O <=> OH + O ₂	1.63E+13	0.0	-446.4
15. HO ₂ + OH <=> H ₂ O + O ₂	9.28E+15	0.0	17580
16. HO ₂ + HO ₂ <=> H ₂ O ₂ + O ₂	4.22E+14	0.0	12033.6
DUPLICATE			
17. HO ₂ + HO ₂ <=> H ₂ O ₂ + O ₂	1.32E+11	0.0	-1636.8
DUPLICATE			
18. OH + OH + M <=> H ₂ O ₂ + M	1.57E+13	0.0	0.0
H ₂ /1/H ₂ O/6.5/O ₂ /0.4/N ₂ /0.4/CO/0.75/CO ₂ /1.5/CH ₄ /3.0/AR/0.35/			
19. H ₂ O ₂ + H <=> H ₂ + HO ₂	1.69E+12	0.0	3770.4
20. H ₂ O ₂ + H <=> H ₂ O + OH	1.02E+13	0.0	3592.8
21. H ₂ O ₂ + O <=> OH + HO ₂	4.22E+11	0.0	3991.2
22. H ₂ O ₂ + O <=> H ₂ O + O ₂	4.22E+11	0.0	3991.2

Reactions	A	n	E _a (cal/mol)
23. H2O2 + OH <=>H2O + HO2 DUPLICATE	1.64E+18	0.0	29532.0
24. H2O2 + OH <=>H2O + HO2 DUPLICATE	1.92E+12	0.0	429.6
25. CH + H <=>C + H2	1.20E+14	0.0	0.0
26. C + O2 <=>CO + O	6.02E+13	0.0	638.4
27. CH + O <=>CO + H	4.00E+13	0.0	0.0
28. CH + OH <=>CHO + H	3.00E+13	0.0	0.0
29. CH + O2 <=>CHO + O	1.69E+13	0.0	0.0
30. CH + CO <=>HCCO	2.80E+11	0.0	-1704.0
31. CH + CO2 <=>CHO + CO	6.38E+7	1.51	-717.6
32. CH + H2O <=>CH2O + H	4.58E+16	-1.42	0.0
33. CH + H2O <=>H2C + OH	4.58E+16	-1.42	0.0
34. CHO + M <=>CO + H + M H2/1/H2O/6.5/O2/0.4/N2/0.4/CO/0.75/CO2/1.5/CH4/3.0/AR/0.35/	1.14E+14	0.0	15604.8
35. CHO + H <=>CO + H2	9.03E+13	0.0	0.0
36. CHO + O <=>CO + OH	3.01E+13	0.0	0.0
37. CHO + O <=>CO2 + H	3.01E+13	0.0	0.0
38. CHO + OH <=>CO + H2O	1.08E+14	0.0	0.0
39. CHO + O2 <=>CO + HO2	7.59E+12	0.0	408.0
40. CHO + CHO <=>CH2O + CO	3.00E+13	0.0	0.0
41. H2C + H <=>CH + H2	1.20E+14	0.0	0.0
42. H2C + O => CO + H + H	1.23E+14	0.0	537.6
43. H2C + O <=>CO + H2	8.19E+13	0.0	537.6
44. H2C + O2 <=>CO + OH + H	1.81E+12	0.0	0.0
45. H2C + O2 <=>CO2 + H2	1.81E+12	0.0	0.0
46. H2C + H2C <=>C2H2 + H2	1.81E+14	0.0	11971.2
47. H2C + H2C <=>C2H2 + H + H	1.63E+15	0.0	11971.2
48. H2C + CH3 <=>C2H4 + H	7.23E+13	0.0	0.0
49. CH2 + M <=>H2C + M H2/1/H2O/6.5/O2/0.4/N2/0.4/CO/0.75/CO2/1.5/CH4/3.0/AR/0.35/	6.02E+12	0.0	0.0
50. CH2 + H2 <=>CH3 + H	1.26E+16	-0.56	15960.0
51. CH2 + O2 <=>CO + OH + H	3.10E+13	0.0	0.0
52. CH2O + M <=>CHO + H + M H2/1/H2O/6.5/O2/0.4/N2/0.4/CO/0.75/CO2/1.5/CH4/3.0/AR/0.35/	4.87E+15	0.0	75924.0
53. CH2O + M <=>CO + H2 + M H2/1/H2O/6.5/O2/0.4/N2/0.4/CO/0.75/CO2/1.5/CH4/3.0/AR/0.35/	2.83E+15	0.0	64070.4
54. CH2O + H <=>CHO + H2	4.10E+8	1.47	2455.2
55. CH2O + O <=>CHO + OH	4.16E+11	0.57	2774.4
56. CH2O + OH <=>CHO + H2O	1.39E+13	0.0	607.2
57. CH2O + HO2 <=>CHO + H2O2	4.10E+4	2.5	10255.2
58. CH2O + O2 <=>CHO + HO2	2.44E+5	2.5	36614.4
59. CH2O + CH3 <=>CHO + CH4	3.19E+1	3.36	4329.6
60. CH2OH + M <=>CH2O + H + M H2/1/H2O/6.5/O2/0.4/N2/0.4/CO/0.75/CO2/1.5/CH4/3.0/AR/0.35/	2.80E+14	-0.73	32954.4
61. CH2OH + H <=>CH2O + H2	2.44E+13	0.0	0.0
62. CH2OH + H <=>CH3 + OH	1.05E+13	0.0	0.0
63. CH2OH + O2 <=>CH2O + HO2 DUPLICATE	2.89E+16	-1.5	0.0
64. CH2OH + O2 <=>CH2O + HO2 DUPLICATE	7.23E+13	0.0	3751.2
65. CH3 + M <=>H2C + H + M H2/1/H2O/6.5/O2/0.4/N2/0.4/CO/0.75/CO2/1.5/CH4/3.0/AR/0.35/	2.92E+16	0.0	90960.0

Reactions	A	n	E _a (cal/mol)
66. CH ₃ + M <=>CH + H ₂ + M H2/1/H2O/6.5/O2/0.4/N2/0.4/CO/0.75/CO2/1.5/CH4/3.0/AR/0.35/	1.89E+16	0.0	85401.6
67. CH ₃ + O <=>CH ₂ O + H	6.74E+13	0.0	0.0
68. CH ₃ + OH => CH ₃ O + H	1.20E+10	0.0	13946.4
69. CH ₃ + OH <=>CH ₂ + H ₂ O	3.00E+13	0.0	2793.6
70. CH ₃ + OH +M <=>CH ₃ OH+M H2/1/H2O/6.5/O2/0.4/N2/0.4/CO/0.75/CO2/1.5/CH4/3.0/AR/0.35/	4.34E+15	-0.79	0.0
71. CH ₃ + HO ₂ <=>CH ₃ O + OH	1.60E+13	0.0	0.0
72. CH ₃ + O ₂ <=>CH ₂ O + OH	6.86E+1	2.86	9808.8
73. CH ₃ + O ₂ => O + CH ₃ O	6.08E+7	1.54	27945.6
74. CH ₃ + O ₂ +M <=>CH ₃ O ₂ + M H2/1/H2O/6.5/O2/0.4/N2/0.4/CO/0.75/CO2/1.5/CH4/3.0/AR/0.35/	7.83E+8	1.2	0.0
75. CH ₃ + CO +M <=>CH ₃ CO + M H2/1/H2O/6.5/O2/0.4/N2/0.4/CO/0.75/CO2/1.5/CH4/3.0/AR/0.35/	5.06E+11	0.0	6904.8
76. CH ₃ + CH ₂ <=>C ₂ H ₄ + H	7.23E+13	0.0	0.0
77. CH ₃ + CH ₃ +M <=>C ₂ H ₆ + M 3.61E+13 0.0 0.0 H2/1/H2O/6.5/O2/0.4/N2/0.4/CO/0.75/CO2/1.5/CH4/3.0/AR/0.35/	3.61E+13	0.0	0.0
78. CH ₃ O + M <=>CH ₂ O + H + M H2/1/H2O/6.5/O2/0.4/N2/0.4/CO/0.75/CO2/1.5/CH4/3.0/AR/0.35/	6.80E+13	0.0	26277.6
79. CH ₃ O + H => CH ₃ + OH	1.63E+13	0.0	597.6
80. CH ₃ O + H <=>CH ₂ O + H ₂	3.79E+13	0.0	597.6
81. CH ₃ O + O => O ₂ + CH ₃	1.13E+13	0.0	0.0
82. CH ₃ O + O <=>OH + CH ₂ O	3.76E+12	0.0	0.0
83. CH ₃ O + OH <=>CH ₂ O + H ₂ O	1.81E+13	0.0	0.0
84. CH ₃ O + O ₂ <=>CH ₂ O + HO ₂	2.17E+10	0.0	1752.0
85. CH ₃ O + CH ₂ O <=>CH ₃ OH + CHO	1.15E+11	0.0	1248.0
86. CH ₃ O ₂ + HO ₂ <=>CH ₃ O ₂ H + O ₂	2.28E+11	0.0	-1497.6
87. CH ₃ O ₂ + CH ₃ <=>CH ₃ O + CH ₃ O	1.50E+13	0.0	-1200.0
88. CH ₃ O ₂ + CH ₃ O ₂ => CH ₂ O + CH ₃ OH + O ₂	3.43E+10	0.0	-777.6
89. CH ₃ O ₂ + CH ₃ O ₂ => CH ₃ O + CH ₃ O + O ₂	2.29E+10	0.0	-777.6
90. CH ₃ O ₂ + H ₂ O ₂ <=>CH ₃ O ₂ H + HO ₂	2.40E+12	0.0	10032.0
91. CH ₃ O ₂ + CH ₂ O <=>CH ₃ O ₂ H + CHO	1.30E+11	0.0	9048.0
92. CH ₃ O ₂ + CH ₄ <=>CH ₃ O ₂ H + CH ₃	1.81E+11	0.0	18672.0
93. CH ₃ O ₂ + CH ₃ OH <=>CH ₃ O ₂ H + CH ₂ OH	1.81E+11	0.0	13848.0
94. CH ₄ + M <=>CH ₃ + H + M H2/1/H2O/6.5/O2/0.4/N2/0.4/CO/0.75/CO2/1.5/CH4/0.7/AR/0.35/	2.46E+16	0.0	105360.0
95. CH ₄ + H <=>H ₂ + CH ₃	6.14E+5	2.5	9628.8
96. CH ₄ + O <=>OH + CH ₃	4.40E+5	2.5	6604.8
97. CH ₄ + OH <=>H ₂ O + CH ₃	1.37E+6	2.18	2692.8
98. CH ₄ + HO ₂ <=>H ₂ O ₂ + CH ₃	4.70E+4	2.5	21091.2
99. CH ₄ + O ₂ <=>CH ₃ + HO ₂	4.88E+5	2.5	52617.6
100. CH ₄ + CH <=>C ₂ H ₄ + H	1.32E+16	-0.94	57.6
101. CH ₄ + H ₂ C <=>CH ₃ +CH ₃	8.40E+12	0.0	-499.2
102. CH ₃ OH + H <=>CH ₂ OH + H ₂	2.75E+9	1.24	4509.6
103. CH ₃ OH + H <=>CH ₃ O + H ₂	6.87E+8	1.24	4509.6
104. CH ₃ OH + O <=>CH ₂ OH + OH	1.98E+13	0.0	5328.0
105. CH ₃ OH + O <=>CH ₃ O + OH	4.94E+12	0.0	5328.0
106. CH ₃ OH + OH <=>CH ₂ OH + H ₂ O	5.27E+6	1.92	-288.0
107. CH ₃ OH + OH <=>CH ₃ O + H ₂ O	9.30E+5	1.92	-288.0
108. CH ₃ OH + HO ₂ <=>CH ₂ OH + H ₂ O ₂	6.20E+12	0.0	19464.0
109. CH ₃ OH + O ₂ <=>HO ₂ + CH ₂ OH	2.05E+13	0.0	45384.0
110. CH ₃ OH + CH ₃ <=>CH ₄ + CH ₂ OH	9.94E+0	3.45	8020.8
111. CH ₃ OH + CH ₃ <=>CH ₄ + CH ₃ O	2.02E+1	3.45	8020.8
112. CH ₃ OH + CH ₃ O <=>CH ₂ OH + CH ₃ OH	1.50E+12	0.0	7032.0

Reactions	A	n	E _a (cal/mol)
113. CH ₃ OH + CH ₂ O => CH ₃ O + CH ₃ O	1.53E+12	0.0	79968.0
114. CH ₃ O ₂ H <=>CH ₃ O + OH	6.00E+14	0.0	42504.0
115. CH ₃ O ₂ H + O <=>OH + CH ₃ O ₂	2.47E+13	0.0	4788.0
116. CH ₃ O ₂ H + OH <=>H ₂ O + CH ₃ O ₂	1.08E+12	0.0	-439.2
117. CO + O +M <=>CO ₂ + M H ₂ /1/H ₂ O/6.5/O ₂ /0.4/N ₂ /0.4/CO/0.75/CO ₂ /1.5/CH ₄ /3.0/AR/0.35/	1.54E+15	0.0	3014.4
118. CO + OH <=>CO ₂ + H DUPLICATE	1.00E+13	0.0	16063.2
119. CO + OH <=>CO ₂ + H DUPLICATE	9.03E+11	0.0	4588.8
120. CO + OH <=>CO ₂ + H DUPLICATE	1.01E+11	0.0	60
121. CO + HO ₂ <=>CO ₂ + OH	1.50E+14	0.0	23688.0
122. CO + O ₂ <=>CO ₂ + O	2.50E+12	0.0	48000.0
123. C ₂ H + O <=>CO + CH	5.96E+13	0.0	0.0
124. C ₂ H + O ₂ <=>HCCO + O	3.25E+14	-0.35	0.0
125. C ₂ H + O ₂ <=>CO ₂ + CH	2.92E+15	-0.35	0.0
126. C ₂ H + CH ₄ <=>C ₂ H ₂ + CH ₃	2.17E+10	0.94	2.73
127. HCCO + H <=>H ₂ C + CO	1.06E+13	0.0	0.0
128. HCCO + O => CO + CO + H	1.53E+14	0.0	0.0
129. HCCO + H ₂ C <=>C ₂ H ₃ + CO	3.00E+13	0.0	0.0
130. C ₂ H ₂ + M<=>C ₂ H + H + M H ₂ /1/H ₂ O/6.5/O ₂ /0.4/N ₂ /0.4/CO/0.75/CO ₂ /1.5/CH ₄ /3.0/AR/0.35/	3.60E+16	0.0	446.0
131. C ₂ H ₂ + H <=>C ₂ H + H ₂	2.01E+9	1.64	126.79
132. C ₂ H ₂ + O <=>H ₂ C + CO	1.48E+8	1.4	9.23
133. C ₂ H ₂ + O <=>HCCO + H	9.40E+8	1.4	9.23
134. C ₂ H ₂ + OH <=>H ₂ O + C ₂ H	6.42E+14	0.0	56.54
135. C ₂ H ₂ + O ₂ <=>HCCO + OH	2.00E+8	1.5	126.0
136. C ₂ H ₂ + C ₂ H <=>C ₄ H ₂ + H	7.83E+13	0.0	0.0
137. CH ₂ CO + M <=>H ₂ C + CO + M H ₂ /1/H ₂ O/6.5/O ₂ /0.4/N ₂ /0.4/CO/0.75/CO ₂ /1.5/CH ₄ /3.0/AR/0.35/	1.00E+16	0.0	248.0
138. CH ₂ CO + H <=>CH ₃ + CO	3.25E+10	0.85	11.89
139. CH ₂ CO + O <=>CH ₂ O + CO	3.61E+11	0.0	5.65
140. CH ₂ CO + O => CHO + H + CO	1.81E+11	0.0	5.65
141. CH ₂ CO + O <=>CHO + CHO	1.81E+11	0.0	5.65
142. CH ₂ CO + OH <=>CH ₃ + CO ₂	6.24E+11	0.0	4.24
143. CH ₂ CO + OH <=>CH ₂ O + CHO	3.37E+10	0.0	4.24
144. C ₂ H ₃ (+ M) <=>C ₂ H ₂ + H (+ M) LOW / 3.24E+27 -3.4 149.82/ TROE/ 0.35 0.0 0.0 0.0/ H ₂ /1/H ₂ O/6.5/O ₂ /0.4/N ₂ /0.4/CO/0.75/CO ₂ /1.5/CH ₄ /3.0/AR/0.35/	7.80E+8	1.62	155.06
145. C ₂ H ₃ + H <=>C ₂ H ₂ + H ₂	4.22E+13	0.0	0.0
146. C ₂ H ₃ + O <=>C ₂ H ₂ + OH	3.01E+13	0.0	0.0
147. C ₂ H ₃ + O <=>CH ₃ + CO	3.01E+13	0.0	0.0
148. C ₂ H ₃ + O <=>CHO + H ₂ C	3.01E+13	0.0	0.0
149. C ₂ H ₃ + OH <=>C ₂ H ₂ + H ₂ O	5.00E+12	0.0	0.0
150. C ₂ H ₃ + O ₂ <=>CH ₂ O + CHO	7.71E+12	0.0	-1.0
151. C ₂ H ₃ + O ₂ <=>CH ₂ CHO + O	8.15E+12	0.0	-1.04
152. C ₂ H ₃ + O ₂ <=>C ₂ H ₂ + HO ₂	4.65E+11	0.0	-1.04
153. CH ₃ CO + H <=>CH ₂ CO + H ₂	2.00E+13	0.0	0.0
154. CH ₂ CHO + H <=>CH ₂ CO + H ₂	2.00E+13	0.0	0.0
155. C ₂ H ₄ + M <=>C ₂ H ₂ + H ₂ + M H ₂ /1/H ₂ O/6.5/O ₂ /0.4/N ₂ /0.4/CO/0.75/CO ₂ /1.5/CH ₄ /3.0/AR/0.35/	2.92E+17	1.0	327.49

Reactions	A	n	E _a (cal/mol)
156. C2H4 + M <=> C2H3 + H + M H2/1/H2O/6.5/O2/0.4/N2/0.4/CO/0.75/CO2/1.5/CH4/3.0/AR/0.35/	7.40E+17	0.0	404.06
157. C2H4 + H (+M) => C2H5 (+ M) LOW / 1.18E+19 0.0 3.2/ TROE/ 0.76 40.0 1025.0 0.0/ H2/1/H2O/6.5/O2/0.4/N2/0.4/CO/0.75/CO2/1.5/CH4/3.0/AR/0.35/	3.98E+9	1.28	5.4
158. C2H4 + H <=> C2H3 + H2	2.35E+2	3.62	47.14
159. C2H4 + O <=> CH2CHO + H	4.74E+6	1.88	0.76
160. C2H4 + O <=> CHO + CH3	8.13E+6	1.88	0.76
161. C2H4 + O <=> CH2CO + H2	6.77E+5	1.88	0.76
162. C2H4 + OH <=> C2H3 + H2O	6.48E+12	0.0	24.9
163. C2H4 + CH <=> C3H4 + H	1.32E+14	0.0	-1.44
164. C2H4 + CH2 <=> C3H6	7.24E+13	0.0	0.0
165. C2H4 + CH3 <=> C2H3 + CH4	6.02E+7	1.56	69.6
166. CH3CHO (+ M) <=> CH3 + CHO (+ M) LOW / 7.83E+17 0.0 342.0/ TROE/ 0.5 0.0 0.0 0.0/ H2/1/H2O/6.5/O2/0.4/N2/0.4/CO/0.75/CO2/1.5/CH4/3.0/AR/0.35/	2.10E+16	0.0	342.0
167. CH3CHO + H <=> CH3CO + H2	2.05E+9	1.16	10.06
168. CH3CHO + H <=> CH2CHO + H2	2.05E+9	1.16	10.06
169. CH3CHO + O <=> CH3CO + OH	5.26E+12	0.0	7.6
170. CH3CHO + O <=> CH2CHO + OH	5.84E+11	0.0	7.6
171. CH3CHO + OH <=> CH3CO + H2O	2.69E+8	1.35	-6.58
172. CH3CHO + OH <=> CH2CHO + H2O	2.02E+7	1.35	-6.58
173. CH3CHO + HO2 <=> CH3CO + H2O2	4.10E+4	2.5	42.69
174. CH3CHO + O2 <=> CH3CO + HO2	1.20E+5	2.5	157.14
175. CH3CHO + H2C <=> CH3CO + CH3	2.50E+12	0.0	15.9
176. CH3CHO + CH3 <=> CH3CO + CH4	3.49E-10	6.21	6.82
177. C2H5 (+ M) => C2H4 + H (+ M) LOW / 3.65E+18 0.0 139.68/ TROE/ 0.75 97.0 1379.0 0.0/ H2/1/H2O/6.5/O2/0.4/N2/0.4/CO/0.75/CO2/1.5/CH4/3.0/AR/0.35/	4.10E+13	0.0	166.8
178. C2H5 + H <=> CH3 + CH3	4.22E+13	0.0	0.0
179. C2H5 + O <=> CH3CHO + H	5.32E+13	0.0	0.0
180. C2H5 + O <=> CH2O + CH3	3.98E+13	0.0	0.0
181. C2H5 + O2 <=> C2H4 + HO2	2.41E+10	0.0	0.0
182. C2H5 + CH3 <=> C2H4 + CH4	9.03E+11	0.0	0.0
183. C2H5 + C2H5 <=> C2H4 + C2H6	1.40E+12	0.0	0.0
184. C2H5O <=> CH3CHO + H	2.00E+14	0.0	97.0
185. C2H5O <=> CH2O + CH3	8.00E+13	0.0	90.0
186. C2H5O + H <=> CH3CHO + H2	1.00E+14	0.0	0.0
187. C2H5O + O <=> CH3CHO + OH	1.21E+14	0.0	0.0
188. C2H5O + OH <=> CH3CHO + H2O	1.00E+14	0.0	0.0
189. C2H5O + O2 <=> CH3CHO + HO2	6.00E+10	0.0	7.0
190. CH3CHOH <=> CH3CHO + H	1.00E+14	0.0	105.0
191. CH3CHOH + H <=> CH3CHO + H2	3.00E+13	0.0	0.0
192. CH3CHOH + O <=> CH3CHO + OH	1.20E+14	0.0	0.0
193. CH3CHOH + OH <=> CH3CHO + H2O	1.51E+13	0.0	0.0
194. CH3CHOH + O2 <=> CH3CHO + HO2 DUPLICATE	8.43E+15	-1.2	0.0
195. CH3CHOH + O2 <=> CH3CHO + HO2 DUPLICATE	4.82E+14	0.0	20.1
196. CH2CH2OH <=> C2H4 + OH	1.00E+14	0.0	140.0
197. CH2CH2OH + H <=> CH3CHO + H2	5.00E+13	0.0	0.0

Reactions	A	n	E _a (cal/mol)
198. C2H5OH <=>CH3 + CH2OH	3.10E+15	0.0	337.2
199. C2H5OH <=>C2H5 + OH	5.00E+16	0.0	381.6
200. C2H5OH <=>C2H4 + H2O	1.00E+14	0.0	320.9
201. C2H5OH + H <=>CH3CHOH + H2	4.40E+12	0.0	19.1
202. C2H5OH + H <=>C2H5 + H2O	5.90E+11	0.0	14.4
203. C2H5OH + O <=>CH3CHOH + OH	5.42E+5	2.5	7.73
204. C2H5OH + O <=>C2H5O + OH	3.01E+4	2.5	7.73
205. C2H5OH + O <=>CH2CH2OH + OH	3.01E+4	2.5	7.73
206. C2H5OH + OH <=>CH3CHOH + H2O	2.14E+7	1.78	-3.53
207. C2H5OH + OH <=>C2H5O + H2O	9.03E+5	1.78	-3.53
208. C2H5OH + OH <=>CH2CH2OH + H2O	1.13E+6	1.78	-3.53
209. C2H5OH + HO2 <=>CH3CHOH + H2O2	6.30E+12	0.0	81.1
210. C2H5OH + CH3 <=>CH3CHOH + CH4	4.70E+11	0.0	40.57
211. C2H5OH + CH3 <=>CH2CH2OH + CH4	3.61E+10	0.0	39.91
212. C2H5OH + CH3 <=>C2H5O + CH4	9.03E+10	0.0	39.32
213. C2H5OH + CH3O <=>CH3CHOH + CH3OH	2.00E+11	0.0	29.3
214. C2H5OH + CH2O <=>C2H5O + CH3O	1.53E+12	0.0	333.2
215. C2H5OH + C2H5O <=>C2H5OH + CH3CHOH	2.00E+11	0.0	29.3
216. C2H6 + H <=>C2H5 + H2	9.82E+13	0.0	38.58
217. C2H6 + O <=>C2H5 + OH	1.00E+9	1.5	24.4
218. C2H6 + OH <=>C2H5 + H2O	9.15E+6	2.0	4.16
219. C2H6 + HO2 <=>C2H5 + H2O2	1.10E+5	2.5	70.5
220. C2H6 + O2 <=>C2H5 + HO2	7.29E+5	2.5	205.69
221. C2H6 + H2C <=>C2H5 + CH3	2.20E+13	0.0	36.3
222. C2H6 + CH3 <=>C2H5 + CH4	5.60E+10	0.0	39.41
DUPLICATE			
223. C2H6 + CH3 <=>C2H5 + CH4	8.43E+14	0.0	93.12
DUPLICATE			
224. C2H6 + CH <=>C2H4 + CH3	1.08E+14	0.0	-1.1
225. C3H2 + O2 <=>CHO + HCCO	1.00E+13	0.0	0.0
226. C3H3 + OH <=>C3H2 + H2O	2.00E+13	0.0	0.0
227. C3H3 + O => CO + C2H3	3.80E+13	0.0	0.0
228. C3H3 + O2 => HCCO + CH2O	6.00E+12	0.0	0.0
229. C3H4 + O <=>CH2O + C2H2	1.00E+12	0.0	0.0
230. C3H4 + O <=>CHO + C2H3	1.00E+12	0.0	0.0
231. C3H4 + OH <=>CH2O + C2H3	1.00E+12	0.0	0.0
232. C3H4 + OH <=>CHO + C2H4	1.00E+12	0.0	0.0
233. C3H4 + M <=>H + C3H3 + M	1.00E+17	0.0	293.0
H2/1/H2O/6.5/O2/0.4/N2/0.4/CO/0.75/CO2/1.5/CH4/3.0/AR/0.35/			
234. C3H4 + H <=>CH3 + C2H2	2.00E+13	0.0	10.0
235. C3H4 + H <=>H2 + C3H3	1.00E+12	0.0	6.3
236. C3H4 + C2H <=>C2H2 + C3H3	1.00E+13	0.0	0.0
237. C3H4 + CH3 <=>C3H3 + CH4	2.00E+12	0.0	32.2
238. C3H5 <=>C3H4 + H	3.98E+13	0.0	293.1
239. C3H5 + H <=>C3H4 + H2	1.81E+13	0.0	0.0
240. C3H5 + O2 <=>C3H4 + HO2	1.02E+12	0.0	94.78
241. C3H5 + OH <=>C3H4 + H2O	6.02E+12	0.0	0.0
242. C3H6 + O2 <=>C3H5 + HO2	1.90E+12	0.0	163.8
243. C3H5 + CH3 <=>C3H4 + CH4	3.61E+11	0.0	0.0
244. C3H5 + C3H5 <=>C3H6 + C3H4	6.02E+10	0.0	0.0
245. CH3 + C2H2 <=>C3H5	6.00E+11	0.0	32.4
246. C3H6 <=>C3H5 + H	1.00E+13	0.0	326.0
247. C3H6 <=>C2H3 + CH3	1.10E+21	-1.2	408.8
248. C3H6 + H <=>C3H5 + H2	5.00E+12	0.0	6.3

Reactions	A	n	E _a (cal/mol)
249. C3H6 + O <=>C2H4 + CH2O	5.90E+13	0.0	21.0
250. C3H6 + O <=>C2H5 + CHO	3.60E+12	0.0	0.0
251. C3H6 + O <=>CH3 + CH3CO	5.00E+12	0.0	2.5
252. C3H6 + OH <=>C2H5 + CH2O	7.90E+12	0.0	0.0
253. C3H6 + OH <=>CH3 + CH3CHO	5.10E+12	0.0	0.0
254. C3H6 + OH <=>C3H5 + H2O	4.00E+12	0.0	0.0
255. C3H6 + CH3 <=>CH4 + C3H5	8.91E+10	0.0	35.6
256. C3H6 + C2H5 <=>C3H5 + C2H6	1.00E+11	0.0	38.5
257. C3H7 <=>CH3 + C2H4	9.60E+13	0.0	129.8
258. C3H7 <=>H + C3H6	1.25E+14	0.0	154.9
259. C3H7 + O2 <=>C3H6 + HO2	1.00E+12	0.0	20.9
260. H7C3 <=>H + C3H6	6.30E+13	0.0	154.5
261. H7C3 <=>CH3 + C2H4	2.00E+10	0.0	123.5
262. H7C3 + O2 <=>C3H6 + HO2	1.99E+10	0.0	-10.72
263. C3H8 (+ M) <=>CH3 + C2H5 (+ M)	4.00E+23	-1.87	377.41
LOW / 2.24E+19 0.0 271.87/			
TROE/ 0.76 1946.0 38.0 0.0/			
H2/1/H2O/6.5/O2/0.4/N2/0.4/CO/0.75/CO2/1.5/CH4/3.0/AR/0.35/			
264. C3H8 + H <=>H2 + C3H7	1.30E+14	0.0	40.6
265. C3H8 + H <=>H2 + H7C3	1.00E+14	0.0	34.9
266. C3H8 + O <=>C3H7 + OH	3.00E+13	0.0	24.1
267. C3H8 + O <=>H7C3 + OH	2.60E+13	0.0	18.7
268. C3H8 + OH <=>C3H7 + H2O	3.70E+12	0.0	6.9
269. C3H8 + OH <=>H7C3 + H2O	2.80E+12	0.0	3.6
270. C3H8 + HO2 => C3H7 + H2O2	1.14E+13	0.0	81.2
271. C3H7 + H2O2 => C3H8 + HO2	2.33E+12	0.0	41.1
272. C3H8 + HO2 => H7C3 + H2O2	3.40E+12	0.0	71.2
273. H7C3 + H2O2 => C3H8 + HO2	4.16E+11	0.0	31.1
274. C3H8 + CH3 => CH4 + C3H7	4.00E+11	0.0	39.8
275. C3H7 + CH4 => CH3 + C3H8	3.12E+12	0.0	68.9
276. C3H8 + CH3 => CH4 + H7C3	1.30E+12	0.0	48.6
277. H7C3 + CH4 => CH3 + C3H8	1.01E+13	0.0	77.7
278. C3H8 + O2 => C3H7 + HO2	2.52E+13	0.0	205.2
279. C3H7 + HO2 => C3H8 + O2	2.08E+12	0.0	0.0
280. C3H8 + O2 => H7C3 + HO2	2.00E+13	0.0	199.3
281. H7C3 + HO2 => C3H8 + O2	2.08E+12	0.0	0.0
282. C3H8 + CH3O => C3H7 + CH3OH	3.00E+11	0.0	29.3
283. C3H7 + CH3OH => C3H8 + CH3O	1.22E+10	0.0	38.5
284. C3H8 + CH3O => H7C3 + CH3OH	3.00E+11	0.0	29.3
285. H7C3 + CH3OH => C3H8 + CH3O	1.22E+10	0.0	38.5
END			

Appendix B: A 19 Elementary Reactions Mechanism used in CHMKIN

Reactions	A	n	E _a (cal/mol)
1.H+O ₂ = O+OH	5.10E+16	-0.82	16510
2.H ₂ +O = H+OH	1.80E+10	1	8830
3.H ₂ +OH = H ₂ O+H	1.20E+09	1.3	3630
4.OH+OH = H ₂ O+O	6.00E+08	1.3	0
5.H+OH+M = H ₂ O+M	7.50E+23	-2.6	0
6.O ₂ +M = O+O+M	1.90E+11	0.5	95560
7.H ₂ +M = H+H+M	2.20E+12	0.5	92600
8.H ₂ +O ₂ = OH+OH	1.70E+13	0	47780
9.H+O ₂ +M = HO ₂ +M	2.10E+18	-1	0
10.H+O ₂ +O ₂ = HO ₂ +O ₂	6.70E+19	-1.42	0
11.H+O ₂ +N ₂ = HO ₂ +N ₂	6.70E+19	-1.42	0
12.HO ₂ +H = H ₂ +O ₂	2.50E+13	0	700
13.HO ₂ +H = OH+OH	2.50E+14	0	1900
14.HO ₂ +O = OH+O ₂	4.80E+13	0	1000
15.HO ₂ +OH = H ₂ O+O ₂	5.00E+13	0	1000
16.HO ₂ +HO ₂ =H ₂ O ₂ +O ₂	2.00E+12	0	0
17.H ₂ O ₂ +M=OH+OH+M	1.20E+17	0	45500
18.H ₂ O ₂ +H = HO ₂ + H ₂	1.70E+12	0	3750
19.H ₂ O ₂ +OH=H ₂ O+HO ₂	1.00E+13	0	1800

Appendix C: Complete H₂ Combustion Mechanism (Dimitrov, 1977)

Maximum Scheme, Mechanism, and Parameters

Reactions	A^+	n^+	E^+	A^-	n^-	E^-
1. $H_2 + O_2 \leftrightarrow 2OH$	$2.81 \cdot 10^{10} *$	0	38.90	$6.24 \cdot 10^8$	0	20.38
2. $H_2 + OH \leftrightarrow H_2O + H$	$8.65 \cdot 10^{10} *$	0	5.4	$3.21 \cdot 10^{11}$	0	20.82
3. $O_2 + H \leftrightarrow OH + O$	$4.42 \cdot 10^{11} *$	0	17.60	$2.20 \cdot 10^{10}$	0	0.98
4. $H_2 + O \leftrightarrow OH + H$	$7.07 \cdot 10^7 *$	1	8.95	$3.15 \cdot 10^8$	1	7.05
5. $H_2O + O \leftrightarrow 2OH$	$8.00 \cdot 10^{10}$	0	18.80	$9.63 \cdot 10^9$	0	1.47
6. $H + H + M \leftrightarrow H_2 + M$	$2.00 \cdot 10^8$	0	0	$2.20 \cdot 10^{16}$	-1	103.26
7. $O + O + M \leftrightarrow O_2 + M$	$4.53 \cdot 10^8$	0	0.53	$4.37 \cdot 10^{17}$	-1	118.50
8. $H + OH + M \leftrightarrow H_2O + M$	$1.27 \cdot 10^{16} *$	-2	0	$1.81 \cdot 10^{16}$	0	118.20
9. $OH + OH + M \leftrightarrow H_2O_2 + M$	$9.10 \cdot 10^8$	0	0	$9.53 \cdot 10^{15}$	0	51.06
10. $OH + O + M \leftrightarrow HO_2 + M$	$8.50 \cdot 10^{10}$	0	6.69	$1.11 \cdot 10^{17}$	0	73.50
11. $H + O_2 + M \leftrightarrow HO_2 + M$	$3.78 \cdot 10^9 *$	0	-1.89	$2.48 \cdot 10^{14}$	0	48.30
12. $H_2 + HO_2 \leftrightarrow H_2O_2 + H$	$9.50 \cdot 10^8$	0	21.80	$3.38 \cdot 10^9$	0	4.15
13. $H_2 + HO_2 \leftrightarrow H_2O + OH$	$1.50 \cdot 10^8$	0	24.80	$9.71 \cdot 10^5$	0.5	77.94
14. $H_2O + HO_2 \leftrightarrow H_2O_2 + OH$	$4.00 \cdot 10^{10}$	0	34.00	$3.83 \cdot 10^{10}$	0	4.08
15. $HO_2 + HO_2 \leftrightarrow H_2O_2 + O_2$	$4.00 \cdot 10^9$	0	0	$1.11 \cdot 10^9$	0.5	41.70
16. $H + HO_2 \leftrightarrow OH + OH$	$8.90 \cdot 10^9$	0	2.58	$4.28 \cdot 10^8$	0	37.13
17. $H + HO_2 \leftrightarrow H_2O + O$	$2.00 \cdot 10^{10}$	0	3.58	$7.99 \cdot 10^9$	0	58.62
18. $H + HO_2 \leftrightarrow H_2 + O_2$	$5.00 \cdot 10^9$	0	1.20	$1.08 \cdot 10^{10}$	0	54.27
19. $O + HO_2 \leftrightarrow OH + O_2$	$6.00 \cdot 10^{10}$	0	0	$5.86 \cdot 10^{10}$	0	51.17
20. $H + H_2O_2 \leftrightarrow H_2O + OH$	$1.30 \cdot 10^{12}$	0	11.90	$6.52 \cdot 10^{11}$	0	79.53
21. $O + H_2O_2 \leftrightarrow OH + HO_2$	$4.00 \cdot 10^{10} *$	0	1.30	$5.02 \cdot 10^{10}$	0	13.89
22. $H_2 + O_2 \leftrightarrow H_2O + O$	$8.00 \cdot 10^{10}$	0	57.62	$4.00 \cdot 10^{10}$	0	61.28
23. $H_2 + O_2 + M \leftrightarrow H_2O_2 + M$	$5.00 \cdot 10^6$	0	21.90	$1.16 \cdot 10^{12}$	0	54.44
24. $OH + M \leftrightarrow O + H + M$	$4.00 \cdot 10^{13}$	0	105.3	$6.31 \cdot 10^8$	0	3.94
25. $HO_2 + OH \leftrightarrow H_2O + O_2$	$3.00 \cdot 10^{10}$	0	0.6	$8.75 \cdot 10^9$	0.5	69.97
26. $H_2 + O + M \leftrightarrow H_2O + M$	$5.00 \cdot 10^8$	0	0	$1.17 \cdot 10^{14}$	0	116.78
27. $H_2O + O + M \leftrightarrow H_2O_2 + M$	$9.00 \cdot 10^7$	0	13.00	$1.13 \cdot 10^{14}$	0	46.73
28. $H_2O_2 + O \leftrightarrow H_2O + O_2$	$2.00 \cdot 10^8$	0	29.00	$2.01 \cdot 10^8$	0	113.24
29. $H_2O_2 + H_2 \leftrightarrow 2H_2O$	$2.00 \cdot 10^{10}$	0	22.00	$3.72 \cdot 10^9$	0	105.06
30. $HO_2 + H + M \leftrightarrow H_2O_2 + M$	$3.00 \cdot 10^8$	0	1.50	$1.51 \cdot 10^{14}$	0	87.11
31. $OH + wall \leftrightarrow OH_s$	30.4	0	0	0.1	0	0
32. $H + wall \leftrightarrow H_s$	10.5*	0	0	0.1	0	0
33. $O + wall \leftrightarrow O_s$	29.5	0	0	0.1	0	0
34. $HO_2 + wall \leftrightarrow HO_{2s}$	46.4	0	0	0.1	0	0

APPENDIX E: Gri-Mech 3.0 Methane Combustion Mechanism (Smith et al.)

	Reactions	A	n	E _a (cal/mol)
1	2O+M<=>O2+M	1.20E+17	-1	0
2	O+H+M<=>OH+M	5.00E+17	-1	0
3	O+H2<=>H+OH	3.87E+04	2.7	6260
4	O+HO2<=>OH+O2	2.00E+13	0	0
5	O+H2O2<=>OH+HO2	9.63E+06	2	4000
6	O+CH<=>H+CO	5.70E+13	0	0
7	O+CH2<=>H+HCO	8.00E+13	0	0
8	O+CH2(S)<=>H2+CO	1.50E+13	0	0
9	O+CH2(S)<=>H+HCO	1.50E+13	0	0
10	O+CH3<=>H+CH2O	5.06E+13	0	0
11	O+CH4<=>OH+CH3	1.02E+09	1.5	8600
12	O+CO(+M)<=>CO2(+M)	1.80E+10	0	2385
13	O+HCO<=>OH+CO	3.00E+13	0	0
14	O+HCO<=>H+CO2	3.00E+13	0	0
15	O+CH2O<=>OH+HCO	3.90E+13	0	3540
16	O+CH2OH<=>OH+CH2O	1.00E+13	0	0
17	O+CH3O<=>OH+CH2O	1.00E+13	0	0
18	O+CH3OH<=>OH+CH2OH	3.88E+05	2.5	3100
19	O+CH3OH<=>OH+CH3O	1.30E+05	2.5	5000
20	O+C2H<=>CH+CO	5.00E+13	0	0
21	O+C2H2<=>H+HCCO	1.35E+07	2	1900
22	O+C2H2<=>OH+C2H	4.60E+19	-1.41	28950
23	O+C2H2<=>CO+CH2	6.94E+06	2	1900
24	O+C2H3<=>H+CH2CO	3.00E+13	0	0
25	O+C2H4<=>CH3+HCO	1.25E+07	1.83	220
26	O+C2H5<=>CH3+CH2O	2.24E+13	0	0
27	O+C2H6<=>OH+C2H5	8.98E+07	1.92	5690
28	O+HCCO<=>H+2CO	1.00E+14	0	0
29	O+CH2CO<=>OH+HCCO	1.00E+13	0	8000
30	O+CH2CO<=>CH2+CO2	1.75E+12	0	1350
31	O2+CO<=>O+CO2	2.50E+12	0	47800
32	O2+CH2O<=>HO2+HCO	1.00E+14	0	40000
33	H+O2+M<=>HO2+M	2.80E+18	-0.86	0
34	H+2O2<=>HO2+O2	2.08E+19	-1.24	0
35	H+O2+H2O<=>HO2+H2O	1.13E+19	-0.76	0
36	H+O2+N2<=>HO2+N2	2.60E+19	-1.24	0
37	H+O2+AR<=>HO2+AR	7.00E+17	-0.8	0
38	H+O2<=>O+OH	2.65E+16	-0.6707	17041
39	2H+M<=>H2+M	1.00E+18	-1	0
40	2H+H2<=>2H2	9.00E+16	-0.6	0
41	2H+H2O<=>H2+H2O	6.00E+19	-1.25	0

	Reactions	A	n	E _a (cal/mol)
42	2H+CO2<=>H2+CO2	5.50E+20	-2	0
43	H+OH+M<=>H2O+M	2.20E+22	-2	0
44	H+HO2<=>O+H2O	3.97E+12	0	671
45	H+HO2<=>O2+H2	4.48E+13	0	1068
46	H+HO2<=>2OH	8.40E+13	0	635
47	H+H2O2<=>HO2+H2	1.21E+07	2	5200
48	H+H2O2<=>OH+H2O	1.00E+13	0	3600
49	H+CH<=>C+H2	1.65E+14	0	0
50	H+CH2(+M)<=>CH3(+M)	6.00E+14	0	0
51	H+CH2(S)<=>CH+H2	3.00E+13	0	0
52	H+CH3(+M)<=>CH4(+M)	1.39E+16	-0.534	536
53	H+CH4<=>CH3+H2	6.60E+08	1.62	10840
54	H+HCO(+M)<=>CH2O(+M)	1.09E+12	0.48	-260
55	H+HCO<=>H2+CO	7.34E+13	0	0
56	H+CH2O(+M)<=>CH2OH(+M)	5.40E+11	0.454	3600
57	H+CH2O(+M)<=>CH3O(+M)	5.40E+11	0.454	2600
58	H+CH2O<=>HCO+H2	5.74E+07	1.9	2742
59	H+CH2OH(+M)<=>CH3OH(+M)	1.06E+12	0.5	86
60	H+CH2OH<=>H2+CH2O	2.00E+13	0	0
61	H+CH2OH<=>OH+CH3	1.65E+11	0.65	-284
62	H+CH2OH<=>CH2(S)+H2O	3.28E+13	-0.09	610
63	H+CH3O(+M)<=>CH3OH(+M)	2.43E+12	0.515	50
64	H+CH3O<=>H+CH2OH	4.15E+07	1.63	1924
65	H+CH3O<=>H2+CH2O	2.00E+13	0	0
66	H+CH3O<=>OH+CH3	1.50E+12	0.5	-110
67	H+CH3O<=>CH2(S)+H2O	2.62E+14	-0.23	1070
68	H+CH3OH<=>CH2OH+H2	1.70E+07	2.1	4870
69	H+CH3OH<=>CH3O+H2	4.20E+06	2.1	4870
70	H+C2H(+M)<=>C2H2(+M)	1.00E+17	-1	0
71	H+C2H2(+M)<=>C2H3(+M)	5.60E+12	0	2400
72	H+C2H3(+M)<=>C2H4(+M)	6.08E+12	0.27	280
73	H+C2H3<=>H2+C2H2	3.00E+13	0	0
74	H+C2H4(+M)<=>C2H5(+M)	5.40E+11	0.454	1820
75	H+C2H4<=>C2H3+H2	1.33E+06	2.53	12240
76	H+C2H5(+M)<=>C2H6(+M)	5.21E+17	-0.99	1580
77	H+C2H5<=>H2+C2H4	2.00E+12	0	0
78	H+C2H6<=>C2H5+H2	1.15E+08	1.9	7530
79	H+HCCO<=>CH2(S)+CO	1.00E+14	0	0
80	H+CH2CO<=>HCCO+H2	5.00E+13	0	8000
81	H+CH2CO<=>CH3+CO	1.13E+13	0	3428
82	H+HCCOH<=>H+CH2CO	1.00E+13	0	0
83	H2+CO(+M)<=>CH2O(+M)	4.30E+07	1.5	79600
84	OH+H2<=>H+H2O	2.16E+08	1.51	3430
85	2OH(+M)<=>H2O2(+M)	7.40E+13	-0.37	0

	Reactions	A	n	Ea (cal/mol)
86	2OH<=>O+H2O	3.57E+04	2.4	-2110
87	OH+HO2<=>O2+H2O	1.45E+13	0	-500
88	OH+H2O2<=>HO2+H2O	2.00E+12	0	427
89	OH+H2O2<=>HO2+H2O	1.70E+18	0	29410
90	OH+C<=>H+CO	5.00E+13	0	0
91	OH+CH<=>H+HCO	3.00E+13	0	0
92	OH+CH2<=>H+CH2O	2.00E+13	0	0
93	OH+CH2<=>CH+H2O	1.13E+07	2	3000
94	OH+CH2(S)<=>H+CH2O	3.00E+13	0	0
95	OH+CH3(+M)<=>CH3OH(+M)	2.79E+18	-1.43	1330
96	OH+CH3<=>CH2+H2O	5.60E+07	1.6	5420
97	OH+CH3<=>CH2(S)+H2O	6.44E+17	-1.34	1417
98	OH+CH4<=>CH3+H2O	1.00E+08	1.6	3120
99	OH+CO<=>H+CO2	4.76E+07	1.228	70
100	OH+HCO<=>H2O+CO	5.00E+13	0	0
101	OH+CH2O<=>HCO+H2O	3.43E+09	1.18	-447
102	OH+CH2OH<=>H2O+CH2O	5.00E+12	0	0
103	OH+CH3O<=>H2O+CH2O	5.00E+12	0	0
104	OH+CH3OH<=>CH2OH+H2O	1.44E+06	2	-840
105	OH+CH3OH<=>CH3O+H2O	6.30E+06	2	1500
106	OH+C2H<=>H+HCCO	2.00E+13	0	0
107	OH+C2H2<=>H+CH2CO	2.18E-04	4.5	-1000
108	OH+C2H2<=>H+HCCOH	5.04E+05	2.3	13500
109	OH+C2H2<=>C2H+H2O	3.37E+07	2	14000
110	OH+C2H2<=>CH3+CO	4.83E-04	4	-2000
111	OH+C2H3<=>H2O+C2H2	5.00E+12	0	0
112	OH+C2H4<=>C2H3+H2O	3.60E+06	2	2500
113	OH+C2H6<=>C2H5+H2O	3.54E+06	2.12	870
114	OH+CH2CO<=>HCCO+H2O	7.50E+12	0	2000
115	2HO2<=>O2+H2O2	1.30E+11	0	-1630
116	2HO2<=>O2+H2O2	4.20E+14	0	12000
117	HO2+CH2<=>OH+CH2O	2.00E+13	0	0
118	HO2+CH3<=>O2+CH4	1.00E+12	0	0
119	HO2+CH3<=>OH+CH3O	3.78E+13	0	0
120	HO2+CO<=>OH+CO2	1.50E+14	0	23600
121	HO2+CH2O<=>HCO+H2O2	5.60E+06	2	12000
122	C+O2<=>O+CO	5.80E+13	0	576
123	C+CH2<=>H+C2H	5.00E+13	0	0
124	C+CH3<=>H+C2H2	5.00E+13	0	0
125	CH+O2<=>O+HCO	6.71E+13	0	0
126	CH+H2<=>H+CH2	1.08E+14	0	3110
127	CH+H2O<=>H+CH2O	5.71E+12	0	-755
128	CH+CH2<=>H+C2H2	4.00E+13	0	0
129	CH+CH3<=>H+C2H3	3.00E+13	0	0

	Reactions	A	n	E _a (cal/mol)
130	CH+CH4<=>H+C2H4	6.00E+13	0	0
131	CH+CO(+M)<=>HCCO(+M)	5.00E+13	0	0
132	CH+CO2<=>HCO+CO	1.90E+14	0	15792
133	CH+CH2O<=>H+CH2CO	9.46E+13	0	-515
134	CH+HCCO<=>CO+C2H2	5.00E+13	0	0
135	CH2+O2=>OH+H+CO	5.00E+12	0	1500
136	CH2+H2<=>H+CH3	5.00E+05	2	7230
137	2CH2<=>H2+C2H2	1.60E+15	0	11944
138	CH2+CH3<=>H+C2H4	4.00E+13	0	0
139	CH2+CH4<=>2CH3	2.46E+06	2	8270
140	CH2+CO(+M)<=>CH2CO(+M)	8.10E+11	0.5	4510
141	CH2+HCCO<=>C2H3+CO	3.00E+13	0	0
142	CH2(S)+N2<=>CH2+N2	1.50E+13	0	600
143	CH2(S)+AR<=>CH2+AR	9.00E+12	0	600
144	CH2(S)+O2<=>H+OH+CO	2.80E+13	0	0
145	CH2(S)+O2<=>CO+H2O	1.20E+13	0	0
146	CH2(S)+H2<=>CH3+H	7.00E+13	0	0
147	CH2(S)+H2O(+M)<=>CH3OH(+M)	4.82E+17	-1.16	1145
148	CH2(S)+H2O<=>CH2+H2O	3.00E+13	0	0
149	CH2(S)+CH3<=>H+C2H4	1.20E+13	0	-570
150	CH2(S)+CH4<=>2CH3	1.60E+13	0	-570
151	CH2(S)+CO<=>CH2+CO	9.00E+12	0	0
152	CH2(S)+CO2<=>CH2+CO2	7.00E+12	0	0
153	CH2(S)+CO2<=>CO+CH2O	1.40E+13	0	0
154	CH2(S)+C2H6<=>CH3+C2H5	4.00E+13	0	-550
155	CH3+O2<=>O+CH3O	3.56E+13	0	30480
156	CH3+O2<=>OH+CH2O	2.31E+12	0	20315
157	CH3+H2O2<=>HO2+CH4	2.45E+04	2.47	5180
158	2CH3(+M)<=>C2H6(+M)	6.77E+16	-1.18	654
159	2CH3<=>H+C2H5	6.84E+12	0.1	10600
160	CH3+HCO<=>CH4+CO	2.65E+13	0	0
161	CH3+CH2O<=>HCO+CH4	3.32E+03	2.81	5860
162	CH3+CH3OH<=>CH2OH+CH4	3.00E+07	1.5	9940
163	CH3+CH3OH<=>CH3O+CH4	1.00E+07	1.5	9940
164	CH3+C2H4<=>C2H3+CH4	2.27E+05	2	9200
165	CH3+C2H6<=>C2H5+CH4	6.14E+06	1.74	10450
166	HCO+H2O<=>H+CO+H2O	1.50E+18	-1	17000
167	HCO+M<=>H+CO+M	1.87E+17	-1	17000
168	HCO+O2<=>HO2+CO	1.35E+13	0	400
169	CH2OH+O2<=>HO2+CH2O	1.80E+13	0	900
170	CH3O+O2<=>HO2+CH2O	4.28E-13	7.6	-3530
171	C2H+O2<=>HCO+CO	1.00E+13	0	-755
172	C2H+H2<=>H+C2H2	5.68E+10	0.9	1993
173	C2H3+O2<=>HCO+CH2O	4.58E+16	-1.39	1015

	Reactions	A	n	E _a (cal/mol)
174	C2H4(+M) \rightleftharpoons H2+C2H2(+M)	8.00E+12	0.44	86770
175	C2H5+O2 \rightleftharpoons HO2+C2H4	8.40E+11	0	3875
176	HCCO+O2 \rightleftharpoons OH+2CO	3.20E+12	0	854
177	2HCCO \rightleftharpoons 2CO+C2H2	1.00E+13	0	0
178	N+NO \rightleftharpoons N2+O	2.70E+13	0	355
179	N+O2 \rightleftharpoons NO+O	9.00E+09	1	6500
180	N+OH \rightleftharpoons NO+H	3.36E+13	0	385
181	N2O+O \rightleftharpoons N2+O2	1.40E+12	0	10810
182	N2O+O \rightleftharpoons 2NO	2.90E+13	0	23150
183	N2O+H \rightleftharpoons N2+OH	3.87E+14	0	18880
184	N2O+OH \rightleftharpoons N2+HO2	2.00E+12	0	21060
185	N2O(+M) \rightleftharpoons N2+O(+M)	7.91E+10	0	56020
186	HO2+NO \rightleftharpoons NO2+OH	2.11E+12	0	-480
187	NO+O+M \rightleftharpoons NO2+M	1.06E+20	-1.41	0
188	NO2+O \rightleftharpoons NO+O2	3.90E+12	0	-240
189	NO2+H \rightleftharpoons NO+OH	1.32E+14	0	360
190	NH+O \rightleftharpoons NO+H	4.00E+13	0	0
191	NH+H \rightleftharpoons N+H2	3.20E+13	0	330
192	NH+OH \rightleftharpoons HNO+H	2.00E+13	0	0
193	NH+OH \rightleftharpoons N+H2O	2.00E+09	1.2	0
194	NH+O2 \rightleftharpoons HNO+O	4.61E+05	2	6500
195	NH+O2 \rightleftharpoons NO+OH	1.28E+06	1.5	100
196	NH+N \rightleftharpoons N2+H	1.50E+13	0	0
197	NH+H2O \rightleftharpoons HNO+H2	2.00E+13	0	13850
198	NH+NO \rightleftharpoons N2+OH	2.16E+13	-0.23	0
199	NH+NO \rightleftharpoons N2O+H	3.65E+14	-0.45	0
200	NH2+O \rightleftharpoons OH+NH	3.00E+12	0	0
201	NH2+O \rightleftharpoons H+HNO	3.90E+13	0	0
202	NH2+H \rightleftharpoons NH+H2	4.00E+13	0	3650
203	NH2+OH \rightleftharpoons NH+H2O	9.00E+07	1.5	-460
204	NNH \rightleftharpoons N2+H	3.30E+08	0	0
205	NNH+M \rightleftharpoons N2+H+M	1.30E+14	-0.11	4980
206	NNH+O2 \rightleftharpoons HO2+N2	5.00E+12	0	0
207	NNH+O \rightleftharpoons OH+N2	2.50E+13	0	0
208	NNH+O \rightleftharpoons NH+NO	7.00E+13	0	0
209	NNH+H \rightleftharpoons H2+N2	5.00E+13	0	0
210	NNH+OH \rightleftharpoons H2O+N2	2.00E+13	0	0
211	NNH+CH3 \rightleftharpoons CH4+N2	2.50E+13	0	0
212	H+NO+M \rightleftharpoons HNO+M	4.48E+19	-1.32	740
213	HNO+O \rightleftharpoons NO+OH	2.50E+13	0	0
214	HNO+H \rightleftharpoons H2+NO	9.00E+11	0.72	660
215	HNO+OH \rightleftharpoons NO+H2O	1.30E+07	1.9	-950
216	HNO+O2 \rightleftharpoons HO2+NO	1.00E+13	0	13000
217	CN+O \rightleftharpoons CO+N	7.70E+13	0	0

	Reactions	A	n	E _a (cal/mol)
218	CN+OH<=>NCO+H	4.00E+13	0	0
219	CN+H2O<=>HCN+OH	8.00E+12	0	7460
220	CN+O2<=>NCO+O	6.14E+12	0	-440
221	CN+H2<=>HCN+H	2.95E+05	2.45	2240
222	NCO+O<=>NO+CO	2.35E+13	0	0
223	NCO+H<=>NH+CO	5.40E+13	0	0
224	NCO+OH<=>NO+H+CO	2.50E+12	0	0
225	NCO+N<=>N2+CO	2.00E+13	0	0
226	NCO+O2<=>NO+CO2	2.00E+12	0	20000
227	NCO+M<=>N+CO+M	3.10E+14	0	54050
228	NCO+NO<=>N2O+CO	1.90E+17	-1.52	740
229	NCO+NO<=>N2+CO2	3.80E+18	-2	800
230	HCN+M<=>H+CN+M	1.04E+29	-3.3	126600
231	HCN+O<=>NCO+H	2.03E+04	2.64	4980
232	HCN+O<=>NH+CO	5.07E+03	2.64	4980
233	HCN+O<=>CN+OH	3.91E+09	1.58	26600
234	HCN+OH<=>HOCN+H	1.10E+06	2.03	13370
235	HCN+OH<=>HNCO+H	4.40E+03	2.26	6400
236	HCN+OH<=>NH2+CO	1.60E+02	2.56	9000
237	H+HCN(+M)<=>H2CN(+M)	3.30E+13	0	0
238	H2CN+N<=>N2+CH2	6.00E+13	0	400
239	C+N2<=>CN+N	6.30E+13	0	46020
240	CH+N2<=>HCN+N	3.12E+09	0.88	20130
241	CH+N2(+M)<=>HCNN(+M)	3.10E+12	0.15	0
242	CH2+N2<=>HCN+NH	1.00E+13	0	74000
243	CH2(S)+N2<=>NH+HCN	1.00E+11	0	65000
244	C+NO<=>CN+O	1.90E+13	0	0
245	C+NO<=>CO+N	2.90E+13	0	0
246	CH+NO<=>HCN+O	4.10E+13	0	0
247	CH+NO<=>H+NCO	1.62E+13	0	0
248	CH+NO<=>N+HCO	2.46E+13	0	0
249	CH2+NO<=>H+HNCO	3.10E+17	-1.38	1270
250	CH2+NO<=>OH+HCN	2.90E+14	-0.69	760
251	CH2+NO<=>H+HCNO	3.80E+13	-0.36	580
252	CH2(S)+NO<=>H+HNCO	3.10E+17	-1.38	1270
253	CH2(S)+NO<=>OH+HCN	2.90E+14	-0.69	760
254	CH2(S)+NO<=>H+HCNO	3.80E+13	-0.36	580
255	CH3+NO<=>HCN+H2O	9.60E+13	0	28800
256	CH3+NO<=>H2CN+OH	1.00E+12	0	21750
257	HCNN+O<=>CO+H+N2	2.20E+13	0	0
258	HCNN+O<=>HCN+NO	2.00E+12	0	0
259	HCNN+O2<=>O+HCO+N2	1.20E+13	0	0
260	HCNN+OH<=>H+HCO+N2	1.20E+13	0	0
261	HCNN+H<=>CH2+N2	1.00E+14	0	0

	Reactions	A	n	E _a (cal/mol)
262	HNCO+O<=>NH+CO2	9.80E+07	1.41	8500
263	HNCO+O<=>HNO+CO	1.50E+08	1.57	44000
264	HNCO+O<=>NCO+OH	2.20E+06	2.11	11400
265	HNCO+H<=>NH2+CO	2.25E+07	1.7	3800
266	HNCO+H<=>H2+NCO	1.05E+05	2.5	13300
267	HNCO+OH<=>NCO+H2O	3.30E+07	1.5	3600
268	HNCO+OH<=>NH2+CO2	3.30E+06	1.5	3600
269	HNCO+M<=>NH+CO+M	1.18E+16	0	84720
270	HCNO+H<=>H+HNCO	2.10E+15	-0.69	2850
271	HCNO+H<=>OH+HCN	2.70E+11	0.18	2120
272	HCNO+H<=>NH2+CO	1.70E+14	-0.75	2890
273	HOCN+H<=>H+HNCO	2.00E+07	2	2000
274	HCCO+NO<=>HCNO+CO	9.00E+12	0	0
275	CH3+N<=>H2CN+H	6.10E+14	-0.31	290
276	CH3+N<=>HCN+H2	3.70E+12	0.15	-90
277	NH3+H<=>NH2+H2	5.40E+05	2.4	9915
278	NH3+OH<=>NH2+H2O	5.00E+07	1.6	955
279	NH3+O<=>NH2+OH	9.40E+06	1.94	6460
280	NH+CO2<=>HNO+CO	1.00E+13	0	14350
281	CN+NO2<=>NCO+NO	6.16E+15	-0.752	345
282	NCO+NO2<=>N2O+CO2	3.25E+12	0	-705
283	N+CO2<=>NO+CO	3.00E+12	0	11300
284	O+CH3=>H+H2+CO	3.37E+13	0	0
285	O+C2H4<=>H+CH2CHO	6.70E+06	1.83	220
286	O+C2H5<=>H+CH3CHO	1.10E+14	0	0
287	OH+HO2<=>O2+H2O	5.00E+15	0	17330
288	OH+CH3=>H2+CH2O	8.00E+09	0.5	-1755
289	CH+H2(+M)<=>CH3(+M)	1.97E+12	0.43	-370
290	CH2+O2=>2H+CO2	5.80E+12	0	1500
291	CH2+O2<=>O+CH2O	2.40E+12	0	1500
292	CH2+CH2=>2H+C2H2	2.00E+14	0	10989
293	CH2(S)+H2O=>H2+CH2O	6.82E+10	0.25	-935
294	C2H3+O2<=>O+CH2CHO	3.03E+11	0.29	11
295	C2H3+O2<=>HO2+C2H2	1.34E+06	1.61	-384
296	O+CH3CHO<=>OH+CH2CHO	2.92E+12	0	1808
297	O+CH3CHO=>OH+CH3+CO	2.92E+12	0	1808
298	O2+CH3CHO=>HO2+CH3+CO	3.01E+13	0	39150
299	H+CH3CHO<=>CH2CHO+H2	2.05E+09	1.16	2405
300	H+CH3CHO=>CH3+H2+CO	2.05E+09	1.16	2405
301	OH+CH3CHO=>CH3+H2O+CO	2.34E+10	0.73	-1113
302	HO2+CH3CHO=>CH3+H2O2+CO	3.01E+12	0	11923
303	CH3+CH3CHO=>CH3+CH4+CO	2.72E+06	1.77	5920
304	H+CH2CO(+M)<=>CH2CHO(+M)	4.87E+11	0.422	-1755
305	O+CH2CHO=>H+CH2+CO2	1.50E+14	0	0

	Reactions	A	n	E _a (cal/mol)
306	O ₂ +CH ₂ CHO=>OH+CO+CH ₂ O	1.81E+10	0	0
307	O ₂ +CH ₂ CHO=>OH+2HCO	2.35E+10	0	0
308	H+CH ₂ CHO<=>CH ₃ +HCO	2.20E+13	0	0
309	H+CH ₂ CHO<=>CH ₂ CO+H ₂	1.10E+13	0	0
310	OH+CH ₂ CHO<=>H ₂ O+CH ₂ CO	1.20E+13	0	0
311	OH+CH ₂ CHO<=>HCO+CH ₂ OH	3.01E+13	0	0
312	CH ₃ +C ₂ H ₅ (+M)<=>C ₃ H ₈ (+M)	9.43E+12	0	0
313	O+C ₃ H ₈ <=>OH+C ₃ H ₇	1.93E+05	2.68	3716
314	H+C ₃ H ₈ <=>C ₃ H ₇ +H ₂	1.32E+06	2.54	6756
315	OH+C ₃ H ₈ <=>C ₃ H ₇ +H ₂ O	3.16E+07	1.8	934
316	C ₃ H ₇ +H ₂ O ₂ <=>HO ₂ +C ₃ H ₈	3.78E+02	2.72	1500
317	CH ₃ +C ₃ H ₈ <=>C ₃ H ₇ +CH ₄	9.03E-01	3.65	7154
318	CH ₃ +C ₂ H ₄ (+M)<=>C ₃ H ₇ (+M)	2.55E+06	1.6	5700
319	O+C ₃ H ₇ <=>C ₂ H ₅ +CH ₂ O	9.64E+13	0	0
320	H+C ₃ H ₇ (+M)<=>C ₃ H ₈ (+M)	3.61E+13	0	0
321	H+C ₃ H ₇ <=>CH ₃ +C ₂ H ₅	4.06E+06	2.19	890
322	OH+C ₃ H ₇ <=>C ₂ H ₅ +CH ₂ OH	2.41E+13	0	0
323	HO ₂ +C ₃ H ₇ <=>O ₂ +C ₃ H ₈	2.55E+10	0.255	-943
324	HO ₂ +C ₃ H ₇ =>OH+C ₂ H ₅ +CH ₂ O	2.41E+13	0	0
325	CH ₃ +C ₃ H ₇ <=>2C ₂ H ₅	1.93E+13	-0.32	0

Appendix F: The Test Condition for H₂-CH₄ Jet Diffusion Flames

H ₂ flow rate [l/min]	CH ₄ flow rate [l/min]	P (Bar)	Actual H ₂ flow rate [l/min]	Actual CH ₄ flow rate [l/min]	Total flow rate [L/min]	Exit velocity [m/s]	CH ₄ vol. %
20	0	1	20	0	20	106	0
20	1	1	20	1	21	111	5
20	2	1	20	2	22	117	9
20	3	1	20	3	23	122	13
20	4	1	20	4	24	127	17
20	5	1	20	5	25	133	20
20	6	1	20	6	26	138	23
20	7	1	20	7	27	143	26
20	8	1	20	8	28	149	29
20	9	1	20	9	29	154	31
20	10	1.1	21	10	31	167	33
20	11	1.1	21	12	32	172	35
20	12	1.1	21	13	34	178	38
20	13	1.2	22	14	36	192	39
20	14	1.2	22	15	37	197	41
40	0	1	40	0	40	212	0
40	1	1.1	42	1	43	228	2
40	2	1.2	44	2	46	244	5
40	3	1.2	44	3	47	250	7
40	4	1.2	44	4	48	255	9
40	5	1.2	44	5	49	261	11

40	6	1.2	44	7	50	267	13
40	7	1.2	44	8	51	273	15
40	8	1.2	44	9	53	279	17
40	9	1.3	46	10	56	296	18
40	10	1.3	46	11	57	302	20
40	11	1.4	47	13	60	320	22
40	12	1.4	47	14	61	326	23
40	13	1.4	47	15	63	332	25
40	14	1.4	47	17	64	338	26
40	15	1.4	47	18	65	345	27
40	16	1.5	49	20	68	363	29
40	17	1.5	49	21	70	370	30

Appendix G: The Test Condition for H₂-C₂H₆ Jet Diffusion Flames

H ₂ flow rate [l/min]	C ₂ H ₆ flow rate [l/min]	P (Bar)	Actual H ₂ flow rate [l/min]	Actual C ₂ H ₆ flow rate [l/min]	Total flow rate [L/min]	Exit velocity [m/s]	C ₂ H ₆ vol.%
20	0	1	20	0	20	106	0
20	1	1	20	1	21	110	4
20	2	1	20	1	21	114	7
20	3	1	20	2	22	118	10
20	4	1	20	3	23	122	13
20	5	1	20	4	24	125	15
20	6	1	20	4	24	129	18
20	7	1	20	5	25	133	20
20	8	1.1	21	6	27	144	23
20	9	1.1	21	7	28	148	25
20	10	1.2	22	8	30	159	27
20	11	1.2	22	9	31	163	29
20	12	1.2	22	10	31	167	30
40	0	1	40	0	40	212	0
40	1	1.1	42	1	43	226	2
40	2	1.2	44	2	45	241	4
40	3	1.2	44	2	46	245	5
40	4	1.2	44	3	47	249	7
40	5	1.2	44	4	48	253	8

40	6	1.2	44	5	49	258	10
40	7	1.2	44	6	49	262	11
40	8	1.2	44	6	50	266	13
40	9	1.3	46	7	53	281	14
40	10	1.3	46	8	54	286	15
40	11	1.4	47	9	57	301	17
40	12	1.4	47	10	58	306	18
40	13	1.4	47	11	58	310	19
40	14	1.5	49	12	61	326	20

Appendix H: The Test Conditions for H₂-C₃H₈ Jet Diffusion Flames

H ₂ flow rate [l/min]	C ₃ H ₈ flow rate [l/min]	P (Bar)	Actual H ₂ flow rate [l/min]	Actual C ₃ H ₈ flow rate [l/min]	Total flow rate [L/min]	Exit velocity [m/s]	C ₃ H ₈ vol. %
20	4	1	20	2	22	119	11
20	6	1.2	22	4	26	137	15
20	8	1.2	22	5	27	144	19
20	9	1.2	22	6	28	148	21
20	10	1.2	22	7	28	151	23
20	11	1.2	22	7	29	155	25
40	4	1.2	44	3	46	246	6
40	6	1.2	44	4	48	253	8
40	7	1.2	44	5	48	257	10
40	8	1.2	44	5	49	260	11
40	10	1.2	44	7	50	267	13
40	12	1.2	44	8	52	274	15

Appendix I: The Test Conditions for H₂-CH₄-CO₂ Jet Diffusion Flames, at H₂ Flowrate of 20 l/min

P(G)	H ₂ flow rate [l/min]	Actual H ₂ flow rate [l/min]	CH ₄ flow rate [l/min]	Actual CH ₄ flow rate [l/min]	CO ₂ flow rate [l/min]	Actual CO ₂ flow rate [l/min]	Total flow rate [l/min]	Jet Exit Velocity [m/s]	H ₂ vol.%	CH ₄ vol.%	CO ₂ vol.%
0	20	20	0	0	2	0.43	20.43	108.4	97.9	0.0	2.1
0	20	20	1	1	2	0.43	21.43	113.7	93.3	4.7	2.0
0	20	20	2	2	2	0.43	22.43	119.1	89.2	8.9	1.9
0	20	20	3	3	2	0.43	23.43	124.4	85.4	12.8	1.8
0	20	20	4	4	2	0.43	24.43	129.7	81.9	16.4	1.8
0	20	20	5	5	2	0.43	25.43	135.0	78.6	19.7	1.7
0.1	20	20.95	6	6.28	2	0.45	27.68	146.9	75.7	22.7	1.6
0.1	20	20.95	7	7.33	2	0.45	28.73	152.5	72.9	25.5	1.6
0.2	20	21.85	8	8.74	2	0.47	31.06	164.9	70.3	28.1	1.5
0.2	20	21.85	9	9.83	2	0.47	32.15	170.7	68.0	30.6	1.5
0.2	20	21.85	10	10.92	2	0.47	33.24	176.5	65.7	32.9	1.4
0.2	20	21.85	11	12.02	2	0.47	34.34	182.3	63.6	35.0	1.4
0.2	20	21.85	12	13.11	2	0.47	35.43	188.1	61.7	37.0	1.3
0.2	20	21.85	13	14.20	2	0.47	36.52	193.8	59.8	38.9	1.3
0	20	20	0	0	4	0.86	20.86	110.7	95.9	0.0	4.1
0	20	20	1	1	4	0.86	21.86	116.0	91.5	4.6	3.9
0	20	20	2	2	4	0.86	22.86	121.3	87.5	8.7	3.8
0	20	20	3	3	4	0.86	23.86	126.6	83.8	12.6	3.6
0.1	20	20.95	4	4.19	4	0.90	26.03	138.2	80.5	16.1	3.5
0.1	20	20.95	5	5.24	4	0.90	27.08	143.7	77.3	19.3	3.3

0.1	20	20.95	6	6.28	4	0.90	28.13	149.3	74.5	22.3	3.2
0.1	20	20.95	7	7.33	4	0.90	29.18	154.9	71.8	25.1	3.1
0.1	20	20.95	8	8.38	4	0.90	30.22	160.4	69.3	27.7	3.0
0.2	20	21.85	9	9.83	4	0.93	32.61	173.1	67.0	30.2	2.8
0.2	20	21.85	10	10.92	4	0.93	33.70	178.9	64.8	32.4	2.8
0.2	20	21.85	11	12.02	4	0.93	34.80	184.7	62.8	34.5	2.7
0.2	20	21.85	12	13.11	4	0.93	35.89	190.5	60.9	36.5	2.6
0	20	20	0	0	6	1.28	21.28	113.0	94.0	0.0	6.0
0	20	20	1	1	6	1.28	22.28	118.3	89.8	4.5	5.7
0	20	20	2	2	6	1.28	23.28	123.6	85.9	8.6	5.5
0.1	20	20.95	3	3.14	6	1.34	25.43	135.0	82.4	12.4	5.3
0.1	20	20.95	4	4.19	6	1.34	26.47	140.5	79.1	15.8	5.1
0.1	20	20.95	5	5.24	6	1.34	27.52	146.1	76.1	19.0	4.9
0.2	20	21.85	6	6.55	6	1.40	29.80	158.2	73.3	22.0	4.7
0.2	20	21.85	7	7.65	6	1.40	30.89	164.0	70.7	24.8	4.5
0.2	20	21.85	8	8.74	6	1.40	31.99	169.8	68.3	27.3	4.4
0.2	20	21.85	9	9.83	6	1.40	33.08	175.6	66.1	29.7	4.2
0.2	20	21.85	10	10.92	6	1.40	34.17	181.4	63.9	32.0	4.1
0.2	20	21.85	11	12.02	6	1.40	35.26	187.2	62.0	34.1	4.0
0	20	20	0	0	8	1.71	21.71	115.2	92.1	0.0	7.9
0	20	20	1	1	8	1.71	22.71	120.5	88.1	4.4	7.5
0.1	20	20.95	2	2.09	8	1.79	24.83	131.8	84.4	8.4	7.2
0.1	20	20.95	3	3.14	8	1.79	25.88	137.4	80.9	12.1	6.9
0.1	20	20.95	4	4.19	8	1.79	26.92	142.9	77.8	15.6	6.7
0.1	20	20.95	5	5.24	8	1.79	27.97	148.5	74.9	18.7	6.4
0.1	20	20.95	6	6.28	8	1.79	29.02	154.0	72.2	21.7	6.2

0.2	20	21.85	7	7.65	8	1.87	31.36	166.5	69.7	24.4	6.0
0.2	20	21.85	8	8.74	8	1.87	32.46	172.3	67.3	26.9	5.8
0.2	20	21.85	9	9.83	8	1.87	33.55	178.1	65.1	29.3	5.6
0.2	20	21.85	10	10.92	8	1.87	34.64	183.9	63.1	31.5	5.4
0	20	20	0	0	10	2.14	22.14	117.5	90.3	0.0	9.7
0.1	20	20.95	1	1.05	10	2.24	24.23	128.6	86.4	4.3	9.2
0.1	20	20.95	2	2.09	10	2.24	25.28	134.2	82.9	8.3	8.9
0.1	20	20.95	3	3.14	10	2.24	26.33	139.7	79.6	11.9	8.5
0.1	20	20.95	4	4.19	10	2.24	27.38	145.3	76.5	15.3	8.2
0.2	20	21.85	5	5.46	10	2.33	29.64	157.3	73.7	18.4	7.9
0.2	20	21.85	6	6.55	10	2.33	30.73	163.1	71.1	21.3	7.6
0.2	20	21.85	7	7.65	10	2.33	31.82	168.9	68.7	24.0	7.3
0.2	20	21.85	8	8.74	10	2.33	32.92	174.7	66.4	26.6	7.1
0.2	20	21.85	9	9.83	10	2.33	34.01	180.5	64.2	28.9	6.8
0	20	20	0	0	12	2.57	22.57	119.8	88.6	0.0	11.4
0	20	20	1	1	12	2.57	23.57	125.1	84.9	4.2	10.9
0.2	20	21.85	2	2.18	12	2.8	26.83	142.4	81.4	8.1	10.4
0.2	20	21.85	3	3.28	12	2.8	27.93	148.2	78.2	11.7	10.0
0.2	20	21.85	4	4.37	12	2.8	29.02	154.0	75.3	15.1	9.6
0.2	20	21.85	5	5.46	12	2.8	30.11	159.8	72.6	18.1	9.3
0.2	20	21.85	6	6.55	12	2.8	31.20	165.6	70.0	21.0	9.0
0.2	20	21.85	7	7.65	12	2.8	32.30	171.4	67.7	23.7	8.7
0.2	20	21.85	8	8.74	12	2.8	33.39	177.2	65.4	26.2	8.4
0.2	20	21.85	9	9.83	12	2.8	34.48	183.0	63.4	28.5	8.1
0.2	20	21.85	10	10.92	12	2.8	35.57	188.8	61.4	30.7	7.9
0	20	20	0	0	14	3	23.00	122.1	87.0	0.0	13.0

0.2	20	21.85	1	1.09	14	3.26	26.20	139.1	83.4	4.2	12.4
0.2	20	21.85	2	2.18	14	3.26	27.29	144.9	80.1	8.0	11.9
0.2	20	21.85	3	3.28	14	3.26	28.39	150.7	77.0	11.5	11.5
0.2	20	21.85	4	4.37	14	3.26	29.48	156.5	74.1	14.8	11.1
0.2	20	21.85	5	5.46	14	3.26	30.57	162.3	71.5	17.9	10.7
0.2	20	21.85	6	6.55	14	3.26	31.66	168.1	69.0	20.7	10.3
0.2	20	21.85	7	7.65	14	3.26	32.76	173.9	66.7	23.3	10.0
0.2	20	21.85	8	8.74	14	3.26	33.85	179.7	64.5	25.8	9.6
0.2	20	21.85	9	9.83	14	3.26	34.94	185.5	62.5	28.1	9.3
0	20	20	0	0	16	3.43	23.43	124.4	85.4	0.0	14.6
0.2	20	21.85	1	1.09	16	3.73	26.67	141.6	81.9	4.1	14.0
0.2	20	21.85	2	2.18	16	3.73	27.76	147.4	78.7	7.9	13.4
0.2	20	21.85	3	3.28	16	3.73	28.86	153.2	75.7	11.4	12.9
0.2	20	21.85	4	4.37	16	3.73	29.95	159.0	73.0	14.6	12.5
0.2	20	21.85	5	5.46	16	3.73	31.04	164.8	70.4	17.6	12.0
0.2	20	21.85	6	6.55	16	3.73	32.13	170.6	68.0	20.4	11.6
0.2	20	21.85	7	7.65	16	3.73	33.23	176.4	65.8	23.0	11.2
0.2	20	21.85	8	8.74	16	3.73	34.32	182.2	63.7	25.5	10.9
0.2	20	21.85	9	9.83	16	3.73	35.41	188.0	61.7	27.8	10.5
0	20	20	0	0	18	3.85	23.85	126.6	83.9	0.0	16.1
0.2	20	21.85	1	1.09	18	4.2	27.14	144.1	80.5	4.0	15.5
0.2	20	21.85	2	2.18	18	4.2	28.23	149.9	77.4	7.7	14.9
0.2	20	21.85	3	3.28	18	4.2	29.33	155.7	74.5	11.2	14.3
0.2	20	21.85	4	4.37	18	4.2	30.42	161.5	71.8	14.4	13.8
0.2	20	21.85	5	5.46	18	4.2	31.51	167.3	69.3	17.3	13.3
0.2	20	21.85	6	6.55	18	4.2	32.60	173.1	67.0	20.1	12.9

0.2	20	21.85	7	7.65	18	4.2	33.70	178.9	64.8	22.7	12.5
0	20	20	0	0	20	4.28	24.28	128.9	82.4	0.0	17.6
0.2	20	21.85	1	1.09	20	4.66	27.60	146.5	79.2	4.0	16.9
0.2	20	21.85	2	2.18	20	4.66	28.69	152.3	76.1	7.6	16.2
0.2	20	21.85	3	3.28	20	4.66	29.79	158.1	73.4	11.0	15.6
0.2	20	21.85	4	4.37	20	4.66	30.88	163.9	70.8	14.2	15.1
0.2	20	21.85	5	5.46	20	4.66	31.97	169.7	68.3	17.1	14.6
0.2	20	21.85	6	6.55	20	4.66	33.06	175.5	66.1	19.8	14.1
0.2	20	21.85	7	7.65	20	4.66	34.16	181.3	64.0	22.4	13.6
0	20	20	0	0	22	4.71	24.71	131.2	80.9	0.0	19.1
0.2	20	21.85	1	1.09	22	5.13	28.07	149.0	77.8	3.9	18.3
0.2	20	21.85	2	2.18	22	5.13	29.16	154.8	74.9	7.5	17.6
0.2	20	21.85	3	3.28	22	5.13	30.26	160.6	72.2	10.8	17.0
0.2	20	21.85	4	4.37	22	5.13	31.35	166.4	69.7	13.9	16.4
0.2	20	21.85	5	5.46	22	5.13	32.44	172.2	67.3	16.8	15.8
0.2	20	21.85	6	6.55	22	5.13	33.53	178.0	65.2	19.5	15.3
0.2	20	21.85	7	7.65	22	5.13	34.63	183.8	63.1	22.1	14.8
0.2	20	21.85	0	0	24	5.6	27.45	145.7	79.6	0.0	20.4
0.2	20	21.85	1	1.09	24	5.6	28.54	151.5	76.6	3.8	19.6
0.2	20	21.85	2	2.18	24	5.6	29.63	157.3	73.7	7.4	18.9
0.2	20	21.85	3	3.28	24	5.6	30.73	163.1	71.1	10.7	18.2
0.2	20	21.85	4	4.37	24	5.6	31.82	168.9	68.7	13.7	17.6
0.2	20	21.85	5	5.46	24	5.6	32.91	174.7	66.4	16.6	17.0
0.2	20	21.85	0	0	26	6.06	27.91	148.1	78.3	0.0	21.7
0.2	20	21.85	1	1.09	26	6.06	29.00	153.9	75.3	3.8	20.9
0.2	20	21.85	2	2.18	26	6.06	30.09	159.7	72.6	7.3	20.1

0.2	20	21.85	3	3.28	26	6.06	31.19	165.5	70.1	10.5	19.4
0.2	20	21.85	4	4.37	26	6.06	32.28	171.3	67.7	13.5	18.8
0.2	20	21.85	0	0	28	6.53	28.38	150.6	77.0	0.0	23.0
0.2	20	21.85	1	1.09	28	6.53	29.47	156.4	74.1	3.7	22.2
0.2	20	21.85	2	2.18	28	6.53	30.56	162.2	71.5	7.1	21.4
0.2	20	21.85	3	3.28	28	6.53	31.66	168.0	69.0	10.4	20.6
0.2	20	21.85	4	4.37	28	6.53	32.75	173.8	66.7	13.3	19.9
0.2	20	21.85	5	5.46	28	6.53	33.84	179.6	64.6	16.1	19.3
0.2	20	21.85	0	0	30	7	28.85	153.1	75.7	0.0	24.3
0.2	20	21.85	1	1.09	30	7	29.94	158.9	73.0	3.6	23.4
0.2	20	21.85	2	2.18	30	7	31.03	164.7	70.4	7.0	22.6
0.2	20	21.85	3	3.28	30	7	32.13	170.5	68.0	10.2	21.8
0.2	20	21.85	4	4.37	30	7	33.22	176.3	65.8	13.2	21.1

Appendix J: The Test Condition for H₂-CH₄-CO₂ Jet Diffusion Flames, at H₂ Flowrate of 40 l/min

P(G)	H ₂ flow rate [l/min]	Actual H ₂ flow rate [l/min]	CH ₄ flow rate [l/min]	Actual CH ₄ flow rate [l/min]	CO ₂ flow rate [l/min]	Actual CO ₂ flow rate [l/min]	Total flow rate [l/min]	Jet Exit Velocity [m/s]	H ₂ vol.%	CH ₄ vol.%	CO ₂ vol.%
0.2	40	43.70	0	0.00	2	0.47	44.17	234.4	98.9	0.0	1.1
0.2	40	43.70	1	1.09	2	0.47	45.26	240.2	96.5	2.4	1.0
0.2	40	43.70	2	2.18	2	0.47	46.35	246.0	94.3	4.7	1.0
0.2	40	43.70	3	3.28	2	0.47	47.45	251.8	92.1	6.9	1.0
0.2	40	43.70	4	4.37	2	0.47	48.54	257.6	90.0	9.0	1.0
0.2	40	43.70	5	5.46	2	0.47	49.63	263.4	88.0	11.0	0.9
0.2	40	43.70	6	6.55	2	0.47	50.72	269.2	86.2	12.9	0.9
0.2	40	43.70	7	7.65	2	0.47	51.82	275.0	84.3	14.8	0.9
0.2	40	43.70	8	8.74	2	0.47	52.91	280.8	82.6	16.5	0.9
0.3	40	45.44	9	10.22	2	0.49	56.15	298.0	80.9	18.2	0.9
0.3	40	45.44	10	11.36	2	0.49	57.28	304.0	79.3	19.8	0.9
0.4	40	47.11	11	12.95	2	0.51	60.57	321.5	77.8	21.4	0.8
0.4	40	47.11	12	14.13	2	0.51	61.75	327.7	76.3	22.9	0.8
0.4	40	47.11	13	15.31	2	0.51	62.92	334.0	74.9	24.3	0.8
0.4	40	47.11	14	16.49	2	0.51	64.10	340.2	73.5	25.7	0.8
0.4	40	47.11	15	17.67	2	0.51	65.28	346.5	72.2	27.1	0.8
0.4	40	47.11	16	18.84	2	0.51	66.46	352.7	70.9	28.4	0.8
0.2	40	43.70	0	0.00	4	0.93	44.63	236.9	97.9	0.0	2.1
0.2	40	43.70	1	1.09	4	0.93	45.72	242.7	95.6	2.4	2.0

0.2	40	43.70	2	2.18	4	0.93	46.81	248.5	93.3	4.7	2.0
0.2	40	43.70	3	3.28	4	0.93	47.90	254.3	91.2	6.8	1.9
0.2	40	43.70	4	4.37	4	0.93	49.00	260.1	89.2	8.9	1.9
0.2	40	43.70	5	5.46	4	0.93	50.09	265.9	87.2	10.9	1.9
0.2	40	43.70	6	6.55	4	0.93	51.18	271.7	85.4	12.8	1.8
0.2	40	43.70	7	7.65	4	0.93	52.27	277.5	83.6	14.6	1.8
0.4	40	47.11	8	9.42	4	1.01	57.54	305.4	81.9	16.4	1.8
0.4	40	47.11	9	10.60	4	1.01	58.72	311.7	80.2	18.1	1.7
0.4	40	47.11	10	11.78	4	1.01	59.90	317.9	78.6	19.7	1.7
0.4	40	47.11	11	12.95	4	1.01	61.08	324.2	77.1	21.2	1.7
0.4	40	47.11	12	14.13	4	1.01	62.25	330.4	75.7	22.7	1.6
0.4	40	47.11	13	15.31	4	1.01	63.43	336.7	74.3	24.1	1.6
0.5	40	48.72	14	17.05	4	1.01	66.79	354.5	73.0	25.5	1.5
0.5	40	48.72	15	18.27	4	1.01	68.01	361.0	71.6	26.9	1.5
0.2	40	43.70	0	0.00	6	1.40	45.10	239.4	96.9	0.0	3.1
0.2	40	43.70	1	1.09	6	1.40	46.19	245.2	94.6	2.4	3.0
0.2	40	43.70	2	2.18	6	1.40	47.28	251.0	92.4	4.6	3.0
0.2	40	43.70	3	3.28	6	1.40	48.37	256.8	90.3	6.8	2.9
0.2	40	43.70	4	4.37	6	1.40	49.47	262.6	88.3	8.8	2.8
0.3	40	45.44	5	5.68	6	1.45	52.57	279.0	86.4	10.8	2.8
0.3	40	45.44	6	6.82	6	1.45	53.70	285.1	84.6	12.7	2.7
0.3	40	45.44	7	7.95	6	1.45	54.84	291.1	82.9	14.5	2.7
0.3	40	45.44	8	9.09	6	1.45	55.98	297.1	81.2	16.2	2.6
0.4	40	47.11	9	10.60	6	1.51	59.21	314.3	79.6	17.9	2.5
0.4	40	47.11	10	11.78	6	1.51	60.39	320.6	78.0	19.5	2.5
0.4	40	47.11	11	12.95	6	1.51	61.57	326.8	76.5	21.0	2.4

0.4	40	47.11	12	14.13	6	1.51	62.75	333.1	75.1	22.5	2.4
0.5	40	48.72	13	15.84	6	1.51	66.07	350.7	73.7	24.0	2.3
0.2	40	43.70	0	0.00	8	1.87	45.57	241.9	95.9	0.0	4.1
0.2	40	43.70	1	1.09	8	1.87	46.66	247.7	93.7	2.3	4.0
0.2	40	43.70	2	2.18	8	1.87	47.75	253.5	91.5	4.6	3.9
0.2	40	43.70	3	3.28	8	1.87	48.84	259.3	89.5	6.7	3.8
0.2	40	43.70	4	4.37	8	1.87	49.94	265.1	87.5	8.8	3.7
0.3	40	45.44	5	5.68	8	1.94	53.06	281.6	85.6	10.7	3.7
0.3	40	45.44	6	6.82	8	1.94	54.19	287.6	83.8	12.6	3.6
0.3	40	45.44	7	7.95	8	1.94	55.33	293.7	82.1	14.4	3.5
0.4	40	47.11	8	9.42	8	2.01	58.54	310.7	80.5	16.1	3.4
0.4	40	47.11	9	10.60	8	2.01	59.72	317.0	78.9	17.7	3.4
0.4	40	47.11	10	11.78	8	2.01	60.90	323.2	77.4	19.3	3.3
0.5	40	48.72	11	13.40	8	2.08	64.20	340.8	75.9	20.9	3.2
0.5	40	48.72	12	14.62	8	2.08	65.42	347.3	74.5	22.3	3.2
0.2	40	43.70	0	0.00	10	2.33	46.03	244.3	94.9	0.0	5.1
0.2	40	43.70	1	1.09	10	2.33	47.12	250.1	92.7	2.3	4.9
0.2	40	43.70	2	2.18	10	2.33	48.21	255.9	90.6	4.5	4.8
0.2	40	43.70	3	3.28	10	2.33	49.31	261.7	88.6	6.6	4.7
0.2	40	43.70	4	4.37	10	2.33	50.40	267.5	86.7	8.7	4.6
0.2	40	43.70	5	5.46	10	2.33	51.49	273.3	84.9	10.6	4.5
0.2	40	43.70	6	6.55	10	2.33	52.58	279.1	83.1	12.5	4.4
0.4	40	47.11	7	8.24	10	2.52	57.87	307.2	81.4	14.2	4.4
0.4	40	47.11	8	9.42	10	2.52	59.05	313.4	79.8	16.0	4.3
0.2	40	43.70	0	0.00	12	2.8	46.50	246.8	94.0	0.0	6.0
0.2	40	43.70	1	1.09	12	2.8	47.59	252.6	91.8	2.3	5.9

0.2	40	43.70	2	2.18	12	2.8	48.68	258.4	89.8	4.5	5.8
0.3	40	45.44	3	3.41	12	2.91	51.75	274.7	87.8	6.6	5.6
0.4	40	47.11	4	4.71	12	3.02	54.84	291.1	85.9	8.6	5.5
0.4	40	47.11	5	5.89	12	3.02	56.02	297.3	84.1	10.5	5.4
0.4	40	47.11	6	7.07	12	3.02	57.19	303.6	82.4	12.4	5.3
0.4	40	47.11	7	8.24	12	3.02	58.37	309.8	80.7	14.1	5.2
0.2	40	43.70	0	0.00	14	3.26	46.96	249.2	93.1	0.0	6.9
0.2	40	43.70	1	1.09	14	3.26	48.05	255.0	90.9	2.3	6.8
0.3	40	45.44	2	2.18	14	3.4	51.02	270.8	89.1	4.3	6.7
0.4	40	47.11	3	3.41	14	3.53	54.05	286.9	87.2	6.3	6.5
0.4	40	47.11	4	4.71	14	3.53	55.35	293.8	85.1	8.5	6.4
0.4	40	47.11	5	5.89	14	3.53	56.53	300.0	83.3	10.4	6.2
0.4	40	47.11	6	7.07	14	3.53	57.70	306.3	81.6	12.2	6.1
0.2	40	43.70	0	0.00	16	3.73	47.43	251.7	92.1	0.0	7.9
0.4	40	47.11	1	1.18	16	4.03	52.32	277.7	90.0	2.3	7.7
0.4	40	47.11	2	2.36	16	4.03	53.49	283.9	88.1	4.4	7.5
0.4	40	47.11	3	3.53	16	4.03	54.67	290.2	86.2	6.5	7.4
0.4	40	47.11	4	4.71	16	4.03	55.85	296.4	84.3	8.4	7.2
0.2	40	43.70	0	0.00	18	4.2	47.90	254.2	91.2	0.0	8.8
0.4	40	47.11	1	1.18	18	4.54	52.83	280.4	89.2	2.2	8.6
0.4	40	47.11	2	2.36	18	4.54	54.00	286.6	87.2	4.4	8.4
0.4	40	47.11	3	3.53	18	4.54	55.18	292.9	85.4	6.4	8.2
0.2	40	43.70	0	0.00	20	4.66	48.36	256.7	90.4	0.0	9.6
0.4	40	47.11	1	1.18	20	5.04	53.33	283.0	88.3	2.2	9.5

Appendix K: The Test Conditions for H₂-CO₂ Jet Diffusion Flames

	P(G) (kg/cm ²)	H ₂ flowrate [l/min]	Actual H ₂ flowrate [l/min]	CO ₂ flowrate [l/min]	Actual CO ₂ flowrate [l/min]	Total flowrate [l/min]	Jet Exit Velocity [m/s]	H ₂ . vol. %	CO ₂ vol. %
1	/	20	20	2	0.43	20.4	108.44	97.9	2.1
2	0.2	40	43.70	2	0.47	44.2	234.44	98.9	1.1
3	0.2	60	65.55	2	0.47	66.0	350.41	99.3	0.7
4	0.3	80	90.87	2	0.49	91.4	484.93	99.5	0.5
5	0.4	100	117.77	2	0.51	118.3	627.81	99.6	0.4
6	0.6	110	138.29	2	0.54	138.8	736.88	99.6	0.4
7	0.8	120	159.83	2	0.57	160.4	851.36	99.6	0.4
8	/	20	20	4	0.86	20.9	110.72	95.9	4.1
9	0.2	40	43.7	4	0.93	44.6	236.89	97.9	2.1
10	0.2	60	65.55	4	0.93	66.5	352.87	98.6	1.4
11	0.3	80	90.87	4	0.97	91.8	487.47	98.9	1.1
12	0.6	100	125.72	4	1.08	126.8	673.02	99.1	0.9
13	0.6	110	138.29	4	1.08	139.4	739.74	99.2	0.8

14	0.8	120	159.83	4	1.14	161.0	854.39	99.3	0.7
15	/	20	20	6	1.28	21.3	112.95	94.0	6.0
16	0.2	40	43.7	6	1.4	45.1	239.38	96.9	3.1
17	0.3	60	68.15	6	1.45	69.6	369.44	97.9	2.1
18	0.4	80	94.22	6	1.51	95.7	508.10	98.4	1.6
19	0.6	100	125.72	6	1.62	127.3	675.88	98.7	1.3
20	0.8	110	146.51	6	1.71	148.2	786.72	98.8	1.2
21	1	120	168.32	6	1.8	170.1	902.96	98.9	1.1
22	/	20	20	8	1.71	21.7	115.23	92.1	7.9
23	0.2	40	43.7	8	1.87	45.6	241.88	95.9	4.1
24	0.4	60	70.66	8	2.01	72.7	385.73	97.2	2.8
25	0.4	80	94.22	8	2.01	96.2	510.77	97.9	2.1
26	0.6	100	125.72	8	2.16	127.9	678.77	98.3	1.7
27	0.8	110	146.51	8	2.29	148.8	789.81	98.5	1.5
28	1	120	168.32	8	2.4	170.7	906.16	98.6	1.4
29	/	20	20	10	2.14	22.1	117.52	90.3	9.7

30	0.2	40	43.7	10	2.33	46.0	244.32	94.9	5.1
31	0.4	60	70.66	10	2.52	73.2	388.43	96.6	3.4
32	0.4	80	94.22	10	2.52	96.7	513.48	97.4	2.6
33	0.6	90	113.14	10	2.69	115.8	614.83	97.7	2.3
34	0.8	100	133.19	10	2.86	136.0	722.13	97.9	2.1
35	1	110	154.29	10	3	157.3	834.88	98.1	1.9
36	1	120	168.32	10	3	171.3	909.33	98.2	1.8
37	/	20	20	12	2.57	22.6	119.80	88.6	11.4
38	0.2	40	43.7	12	2.8	46.5	246.82	94.0	6.0
39	0.4	60	70.66	12	3.02	73.7	391.08	95.9	4.1
40	0.6	80	100.57	12	3.23	103.8	550.97	96.9	3.1
41	0.6	90	113.14	12	3.23	116.4	617.70	97.2	2.8
42	0.8	100	133.19	12	3.42	136.6	725.11	97.5	2.5
43	1	110	154.29	12	3.6	157.9	838.06	97.7	2.3
44	1.2	120	176.40	12	3.76	180.2	956.27	97.9	2.1
45	/	20	20	14	3	23.0	122.08	87.0	13.0

46	0.2	40	43.7	14	3.26	47.0	249.26	93.1	6.9
47	0.4	60	70.66	14	3.53	74.2	393.79	95.2	4.8
48	0.6	80	100.57	14	3.77	104.3	553.82	96.4	3.6
49	0.8	90	119.87	14	3.99	123.9	657.43	96.8	3.2
50	1	100	154.29	14	4.2	158.5	841.24	97.3	2.7
51	1.2	110	161.70	14	4.39	166.1	881.58	97.4	2.6
52	1.4	120	184.13	14	4.6	188.7	1001.74	97.6	2.4
53	/	20	20	16	3.43	23.4	124.36	85.4	14.6
54	0.3	40	45.44	16	3.89	49.3	261.81	92.1	7.9
55	0.4	60	70.66	16	4.003	74.7	396.30	94.6	5.4
56	0.6	80	100.57	16	4.31	104.9	556.69	95.9	4.1
57	1	100	154.29	16	4.8	159.1	844.43	97.0	3.0
58	1.2	120	184.13	16	5.02	189.2	1003.98	97.3	2.7
59	/	20	20	18	3.85	23.9	126.59	83.9	16.1
60	0.4	40	47.11	18	4.54	51.6	274.14	91.2	8.8
61	0.6	60	75.43	18	4.85	80.3	426.11	94.0	6.0

62	0.6	80	100.57	18	4.85	105.4	559.57	95.4	4.6
63	1	100	154.29	18	5.4	159.7	847.61	96.6	3.4
64	0.2	20	21.85	20	4.66	26.5	140.71	82.4	17.6
65	0.4	40	47.11	20	5.04	52.1	276.79	90.3	9.7
66	0.4	50	58.88	20	5.04	63.9	339.30	92.1	7.9
67	0.2	20	21.85	22	5.13	27.0	143.21	81.0	19.0
68	0.4	40	47.11	22	5.54	52.7	279.46	89.5	10.5
69	0.2	20	21.85	24	5.6	27.5	145.70	79.6	20.4
70	0.3	30	34.08	24	5.83	39.9	211.82	85.4	14.6
71	0.4	40	47.11	24	6.05	53.2	282.17	88.6	11.4
72	0.2	20	21.85	26	6.06	27.9	148.14	78.3	21.7
73	0.3	30	34.08	26	6.31	40.4	214.38	84.4	15.6
74	0.4	40	47.11	26	6.55	53.7	284.82	87.8	12.2
75	0.2	20	21.85	28	6.53	28.4	150.64	77.0	23.0
76	0.4	30	35.33	28	7.05	42.4	224.95	83.4	16.6
77	0.2	20	21.85	30	7	28.9	153.13	75.7	24.3

78	0.4	30	35.33	30	7.56	42.9	227.65	82.4	17.6
----	-----	----	-------	----	------	------	--------	------	------

Appendix L: The Test Conditions for Pure H₂ Jet Diffusion Flames

Initial H ₂ flow rate [l/min]	Pressure gauge (bar)	Actual H ₂ flow rate [l/min]	Exit velocity [m/s]
10	1	10	53
20	1	20	106
30	1	30	159
40	1	40	212
50	1.2	55	290
60	1.2	66	348
70	1.2	77	406
80	1.2	88	464
90	1.3	102	544
100	1.4	118	626
110	1.4	130	689
120	1.6	151	803
130	1.7	169	897
140	1.8	187	993
150	1.9	206	1093

Appendix M: The Initial Composition of H₂-CH₄, H₂-C₂H₆ and H₂-C₃H₈ Mixtures applied in Equilibrium Kinetics Simulation

H ₂ Mole Fraction	H ₂ Mole	CH ₄ Mole	O ₂ Mole	N ₂ Mole
0.0	0.0	10.0	20.0	75.2
0.1	1.0	9.0	18.5	69.6
0.2	2.0	8.0	17.0	64.0
0.3	3.0	7.0	15.5	58.1
0.4	4.0	6.0	14.0	52.7
0.5	5.0	5.0	12.5	47.0
0.6	6.0	4.0	11.0	41.4
0.7	7.0	3.0	9.5	35.7
0.8	8.0	2.0	8.0	30.1
0.9	9.0	1.0	6.5	24.5
1	10	0	5	18.8

H ₂ Mole Fraction	H ₂ Mole	C ₂ H ₆ Mole	O ₂ Mole	N ₂ Mole
0.0	0.0	10.0	35.0	131.7
0.1	1.0	9.0	32.0	120.4
0.2	2.0	8.0	29.0	109.1
0.3	3.0	7.0	26.0	97.8
0.4	4.0	6.0	23.0	86.5
0.5	5.0	5.0	20.0	75.2
0.6	6.0	4.0	17.0	64.0
0.7	7.0	3.0	14.0	52.7
0.8	8.0	2.0	11.0	41.4
0.9	9.0	1.0	8.0	30.1
1.0	10.0	0.0	5.0	18.8

H ₂ Mole Fraction	H ₂ Mole	C ₃ H ₈ Mole	O ₂ Mole	N ₂ Mole
0.0	0.0	10.0	50	188.1
0.1	1.0	9.0	45.5	171.2
0.2	2.0	8.0	41	154.2
0.3	3.0	7.0	36.5	137.3
0.4	4.0	6.0	32	120.4
0.5	5.0	5.0	27.5	103.5
0.6	6.0	4.0	23	86.5
0.7	7.0	3.0	18.5	69.6
0.8	8.0	2.0	14	52.7
0.9	9.0	1.0	9.5	35.7
1.0	10.0	0.0	5	18.8

Appendix N: CHEMKIN Output File of the Final Solution of Laminar Burning Velocity Simulation for CH₄/Air

TWOPNT: SOLVE THE PROBLEM.

TASK	LOG10 NORM F	LOG10 COND J	REMARK
START	-3.34		48 GRID POINTS
SEARCH	-3.34	14.31	0 SEARCH STEPS
REFINE			0.67 AND 0.66 RATIOS

TWOPNT: FINAL SOLUTION:

	X (cm)	T (K)	AREA (cm ²)	V (cm/s)	RHO (g/cm ³)	HDOT (cal/s/cm ³)
1	0.0000	2.980E+02	1.000E+00	4.159E+01	1.130E-03	4.779E-07
2	0.0150	2.984E+02	1.000E+00	4.166E+01	1.128E-03	2.983E-06
3	0.0300	3.000E+02	1.000E+00	4.190E+01	1.122E-03	4.406E-05
4	0.0985	3.582E+02	1.000E+00	5.033E+01	9.336E-04	1.457E-02
5	0.1156	4.580E+02	1.000E+00	6.471E+01	7.262E-04	3.399E-01
6	0.1242	5.748E+02	1.000E+00	8.156E+01	5.761E-04	3.104E+00
7	0.1285	6.636E+02	1.000E+00	9.441E+01	4.977E-04	1.120E+01
8	0.1328	7.761E+02	1.000E+00	1.108E+02	4.243E-04	3.081E+01
9	0.1370	9.119E+02	1.000E+00	1.305E+02	3.600E-04	7.254E+01
10	0.1413	1.068E+03	1.000E+00	1.533E+02	3.064E-04	1.655E+02
11	0.1499	1.416E+03	1.000E+00	2.046E+02	2.297E-04	5.854E+02
12	0.1542	1.571E+03	1.000E+00	2.275E+02	2.066E-04	9.155E+02
13	0.1585	1.693E+03	1.000E+00	2.455E+02	1.914E-04	1.060E+03
14	0.1627	1.775E+03	1.000E+00	2.573E+02	1.826E-04	8.616E+02
15	0.1670	1.822E+03	1.000E+00	2.639E+02	1.781E-04	5.078E+02
44	11.1111	2.227E+03	1.000E+00	3.134E+02	1.499E-04	-1.164E-03
45	13.3333	2.227E+03	1.000E+00	3.134E+02	1.500E-04	-1.250E-03
46	15.5556	2.227E+03	1.000E+00	3.133E+02	1.500E-04	-1.245E-03
47	17.7778	2.227E+03	1.000E+00	3.133E+02	1.500E-04	-1.220E-03
48	20.0000	2.227E+03	1.000E+00	3.133E+02	1.500E-04	-1.220E-03

Appendix O: CHEMKIN Output File of the Final Solution of Laminar Burning Velocity Simulation for C₂H₆/Air

TWOPNT: SOLVE THE PROBLEM.

	LOG10	LOG10	
TASK	NORM F	COND J	REMARK
START	-1.49		52 GRID POINTS
SEARCH	-1.49	14.34	0 SEARCH STEPS
REFINE			0.57 AND 0.73 RATIOS

TWOPNT: FINAL SOLUTION:

	X (cm)	T (K)	AREA (cm ²)	V (cm/s)	RHO (g/cm ³)	HDOT (cal/s/cm ³)
1	0.0000	2.980E+02	1.000E+00	4.924E+01	1.182E-03	1.009E-07
2	0.0150	2.983E+02	1.000E+00	4.929E+01	1.181E-03	1.304E-06
3	0.0225	2.987E+02	1.000E+00	4.938E+01	1.179E-03	8.460E-06
4	0.0300	3.000E+02	1.000E+00	4.961E+01	1.174E-03	6.086E-05
5	0.0985	4.004E+02	1.000E+00	6.701E+01	8.689E-04	4.208E-02
6	0.1156	5.813E+02	1.000E+00	9.855E+01	5.908E-04	1.277E+00
7	0.1199	6.804E+02	1.000E+00	1.160E+02	5.018E-04	8.867E+00
8	0.1242	8.143E+02	1.000E+00	1.398E+02	4.164E-04	3.719E+01
9	0.1285	9.830E+02	1.000E+00	1.702E+02	3.421E-04	1.209E+02
10	0.1328	1.181E+03	1.000E+00	2.064E+02	2.821E-04	3.358E+02
48	11.1111	2.287E+03	1.000E+00	3.946E+02	1.475E-04	-2.253E-03
49	13.3333	2.286E+03	1.000E+00	3.946E+02	1.475E-04	-2.519E-03
50	15.5556	2.286E+03	1.000E+00	3.946E+02	1.476E-04	-2.503E-03
51	17.7778	2.286E+03	1.000E+00	3.945E+02	1.476E-04	-2.417E-03
52	20.0000	2.286E+03	1.000E+00	3.945E+02	1.476E-04	-2.417E-03

Appendix P: CHEMKIN Output File of the Final Solution of Laminar Burning Velocity Simulation for C₃H₈/Air

TWOPNT: SOLVE THE PROBLEM.

	LOG10	LOG10	
TASK	NORM F	COND J	REMARK
START	-1.78		46 GRID POINTS
SEARCH	-2.43	14.04	1 SEARCH STEP
REFINE			0.70 AND 0.83 RATIOS

TWOPNT: FINAL SOLUTION:

	X (cm)	T (K)	AREA (cm ²)	V (cm/s)	RHO (g/cm ³)	HDOT (cal/s/cm ³)
1	0.0000	2.980E+02	1.000E+00	5.569E+01	1.205E-03	1.175E-06
2	0.0150	2.983E+02	1.000E+00	5.577E+01	1.203E-03	9.450E-06
3	0.0300	3.000E+02	1.000E+00	5.612E+01	1.195E-03	2.411E-04
4	0.0643	3.278E+02	1.000E+00	6.163E+01	1.089E-03	3.794E-02
5	0.0814	4.186E+02	1.000E+00	7.938E+01	8.451E-04	1.018E+00
6	0.0899	5.585E+02	1.000E+00	1.070E+02	6.268E-04	1.068E+01
7	0.0985	8.234E+02	1.000E+00	1.606E+02	4.177E-04	7.776E+01
8	0.1028	1.014E+03	1.000E+00	2.002E+02	3.350E-04	2.529E+02
9	0.1071	1.233E+03	1.000E+00	2.472E+02	2.714E-04	6.960E+02
10	0.1114	1.452E+03	1.000E+00	2.947E+02	2.276E-04	1.420E+03
41	8.8889	2.284E+03	1.000E+00	4.496E+02	1.492E-04	1.109E-03
42	11.1111	2.284E+03	1.000E+00	4.496E+02	1.492E-04	-1.702E-03
43	13.3333	2.284E+03	1.000E+00	4.495E+02	1.492E-04	-2.409E-03
44	15.5556	2.283E+03	1.000E+00	4.495E+02	1.492E-04	-2.537E-03
45	17.7778	2.283E+03	1.000E+00	4.494E+02	1.493E-04	-2.507E-03
46	20.0000	2.283E+03	1.000E+00	4.494E+02	1.493E-04	-2.507E-03

Appendix Q: CHEMKIN Output File of the Final Solution of Laminar Burning Velocity Simulation for H₂/Air

TWOPNT: SOLVE THE PROBLEM.

	LOG10	LOG10	
TASK	NORM F	COND J	REMARK
START	-0.71		44 GRID POINTS
SEARCH	-0.71	12.35	0 SEARCH STEPS
REFINE			0.49 AND 0.67 RATIOS

TWOPNT: FINAL SOLUTION:

	X (cm)	T (K)	AREA (cm ²)	V (cm/s)	RHO (g/cm ³)	HDOT (cal/s/cm ³)
1	0.0000	2.980E+02	1.000E+00	2.486E+02	8.550E-04	3.105E-07
2	0.0075	2.980E+02	1.000E+00	2.486E+02	8.550E-04	8.311E-07
3	0.0150	2.980E+02	1.000E+00	2.486E+02	8.551E-04	9.648E-06
4	0.0187	2.981E+02	1.000E+00	2.486E+02	8.550E-04	5.171E-05
5	0.0225	2.981E+02	1.000E+00	2.487E+02	8.549E-04	2.710E-04
6	0.0244	2.983E+02	1.000E+00	2.487E+02	8.547E-04	7.392E-04
7	0.0262	2.985E+02	1.000E+00	2.489E+02	8.543E-04	2.073E-03
8	0.0281	2.990E+02	1.000E+00	2.492E+02	8.533E-04	6.162E-03
9	0.0300	3.000E+02	1.000E+00	2.498E+02	8.510E-04	2.166E-02
10	0.0386	3.170E+02	1.000E+00	2.620E+02	8.115E-04	1.335E+00
40	11.1111	2.372E+03	1.000E+00	1.695E+03	1.254E-04	-4.935E-03
41	13.3333	2.372E+03	1.000E+00	1.695E+03	1.254E-04	-6.303E-03
42	15.5556	2.372E+03	1.000E+00	1.695E+03	1.254E-04	-6.506E-03
43	17.7778	2.372E+03	1.000E+00	1.695E+03	1.254E-04	-6.460E-03
44	20.0000	2.372E+03	1.000E+00	1.695E+03	1.254E-04	-6.460E-03